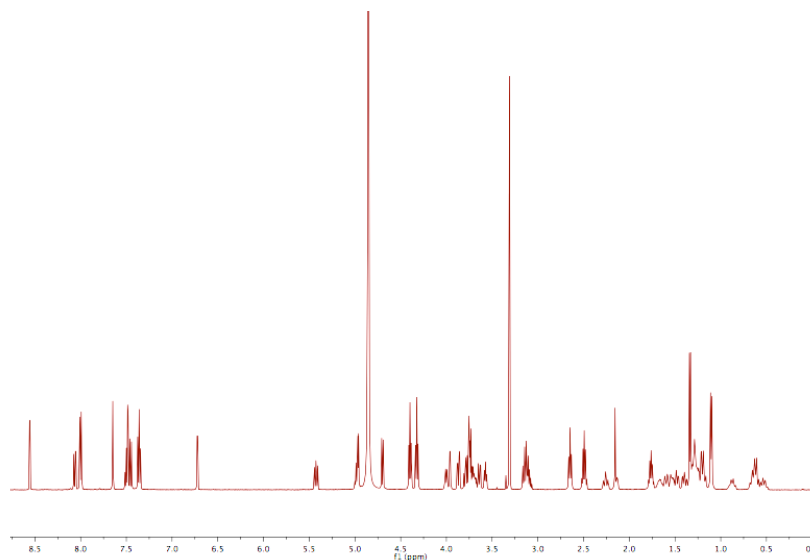


E-selectin Antagonists: Fragment-Based Drug Discovery and Lead Optimization by NMR and BIAcore



Inauguraldissertation zur Erlangung der Würde eines Doktors der Philosophie
vorgelegt der Philosophisch-Naturwissenschaftlichen Fakultät der Universität Basel

Von

Céline Weckerle
aus Strasbourg, Frankreich

Referent: Prof. Dr. Beat Enst
Korreferent: Prof. Dr. Ernest Giralt
Expert: Dr. Brian Cutting

Basel, 2012

Genehmigt von der Philosophisch-Naturwissenschaftlichen Fakultät auf Antrag von:

Prof. Dr. Beat Ernst, Institut für Molekulare Pharmazie, Universität Basel

Prof. Dr. Ernest Giralt, Institute for Research in Biomedicine, Parc Cientific de Barcelona, University of Barcelona, Spain

Dr. Brian Cutting, Institut für Molekulare Pharmazie, Universität Basel

Basel, den 22 Juni 2010

Prof. Dr. Eberhard Parlow

Dekan der Philosophisch-Naturwissenschaftlichen Fakultät

“Obstacles are those frightful things we see when we take our eyes off our goals”

Henry Ford
1863-1947

ACKNOWLEDGEMENTS

First, I would like to thank Prof. Dr. Beat Ernst who gave me the opportunity to do my Ph.D. thesis at the Institute of Molecular Pharmacy (IMP). I express all my gratitude for his support during the past three and a half years. The interdisciplinary scientific atmosphere, the available pool of modern infrastructures and the innovative approaches in drug discovery projects created a unique environment at the IMP, which with no doubt contributed to my scientific education and made this work possible.

I would like to thank Prof. Dr. Ernest Giralt for accepting to be the co-referee of my thesis.

My deep and special thanks are also going to Dr. Brian Cutting for the scientific and project-related discussions, for encouraging me to pursue and develop my own ideas, and for introducing me into the NMR technology.

I would like to specifically name people who worked with me on the selectin project: Jonas Egger, Beatrice Wagner and Dr. Daniel Schwizer for providing me with analytes, Katrin Lemme, Roland Preston and Dr. Said Rabbani for providing me with proteins, and Dr. Daniel Strasser for introducing me into the surface plasmon resonance technology. I also would like to mention Stefanie Mesch, Florian Binder, Matthias Wittwer, Meike Scharenberg and Dr. Alex Titz for our scientific discussions.

My gratefulness goes to all IMP members, former and present, who make the IMP as it is. They provided me with assistance, new inputs, an encouraging working atmosphere and most of them became more than colleagues: friends.

Finally, I want to thank the most important people in my life: my family. Thanks to my parents, Patrick and Viviane, for their love, support and encouragements. Thanks to my sister, Fanny, available 24 hours a day, seven days per week. Thanks to my better half, Cédric, for his love, his patience and for encouraging me to pursue my dreams. Thanks to my little sunshine, Louis, for giving me the strength. This work would not have been possible without them.

SUMMARY

The inflammatory response consists of a well-defined and regulated multi-step cascade leading to extravasation of leukocytes from the blood to sites of inflammation. The transmigration of leukocytes is initiated by their interaction with the endothelium, a process regulated by selectins, a family of cell adhesion molecules. This Ph.D. thesis is focused on E-selectin - a C-type type (Ca^{2+} -dependent) lectin.

Excessive recruitment of leukocytes, as observed in inflammatory diseases (e.g. asthma or arthritis), is problematic because the inflammatory response itself becomes harmful. Consequently, the modulation of leukocyte recruitment by interfering with cell tethering is of therapeutical interest.

Sialyl Lewis^x (sLe^x) is the minimal carbohydrate epitope of physiological ligands recognized by E-selectin. This moderate binder (in the millimolar range) has served as a lead structure for the design of more potent E-selectin antagonists. This optimization process was supported by NMR and SPR, leading to the first generation of low micromolar antagonists of E-selectin. These contributions are presented in this thesis. By ligand-based NMR experiments a better understanding of the physical basis of the interaction was obtained.

In a next step, fragment-based methods that have emerged as a new strategy in drug discovery were successfully applied to the lead optimization of E-selectin antagonists. The improved affinities as well as the increased residence time impressively demonstrate the potential of the applied fragment-based approach.

ABBREVIATIONS

ADMET	Absorption, Distribution, Metabolism, Elimination, Toxicity
bb	Backbone
BIA	Biomolecular Interaction Analysis
BPA	Bradford protein assay
CMD	Carboxymethyl dextran
CRDs	Consensus repeat domains
DMSO	Dimethyl sulfoxide
EA	Ethanolamine
<i>e.g.</i>	For example
ESL-1	E-selectin ligand-1
FDA	Food and drug administration (USA)
Fuc	Fucose
Gal	Galactose
GEM	Group epitope mapping
GlcNAc	N-Acetylglucosamine
Glc	Glucose
GlyCAM-1	Glycosylated cell adhesion molecule-1
HTS	High-throughput screening
HPLC	High pressure liquid chromatography
IC ₅₀	50% inhibition concentration
ICAM-1	Intercellular cell adhesion molecule-1
ITC	Isothermal titration calorimetry
K _A	Equilibrium association constant
K _D	Equilibrium dissociation constant
kDa	Kilo Dalton
K _i	Inhibition constant
k _{on}	Association rate constant
k _{off}	Dissociation rate constant
Le ^a	Lewis ^a
Le ^x	Lewis ^x
LMW	Low molecular weight

LPS	Lipopolysaccharide
MadCAM-1	Mucosal vascular addressin cell adhesion molecule
MD	Molecular dynamics
Me	Methyl
MAG	Myelin-associated glycoprotein
min	Minute (s)
NME	New molecular entity
NMR	Nuclear magnetic resonance
NOE	Nuclear Overhauser effect
P20	Polysorbate-20 (Tween-20)
PAGE	Polyacrylamide gel electrophoresis
PSGL-1	P-selectin glycoprotein ligand-1
rIC ₅₀	Relative IC ₅₀
RT	Room temperature
RU	Resonance units
R _{eq}	Equilibrium response
R _{max}	Maximum response
SAR	Structure activity relationship
SDS	Sodium dodecyl sulfate
sLe ^a	Sialyl Lewis ^a
sLe ^x	Sialyl Lewis ^x
ss	Side chain
SPR	Surface plasmon resonance
STD	Saturation transfer difference
TIR	Total internal reflexion
TNF	Tumor necrosis factor
VCAM-1	Endothelial vascular cell-adhesion molecule-1

1.	General introduction	14
1.1	Drug discovery	14
1.1.1	Overview	14
1.1.1	Surface plasmon resonance in drug discovery	16
1.1.2	NMR in drug discovery	17
1.2	Selectins	18
1.2.1	Selectins in the inflammatory cascade	18
1.2.2	Role of selectins in human inflammatory diseases	21
1.2.3	Selectin family	22
1.2.4	Selectin ligands	25
1.2.4.1	Natural ligands	25
1.2.4.2	Sialyl Lewis ^x as a lead for selectin antagonists	27
1.2.4.3	Recent advances in selectin antagonists	30
1.3	References	31
2	Aim of the thesis	37
3	Affinity and kinetic evaluation of the first generation of E-selectin antagonists using Biacore technology	38
3.1	Introduction	38
3.1.1	Locked conformations: a successful strategy for development of Selectin antagonists	38
3.1.2	Biacore Technology	39
3.1.2.1	Surface plasmon resonance phenomenon	39
3.1.2.2	Typical Biacore experiment	40
3.1.2.3	Kinetic and affinity evaluation	44
3.1.3	Structure of E-selectin/IgG and Lec EGF_CRD2 domain constructs	45
3.2	Materials and Methods	48
3.2.1	Biacore	48
3.2.2	Expression and purification of E-selectin/IgG	49

3.2.3	Expression and purification of Lec EGF_CR2 domain	50
3.2.4	Direct amine coupling of E-selectin/IgG	51
3.2.5	Capture-based assay format	52
3.2.5.1	Preparation of protein A surface	52
3.2.5.2	Preparation of anti-human IgG (Fc specific) surface	54
3.2.5.3	Capture of E-selectin/IgG on Protein A or E-selectin IgG surface	55
3.2.5.4	Validation of the capture-based assay	55
3.2.5.5	Evaluation of the surface activity	56
3.2.5.6	DMSO tolerability	57
3.2.5.7	Evaluation of synthesized E-selectin antagonists	58
3.2.6	Thermodynamic analyses	59
3.2.7	Reverse assay: immobilization of an E-selectin antagonist onto the sensor chip surface	60
3.3	Results and discussion	62
3.3.1	Development of an E-selectin Biacore assay	62
3.3.1.1	Direct amine coupling of E-selectin/IgG	62
3.3.1.2	Immobilization of E-selectin/IgG by a capture assay on a Protein A surface	64
3.3.1.3	Immobilization of E-selectin/IgG by a capture assay on a anti-human IgG surface	66
3.3.1.4	Comparison of the capture assay via Protein A and via anti-human IgG	68
3.3.2	Further optimization of the E-selectin/IgG Biacore capture assay	71
3.3.2.1	Dependence of the binding affinity upon surface density	71
3.3.2.2	Non-specific contribution from the intermediate used for the capture to the observed binding	75
3.3.2.3	Impact of the quality of the protein	76
3.3.2.4	Stability of the surface	78
3.3.2.5	Calcium dependence of the binding	79
3.3.2.6	Removal of sample interactant from the captured surface	80
3.3.3	Evaluation of BW-69669 derivatives	83
3.3.4	Kinetic evaluation of BW-69669 derivatives	88
3.3.5	Reproducibility in Biacore experiments	89

3.3.6	Thermodynamic analysis	90
3.3.7	Reverse assay	92
3.4	Conclusion	97
3.5	References	99
4	Binding epitope studies of the first generation of E-selectin antagonists by STD-NMR	103
4.1	Introduction	103
4.1.1	General points	103
4.1.2	Detection of ligand-binding by NMR methods	104
4.1.2.1	Methods based on relaxation enhancement	106
4.1.2.2	Methods based on NOEs measurements	107
4.2	Material and methods	110
4.2.1	Instrumentation	110
4.2.2	Reagent	111
4.2.3	Software	111
4.2.4	Experiments	111
4.2.4.1	Relaxation experiments	111
4.2.4.2	STD-NMR experiments	113
4.2.4.3	Competitive STD-NMR experiment	114
4.2.4.4	Group epitope mapping (GEM)	114
4.2.4.5	selective TOCSY and COSY experiments	115
4.2.4.6	trNOESY experiment	115
4.3	Results and discussion	116
4.3.1	Relaxation experiments of BW-69669 and GMI-1077 in the presence of E-selectin/IgG	116
4.3.1.1	Spin-spin ($T_{1\rho}$) relaxation experiments	116
4.3.1.2	Selective T1 relaxation	119
4.3.1.3	Competitive binding measurements using selective T1 relaxation	120
4.3.2	Transferred NOESY	123
4.3.3	2D-TOCSY experiments for assignment of the resonances of DS-0567 in the presence of E-selectin/IgG	126

4.3.4	STD-NMR experiments of DS-0567 in the presence of E-selectin/IgG	127
4.3.5	Non-specific binding: an issue tested by STD-NMR of DS-0567 with E-selectin/IgG.	129
4.3.6	Artifacts: an issue tested by STD-NMR of DS-0567 with E-selectin/IgG	130
4.3.7	Large STD values of the benzoate in 2-position of galactose due to the dimeric form of the protein: an issue tested by STD-NMR experiments of GMI-1077 and a monomeric E-selectin construct.	131
4.3.8	STD-NMR experiments of BW-580	134
4.3.9	STD-NMR experiments of BW-69669 and DS-04115	136
4.3.10	Additional studies and comparisons of different epitope maps of compound studied	137
4.3.11	STD-NMR experiments of DS-0560	138
4.4	Conclusion	141
4.5	References	143
5	Fragment-based screening approach for design and synthesis of the second generation of E-selectin antagonists	145
5.1	Introduction	145
5.1.1	Need for fragment-based approaches in drug design	145
5.1.2	Fragment-based screening and linked-fragment approaches	146
5.1.3	SAR by NMR	147
5.1.4	Spin-label approach	149
5.2	Materials and methods	151
5.2.1	Biacore capture assay	151
5.2.1.1	Biacore characterization of TEMPO ligands	151
5.2.1.2	Optimization of the Biacore method used for first-second-site ligands analysis	152
5.2.1.3	Affinity ranking experiments	152
5.2.2	NMR	153

5.2.2.1	Pre-selection of promising compounds by screening of small sublibraries of second site compounds	153
5.2.2.2	Analysis of promising hits	154
5.2.2.3	STD and waterLOGSY experiments	154
5.3	Results and discussion	156
5.3.1	Evaluation of JE-16 with the Biacore capture assay	156
5.3.2	NMR evaluation of the paramagnetic activity of JE-16 and reducing conditions	158
5.3.3	Second site screening by NMR	159
5.3.4	Assignment of isolated resonances for each compound of each sublibrary	159
5.3.5	Screening of the sublibraries	160
5.3.6	SH-104-17	166
5.3.7	SH-104-19	168
5.3.8	SH-104-4	171
5.3.9	Analysis of the first compound synthesized and optimization of the Biacore method	177
5.3.10	Optimization of assay conditions for JE-57	179
5.3.11	Ranking	181
5.3.12	Binding assay for JE-55, JE-81, JE-83, JE-85, JE-86 and JE-97	186
5.4	Conclusion	188
5.5	References	190
6	Conclusions and outlook	192
	Appendixes	196
	CV	204

1. General introduction

1.1 Drug discovery

1.1.1 Overview

The drug discovery and development (DDD) process is complex, challenging and expensive. Traditionally, the discovery phase is divided into five steps (Figure 1).

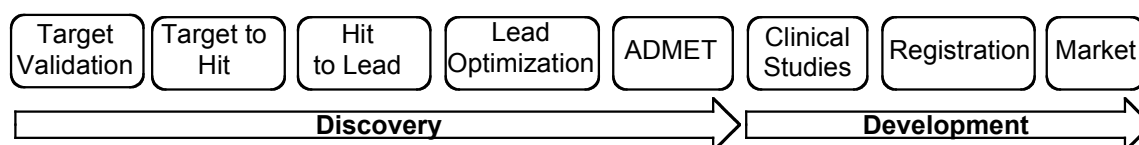


Figure 1. General steps of drug discovery and development process.

The first step is the identification and validation of a target according to its involvement in the particular disease and its “drugability”. Currently, most of the targets are proteins, e.g. G-protein-coupled-receptors [1], and can be classified in different categories: receptors, enzymes, channels and hormones (Figure 2).

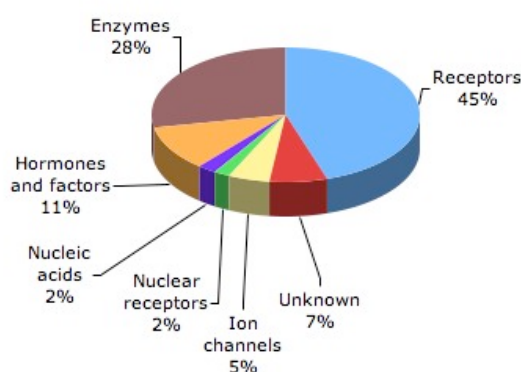


Figure 2. Main classes of current drug targets (adapted from Bleicher et al. [2])

After target discovery and validation, hits have to be identified for the selected target. Thus, a primary screen of large libraries of compounds is rapidly performed. For this purpose, divers types of libraries can be used: natural products (NPs),

collections of synthesized compounds, as well as combinatorial libraries [2,3]. In this step, contributions from computer-aided drug design (CADD) and structure-based drug design often play a key role, especially when NMR and X-ray data of the target are available. After their validation, selected hits enter the dose-response screening in order to choose compounds with the most promising lead profile (selectivity, potency). Lead optimization is achieved in order to improve the drug-like profile of the candidates. Guided by the structure-activity relationship (SAR), medicinal chemists further optimize the leads, their pharmacodynamics (PD) and their pharmacokinetic (PK) properties as adsorption, distribution, metabolism, excretion and toxicity (ADMET).

The time range for the discovery and development phase, resulting in the entry of a new drug in the market is long, approximately 15 years. In 2003, DiMasi *et al.* [4] estimated the cost of the process to be US\$ 800 million. In 2006, Adams *et al.* [5] re-evaluated the total cost as varying between US\$ 0.5 and US\$ 2 billion. This broad range results from the variation of costs depending on the indication and the novelty of both target and drug.

Pharmaceutical industries put significant effort into improving the productivity of the DDD process in order to bring more innovative drugs to the market. As a consequence of the high safety standards, the Food and Drug Administration (FDA) and other worldwide safety authorities approve only a restricted number of New Molecular Entities (NMEs) per year (26 in 2009) [6]. In view of these conflicting goals, a substantial improvement of the DDD process is unavoidable, especially due to growing pressures such as patent expiration or even more demanding regulatory requirements that have to be faced [7,8]. Therefore, in modern-drug discovery, a combination of virtual screening and medicinal chemistry with high throughput technologies tends to reduce time and costs and improve efficacy of the DDD process [8]. In the development phase of the candidates (Figure 1), phase II and phase III of the clinical development are the most expensive ones. Paul *et al.* therefore proposed an alternative development paradigm including the establishment of proof-of-concept (POC) leading to a reduction of the number of NMEs reaching the clinical studies but increasing their probability to reach market [7].

Research for new, efficient and cost effective techniques in the process of drug discovery and development is unambiguous. In that respect, label-free assays

that limit the generation of false positive and false negative results are highly attractive for pharmaceutical firms. Isothermal titration calorimetry (ITC), analytical centrifugation (AUC), mass spectroscopy, nuclear magnetic resonance spectroscopy (NMR) and biosensors represent a set of attractive methods [9]. Frequently, two or more techniques are used simultaneously to improve the reliability of hit identification [10].

1.1.2 Surface plasmon resonance in drug discovery

Optical biosensors can be used in all steps of the discovery and development process, including target identification and validation, screening, assay development, lead selection and optimization, ADME and quality control [9,11-14]. The miniaturization and automation of the platforms make this technology even more attractive. Optical biosensors that exploit surface plasmon resonance (SPR) are nowadays the most popular class of biosensors. Indeed, this surface-sensitive method allows high-throughput, does not require any label for the detection and the measurements are performed in real-time. Those characteristics, as well as considerable recent advance in instrumentation and experimental design place optical biosensors in a key position in drug discovery [12]. As an example, Biacore 4000 commercialized by GE Healthcare is dedicated to screening of fragments and evaluating of low molecular weight compounds. In addition, almost all types of molecule can be immobilized on a biosensor surface (protein, nucleic acids, lipids, carbohydrates) and a broad range in the size of the analytes exists (low molecular weight compounds of a few 100 Da up to large particules such as virus) [15]. Despite recent improvements in the instrument hardware, experimental design and data analysis [14], the analysis of low molecular weight compounds remains challenging. Last but not least, the set of parameters accessible from SPR-biosensor analyses is significant: association and dissociation rates, enthalpy, entropy, stoichiometry, IC_{50} , and inhibition constant.

1.1.3 Nuclear magnetic resonance in drug discovery

Also traditionally dedicated and developed for applications in chemistry and structural biology, nuclear magnetic resonance (NMR) has more recently found a central role in the drug discovery and development process. In 1996, Abbott Laboratories highlighted the role of NMR in the drug discovery process with their SAR-by-NMR, an NMR-driven method based on perturbation of the target spectra in the presence of ligands [16]. Since then, in addition to complementary research areas, NMR increased its range of application in pharmaceutical research and is used throughout numerous research and development steps from the primary high-throughput screening to binding studies [13].

NMR in drug discovery can be divided in two types of methods according to the molecule detected: ligand or target. Ligand-based investigations are focused on the difference in the NMR properties of a ligand in the bound state compared to the free form. In the bound state, a ligand will exhibit the same NMR properties as the target: fast relaxation, slow diffusion and negative NOEs. This approach presents a number of advantages: labeled targets are not required, smaller amount of the target are needed compared to target-based screening, and some degree of information on the binding epitope and binding mode can be extracted. In addition, most of the ligand-based NMR methods rely to 1D experiments, *e.g.* STD and relaxation [17-19]. The limitations of this method are the range of affinity that can be detected (mM to μ M affinities). High affinity ligands can be a source of false negative (undistinguishable from the target). For low affinity ligands, recent publications opened new possibilities [20].

In target-based methods, low affinity ligands can be detected and the specificity of the binding characterized. In addition, detailed structural information can be obtained. Nevertheless, significant quantities of the target, usually isotopically labeled are required, which is a clear limitation to their application. In addition, most of the experiments are 2D, which implies long acquisition time *e.g.* HSQC [17-19].

Both methods exhibit positives and negatives aspects and provide complementary information. The use of one or the other approach is clearly dependent on the material available (labeled or non-labeled target, quantities).

1.2 Selectins

1.2.1 Selectins in the inflammatory cascade

The inflammatory response is a complex biological response of the body to defend itself against various injuries or infections (e.g. viruses, bacteria, fungi, damaged cells). The main actors of this defense are leukocytes, which circulate in the body in search for alert signals from sites of tissue damage or infection. The inflammatory response consists of a well-defined and regulated multi-step cascade leading to extravasation of leukocytes from the blood (mainly post-capillary venules) to the site of inflammation. This process is part of the innate immune response. After reaching the site of damaged tissue by chemotaxis, leukocytes act by phagocytosis and release of pro-inflammatory mediators like chemokines or platelet activating factors. Four major steps are distinguished in the inflammatory response process (Figure 3):

- Inflammatory stimuli
- Tethering and rolling of the leukocytes
- Integrin activation leading to firm adhesion
- Transendothelial migration

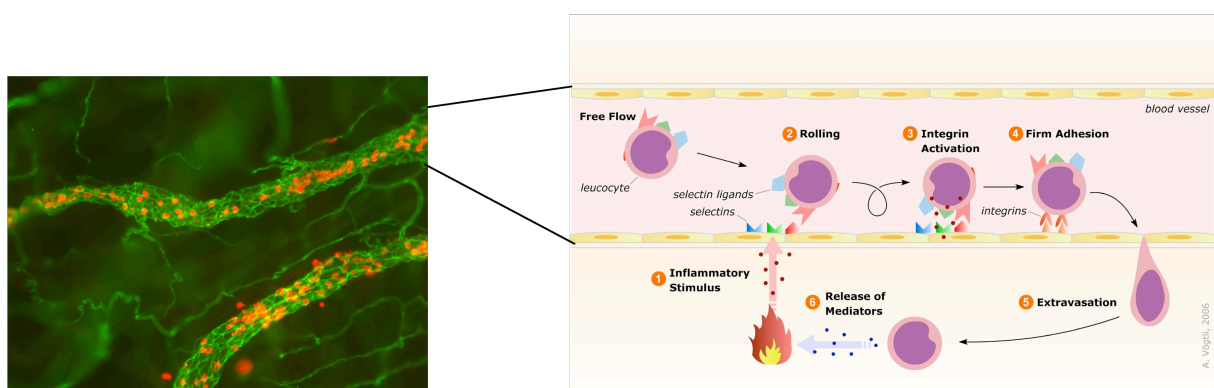


Figure 3. Successive steps of leukocyte transmigration and the role of selectins (adapted from [21] and by courtesy of Dr. A. Voegtli).

In the first step, proinflammatory mediators are released on the site of injury by the immune cells already present in the tissues (e.g. macrophages), which act as an

alert signal for the start of the inflammatory cascade. The consequence is the expression of cell adhesion molecules (CAMs) on the endothelial surface. The leukocyte recruitment is a receptor-mediated process, initiated by interactions between leukocytes and the endothelium [22]. Selectins are a family of CAMs involved in the early stages of those interactions. The expression of E- and P-selectin on the endothelium surface is initiated by the release of proinflammatory mediators (thrombin, histamine). In that process, E-selectin is synthesized *de novo* and its expression is induced by TNF- α , interleukin 1 (IL-1) or lipopolysaccharide (LPS) [23]. In contrast, after stimuli such as histamine or thrombin, P-selectin is transported from α -granules of platelets and Weibel-Palade bodies of endothelial cell to the surface within minutes [24,25]. In addition, a few hours later, stimulation by cytokines such as TNF- α induces the expression of P-selectin. In the next step, selectins bind to endogenous ligands expressed on the leukocyte surface (PSGL-1 and ESL-1) in a fast association/dissociation process which leads to reduced mobility of the leukocytes from 1-10 mm/s down to 5 μ m/s before becoming fully stationary. The principal role of E-selectin in this process was shown in E-selectin deficient mice, where the leukocytes rolled two to four times faster than in wild mice [26]. A third member of the selectin family, the L-selectin, is constitutively expressed on the surface of leukocytes and is involved in interactions with its ligand GlyCAM-1 in the “secondary tethering” process. This process describes the interaction between leukocytes in the flow and leukocytes already associated on the endothelium [27].

At the end of the leukocyte recruitment process, the expression of E-selectin is stopped and return to basic level, P-selectin is removed from the surface by endocytosis and L-selectin is cleaved by metalloproteases. By promoting the tethering and the rolling of leukocytes along the endothelial surface in the early stage of the inflammatory cascade, selectins play a key role in the initiation of the extravasation process [28]. The kinetics of the expression of the different CAMs is precisely regulated and a global maximum level is reached 4 h after activation (Figure 4).

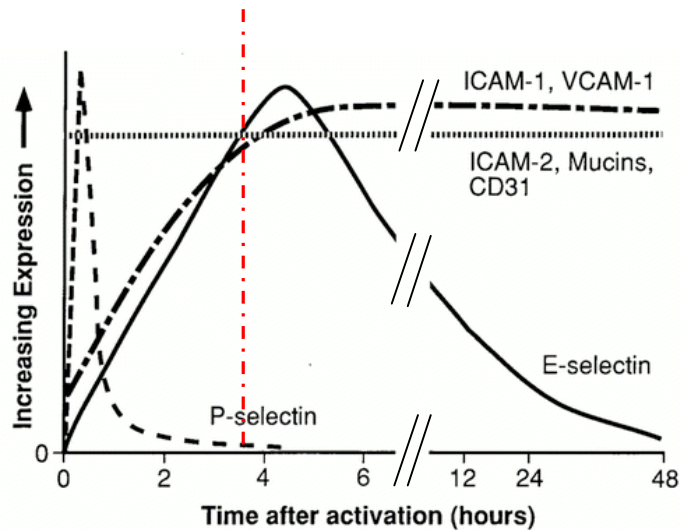
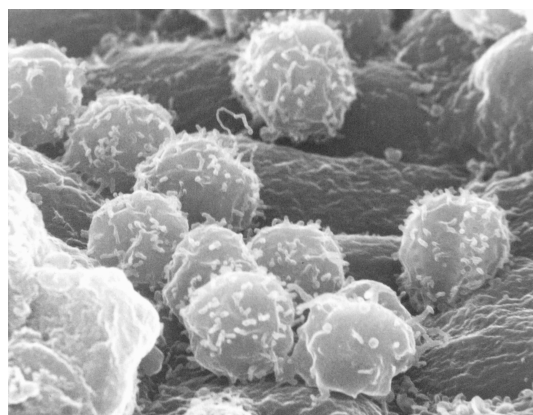


Figure 4. Kinetic profile of the expression of adhesion molecules after activation by inflammatory mediators (Adapted from Bevilacqua et al. 1994).

Fundamental to transmigration, integrin mediates tight adhesion to the endothelium and finally, migration of the leukocytes to the endothelial junctions. The process ends with the passage of the recruited leukocytes across the endothelium via diapedesis (Table 1) [29-31].

Table 1. Proteins involved in the different stage of leukocyte extravasation. Leukocytes adhering on the endothelium are show at the bottom [32].

Steps of homing process	Protein families	Members
Rolling	Selectins	E-selectin P-selectin L-selectin
Firm adhesion	Integrins	LFA-1 VLA-4 Mac-1
Transmigration	Integrins Immunoglobulin superfamily Glycoproteins	LFA-1, VLA-4 PECAM-1 (CD-31), JAM-1 CD-99



1.2.2 Role of selectins in human inflammatory diseases

Two categories of inflammation can be distinguished: acute and chronic. In both, an excessive recruitment of leukocytes, as observed in inflammatory diseases (e.g. asthma or arthritis) is problematic, because the inflammatory response itself becomes harmful. *A contrario*, a lack of leukocytes recruitment also appears problematic by decreasing the host's response. Consequently, the modulation of leukocyte recruitment via interference with cell tethering is of therapeutic interest. The physiological and pathophysiological role of selectins was revealed with the first studies in selectin-deficient mice models where multifocal infections were detected [33,34].

Those first insights revealed the likelihood of the importance of the selectin-leukocytes interaction in inflammatory diseases. The consequences of preventing selectin-ligand interactions lead to a dramatic impact on the progression of diseases in animal models [35,36], and thereby reveal the key role of selectins in numerous diseases. Thus, in vasculitis and atherosclerosis, an enhanced expression of E-selectin was observed inducing an accumulation of leukocytes in the tissues [37-39]. In ischemia and reperfusion injuries, prolonged hypoxia induces an increase of the leukocytes-endothelium interaction mediated by P- and E-selectin [40,41]. The role of selectin was also demonstrated in other diseases like sepsis [42], asthma [43], gastrointestinal inflammation [44] or rheumatoid arthritis [45]. A strong upregulation of the selectin ligands has also been observed in cancer metastasis. Indeed, high levels of expression of sLe^{x/a} were observed in many solid tumors and adenocarcinomas [46-51]. During metastasis, it was shown that malignant cells follow the pathway of leukocytes to be spread in the organism (Figure 5). An enhancement of the sialylation and fucosylation of the mucin surface protein, which interacts with selectins was reported to participate to the progression of carcinoma cells metastasis [52]. Therefore, carbohydrates epitopes, which bind to selectins, are tumor-associated antigens [53] and can be used in diagnosis [52].

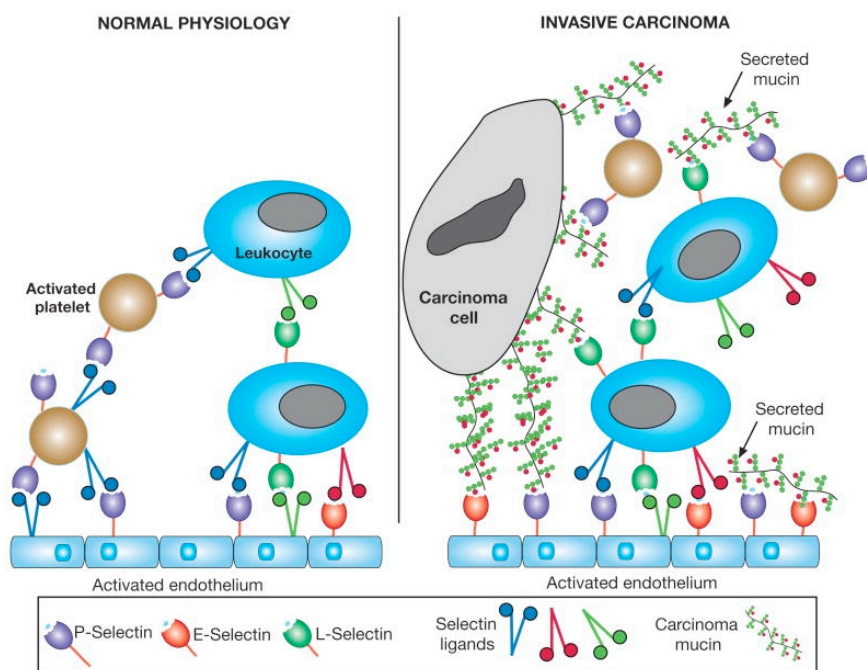


Figure 5. Role of Selectins in cancer metastasis [54].

Based on the studies mentioned above, blocking the selectin-ligand interaction would provide considerable benefits for patients suffering from inflammatory diseases. Established treatments of inflammation are based on non-steroidal anti-inflammatory drugs (NSAIDs, *e.g.* salicylates and cyclooxygenase (COX) inhibitors) as well as steroid-based drugs (*e.g.* cortisol). Such treatments are palliative and short and long term side effects are well documented. An alternative approach is possible with antibody therapies (*e.g.* Enbrel®, Wyeth) but the high costs of treatment limit their use. The development of small molecular antagonists of selectins, which could interfere in the early stage of the inflammatory cascade and limit the leukocytes recruitment, appears extremely attractive, but is nevertheless challenging. This PhD thesis reports the improvement of the potency of E-selectin antagonists guided by Biacore and NMR at the Institute of Molecular Pharmacy.

1.2.3 Selectin family

Lectins recognize carbohydrate structures of glycoconjugates (proteins or lipids) or soluble carbohydrates and are present in plants, in which they were initially discovered, as well as in animals. They are divided into 4 groups [55]:

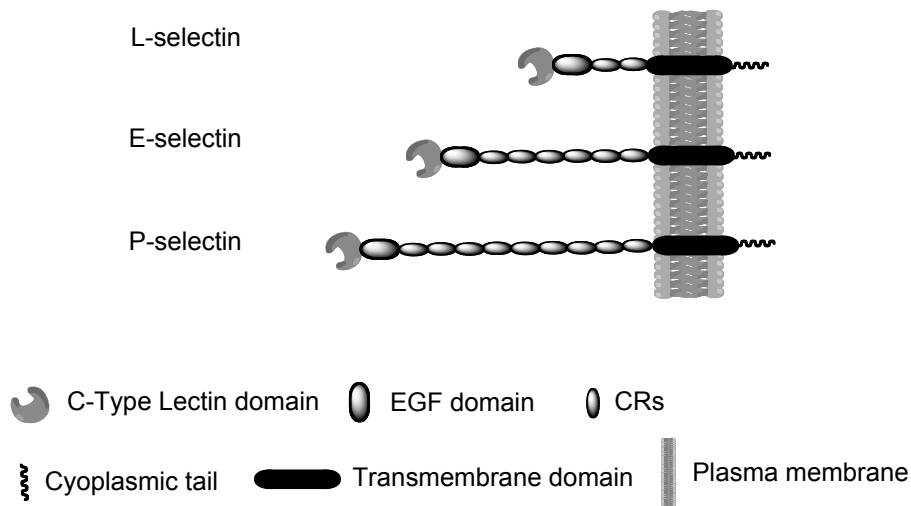
- C-type lectins characterized by a calcium dependant binding
- P-type lectins characterized by recognition of phosphorylated mannose residues
- S-type lectins or galectins characterized by the presence of free thiol groups in their structure
- Other lectins

Selectins are single-chain transmembrane glycoprotein belonging the group of C-type lectins. Three members, E-, P- and L-selectin, represent the selectin family. They are distinguished by their first identification site (Table 2).

Table 2. Selectin family members.

	L-selectin	E-selectin	P-selectin
Date of identification	1983 [56]	Late 1980's [23]	1984 [57]
Site of first identification	Leukocytes	Endothelium	Platelets
Synonyms	CD62L LAM-1 LECAM-1	CD62E ELAM-1 LECAM-2	CD62P LECAM-3 GMP-140 PADGE
Molecular weight calculated	42 kDa	64 kDa	86 kDa
Molecular weight observed	90 kDa [58]	115 kDa [59]	140 kDa [60]

A high degree of glycosylation considerably increases the molecular weight for each selectin (Table 2). All selectins are transmembrane glycoproteins and share common structural motifs (Figure 6). A C-type lectin domain at the *N*-terminus, which contains the carbohydrate recognition domain (CRD) followed by an epidermal growth factor (EGF)-like domain, a variable number of consensus repeats (CRs), a transmembrane segment and a short *C*-terminal tail are present in all selectins [61].



	L-selectin	E-selectin	P-selectin
Lectin domain (with CRD)	120	120	118
EGF domain	35	35	40
CRs	177	380	572
TM domain	23	24	24
Cytoplasmic tail	17	32	35

Figure 6. Structure of L-, E- and P-selectin. Number of amino acids of each motif for each selectin is mentioned in the table.

An overall homology of about 50% is found between the members of the selectin family. For the lectin and the EGF domains, the primary sequence is highly conserved (up to 65 %) [62]. A calcium ion present in the CRD domain plays a major role in the carbohydrate recognition [63] together with the EGF domain that enhances the carbohydrate binding potential. Nevertheless, the role of the EGF domain in the interaction with the ligand remains unclear (stabilization of the conformation of the binding domain and/or direct interaction with the ligand [64,65]).

The major difference between the members of the selectin family is the number of short CRs. The primary sequence of these domains is less conserved between the selectin (40 % of homology [62]). These domains may act as spacers between cells involved in the interaction since it was shown that a depletion of the CRs in P-selectin affect the leukocytes rolling [66,67]. The transmembrane domain anchors the selectin to the plasma membrane and a short C-terminal cytoplasmic domain is postulated to be involved in signal transduction [68].

1.2.4 Selectin ligands

1.2.4.1 Natural ligands

Selectins are carbohydrate binding proteins recognizing sialylated and fucosylated terminal glycan epitopes on glycoproteins and glycolipids. The three members of the selectin family recognize a common carbohydrate epitope found in the trisaccharides Lewis^x (Le^x) and Lewis^a (Le^a) as well as in their sialylated derivatives, sialyl Lewis^x (sLe^x) and sialyl Lewis^a (sLe^a) (Figure 7) [69-72].

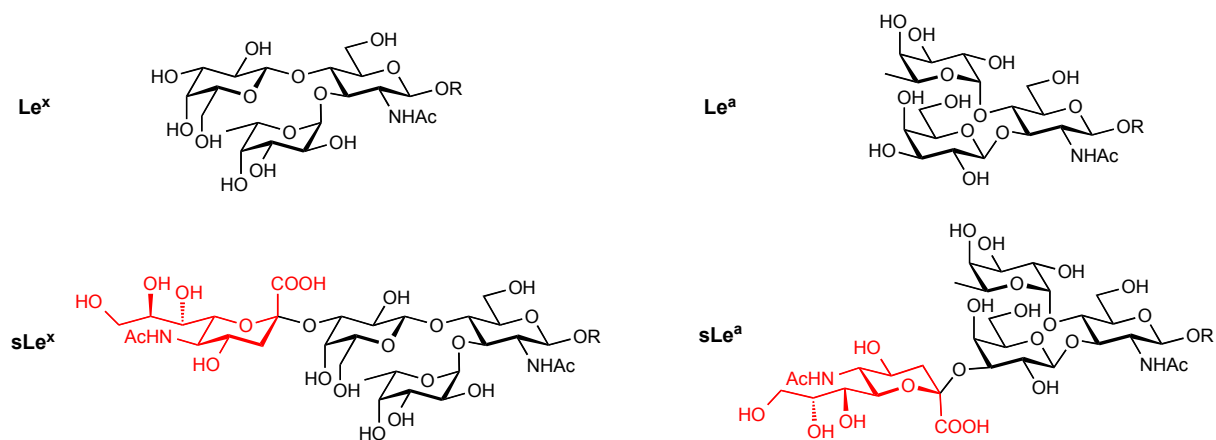


Figure 7. Common carbohydrates epitopes recognized by the selectin family. The sialic acid moieties are highlighted in red.

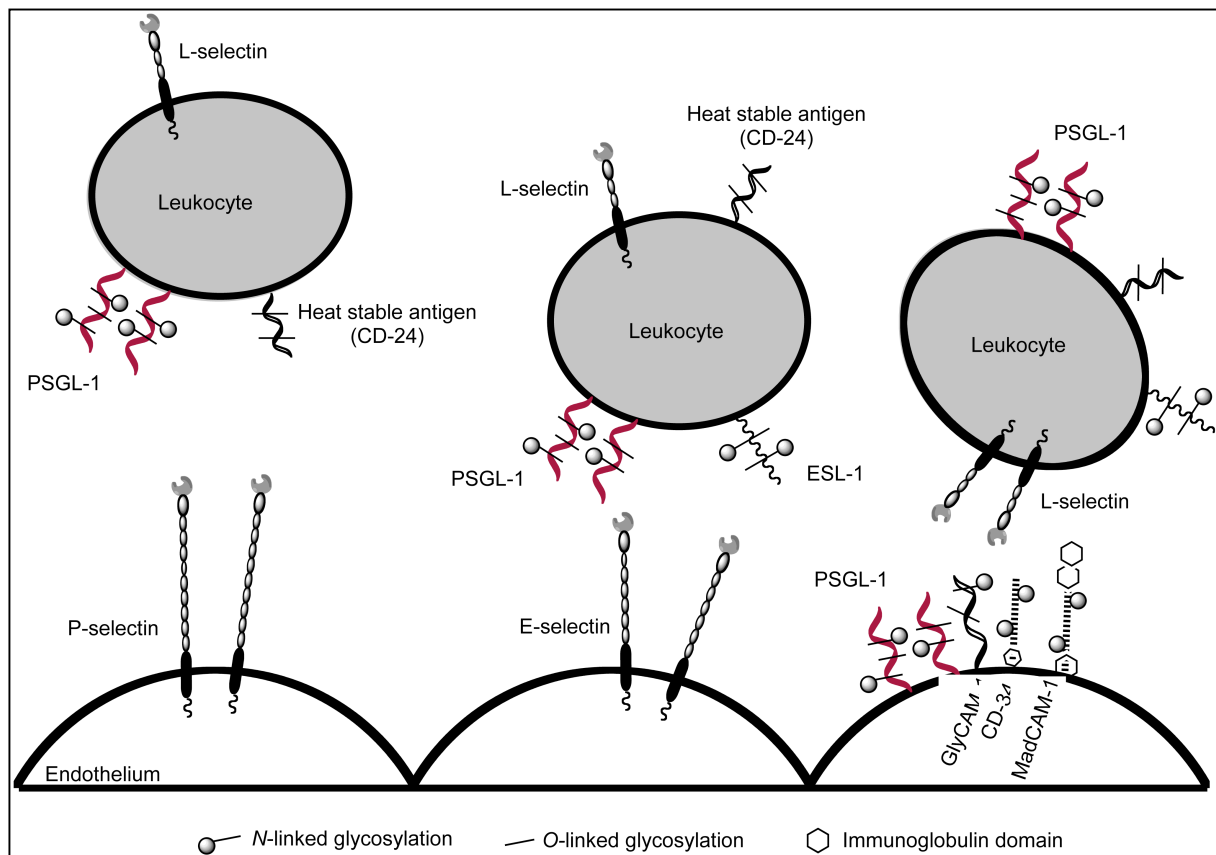
Seven glycoproteins were identified as L-selectin ligands and are shown in Table 3. The glycosylation-dependant cell adhesion molecule 1 (Gly-CAM-1), a sialo-mucin stored in cytoplasmic granula of endothelial cells in lymph node tissue is so far the best characterized L-selectin ligand [73-77]. *N*-acetyl neuraminic acid (Neu5Ac), L-fucose and sulfationated oligosaccharides were found to contribute to the binding [73-79].

In 1993 [80], P-selectin glycoprotein ligand-1 (PSGL-1) was discovered and is so far the best characterized natural P-selectin ligand. This 125 kDa glycoprotein forms dimers via a cysteine disulfide bridge and is also a natural ligand of E- and L-selectin. Nevertheless, the interaction of PSGL-1 with L- and P-selectin required additional sulfation of the three N-terminal tyrosine residues [81,82]. Three natural ligands for E-selectin have been identified: E-selectin ligand-1 (ESL-1), a 150 kDa

non-sulfated *N*-linked glycoprotein ligand [83,84], PSGL-1 and carbohydrates motifs present on L-selectin of human neutrophils [85].

Table 3. L-, P- and E-selectin natural ligands. Major ligands are highlighted on the figure adapted from Kneuer et al., shown below [86].

	L-selectin	P-selectin	E-selectin
Natural Ligands	<ul style="list-style-type: none"> • GlyCAM-1 • CD-34 • MAdCAM-1 • podocalyxin-like protein • endomucin • endoglycan • PSGL-1 	<ul style="list-style-type: none"> • PSGL-1 • Heat stable antigen (CD-24) 	<ul style="list-style-type: none"> • ESL-1 • PSGL-1 • L-selectin



1.2.4.2 Sialyl Lewis^x as a lead for selectin antagonists

The tetrasaccharide sialyl Lewis^x is the minimal carbohydrate epitope recognized by all three selectins [87,88]. Therefore, it serves as a lead structure in selectin antagonist research [89,90]. sLe^x exhibits a relatively low affinity for the selectins (in the mM range) as shown in Table 4 [90-92].

Table 4. Affinity of sLe^x for E-, P- and L-selectin [28].

	E-selectin	P-selectin	L-selectin
K _D [μM]	100-2000	7800	3900
IC ₅₀ [μM]	100-750	520-1300	2300

As for all the natural ligands of selectins, sLe^x exhibits fast association and dissociation constants ($k_{on} \sim 10^4 \text{ M}^{-1} \text{ s}^{-1}$ and $k_{off} \sim 1 \text{ s}^{-1}$) [93].

The essential pharmacophores of sLe^x were determined by studies of systematic variations of functional groups (Figure 8). These are:

- Hydroxyl groups in 3- and 4-position of the fucose moiety [94,95]
- Hydroxyl groups in 4- and 6-position of galactose [96]
- Carboxylic acid of neuraminic acid [95]

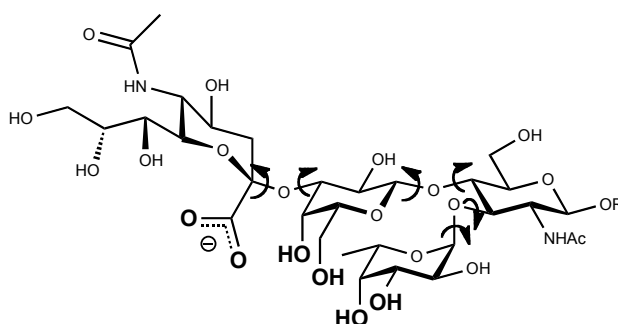


Figure 8. Essential pharmacophores of sLe^x for the binding to E-selectin (in bold).

Several studies showed that the D-GlcNAc moiety is not directly involved in the binding process [97,98]. D-GlcNAc serves as a spacer to optimally position the pharmacophores from L-fucose and the D-galactose for binding.

In order to develop low molecular weight antagonists starting from sLe^x as lead structure, a deeper understanding of the ligand-protein complex is mandatory. Data from NMR spectroscopy, X-ray crystallography and *in-silico* studies provides growing insight into this specific carbohydrate-protein interaction. Dr. D. Schwitzer and Dr. M. Porro gave an overview on this topic in their dissertations [99,100].

Computational studies and NMR experiments agreed in the conformational stability of the core of sLe^x in solution [101-107]. However, the co-existence of two orientations of Neu5Ac in solution is strongly suggested by the presence of NOE's between the proton in the 3-position of galactose and the protons in 3- and 8-position of Neu5Ac [105-107].

Structural information on the bioactive conformation was obtained in the presence of the protein by trNOE-NMR and STD-NMR experiments [108-110]. The pharmacophores of sLe^x in close contact with E-selectin are indicated in Figure 9.

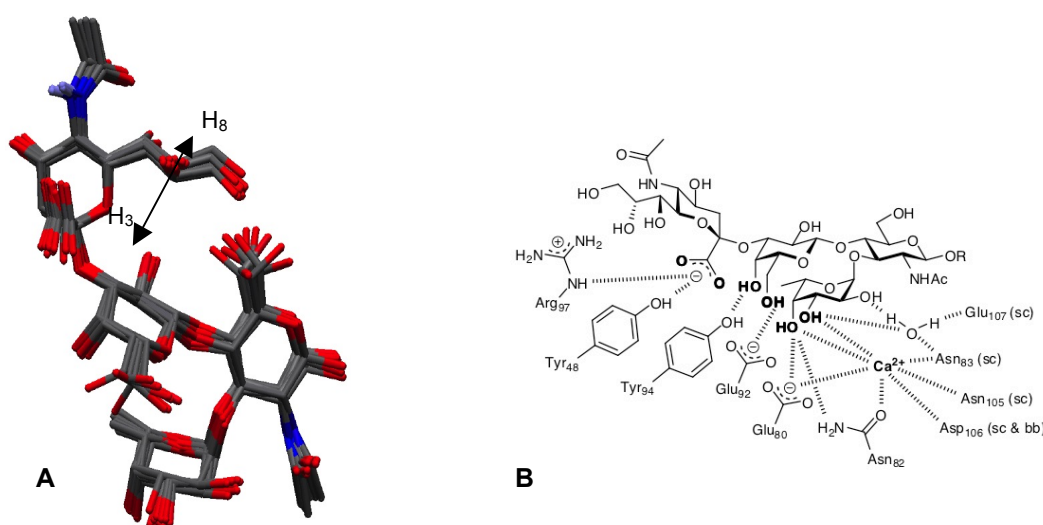


Figure 9. (A) Bioactive conformation of sLe^x from trNOE experiments [108-110]. NOE between proton in the 3-position of D-galactose and the 8-position of Neu5Ac are indicated with arrow. (B) Schematic view of the pharmacophores of sLe^x binding to E-selectin and part of the amino acid involved in the binding (specified under brackets, side chain (sc) or backbone (bb)).

In 2000, Somers *et al.* published X-ray crystallography data of sLe^x in complex with E- and P-selectin based on the crystal structure of the apoprotein published in 1994. These data show the involvement of the hydroxyl in 3- and 4-position of fucose in complexing the calcium ion. In addition, the hydroxyl in the 2-position of fucose binds to Glu₁₀₇ and Asn₈₃ mediated by water molecule. Glu₉₂ and Tyr₉₄ appear to be involved in interactions with hydroxyl groups in the 5- and 6-position of

galactose. The carboxylate of neuraminic acid is involved in a tyrosine supported salt bridge with Arg₉₇ and is the only contact of this moiety with the protein. Finally, the role of the D-GlcNAc moiety as a spacer was finally supported by the X-ray structure (Figure 10).

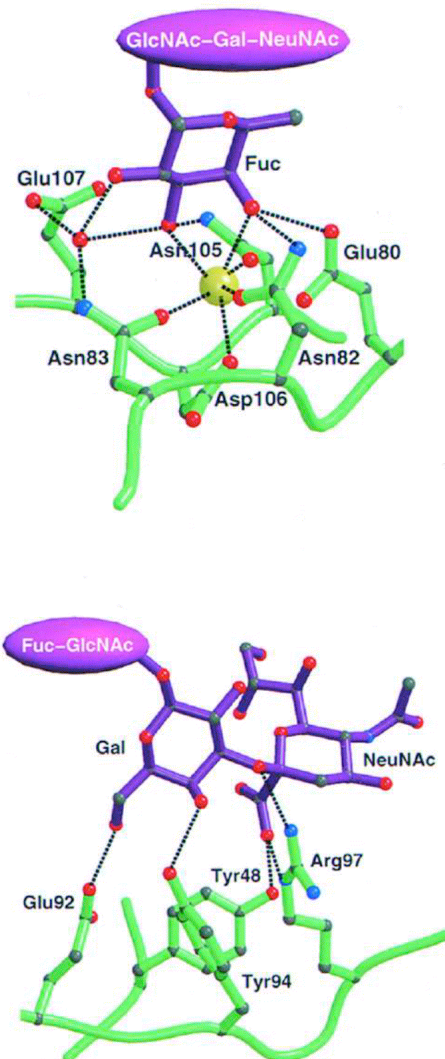


Figure 10. Interaction between sialyl Lewis ^x and E-selectin highlighting the coordination of the calcium by D-fucose (top) and on the interactions from Neu5Ac-D-Gal (bottom) (adapted from Somers *et al.*, 2000).

1.2.4.3 Recent advances in selectin antagonists

An overview of selectin antagonists in preclinical and clinical trials was recently reported by Ernst and Magnani [111]. The numerous glycomimetic, low molecular weight antagonists of the selectins are based on sLe^x and are *de novo* synthesized. An exception is efomycine M (Figure 11), a natural product supposed to bind to the selectins. Efomycine, presented as a potential target in psoriasis treatment, is now in preclinical trials [112]. Nevertheless, a recent publication from Bonin *et al.* suggest a mode of action separate from pan-selectin inhibition [113]. Kaila *et al.* at Wyeth reported in 2005 the activity of quinic acid derivatives as new leads. As a continuity of this work, PSI-697 (Figure 11) was found and is currently in clinical development, although poor IC₅₀s were reported (in the μM range) [114]. As a third example, of special relevance for this thesis, **GMI-1070** (Figure 11) is a promising pan-selectin inhibitor based on sLe^x structure. In march 2009 the successful completion of Phase I clinical trials was announced showing the compounds safety and the positive pharmakinetic evaluation. This compound, developed by GlycoMimetics Inc. Gaithersburg, MD, USA in cooperation with the Institute of Molecular Pharmacy will enter this year in phase II clinical trials.

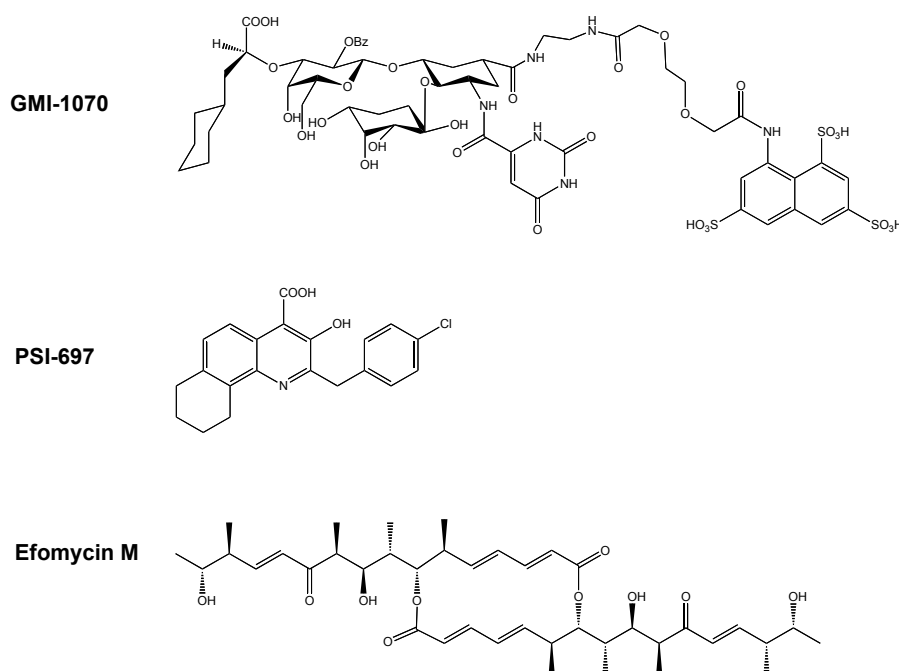


Figure 11. Structure of **GMI-1070**, PSI-687 and efomycine M.

1.3 References

- [1] J.P. Overington, B. Al-Lazikani, L. Hopkins, *Nat. Rev. Drug Discovery* **2006**, 5, 993.
- [2] K.H. Bleicher, H-J. Böhm, K. Müller and A.I. Alanine, *Nat. Rev. Drug Discovery* **2003**, 2, 369.
- [3] M.D. Shotridge, D.S. Hage, G.S. Harbison and R. Powers, *J. Comb. Chem.* **2008**, 6, 948.
- [4] J. DiMasi, R. Hansen, H. Grabowski, *J. Health Econ.* **2003**, 22, 151.
- [5] C. Adams, V. Brantner, *Health Aff. (Millwood)* **2006**, 25, 420.
- [6] A. Smith, *Nat. Rev. Drug Discovery* **2002**, 418, 453.
- [7] S.M. Paul, D.S. Mytelka, C.T. Dunwiddie, C.C. Persinger, B.H. Muos, S.R. Lindborg and A.L. Schacht, *Nat. Rev. Drug Discovery* **2010**, 9, 203.
- [8] P.Gwynne, *Sci. Drug Discov. Biotechnol.* **2007**, 318, 293.
- [9] W. Huber and F. Mueller, *Curr. Pharm. Des.* **2006**, 12, 3999.
- [10] C. Dalvit, *Drug Discovery Today* **2009**, 14, 1051.
- [11] M.A. Cooper, *Nat. Rev. Drug Discovery* **2002**, 1, 515.
- [12] R.L. Rich and D. Myszka, *Anal. Biochem.* **2007**, 361, 1.
- [13] G.C.K. Roberts, *Drug Discovery Today* **2000**, 5, 230.
- [14] D.G. Myszka and R.L. Rich, *Pharm. Sci. Technol. Today* **2000**, 3, 310.
- [15] R.L. Rich and D.G. Myszka, *Drug Discovery Today*, **2004**, 1, 301.
- [16] S.B. Shuker, P.J. Hajduk, R.P. Meadows and S.W. Fesik, *Science*, **1996**, 274,1531.
- [17] J. Klages, M. Coles and H. Kessler, *Mol. Biosyst.* **2006**, 2, 318.
- [18] J.W. Peng, J. Moore and N. Abdul-Manan, *Prog. Nucl. Magn. Reson. Spectrosc.* **2004**, 44, 225.
- [19] M. Pellecchia, D.S. Sem and K. Wüthrich, *Nat. Rev. Drug Discovery* **2002**, 1, 211.
- [20] Y.S. Wand, D. Liu and D.F. Wyss, *Magn. Reson. Chem.* **2004**, 6, 485.
- [21] E. J. Kunkel and E. C. Butcher *Nat. Rev. Immunol.* **2003**, 3, 822
- [22] E.C. Butcher, *Cell* **1991**, 67, 1033.

- [23] M.P. Bevilacqua, J.S. Pober, D.L. Mendrick, R.S. Contran and M.A. Gimbrone Jr., *Proc. Natl. Acad. Sci. USA* **1987**, 84, 9238.
- [24] J.G. Geng, M.P. Bevilacqua, K.L. Moore, T.M. McIntire, S.M. Prescott, J.M. Kim, G.A. Bliss, G. Zimmerman and R.P. McEver, *Nature* **1990**, 343, 757
- [25] R. Hattori, K.K. Hamilton, R.D. Fugate, R.P. Mc Ever and P.J. Sims, *J. Biol. Chem.* **1989**, 264, 7768.
- [26] E.J. Kunkel, J.E. Chomas and K. Ley, *J. Immunol.* **1998**, 82, 30.
- [27] L.J. Picker, R.A. Warnock, A.R. Burns, C. M. Doerschuk, E.L. Berg and E.C. Butcher, *Cell* **1991**, 66, 921.
- [28] C. Kneuer, C. Ehrhardt, M.W. Radomski and U. Bakowsky, *Drug Discovery Today* **2006**, 11, 1034
- [29] A.E. Aplin, A. Howe, S.K. Alahari and R.L. Juliano, *Pharmacological Reviews* **1998**, 50, 197.
- [30] Department of Biomedical Engineering, University of Virginia website
- [31] T. Springer, *Annu. Rev. Physiol.* **1995**, 57, 827.
- [32] M.J. Davies, N. Woolf, P.M. Rowles, J. Pepper, *Br. Heart J.* **1998**, 60, 459.
- [33] T.N. Mayadas, R.C. Johnson H. Rayburn, R.O. Hynes and D.D. Wagner, *Cell*, **1993**, 74, 541.
- [34] M.A. Labow, C.R. Norton, J.M. Rumberger, K.M. Lombard-Gilloly, D.J. Shuster, J. Hubbard, R. Bertko, P.A. Knaak, R.W. Terry, M.L. Harbison et al., *Immunity* **1994**,1, 709.
- [35] T.F. Eder, D. A. Steeber, A. Chen and P. Engel, *FASEB J.* **1995**, 9, 866.
- [36] S.M. Albelda, C.W. Smith and P.A. Ward, *FASEB J.* **1994**, 8, 504.
- [37] R.N. Oston, D.O. Haskard, J.R. Couchier et al., *Am. J. Pathol.* **1992**, 140, 665.
- [38] A.C. van der Wal, P.K. Das, A.J. Tigges et al., *Am. J. Pathol.* **1992**, 141, 1427.
- [39] P.K. Panegyres, R.J. Faull, G.R. Russ et al., *J. Neurol. Neurosurg. Psychiatry* **1992**, 55, 4.
- [40] R. Phreeniwas, S. Koga, M. Karakurum et al., *J. Clin. Invest* **1992**, 90, 2333.
- [41] O. Palluy, L. Morliere, J.C. Gris et al., *Free-Radical. Biol. Med.* **1992**.
- [42] T.A. Drake, J. Cheng, A. Chang et al., *Am. J. Pathol* **1993**, 142, 1458.
- [43] S.N. Georas, M.C. Liu, W. Newman et al., *Am. J. Respir. Cell Mol. Biol.* **1992**, 7, 261.

- [44] R.S. Cotran, M.Jr Gimbrone, M.P. Bevilacqua et al., *J. Exp. Med.* **1986**, 164, 661.
- [45] J.S. Rober, B.L. Bowen, H. Ebling et al., *J. Clin. Invest.* **1993**, 91, 2609.
- [46] W.D. Hanley, M.M. Burdick, K. Konstantopoulos and R. Sackstein, *Canc. Res.* **2005**, 65, 5812.
- [47] U. Jeshke et al., *Anticancer Res.* **2005**, 25, 1615.
- [48] J. Inata et al., *Int. J. Cancer* **2007**, 120, 2643.
- [49] C. Dimitroff et al., *Cancer Res.* **2005**, 65, 5750.
- [50] J.L. Magnani et al., *J. Biol. Chem.* **1982**, 257, 14365.
- [51] D.S. Krause, K. Lazarides, U.H. von Adrian, R.A. van Etten, *Nature Med.* **2006**, 12, 1175.
- [52] L. Borsig, News, *Physiol. Sci.* **2004**, 19, 16
- [53] T. Feizi, *Nature* **1985**, 314, 53.
- [54] A. Varki, R. Kannagi, B.P. Toole, *Essential of Glycobiology*, 2nd Ed. **2009**, chap. 44.
- [55] S. H. Barondes, D. N. W. Cooper, M. A. Gitt and H. Leffler, *J. Biol. Chem.* **1994**, 269, 20807.
- [56] W.M. Gallatin, I.L. Weissman, E.C. Butcher, *Nature* **1983**, 304, 30.
- [57] R.P. McEver, M.N. Martin, *J. Biol. Chem.* **1984**, 259, 9799.
- [58] L.A. Lasky, M.S. Singer, T.A. Yednock, D. Dowbenko, C. Fennie, H. Rodriguez, T. NguyenS. Stachel, S.D. Rosen, *Cell* **1989**, 56, 1045.
- [59] M. P. Bevilacqua, S. Stengelin, M. A. Gimbrone Jr., B. Seed, *Science* **1989**, 243, 1160.
- [60] G.I. Johnston, A. Kurosky, R.P. McEver, *J. Biol. Chem.* **1989**, 264, 1816.
- [61] D. V. Erbe, B. A. Wolitzky, L. G. Presta, C. R. Norton, R. J. Ramos, D. K. Burns, J. M. Rumberger, B. N. N. Rao, C. Foxall *et al.*, *J. Cell Biol.* **1992**, 119, 215.
- [62] J.K. Welply, J.L. Keene, J.J. Schmuke, S.C. Howard, *BBA*, **1994**, 1197, 215-226.
- [63] D.V. Erbe, B.A. Wolitzky, L.G. Presta, C.R. Norton, R.J. Ramos, D.K. Burns, J.M. Rumberger, B.N.N. Rao, C. Foxall *et al.*, *J. Cell Biol.* **1992**, 119, 215.
- [64] R. Piggot, L. A. Needham, R. M. Edwards, C. Walker, C. Power, *J. Immunol.* **1991**, 147, 130.
- [65] G.S. Kansas, K.B. Saunders, K. Ley, A. Zarkzewich, R. M. Gibson, B. C. Furie

- and T. F. Tedder, *J. Cell. Biol.* **1994**, *124*, 609.
- [66] T. P. Patel, M. U. Nollert, R. P. McEver, *J. Cell. Biol.* **1995**, *131*, 1893.
- [67] S. H. Li, D. K. Burns, J. M. Rumberger, D. H. Presky, V. L. Wilkinson, M. Anostario, B. A. Wolitzky, C. R. Norton, P. C. Familletti, K. J. Kim, A. L. Goldstein, D. S. Cox and K. S. Huang, *J. Biol. Chem.* **1994**, *269*, 4431.
- [68] C. Laudanna, G. Constantin, P. Baron, E. Scarpini, G. Scarlano, G. Caprini, C. Dehecchi, F. Rossi, M. A. Cassatella and G. Berton, *J. Biol. Chem.* **1994**, *269*, 4021
- [69] S. A. Mousa, *Drugs Fut.* **1996**, *21*, 283.
- [70] S. A. Mousa, D. A. Cheresch, *Drug Discovery Today* **1997**, *2*, 187.
- [71] D. B. Cines, E. S. Pollak, J. Loscalzo C. A. Buck, G. A. Zimmerman, R. P. McEver, J. S. Pober, T. M. Wick, B. A. Konkle, B. S. Schwartz, E. S. Barnathan, K. R. McCrae, B. A. Hug, A.-M. Schmidt and D. M. Stern, *Blood* **1998**, *91*, 3527.
- [72] G. S. Kansas, *Blood* **1996**, *88*, 3259-3287.
- [73] M. Brustein, G. Kraal, R. Mebius, S. Watson, *J. Exp. Med.* **1992**, *176*, 1415.
- [74] S. D. Rosen, A. Kikuta, *Blood* **1994**, *84*, 3766.
- [75] S. Hemmerich, C. R. Bertozzi, H. Leffler and S. D. Rosen, *Biochemistry* **1994**, *33*, 4820.
- [76] S. Hemmerich, S. D. Rosen, *Biochemistry* **1994**, *33*, 4830.
- [77] Y. Imai, L. A. Lasky, S. D. Rosen, *Nature* **1993**, *361*, 555.
- [78] S. R. Watson, Glycoprotein ligands for L-selectins. In: *The Selectins*, edited by D. Vestweber. Amsterdam: Harwood, **1997**, vol. 3, 179.
- [79] D. Vestweber, J. E. Blanks, *Physiol. Rev.* **1999**, *79*, 181.
- [80] K. L. Moore, N. L. Stultz, S. Diaz, D. L. Smith, R. D. Cummings, A. Varki, R. P. McEver, *J. Cell Biol.* **1992**, *118*, 445.
- [81] D. Sako, K. M. Comess, K. M. Barone, R. T. Camphausen, D. A. Cumming and G. Shaw, *Cell* **1995**, *83*, 323.
- [82] T. Pouyani, B. Seed, *Cell* **1995**, *83*, 333.
- [83] A. Levinovitz, J. Mühlhoff, S. Isenmann, D. Vestweber, *J. Cell. Biol.* **1993**, *121*, 449.
- [84] M. Lenter, A. Levinovitz, S. Isenmann, D. Vestweber, *J. Cell. Biol.* **1994**, *125*, 471.
- [85] W. M. Jones, G. M. Watts, M. K. Robinson, D. Vestweber, M. A. Jutila, *J.*

Immunol. **1997**, *159*, 3574.

[86] C. Kneuer, C. Ehrhardt, M. W. Radomski, U. Badowsky, *Drug Discovery Today* **2006**, *11*, 1034.

[87] M.L. Philips, E. Nudelman, F.C.A. Gaeta, M. Perez, A.K. Singhal, S.I. Hakomori, J.C. Paulson, *Science* **1990**, *250*, 1130.

[88] E.L. Berg, M.K. Robinson, O. Mansson, E.C. Butcher, J.L. Magnani, *J. Biol. Chem.* **1991**, *266*, 14869.

[89] C.R. Bertozzi, *Chem. Biol.* **1995**, *2*, 703.

[90] J.H. Musser, M.B. Anderson, D.E. Levy, *Curr. Pharm. Des.* **1995**, *1*, 221.

[91] H. Sagara, C. Ra, T. Okada, S. Shinohara, T. Fukuda, K. Okumura, S. Makino, *Int. Arch. Allergy Immunol.* **1996**, *111*, 32.

[92] I.Y. Park, D.S. Lee, M.H. Song, W. Kim, J.M. Wong, *Transplant. Proc.* **1998**, *30*, 2927.

[93] M. K. Wild, M.-C. Huang, U. Schulze-Horsel, P. A. van der Merwe, D. Vestweber, *J. Biol. Chem.* **2001**, *276*, 31602.

[94] J. Y. Ramphal, Z. L. Zheng, C. Perez, L. E. Walker, S. A. DeFrees, F. A. Gaeta, *J. Med. Chem.* **1994**, *37*, 3459.

[95] B. K. Brandley, M. Kiso, S. Abbas, P. Nikrad, O. Srivasatava, C. Foxall, Y. Oda, A. Hasegawa, *Glycobiology* **1993**, *3*, 633.

[96] W. Stahl, U. Sprengard, G. Kretzschmar, H. Kunz, *Angew. Chem. Int. Ed. Engl.* **1994**, *22*, 2096.

[96] S.A. DeFrees, F.A. Gaeta, Y.C. Lin, Y. Ichikawa, C.-H. Wong, *J. Am. Chem. Soc.* **1993**, *115*, 7549.

[98] Y. Hiramatsu, H. Tsujishita, H. Kondo, *J. Med. Chem.* **1996**, *39*, 45.

[99] M. Porro, dissertation, University of Basel, **2006**.

[100] D. Schwitzer, dissertation, University of Basel, **2007**.

[101] R. M. Cooke, R. S. Hale, S. G. Lister, G. Shah, M. P. Weir, *Biochem. Biophys. Res. Commun.* **1994**, *33*, 10591.

[102] G. E. Ball, R. A. O'Neill, J. E. Schultz, J. B. Lowe, B. W. Weston, J. O. Nagy, E. G. Brown, C. J. Hobbs, M. D. Bednarski, *J. Am. Chem. Soc.* **1992**, *114*, 5449.

[103] R. Harris, G. R. Kiddle, R. A. Field, M. J. Milton, B. Ernst, J. L. Magnani, S.W. Homans, *J. Am. Chem. Soc.* **1999**, *121*, 2546.

- [104] K. Veluraja, C. J. Margulis, *J. of Biomol. Struct. & Dynamics* **2005**, 23, 101.
- [105] C.-Y. Lin, C. W. Hummel, D.-H. Huang, Y. Ishikawa, K. C. Nicolaou, C.-H. Wong, *J. Am. Chem. Soc.* **1992**, 114, 5452.
- [106] L. Poppe, G. S. Brown, J. S. Philo, P. V. Nikrad, B. H. Shah, *J. Am. Chem. Soc.* **1997**, 119, 1727.
- [107] Y. Ichikawa, Y. C. Lin, D. P. Dumas, G. J. Shen, E. Garcia-Junceda, M. A. Williams, R. Bayer, C. Ketcham, L. E. Walker, J. Paulson, C. H. Wong, *J. Am. Chem. Soc.* **1992**, 114, 9283.
- [108] K. Scheffler, B. Ernst, A. Katopodis, J. L. Magnani, W. T. Wang, R. Weisemann, T. Peters, *Ang. Chem. Int. Ed.* **1995**, 34, 1841.
- [109] K. Scheffler, J. R. Brisson, R. Weisemann, J. L. Magnani, W. T. Wong, B. Ernst, T. Peters, *J. Biomol. NMR* **1997**, 9, 423.
- [110] M. Rinnbauer, B. Ernst, B. Wagner, J. Magnani, A.J. Benie, T. Peters, *Glycobiology* **2003**, 13, 435.
- [111] B. Ernst and L. Magnani, *Nat. Rev. Drug Discovery* **2009**, 8, 661.
- [112] M.P. Schon et al. *Nature Medicine*, **2002**, 8, 366.
- [113] A. von Bodin et al. *Nature Med.* **2006**, 12, 873.
- [114] Kaila, N. et al. *J. Med. Chem.* **2007**, 50, 40.

2. Aim of the thesis

Selectins are a family of cell adhesion molecules involved in the inflammatory cascade, *i.e.* in the interaction of leukocytes with the endothelium. As a result, extravasation of leukocytes from the circulation to the site of inflammation is observed. Excessive extravasation of leukocytes as observed in inflammatory diseases is problematic. The modulation of leukocyte recruitment by interfering with cell tethering is therefore of therapeutical interest and selectins, involved in the early stage of the process, are a possible target. At the IMP, the selectin project is aimed at the synthesis of carbohydrate mimics antagonizing selectins.

Sialyl Lewis^x (sLe^x), the minimal carbohydrate epitope of the physiological E-selectin ligand, has served as a starting point for the design of more potent selectin antagonists. In the literature, sLe^x and selectin ligands in general have been reported with various affinities as a result of the wide variety of biological *in vitro* and *in vivo* assays applied. As a result, the reported values display a large variance and make the comparison of antagonists synthesized almost impossible. Therefore, the necessity of an assay that delivers accurate affinity data was fundamental. SPR biosensor technology is an excellent method for that purpose. In addition to evaluating the potency of the antagonists, kinetic rate constants and thermodynamic parameters can be assessed leading to a more thorough understanding of the binding event. One aim of the thesis was to implement SPR technology into the ligand optimization process of E-selectin antagonists.

In parallel, ligand-based NMR methods were planned for a further understanding of the physical basis responsible for the observed affinity. A particular focus was binding epitope studies by STD-NMR with the first generation of E-selectin antagonists synthesized at the IMP.

By Biacore and NMR characterization of selectin/antagonist interactions, guidance for the design of the second generation of E-selectin ligands should be established.

3. Affinity and kinetic evaluation of the first generation of E-selectin antagonists using Biacore Technology

3.1 Introduction

3.1.1 Locked conformations: a successful strategy for development of selectin antagonists

The optimization of ligands in a spatial pre-organization corresponding to the bioactive conformation is a well-known concept in medicinal chemistry. By reducing the entropic cost required for adopting the appropriate binding conformation, a higher binding affinity can be obtained. In 1993, Carver described a new approach that he called “site-directed presentation”. Based on the reduction of the flexibility of oligosaccharides, this mechanism should improve the affinity and the specificity towards their target [1]. Success of this approach was reported in many publications, including applications to HIV proteases inhibitors [2-5], as well as the stabilization of the bioactive conformation of a trisaccharide mimicking the LPS of bacteria to improve the binding of an antibody [3,4]. More recently, in 2006, Bastida *et al.* reported a new strategy for the design of aminoglycosides to overcome bacterial resistance by using conformationally locked compounds [6].

The development of selectin antagonists in our research group is based on the design of sLe^x mimics with preorganized pharmacophores [7]. In 1997, Kolb and Ernst reported the existence of a correlation between the affinity of E-selectin to sLe^x and the preferential conformation, predicted *in-silico* [8,9]. Later on, an agreement between computational predictions and the bioactive conformation determined by trNOE NMR was observed [10].

Following the idea of a pre-organization of the antagonists in their bioactive conformation, series of sLe^x mimics were synthesized with different strategies by Dr. D. Schwitzer and Dr. A. Titz during their Ph.D. studies [11,12]. Therefore, a compensation of the low enthalpic contributions would be obtained by reduction of the entropy costs [13]. In this chapter of the present thesis the development of a Biacore assay for the characterization of a first generation of more potent E-selectin antagonists is shown. Dr. Daniel Schwitzer synthesized the majority of these ligands

by focusing on minimizing the entropic costs upon binding by modifying substituents of the lead compound **BW-69669** with the idea of a stabilization of the bioactive conformation. The Biacore assay developed allowed a direct evaluation of the improved potencies of the antagonists, in a real-time measurement format under flow conditions.

3.1.2 Biacore Technology

3.1.2.1 Surface plasmon resonance (SPR) phenomenon

The Biacore system uses a detection principle based on the phenomenon of surface plasmon resonance. Sensor chip chemistry and an integrated flow system allow real-time detection of molecular interactions on the sensor surface. Surface plasmon resonance arises as a result of an electron charge density wave and is based on total internal reflexion (TIR), an evanescence electric field (E) and surface plasmon waves. A light beam that propagates through two non-absorbing media of different refractive indices will only be totally reflected at the interface at a critical incidence angle (θ). When this angle is exceeded, the energy of the refracted light beam is kept constant but an electric field intensity called evanescence wave (E) leaks into the medium of lower refractive index. E decreases exponentially with the distance to the surface. The presence of a thin metal film (usually a non-magnetic metal like gold) at the interface induces the excitation of surface plasmons when E penetrates this layer. Surface plasmons are waves of oscillating surface charge densities in a conducting metal. Resonance occurs for a specific incidence angle and leads to a drop in the intensity of the reflected light [14,15].

In an experimental setup, resonance is only dependent of the angle of the incident light and the refractive index of the second medium. Biosensors monitor changes in refractive index of the solution very near to the surface by adjusting the incident light angle until resonance is detectable [16-18]. Such a change is converted into a response signal measured in resonance units (RU) that corresponds to a shift in the resonance angle of 10^{-4} degree [17]. The measurement of a biomolecular interaction by SPR is based on the fact that binding of molecules to the surface alters the refractive index. Indeed, the mass of the molecules directly influences the

refractive index (1 RU = 1pg/mm² in the case of proteins) [18]. The sensitivity of the detection depends on:

- the type of ligands,
- the distance from the surface (due to the exponential decay of E),
- effects occurring around the interface (e.g. electrostatic attraction, conformational changes).

3.1.2.2 Typical Biacore experiment

In a typical Biacore experiment, one binding partner is immobilized on the sensor chip (name as target) and the other is injected (name as ligand or analyte) (Figure 1).

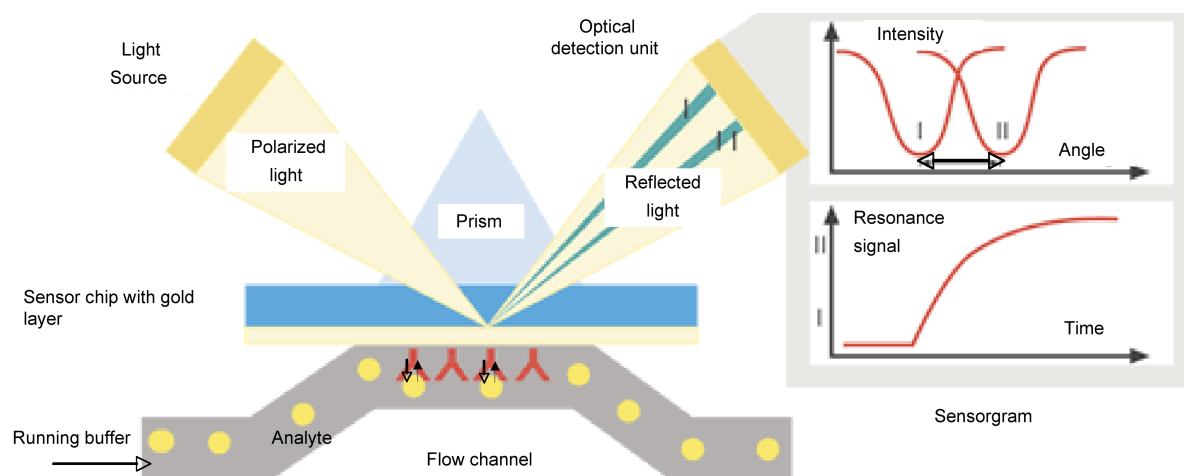


Figure 1. Schematic overview of the experimental set-up of a Biacore 3000. The SPR-based detection mode (schematized on the right) allows to monitor the binding of an analyte to the target in real-time.

Different types of molecules can be immobilized on the biosensor surface (oligosaccharides, nucleotides, proteins). In the following, I will focus on an assay involving a protein as a target immobilized on a CM5 sensorchip. The CM5 is the most frequently used, commercially available biosensor chip. In such a surface, a protecting polymer made from carboxymethyl dextran chains covers a gold layer in order to limit non-specific binding to the gold surface and to facilitate immobilization.

The immobilization of a protein is a crucial step in a Biacore assay, because the natural folding and the binding affinity must be retained. Two parameters of the immobilization have to be considered: the orientation (random or site-specific) and the type of linkage (covalent or non-covalent) [19]. Random and covalent coupling usually generates stable surfaces with high density. In the covalent coupling approach, functional groups of the target are utilized to form covalent bonds (e.g. amine, hydroxy, thiol). The randomization of the attachment, due to multiple immobilization sites, might result in a loss of activity due to involvement of amino acids in or close to the binding site, conformational changes and/or steric hindrance.

Amine coupling is the most frequently used immobilization technique for proteins due to the high availability of accessible primary amine groups on protein surfaces (lysine residues and N-terminus) (Figure 2A). In a first step, the carboxyl groups of the dextran matrix are activated by *N*-hydroxysuccinimide (NHS) / 1-ethyl-3-(3-dimethylaminopropyl) carbodiimide (EDC), leading to reactive esters. Then, these reactive esters react with accessible primary amino groups of the protein resulting in a covalent coupling. The efficiency of the process is increased by working at a pH just below the pI of the protein inducing an optimum surface attraction. At that pH, only small fraction of the primary amines are deprotonated. The protonated amines cannot react with the activated esters of the dextran matrix but interact with the negative charges of the matrix. Only the deprotonated amino groups are available for the covalent coupling [20].

Thiol coupling could be used for a direct immobilization of protein with a more defined orientation due to the lower abundance of cysteine residues in proteins compared to amino groups. Finally, aldehyde coupling is used in some studies, since it offers a possibility for direct immobilization. These groups can be natively present on carbohydrate residues of the protein or can be artificially introduced. Therefore, this coupling mode enables a better-oriented immobilization.

Another approach for the immobilization is the capture approach based on a specific biomolecular interaction between the target and a high affinity capturing molecule covalently immobilized on the surface (Figure 2B). This approach leads to a site-oriented immobilization. Three major classes of capture can be described:

antibody-antigens, protein-natural ligand and capture *via* introduction of an affinity tag. The disadvantage of these methods is the non-covalent character of the immobilization that can lead to instability of the surface. Indeed, bleeding of the surface is frequently observed and can significantly influence the quality of the data, especially in the case of low molecular weight ligand characterization with low signal intensities. One non-negligible advantage is the possibility of regeneration of the surface, which reduces the amount of sensor chips needed and ensure a good quality of the target throughout the studies. However, as it will be shown in this work, the regeneration of capture surface is not always possible.

To overcome the instability of capture surfaces, the use of a crosslink capture method was suggested (Figure 2C). In this approach, the target is covalently linked to the intermediate of immobilization [21].

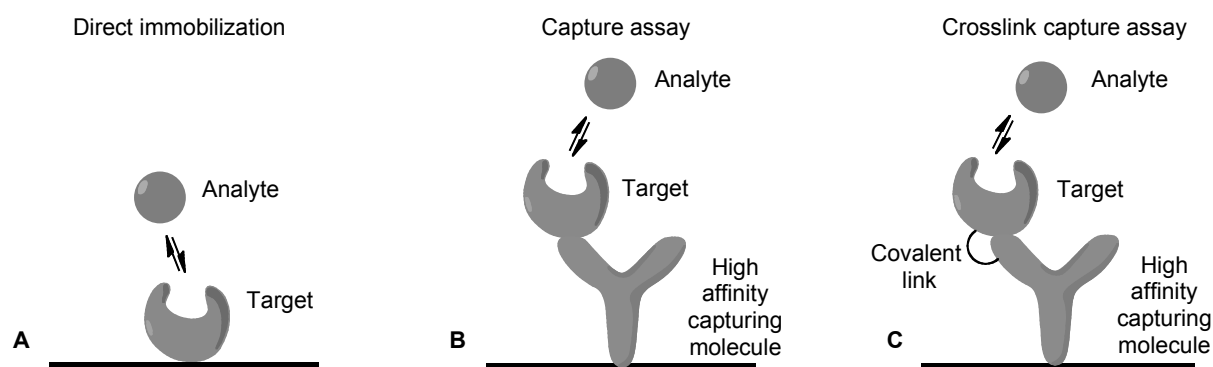


Figure 2. Different possibilities for target immobilization. **A:** Direct immobilization (*e.g.* *via* amine coupling); **B:** capture assay *via* a high-affinity capturing molecule; **C:** crosslink capture assay.

Frequently, in drug discovery large molecules (*e.g.* proteins) are immobilized and small ligands are screened resulting in low signal intensity. Different approaches can ameliorate insufficient signal intensities, such as attaching the small ligand on the surface and injecting the large molecule [22] or performing a competitive assay [23]. Unfortunately, both alternatives contain disadvantages *e.g.* the higher protein consumption. Non-specific binding cannot be avoided in either of the assay formats previously described. In addition, the problem of mass transport is a factor that complicates the measurement [24,25]. This phenomenon might occur, when the interaction between ligand and target is comparable or faster than the diffusion of the

ligand from the bulk solvent to the surface. Increasing on the flow rate and reducing the surface density can reduce mass transport effects.

In summary, each immobilization strategy presents advantages and disadvantages. The Biacore technology offers a broad range of alternative immobilization procedures and for every target the most appropriate should be carefully selected.

As described above, when a ligand is injected onto the surface, a shift in the resonance angle is monitored in real time. The plot of the signal *versus* time is called a sensorgram and the different phases of a binding event can be visualized on it: association, steady-state, dissociation and regeneration (Figure 3A-D). The steady state is reached when associating and dissociating molecules are in equilibrium.

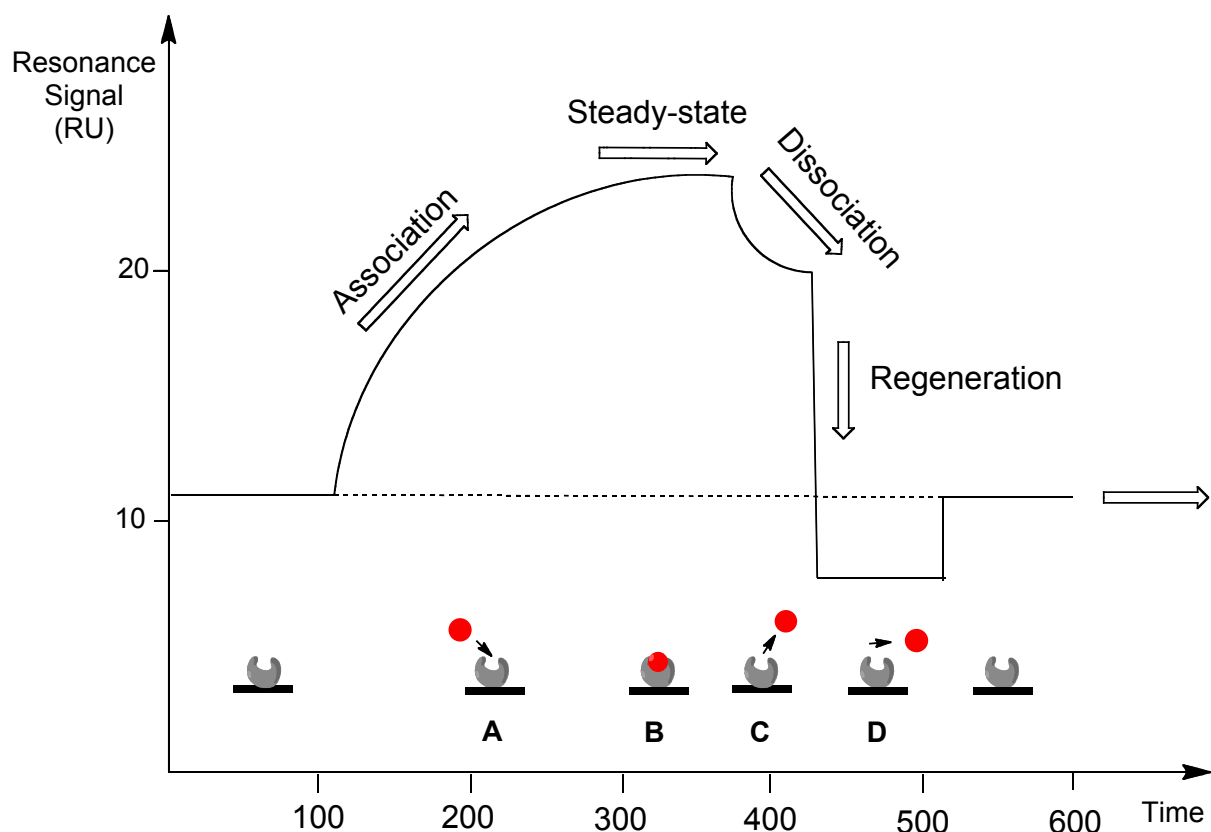
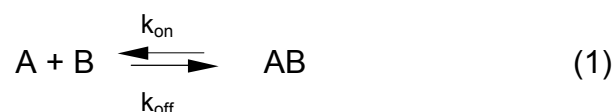


Figure 3. Typical sensorgram obtained for a standard interaction measurement. The different phases of the binding are indicated: the injected ligand starts to bind to the target (**A**) until reaching a steady-state (**B**). When the injection of the ligand is interrupted and replaced by running buffer, the dissociation of the ligand becomes visible (**C**). The regeneration step (**D**) is needed only if remaining ligand has to be removed from the surface.

3.1.2.3 Kinetic and affinity evaluation

Proper data evaluation and interpretation is critical, especially when measuring low molecular weight compounds like carbohydrates. There is a risk of fitting data that deviates from an expected model (e.g. due to poor experimental design, low purity of ligands and/or target heterogeneity) with a more complex model [26,27]. Therefore, assay design should be kept easy and data fit with a simple 1:1 binding model should be the method of choice in a first attempt [Eq. (1)].



The 1:1 binding model can be extended to 1:2 binding site model and, if suspected or reported, a mass transfer coefficient might be introduced. A global analysis approach is implemented in the Scrubber software package and provides accurate and robust results by fitting simultaneously the association and dissociation phases of the entire data set [28]. The equilibrium binding constant is accessible from two approaches:

- The kinetic rate constant ratio [Eq. (2)]

$$K_D = \frac{k_{\text{off}}}{k_{\text{on}}} [M] \quad \text{and} \quad K_A = \frac{k_{\text{on}}}{k_{\text{off}}} [M^{-1}] \quad (2)$$

- Steady state signals at different concentrations using the saturation binding plot [Eq. (3)]

$$R_{\text{eq}} = \frac{K_A \cdot C \cdot R_{\text{max}}}{1 + (K_A \cdot C \cdot n)} [RU] \quad (3)$$

R_{eq} : equilibrium response signal, R_{max} : maximum response, C : concentration, K_A : equilibrium association constant, n : steric interference factor

The possibility to assess specificity, affinity and kinetics is of particular interest, placing SPR as an indispensable tool in drug discovery. In the traditional drug

discovery process, high throughput screening (HTS) is used for the identification of new lead compounds. To be identified as a hit, molecules must preferably fulfill criteria like specificity, low affinity, low molecular weight (LMW), low molecular complexity [29], small number of rings [30], small number of rotatable bonds [30], and low polarity [31]. After validation, the optimization of the pharmacokinetic and pharmacodynamic profile is performed *via* structure-based drug design in medicinal chemistry [32]. In the two steps previously described, compounds are rated by an *in vitro* evaluation of their affinity for the target (K_D or IC_{50}). This is not representative of an *in vivo* environment where the kinetics of the interaction ought to play an important role. Having early information on the kinetics of the lead molecule could reduce attrition rates in later stages of the drug development process, which is economically highly desired. Indeed, a long residence time of the drug-target binary complex characterized by the dissociation half-life ($t_{1/2}$) is reported as beneficial for pharmacological profiles [33]. Prolonged drug-target dissociation times enable dosage reduction, which is an effective gain for drug discovery. In a Biacore analysis, molecules can be rated according to their affinity and kinetic parameters, both accessible from the sensorgrams. Therefore, compounds exhibiting an identical affinity (K_D) can show completely different binding kinetics. The high degree of reproducibility and the close agreement with other techniques such as analytical ultracentrifugation (AUC), stop-flow fluorescence (SFF) and isothermal titration calorimetry (ITC) for kinetic as well as for thermodynamic parameter are the main reason for the important role Biacore plays in the drug discovery process [34,35]. Nevertheless, it has to be mentioned that immobilization of a target is a critical and delicate step that has to be designed properly for each assay. A disadvantage of working with immobilized target is the risk of restriction in rotational freedom and accessibility of the binding site that can influence affinity and kinetics [33].

3.1.3 Structure of E-selectin/IgG and LecEGF_CR2 constructs

E-selectin/IgG was produced in Chinese hamster ovary (CHO-K1) cells kindly provided by Dr. Frank Kolbinger from Novartis (Basel, Switzerland). The E-selectin construct consists of the C-type lectin domain (Lec domain), the epidermal growth factor (EGF) domain and six consensus repeats (CRs) of human selectin fused to a

human IgG1 (Fc part) tail (Figure 4A and B). The fused Fc region is part of the human immunoglobulin G type 1. The human immunoglobulin G contains two light (L) and two heavy chains (H). Each heavy chain is composed of four units: one variable (V_H) and three constant (C_{H1} , C_{H2} and C_{H3}). A hinge region exists between C_{H1} and C_{H2} . This flexible area contains the cleavage site of papain (Figure 4A). E-selectin/IgG contains the hinge region, C_{H2} and C_{H3} domains (Figure 4B). The theoretical molecular weight of the chimeric protein is 86.7 kDa. Because of a high degree of glycosylation, the observed molecular weight was evaluated to be 148 kDa.

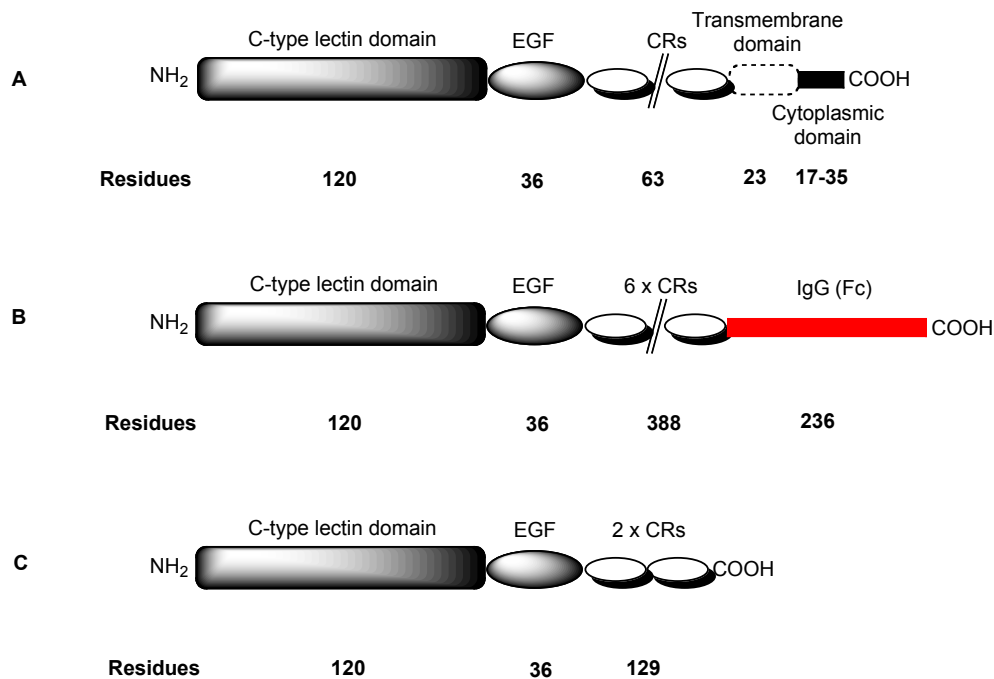


Figure 4: Structure of wild-type selectin (**A**), E-selectin/IgG construct (**B**) and LecEGF_CR2 construct (**C**) produced in CHO-K1 cells.

The LecEGF_CR2 construct (Figure 4C and 5C) was also produced in CHO-K1 cells. Cell transformation, culture and LecEGF_CR2 purification were done in house by Roland Preston. LecEGF_CR2 construct consist of the lectin domain followed by the EGF domain and two CRs. The theoretical molecular weight of the chimera protein is 31.3 kDa. Because of a high degree of glycosylation, the observed molecular weight was evaluated to 70 kDa by SDS-PAGE electrophoresis under denaturated conditions.

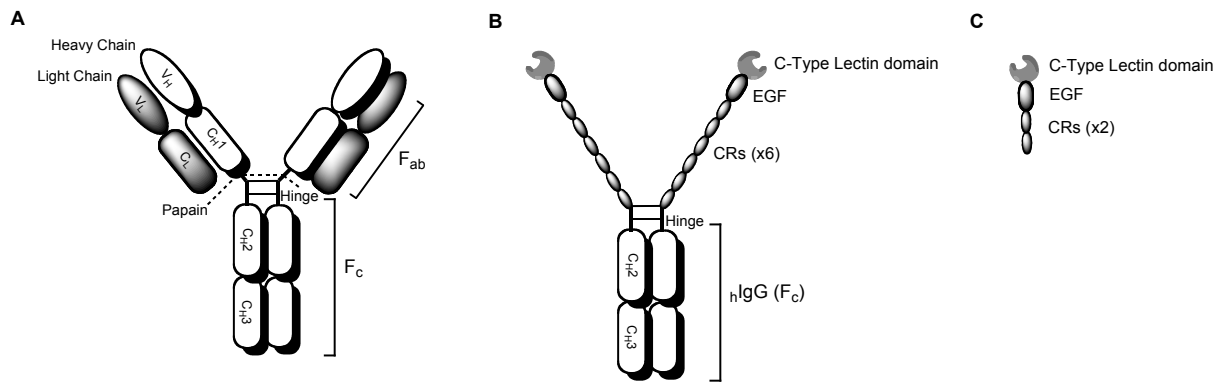


Figure 5: Representative structure of human immunoglobulin G (A), E-selectin/IgG (B) and LecEGF_CR2 construct (C).

3.2 Materials and Methods

For all ligands measured, the chemical structure can be found in Appendix III.

3.2.1 Biacore

Instrumentation

Biomolecular interaction analyses by surface plasmon resonance (SPR) were performed on a Biacore® 3000 system (GE Healthcare, Upsalaa, Sweden). All vials, caps and other consumables were purchased by GE Healthcare. Research grade CM5 sensor chips were used in all analyses (GE Healthcare, Freiburg, Germany). *Desorb* and *sanitize* procedures were regularly performed in accordance to manufacturer recommendations as well as an annual check by a service technician.

Reagents

Immobilization buffers (10 mM sodium acetate at pH values of 4.0, 4.5, 5.0 and 5.5), BIAdisinfecant solutions, normalizing solutions, BIAdesorb solutions and amine coupling kit including ready-to-use EDC, NHS and ethanolamine were purchased from GE Healthcare.

HBS-P buffer (10 mM HEPES, 150 mM NaCl, 0.005% polysorbate 20 (v/v), pH 7.4) ready-to-use was purchased from GE Healthcare and used as the running buffer in all the immobilization procedures. For the interaction analyses, 5% DMSO (v/v) (D8418, Sigma-Aldrich Chemie, Steinheim, Germany) and 20 mM calcium chloride (C3306, Sigma-Aldrich Chemie, Steinheim, Germany) were added to HBS-P buffer. This running buffer was filtrated (using nitrocellulose membranes with a pore size of 0.44 µm) before adding DMSO and degazed [ultrasonic bath for 10 min under reduced pressure (50 mbar)].

Software

Data were processed with Scrubber-2.0a (BioLogic Software Pty Ltd., Campbell, Australia). Equilibrium binding constants were determined using a simple steady-state affinity 1:1 binding model. Kinetic data were also fit with Scrubber-2.0a. Double referencing was applied to correct bulk effects and other systematic artifacts (subtraction of reference surface and blank injection) [36].

3.2.2 Expression and purification of E-selectin/IgG

CHO-K1 cells were transformed with the cloned gene of E-selectin/IgG (Appendix I) in the laboratory of Dr. Frank Kolbinger from Novartis (Basel, Switzerland) [37,38]. Cell culture and purification of E-selectin/IgG were done in-house by Katrin Lemme and Dr. Said Rabbani. Cells were cultivated at 37 °C with 5 % CO₂ and 80 – 90% humidity in TC-Flask Nunclon™ Δ Surface (Nunc™, Rochester, NY). The culture medium was Ham's Nutrient Mixture F-12 with L-glutamine (GIBCO® Invitrogen, Switzerland) supplemented with Fetal Calf Serum (GIBCO® Invitrogen, Switzerland) 10% (v/v), Penicillin 50 000 U (10 000 U/ml Sigma-Aldrich, Switzerland) and Streptomycin (10 mg/ml Sigma-Aldrich, Switzerland) 50 mg. The medium from CHO-K1 cell culture containing the secreted E-selectin/IgG was collected weekly and filtrated through a 0.45 µm sterile filter. The protein was purified in two steps by Fast Protein Liquid Chromatography (FPLC-apparatus Biologic-HR from Bio-Rad) at 4 °C. The first affinity chromatography was performed with a protein A column (HiTrap™ protein A HP from GE Healthcare, Switzerland) following standard procedure from the manufacturer [39]. In a second purification step, the monoclonal anti-E-selectin blocking antibody 7A9 was used as a ligand in the stationary phase. This antibody was expressed in B lymphocyte hybridoma cells (HB-10135™, ATCC®, Otsuka Pharmaceutical Co., Japan) and purified at the IMP by Dr. Jing Yu [40]. The 7A9 was coupled to cyanogen bromide activated sepharose (Cyanogen bromide-activated-Sepharose® 4B, Sigma Aldrich, Buchs, Switzerland) according to the manufacturer's protocol [41]. After elution, the pH was adjusted to pH 7 with 2.5 M Tris buffer and cooled on ice. For both chromatography, proteins

were detected at 280 nm and the progress was controlled by Biologic HR software (version 2.10, Bio-Rad). The eluted E-selectin/IgG was concentrated using centrifugal filter devices (Amicon® Ultra-4, 10k molecular weight cut-off from Millipore Corporation, Billerica, MA, USA) at 6'000 rpm at 4 °C.

SDS-PAGE and Coomassie Brilliant Blue Staining were used to check the purity of the E-selectin/IgG. Western-blot analysis for a specific detection of E-selectin/IgG was also performed [42-44]. The concentration of E-selectin/IgG was determined by Bradford Protein Assay (BPA) [45] and/or High Pressure Liquid Chromatography (HPLC) [46]. The HPLC measurement was performed on an HPLC system Model 2695 (Waters Alliance, Milford, MA) employing a 100 x 2 mm column packed with POROS R1/10 (Dr. Maisch HPLC, Morvay Analytic GmbH, Basel, Switzerland). The column was kept at 60 °C. Eluant A was water containing 0.1% TFA. Eluant B was a 1:9 mixture of water:acetonitrile containing 0.09% TFA. A gradient from 20% B to 90% B was run for 20 min at a flow rate of 0.2 ml/min. UV detection was performed at 214 nm and the progress was controlled using Empower Pro software.

Figure 6A shows a single band below 150 kDa on the SDS-PAGE. The Western-blot analysis (Figure 6B) confirmed that the protein isolated was E-selectin/IgG.

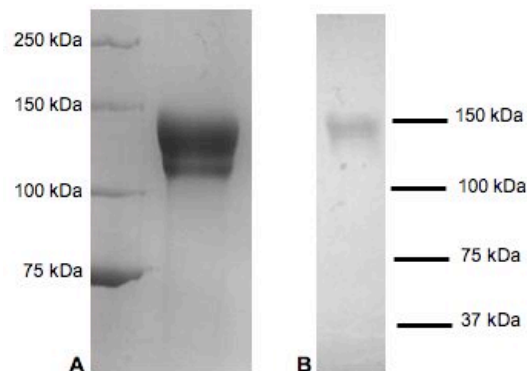


Figure 6: SDS-PAGE (A) and Western-blot (B) of E-selectin/IgG after purification.

3.2.3 Expression and purification of LecEGF_CR2 construct

CHO-K1 cells were transformed with the cloned gene for the LecEGF_CR2 construct (Appendix II). Cloning, expression and purification of LecEGF_CR2 construct was done in-house by Roland Preston [44]. The methods to produce this protein were similar to those previously described for E-selectin/IgG construct (see section 3.2.2). In contrast to the purification procedure used for the E-selectin/IgG construct, only a one-step affinity chromatography on a 7A9 antibody substituted column was performed for purification.

3.2.4 Direct amine coupling of E-selectin/IgG

pH scouting

A pH scouting was performed in order to evaluate the pH dependence for an optimal immobilization of E-selectin/IgG onto the biosensor surface. E-selectin/IgG was diluted to a concentration of 40 µg/ml with different acetate buffers (10 mM, pH 4.0, 4.5, 5.0 and 5.5) or HBS-N buffer (10 mM HEPES, 150 mM NaCl, pH 7.4) purchased from GE Healthcare. These solutions were sequentially injected over a CM5 sensor chip for 3 min at a flow rate of 10 µl/min. A 50 mM NaOH solution was injected for 30 sec at a flow rate of 20 µl/min in order to wash the surface between each sample injection. An optimal attraction of E-selectin/IgG to the surface was observed at pH 5.0.

Immobilization procedure

A preconditioning of the surface was achieved prior to usage by injecting successively 20 µl of 50 mM NaOH, 10 mM HCl, 0.1% SDS and 100 mM H₃PO₄ at a flow rate of 50 µl/min. The cycle of injections was repeated twice. After preconditioning, the sensor chip was used within the next four hours for the immobilization.

HBS-P buffer was used as running buffer for the amine coupling procedure. The carboxy groups of the dextran matrix of the CM5 sensor chip were activated for 10 min with a 1:1 mixture of 0.1 M 3-(N,N-dimethylamino)propyl-N-ethylcarbo-diimide

(EDC), and 0.1 M *N*-hydroxysuccinimide (NHS) at a flow rate of 10 μ l/min. This activation step produced reactive succinimide esters on the CM5 surface. A stock solution of E-selectin/IgG (0.4 mg/ml in 50 mM Tris buffer, 150 mM sodium chloride, pH 7.6) was diluted to 40 μ g/ml in 10 mM sodium acetate buffer pH 5.0. Injection of 100 μ l of the 40 μ g/ml solution was performed onto the activated surface at a flow rate of 10 μ l/min. A surface capacity of 7'500 RU of E-selectin/IgG was achieved. Finally, the residual activated sites of the surface were blocked by injection of 1 M ethanolamine•HCl, pH 8.0. The flow path was changed to the reference flow cell. The same protocol was applied without injection of E-selectin/IgG sample to prepare a reference surface.

Assay validation

DS-04115 was synthesized in-house by Dr. Daniel Schwitzer [47] and used as a test compound for the validation of the assay. A 20 mM stock solution was prepared in HBS-N buffer.

HBS-P buffer was supplemented with 20 mM calcium chloride and used for all interaction experiments. In order to evaluate the binding affinity, a serial dilution of a broad range of concentrations starting at 8 mM was injected at a flow rate of 20 μ l/min for 1 minute. Analysis of the data was accomplished with Scrubber[®] (version 2.0a). Five buffer blanks preceded the injection of the serial dilution. One buffer blank was also injected at the end of the run.

3.2.5 Capture-based assay format

3.2.5.1 Preparation of protein A surface

Staphylococcus protein A was purchased from Sigma (P6031, Sigma-Aldrich Chemie GmbH, Buchs, Switzerland) and the amine coupling kit from GE Healthcare. The kit included all reagents needed for the immobilization procedure [*N*-hydroxysuccinimide (NHS), 3-(*N,N*-dimethylamino)propyl-*N*-ethylcarbo-diimide (EDC), ethanolamine•HCl (EA)].

Concentration and pH scouting of protein A

Stock solution of protein A was prepared by dissolving 1 mg lyophilized protein in 1 ml water. pH and concentration scouting were performed in order to evaluate the pH and concentration dependence for an optimum immobilization of protein A onto the biosensor surface. Protein A was diluted to a 40 µg/ml concentration with different acetate buffers (10 mM, pH 4.0, 4.5, 5.0 and 5.5) or HBS-N buffer (10 mM HEPES, 150 mM NaCl, pH 7.4) purchased from GE Healthcare. These solutions were sequentially injected over a CM5 sensor chip for 3 min at a flow rate of 10 µl/min. A 50 mM NaOH solution was injected for 30 sec at a flow rate of 20 µl/min in order to wash the surface between each sample injection. The best interaction between the dextran matrix of the biosensor surface and protein A was observed at pH 5.0. Therefore, the concentration scouting was performed by injection of a serial dilution of protein A (10, 20 and 40 µg/ml) in acetate buffer, pH 5.0. The same injection parameters as those used for the pH scouting were applied and 30 µg/ml was a suitable concentration to achieve appropriate level of immobilization.

Immobilization procedure of protein A

Two cycles of injections prior to usage were done for the preconditioning of the surface. The cycle consisting of successive injections of 20 µl of 50 mM NaOH, 10 mM HCl, 0.1% SDS and 100 mM H₃PO₄ at a flow rate of 50 µl/min were performed. After preconditioning, the sensor chip was used within the next four hours for the immobilization.

HBS-P buffer was used as running buffer for the amine coupling procedure. The carboxy groups of the dextran matrix of the CM5 sensor chip were activated for 10 min with a 1:1 mixture of 0.1 M 3-(N,N-dimethylamino)propyl-N-ethylcarbo-diimide (EDC), and 0.1 M N-hydroxysuccinimide (NHS) at a flow rate of 10 µl/min. A stock solution of protein A (1 mg/ml in 50mM phosphate buffer, pH 7.0) was diluted to 30 µg/ml in 10 mM sodium acetate buffer pH 5.0. Injection of 100µl of the prepared dilution was performed onto the activated surface at a flow rate of 10 µl/min. Surface capacities of protein A from 6'800 to 7'800 RU were achieved. Finally, the residual activated sites of the surface were blocked by injection of 1 M ethanolamine HCl, pH

8.0. The same protocol was applied with a protein A sample prepared sequentially or in parallel and used to prepare a reference surface.

3.2.5.2 Preparation of anti-human IgG (Fc specific) surface

Polyclonal goat anti-human IgG (Fc specific) was purchased from Sigma (I2136, Sigma-Aldrich Chemie GmbH, Buchs, Switzerland) and the amine coupling kit from GE Healthcare.

Concentration and pH scouting of anti-human IgG

A 2.1 mg/ml stock solution of antibody anti-human IgG in 10 mM phosphate buffer, pH 7.0 containing 15 mM sodium azide was used for scouting procedures. Both pH and concentration scouting assays were performed in order to evaluate the optimal immobilization conditions for anti-human IgG onto the biosensor surface. Anti-human IgG was diluted to a 42 µg/ml concentration with different acetate buffers (10 mM, pH 4.0, 4.5, 5.0 and 5.5) or HBS-N buffer (10 mM HEPES, 150 mM NaCl, pH 7.4) purchased from GE Healthcare. These solutions were sequentially injected over a CM5 sensor chip for 3 min at a flow rate of 10 µl/min. A 50 mM NaOH solution was injected for 30 sec at a flow rate of 20 µl/min in order to wash the surface between each sample injection. The same cycle of injection was repeated with a 14 µg/ml sample of anti-human IgG diluted in acetate buffers (10 mM, pH 4.0, 4.5, 5.0 and 5.5). For both, the 42 µg/ml and the 14 µg/ml concentrations, the best interaction between the dextran matrix of the biosensor surface and anti-human IgG was observed at pH 5.5. Therefore, the concentration scouting was performed by injection of dilutions of anti-human IgG (7, 21 and 30 µg/ml) in acetate buffer, pH 5.5. The same injection parameters as those used for the pH scouting were applied.

Immobilization procedure of anti-human IgG

The preconditioning of the surface prior to usage and the activation of the CM5 sensor chip surface was done as previously described in section 3.2.5.1 for the protein A immobilization procedure.

HBS-P buffer was used as running buffer for the amine coupling procedure. A stock solution of anti-human IgG (2.1 mg/ml) was diluted to 21 µg/ml in 10 mM sodium acetate buffer pH 5.0. A hundred microliter of the 21 µg/ml solution was injected onto the activated surface at a flow rate of 10 µl/min. Surface capacities of anti-human IgG from 14'000 to 16'000 RU were achieved. Finally, the residual activated sites of the surface were blocked by injection of 1 M ethanolamine•HCl, pH 8.0. The same protocol was applied with a anti-human IgG sample prepared sequentially or in parallel and used to prepare a reference surface.

3.2.5.3 Capture of E-selectin/IgG on protein A or E-selectin IgG surface

Following the protein A or anti-human IgG coupling, the flow path was changed to exclude the reference flow cell containing only protein A. E-selectin/IgG was diluted to a 50 µg/ml concentration using 10 mM acetate buffer, pH 5.5. This solution was injected at a flow rate of 5 µl/min for 20 min over a single flow-cell, designated the active flow cell. Densities of approximately 7'800 RU of E-selectin/IgG were achieved on the protein A surface and approximately 9'000 RU on the anti-human IgG surface. The active and reference flow cells were equilibrated for twelve hours in HBS-P buffer containing 20 mM calcium chloride at a flow rate of 2 µl/min. The surface was equilibrated in HBS-P buffer supplemented with 20 mM calcium chloride (C3306, Sigma-Aldrich Chemie, Steinheim, Germany) at a flow rate of 2 µl/min for twelve hours. After usage, the chip was stored in HBS-P buffer containing 20 mM calcium chloride at 4°C.

3.2.5.4 Validation of the capture-based assay

Compounds were synthesized in-house by Dr. Daniel Schwitzer [47], Jonas Egger [48] and Bea Wagner and dissolved to prepare a 50 mM stock solution in DMSO. For all compounds tested, the chemical structure are displayed in Appendix III.

GMI-1077 and **DS-0548** were used as test compounds for the validation of the capture assay. These compound were analyzed in a static cell-free ligand binding assay (Dr. John L. Magnani, Glycomimetics Inc., Rockville, USA) [49,50]. In this

assay, the inhibition of E-selectin was measured under equilibrium conditions. E-selectin/IgG was coated on a 96 well plate and a weak binder competed with sialyl Lewis^a polymer coupled to horseradish peroxidase (sLe^a-PAA-biotin/SA-HRP). IC₅₀ were standardized to the value of **BW-69669** measured in parallel on the same plate. This standardization avoids fluctuation of IC₅₀ values due to variations in the well plate. Affinity values are expressed in relative IC₅₀ (rIC₅₀) after normalization to sialyl Lewis^x (sLe^x), which was taken as a reference compound with an IC₅₀ of 1 mM (rIC₅₀ = 1.0). rIC₅₀ values of 0.080 for **BW-69669**, 0.008 for **DS-0548** and 0.004 for **GMI-1077** were obtained. Stock solutions of compounds (50 mM) were prepared in DMSO (Sigma-Aldrich Chemie, Steinheim, Germany).

HBS-P buffer supplemented with 20 mM calcium chloride and 5% DMSO (v/v) was used for all Biacore experiments. In order to evaluate the binding affinity, a serial dilution with a broad range of concentrations starting at 0.5 mM was injected at a flow rate of 20 µl/min for one minute. Following the assay with a broad range of concentrations, nine concentrations, optimized based on the rough estimate of the affinity constant, of a twofold dilution of ligand was randomly injected in duplicate. Determination of the affinity constant was accomplished in Scrubber[®] (version 2.0a) after double referencing (against buffer blank and reference flow cell) and a solvent correction. The K_D was derived from the equilibrium binding response by applying a single-site model with a 1:1 binding event.




3.2.5.5 Evaluation of the surface activity

The maximum response for a SPR signal can be calculated using Eq. (4):

$$R_{\max} = \frac{MW_{\text{analyte}}}{MW_{\text{target}}} \cdot \text{density}_{\text{target}} \cdot \text{valency} \quad (4)$$

Table 1 summarizes parameters of the equation that differs according to the format of the biacore assay.

Table 1. Parameters of equation 1 according to different Biacore assay format.

Biacore assay	MW_{target}	$\text{density}_{\text{target}}$	valency
Direct amine coupling 	$MW_{\text{E-selectin/IgG}}$	$\text{density}_{\text{E-selectin/IgG}}$	2
Capture assay <i>via</i> protein A 	$MW_{\text{E-selectin/IgG}} + MW_{\text{proteinA}}$	$\text{density}_{\text{E-selectin/IgG}} + \text{density}_{\text{proteinA}}$	2
Capture assay <i>via</i> anti-human IgG 	$MW_{\text{E-selectin/IgG}} + MW_{\text{anti-human IgG}}$	$\text{density}_{\text{E-selectin/IgG}} + \text{density}_{\text{anti-human IgG}}$	4

The surface activity corresponds to the ratio $R_{\text{max}}^{(\text{experimental})} / R_{\text{max}}^{(\text{calculated})}$

3.2.5.6 DMSO tolerability

DMSO was purchased from Sigma (Sigma-Aldrich Chemie, Steinheim, Germany) and stored in a desiccator. A stock solution of 50 mM in DMSO was prepared for all the ligands. The stock solutions were prepared and stored in polypropylene tubes (Treff AG, Degersheim, Switzerland), which are compatible with this solvent. A concentration of 5% DMSO (v/v) was maintained constant in the running buffer (HBS-P, 20 mM calcium chloride, 5% DMSO) and the ligands dilutions. To take into account and eliminate the effect of the high refractive index of DMSO on the signals, a calibration curve was needed [51]. Two solutions were prepared: solution A (1 ml of running buffer + 50 μl HBS-P containing 20 mM calcium chloride) and solution B (1 ml of running buffer + 1 μl of DMSO).

Solutions A and B were mixed in different proportions to prepare a series of five calibration solutions (Table 2) containing an increasing amount of DMSO [respectively 4.76%, 4.84%, 4.93%, 5.01% and 5.09% (v/v)].

Table 2. Calibration solutions of DMSO.

	1	2	3	4	5
A (μl)	400	300	200	100	0
B (μl)	0	100	200	300	400

DMSO calibration solutions were injected prior to each assay. Five blank buffer injections preceded and 1 blank buffer followed the injection of the DMSO calibration solutions.

3.2.5.7 Evaluation of synthesized E-selectin antagonists

Based on the lead structure **BW-69669** [52], several derivatives were synthesized in-house by Dr. Daniel Schwitzer, Jonas Egger and Beatrice Wagner in order to stabilize the bioactive conformation of the ligand in solution. Two capture-based assays for the immobilization of E-selectin/IgG were established and validated (see section 3.2.5). Improvement of the potency of the ligands was evaluated with the capture assay, which used anti-human IgG to immobilize the E-selectin/IgG. Stock solutions of ligands (50 mM) were prepared. The K_D values obtained with Biacore were compared to IC_{50} values obtained from the static cell-free ligand binding assay.

A CM5 sensor chip was prepared as described in section 3.2.5. Binding experiments were performed in HBS-P buffer supplemented with 20 mM calcium chloride and 5% DMSO. Prior to compound evaluation, the surface was equilibrated in HBS-P buffer supplemented with 20 mM calcium chloride and 5% DMSO (v/v) (D8418, Sigma-Aldrich Chemie, Steinheim, Germany) at a flow rate of 5 μ l/min for four hours.

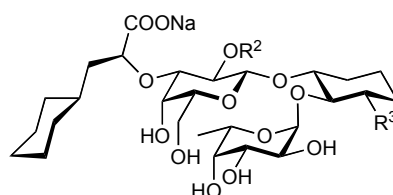
For each experiment, ten twofold dilutions of the ligand were randomly injected. For the initial determination of ligand binding isotherms, each concentration was injected in duplicate or triplicate. In later studies, to increase the throughput, two to three concentrations per assay were repeated in duplicate. **DS-0565** and **GMI-1077** were chosen as reference compounds. The stability of the surface after immobilization and its use to determine binding constants was followed by injection of ten twofold dilutions of a reference compound. Prior to each assay, DMSO solutions and blank injection of buffer were performed as described in section 3.2.4.6. After usage, the chip was stored in HBS-P buffer containing 20 mM calcium chloride at 4°C.

3.2.6 Thermodynamic analyses

Enthalpic and entropic contributions were determined for a better characterization and understanding of the binding affinity of carbohydrate mimics to E-selectin. A set of four ligands **DS-04115**, **GMI-1077**, **DS-0565** and **DS-0567** was selected based on their structural properties and affinity (Table 3).

Table 3. Structure, rIC₅₀ (determined by static cell-free assay) and K_D (mean value, Biacore) of **DS-04115**, **GMI-1077**, **DS-0565** and **DS-0567**. The general structure of **BW-69669** derivatives is shown below.

Compound	R ²	R ³	rIC ₅₀ competitive binding assay GMI, ref. sLe ^x	K _D [μM] [Biacore]
DS-04115	H	Methyl	0.016	7.89
GMI-1077	Benzoate	Methyl	0.004	1.45
DS-0567	Benzoate	Ethyl	0.007	1.49
DS-0565	Benzoate	Cyclopropyl	0.032	5.36



All ligands were measured at several temperatures between 10 and 30 °C and evaluated by applying a van't Hoff plot [53]. The E-selectin/IgG was captured on an anti-human IgG surface as described in section 3.2.5.2 and 3.2.5.3. The binding analyses were carried out as described in section 3.2.5.7. The Biacore 3000 was stabilized over night for each measured temperature.

3.2.7 Reverse assay: immobilization of an E-selectin antagonist onto the sensor chip surface

Immobilization of JE-14

JE-14 was synthesized in-house by Jonas Egger and designed to be coupled to the biosensor surface *via* amine coupling.

Two cycle of injection prior to usage were done for the preconditioning of the surface. Successive injections of 20 μ l of 50 mM NaOH, 10 mM HCl, 0.1% SDS and 100 mM H₃PO₄ at a flow rate of 50 μ l/min were performed. After preconditioning, the sensor chip was used within the next four hours for the immobilization. HBS-P buffer was used as running buffer for the amine coupling procedure. A reference flow cell was first prepared by activation of the carboxy groups of the dextran matrix of the CM5 sensor chip with a 1:1 mixture EDC/NHS at a flow rate of 10 μ l/min for 10 minutes. Afterwards, the residual activated sites of the surface were immediately blocked by injection of 1 M ethanolamine•HCl (EA), pH 8.0.

The flow path was changed to exclude the reference flow cell. A mixture of sodium borate buffer (10 mM sodium tetraborate, 1 M NaCl, pH 8.5, GE Healthcare, Freiburg, Germany) containing 0.004% (v/v) of *N*-ethyl-diisopropylamine (0340, Fluka, Sigma-Aldrich Chemie GmbH, Buchs, Switzerland) was prepared. This solution was used to dissolve **JE-14** to a 20 mM stock solution. A sample of **JE-14**/EA 1:1 was injected onto the activated flow cell at a flow rate of 5 μ l/min for 7 minutes. A final concentration of 1 mM of **JE-14** was used. Finally, the residual activated sites of the surface were blocked by injection of 1 M EA, pH 8.0. Additional active flow cells were prepared with lower densities of **JE-14** on the surface by injecting ratios of **JE-14**/EA at 1:10, 1:50 and 1:100. Biacore experiments were performed in HBP-P buffer supplemented with 20 mM calcium chloride.

Reverse assay with LecEGF_CR2 construct

A stock solution of LecEGF_CR2 construct (6.7 mg/ml in HBS-P, pH 7.4) was diluted to 40 μ M in HBS-P buffer at pH 7.4 supplemented with 20 mM calcium chloride. For determination of the binding constant, ten twofold dilutions of

LecEGF_CR2 construct were injected. HBS-P buffer containing 20 mM calcium chloride was used as running buffer. A series of five buffer blanks was injected prior to protein sample injection and one buffer blank was injected at the end of the run. Equilibrium binding constants were determined using the steady-state response fit to a 1:1 binding model as well as calculated by the ratio of dissociation and association rates.

Reverse assay with E-selectin/IgG

A stock solution of E-selectin/IgG (23 mg/ml in HBS-P, pH 7.4) was diluted to 58 μ M in HBS-P buffer at pH 7.4 supplemented with 20 mM calcium chloride. A final concentration of 5% DMSO was present in the E-selectin/IgG dilution. For the determination of the binding constant, ten twofold dilutions of E-selectin/IgG were injected. HBS-P buffer containing 20 mM calcium chloride and 5% DMSO was used for both, serial dilution of the protein and as running buffer. The surface was equilibrated with the running buffer for two hours before running the protein dilutions. DMSO calibration solutions were injected prior to the protein dilutions. Five blank buffer injections preceded, and one blank buffer followed the injection of the DMSO calibration solutions. One buffer blank was also injected at the end of the run, after the last protein injection. Equilibrium binding constants were determined using the steady-state response fit to a 1:1 and a 1:2 binding models.

3.3 Results and discussion

For all antagonists measured, the chemical structure can be found in Appendix III.

3.3.1 Development of an E-selectin Biacore assay

3.3.1.1 Direct amine coupling of E-selectin/IgG

Immobilization of E-selectin/IgG

Direct covalent immobilization by amine coupling (e.g. Arg₉₇, Lys₁₁₁, Lys₁₁₂, Lys₁₁₃) [54] might involve amino acids located in the binding site of E-selectin and therefore prevent the interaction with an antagonist. Nevertheless, this coupling approach remains interesting, since it generally generates a stable surface with a high density of protein. This is essential for ligands with low signal intensities, such as carbohydrates. For this reason, the possibility of a direct amine coupling of E-selectin/IgG was evaluated. The optimization of the pH attraction is not a necessity but is usually applied to limit sample consumption. In general, proteins adopt different conformations at different pH due to changes in intramolecular hydrogen bonds. Under native conditions, protein can change back to its native folding. Thus, one has to keep in mind the risk of an effect of amine coupling to the matrix on the protein conformation. An optimal pH attraction is usually:

- below the pI of the protein (surface of the protein predominantly positively charged),
- not at the pI (negative and positive charges are canceled, repulsive electrostatic forces are reduced and dispersive forces predominates inducing aggregation and precipitation),
- not too acidic to reduce risk of non denaturation.

High surface attraction of E-selectin/IgG was observed in the range of pH 4.0-5.0. This was in good agreement with the pI of 5.4 for E-selectin/IgG, since the

positively charged protein is electrostatically attracted to the carboxylate surface. For the immobilization, 40 µg/ml of E-selectin/IgG was injected at pH 5.0 (Figure 7). The concentration is chosen in order to have a slow velocity that enable a better control and a better reproducibility of the immobilization level.

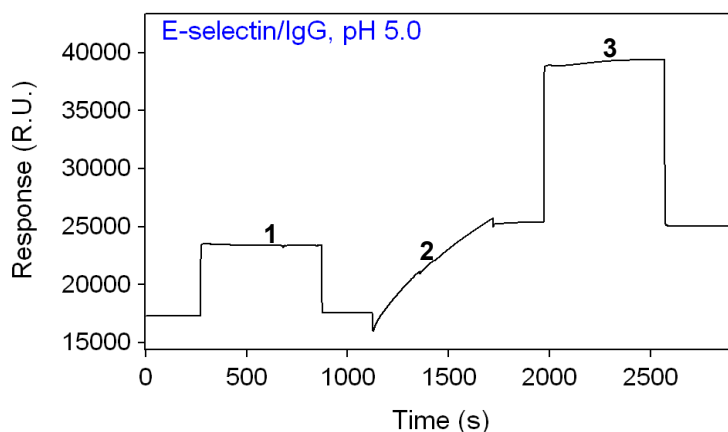


Figure 7: Amine coupling profile of E-selectin/IgG performed at pH 5.0; 1: activation of the surface with EDC/NHS; 2: E-selectin/IgG injection; 3: Deactivation step by ethanolamine injection.

On a CM5 sensor chip, an immobilization level of 7'500 RU was obtained. The system was stabilized for several hours with HBS-P buffer supplemented with 20 mM calcium chloride (5 µl/min).

Validation process of directly coupled E-selectin/IgG

DS-04115 was used for testing the direct covalent coupling of E-selectin/IgG to the biosensor surface. The relative estimated affinity of 0.018 [relative to sLe^x (rIC₅₀)], was known from the static cell-free ligand binding assay (see section 3.2.5.4). This assay is based on a competition between an analyte (here **DS-04115**) and sLe^a-PAA-biotin/SA-HRP. The affinity value was normalized to sLe^x (rIC₅₀ = 1). In addition, to avoid the deviation of the absolute values between different plates, **BW-69669** was measured on the same plate as an internal reference. According to this assay, the K_D of **DS-04115** was expected to be in the µM range.

In the Biacore assay, no response was observed below a concentration of 60 µM of **DS-04115** and no saturation of E-selectin/IgG was achieved even at millimolar concentrations (Figure 8). This observation is rationalized through section 3.2.5.2,

namely that no or only a limited amount of E-selectin/IgG was immobilized on the chip surface with an accessible binding pocket. Therefore, another immobilization strategy had to be considered.

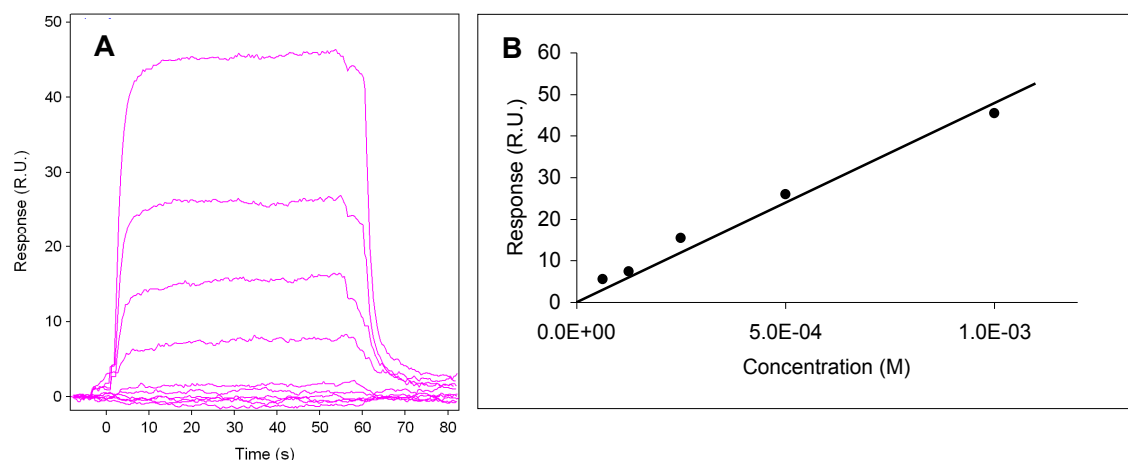


Figure 8: Sensorgrams (A) and binding isotherm plot (B) of **DS-04115** to E-selectin/IgG immobilized via direct amine coupling at pH 5.0.

3.3.1.2 Immobilization of E-selectin/IgG by a capture assay on a protein A surface

The E-selectin/IgG (Figure 9) consists of a C-type Lectin domain which corresponds to the carbohydrate recognition domain, an epidermal growth factor (EGF) and 6 consensus repeats domains (CRs) of E-selectin fused to the Fc part of human immunoglobulin G1 (h IgG1). Initially, the Fc part was introduced for the purification of E-selectin/IgG. Use of staphylococcal protein A or streptococcal protein G to capture an antibody on a sensor chip has been described [55-57]. Therefore, use of protein A was considered to be promising for the immobilization of E-selectin/IgG. Protein A was immobilized by the standard amine coupling procedure and E-selectin/IgG was captured on the prepared surface.

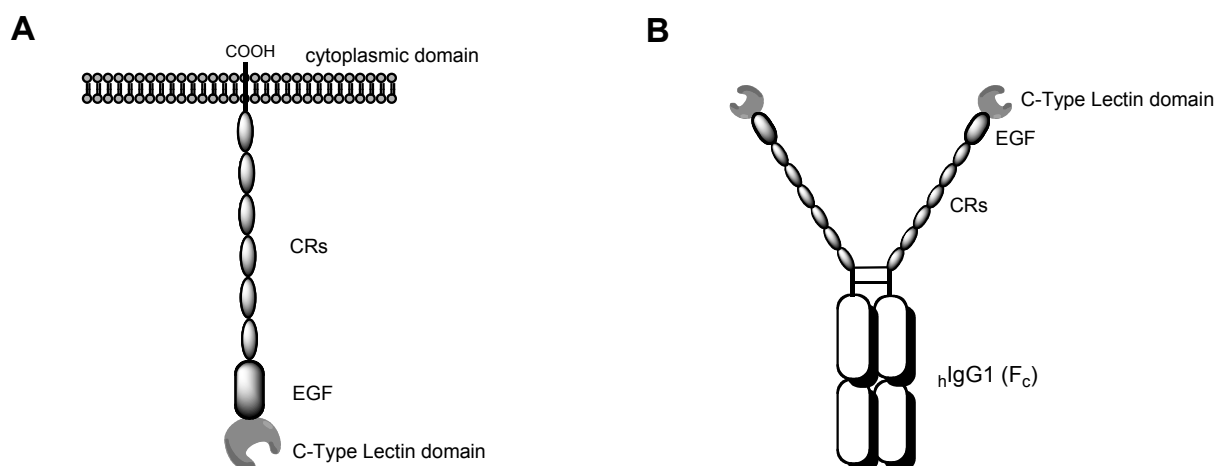


Figure 9: Schematic structure of E-selectin wild type (A) and E-selectin/IgG (B).

Amine coupling of protein A

High surface attraction was observed at pH values of 4.0, 4.5 and 5.0 from a pH scouting procedure which used a 40 µg/ml solution of protein A (Table 4). This result was in agreement with the pI of 5.1 for protein A. Even though protein A should remain native at pH 4.0, a pH of 5.0 was preferred for the coupling reaction. The concentration was decreased to 30 µg/ml in order to achieve the desired level of immobilization (6'000- 8'000 RU).

Table 4. pH scouting profile of protein A at 40 µg/ml.

pH	Response [RU]
7.4	63.7
5.5	4'036
5.0	13'051
4.5	16'552
4.0	12'106

With the optimized conditions, immobilization levels of 7'000-8'000 were obtained on CM5 sensor chips. The procedure was run in parallel for the reference

and the active flow cell. Prior to the capture of E-selectin/IgG, the protein A surface was stabilized under a 5 μ l/min flow of HBS-P for several hours.

Capturing of E-selectin/IgG on the protein A surface

For E-selectin/IgG capture, 100 μ l of a 50 μ g/ml solution of protein was injected at a flow rate of 5 μ l/min for 20 minutes (Figure 10). This procedure enabled the capture of a sufficient amount of E-selectin/IgG (7'800 RU).

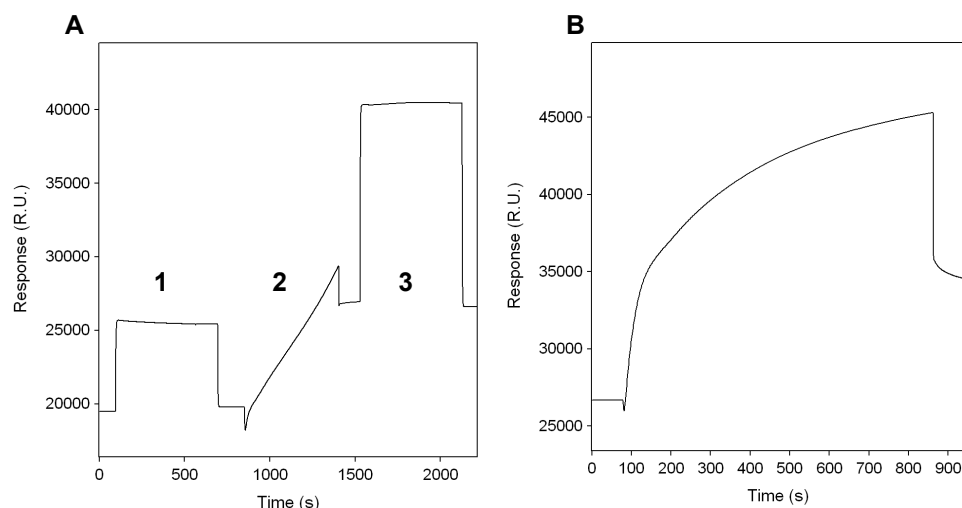


Figure 10: (A) Amine coupling profile of protein A performed at pH 5.0; 1: activation of the surface with EDC/NHS; 2: protein A injection; 3: Deactivation step by ethanolamine injection. (B) Capturing of E-selectin/IgG following the protein A immobilization.

A drift of the baseline was observed at the end of the injection due to the non-covalent binding between protein A and E-selectin/IgG. The surface was stabilized overnight in HBS-P buffer supplemented in 20 mM calcium chloride.

3.3.1.3 Immobilization of E-selectin/IgG by a capture assay on a anti-human IgG surface

An alternative approach for the immobilization of E-selectin/IgG was the use of an anti-human IgG antibody as an intermediate protein for the capture. In 2005, Beauharnois and coworkers reported a similar approach for P-selectin/IgG and L-selectin/IgG [58,59].

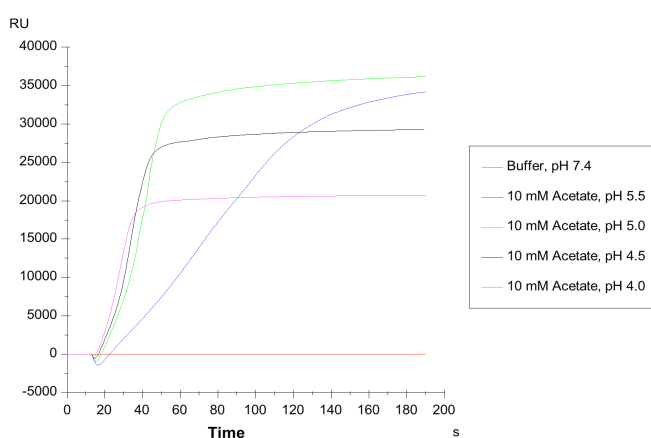
A 2.1 mg/ml stock solution of polyclonal anti-human IgG (Fc specific) purchased from Sigma was used in all capture assays involving an antibody.

Amine coupling of polyclonal anti-human IgG

In a pH scouting procedure, high surface attraction was observed at pH values between 4.0 and 5.5. A 42 µg/ml solution of antibody anti-human IgG was used (Table 5). At pH 5.5, the surface attraction appeared linear with time until reaching saturation. A pH of 5.5 was preferred for the coupling even though a lower pH should not affect the stability of an antibody.

Table 5. pH scouting profile of polyclonal anti-human IgG at 42 µg/ml.

pH	Response [RU]
7.4	26.6
5.5	33'827
5.0	36'084
4.5	29'263
4.0	20'740



According to the pH scouting, five concentrations of antibody (7, 14, 21, 30 and 42 µg/ml) were tested at pH 5.5. A clear correlation between concentration and surface attraction was observed (Table 6). A concentration of 21 µg/ml showed a suitable level of immobilization, while 7 and 14 µg/ml gave a low response and 42 and 30 µg/ml an undesired high response.

Table 6. Concentration scouting profile of anti-human IgG at pH 5.5.

Concentration [µg/ml]	Response [RU]
7	-1'759
14	2'252
21	8'600
30	12'803
42	33'827

Capturing of E-selectin/IgG on the anti-human IgG surface

For the capture of E-selectin/IgG, 100 μ l of a 50 μ g/ml solution of protein were injected at a flow rate of 5 μ l/min for 20 minutes (Figure 11). This procedure enabled the capture of high amount of selectin (10'000 RU) and appeared to be more efficient in terms of surface density.

As for the protein A capture assay, a drift of the baseline was observed at the end of the injection due to the non-covalent binding between anti-human IgG and E-selectin/IgG. The surface showed a high stability after equilibration overnight in HBS-P buffer supplemented with 20 mM calcium chloride.

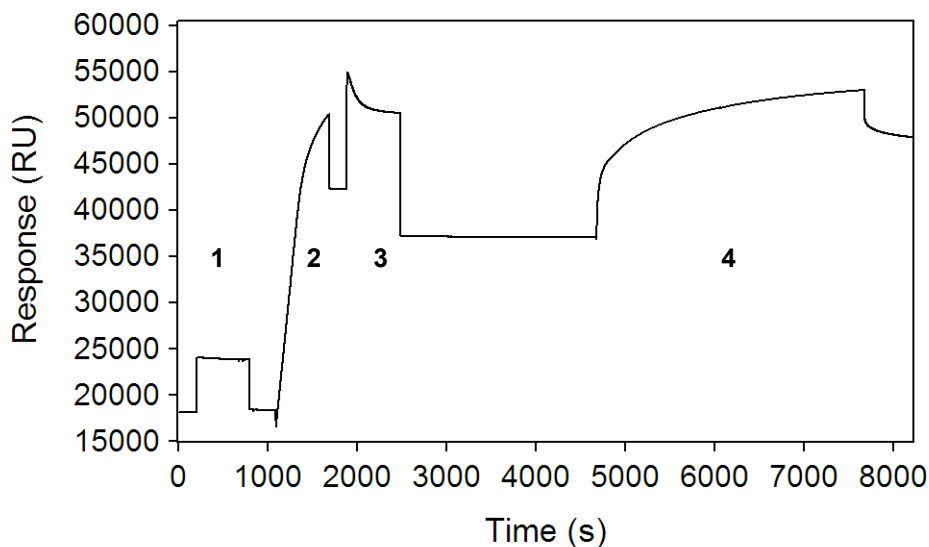


Figure 11. Profile of the capture assay of E-selectin/IgG. 1: activation of the surface with EDC/NHS; 2: amine coupling of anti-human IgG (21 μ g/ml, pH 5.5); 3: deactivation step by ethanolamine injection; 4: capturing of E-selectin/IgG(50 μ g/ml, pH 5.0).

3.3.1.4 Comparison of the capture assay *via* protein A and *via* anti-human IgG

Since we plan to detect low molecular weight antagonists (carbohydrate derivatives, MW 600-1000 Da), a high density of immobilized active E-selectin/IgG will positively influence the quality of the data. As previously shown, a high density of E-selectin/IgG (7'500 RU) can be immobilized by direct amine coupling. Unfortunately, the orientation of the immobilized E-selectin/IgG was not suitable for the binding assay. Capturing approaches led to an oriented attachment of E-

selctin/IgG and were therefore an obvious solution for generating highly active surfaces.

Because of their strong binding affinity to the Fc fragment of human IgG, two intermediates were used for the capture: protein A and anti-human IgG (Fc specific). A strong affinity between the captured target and intermediate protein is a prerequisite for generating stable surface and avoiding surface bleeding frequently observed in capturing assays. E-selectin/IgG was successfully captured on both types of surfaces (see sections 5.2.5.1 and 5.2.5.2). In order to select the approach that leads to the best quality of data, **GMI-1077** and **DS-0548** were tested over the two surfaces. The results are summarized in Table 7 and Figure 12.

Table 7. (A) Active flow cell profiles for comparison of capturing approach *via* protein A and *via* anti-human IgG. **(B)** Evaluation of the surface activity and binding affinity of **GMI-1077** (1-62.5 μ M) on a protein A surface and an anti-human IgG surface. **(C)** Binding affinity of **DS-0548** (0.1-25 μ M) on a protein A surface and an anti-human IgG surface.

A.

Intermediate protein for immobilization [μ g/ml]	pH	Surface capacity [RU]	E-selectin/IgG [μ g/ml]	pH	Surface capacity [RU]
protein A, 30 μ g/ml	5.0	8'500	50	5.0	6'200
anti-hIgG(Fc), 21 μ g/ml	5.5	14'800	50	5.0	11'500

B.

Intermediate protein for immobilization	Exp. K_D [μ M]*	Exp. R_{max} [RU]*	Calc. R_{max} [RU]**	Activity [%]***
protein A	1.77	11.31	58.20	19.40
anti-hIgG(Fc)	2.14	33.61	101.80	33

C.

Intermediate protein for immobilization	Exp. K_D [μ M]*	Exp. R_{max} [RU]*	Calc. R_{max} [RU]**	Activity [%]***
protein A	1.52	12.70	62.20	20.40
anti-hIgG(Fc)	1.82	22.14	103.20	21.50

*Experimental values obtained by fitting the steady state responses to a 1:1 binding model **Calculated value obtained with equation 1 *** Ratio Exp. R_{max} /Calc. R_{max}

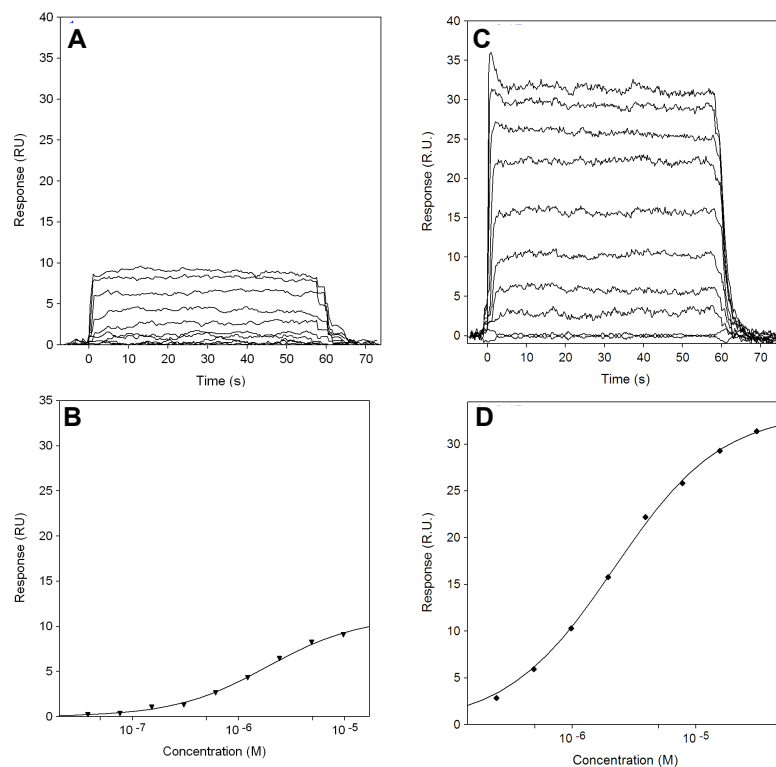


Figure 12. Sensorgrams and binding isotherm plots of **GMI-1077** for E-selectin/IgG. Influence of the intermediate protein for immobilization on the evaluation of the binding activity; **A,B**: protein A; **C,D**: anti-human IgG.

As shown in Figure 12 for **GMI-1077**, the quality of the sensorgrams was improved by using anti-human IgG as an intermediate protein to capture E-selectin/IgG. A better R_{max} and therefore an improvement of the signal-to-noise ratio were achieved. A similar observation was made for **DS-0548**, but at a lower proportion. As a consequence, the surface activity was considerably improved for **GMI-1077**. For both compounds, the dissociation constants (K_D s) obtained by fitting the steady state response with a one-to-one binding model showed comparable values (Table 7) in both formats. As will be shown later, the difference in affinity obtained with the two capturing assays was in the range of the fluctuation observed for the same compound measured on different surfaces with the same capturing procedure. Therefore, this fluctuation cannot be directly attributed to the intermediate protein used for the capture.

In conclusion, the direct amine coupling of the E-selectin/IgG on the surface was aborted due to the poor orientation of the protein. Therefore, a capture assay appeared an obvious solution. Antibody anti-human IgG was chosen as an

intermediate protein in the capture assay of E-selectin/IgG, because it generates more densely packed surfaces and higher R_{max} than protein A. These parameters are required for the detection of small molecules on large targets as this is the case with E-selectin/IgG and carbohydrate-based ligands.

3.3.2 Further optimization of the E-selectin/IgG Biacore capture assay

3.3.2.1 Dependence of the binding affinity upon surface density

An amine coupling of three different concentrations (10, 20 and 30 $\mu\text{g/ml}$ in 10 mM acetate buffer pH 5.5) of the anti-human IgG antibody was performed in order to investigate a dependence of the binding affinity upon the surface density. For this procedure, 100 μl of each antibody solution was injected on activated flow cells for 10 minutes. Increasing capacities were achieved, as shown in Table 8, fourth column. A solution of 50 $\mu\text{g/ml}$ of E-selectin/IgG was prepared in 10 mM acetate buffer, pH 5.0. After deactivation of the residual reactive succinimide esters groups, the protein solution was captured over the antibody surfaces. Each surface was prepared independently and different levels of capture were observed (Table 8, seventh column).

Table 8. Surface capacity of anti-human IgG antibody observed after amine coupling procedure with 3 different concentrations (10, 20 and 30 $\mu\text{g/ml}$) at pH 5.5 (right). Capture of E-selectin/IgG on increasing surface capacities of anti-human IgG (left).

Surface density*	Antibody anti-IgG(Fc) [$\mu\text{g/ml}$]	pH	Surface Capacity [RU]	E-selectin/IgG [$\mu\text{g/ml}$]	pH	Surface Capacity [RU]
Low	10	5.5	5'963	50	5.0	6'270
Medium	20	5.5	12'089	50	5.0	9'405
High	30	5.5	15'860	50	5.0	8'568

*Surface density total (E-selectin/IgG + antibody)

As expected, a correlation between the surface capacity of the immobilized antibody and the surface capacity of E-selectin captured was observed (Table 8, low and medium surface densities). However, this effect was not linear and up to a certain limit ($\approx 13'000$ RU), a further increase of the immobilization level of antibody

(Table 8, high density) showed a decrease of about 1'000 RU of the E-selectin/IgG captured (Table 8, Figure 13 and 15).

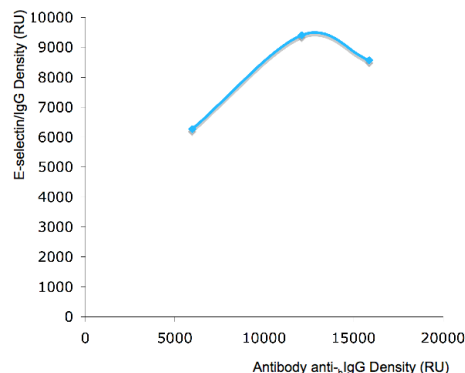


Figure 13. Density of captured E-selectin/IgG with respect to the density of covalently linked anti-human IgG.

The influence of the density of E-selectin/IgG on the detected affinities was evaluated with the ligand **DS-0565**. The relative affinity ($rIC_{50} = 0.032$) was known from the static cell-free ligand binding assay (see section 3.2.5.4). The measurements were done in triplicate over the three surfaces described above (Table 8). A single binding site model was used and fit best with the experimental data. A clear difference was observed between the low density surface (Figure 14A-B) and both medium and high density surfaces (respectively Figures 14C-D and 14E-F).

The sensorgrams in Figure 14A showed a lower response compared to medium and high-density surfaces (Figures 14C and 14E). In addition, the standard deviation was higher and therefore the fit was of poorer quality (Figure 14B). This was most likely due to the overall lower signal intensity leading to a lower signal-to-noise ratio.

No clear differences were observed between medium and high surface densities of protein (Figure 14C and E). This showed that an overload of the antibody on the surface did not improve the quality of the data. Even though the amount of E-selectin/IgG captured was lower at high density of antibody, a minor impact on the data was observed.

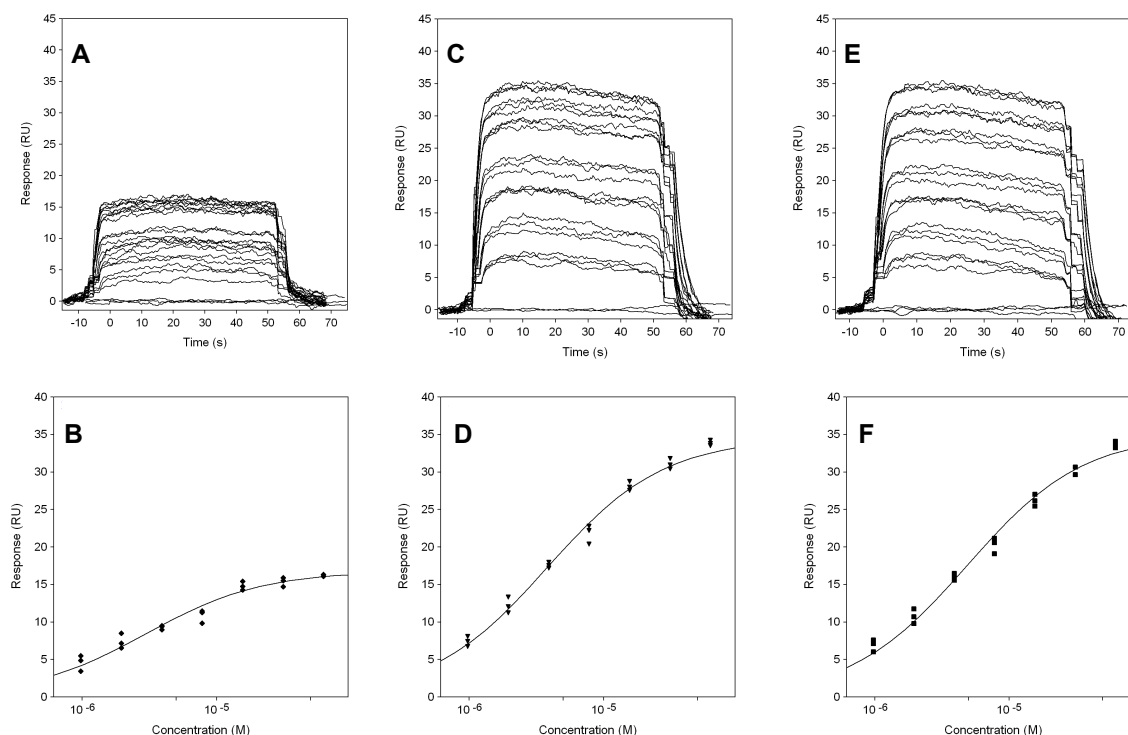


Figure 14. Sensorgrams and binding isotherm plots of **DS-0565** for E-selectin/IgG. Influence of the surface density of the intermediate protein used for the immobilization of E-selectin/IgG on the evaluation of the affinity; **A,B:** 5'963 RU; **C,D:** 12'089 RU; **E,F:** 15'860 RU.

K_D values were obtained by fitting the signals to a single binding site model (Table 9). The K_D value observed with the low surface density differs by a factor of two from the results with medium and high surface densities. This can be explained by the lower signal-to-noise ratio leading to higher standard deviation and poorer fit as already mentioned.

For further understanding of the results obtained with medium and high density surfaces, the surface activity was also evaluated and correlated with the surface densities.

Table 9. Evaluation of the surface activity and binding affinity of **DS-0565** (0.98-62.5 μ M, triplicate injections) at three different anti-human IgG surface densities.

Surface density*	Exp. K_D [μ M]**	Exp. R_{max} [RU]**	Calc. R_{max} [RU]***	Activity [%]****
Low	2.94	16.76	48	34.9
Medium	4.07	35.27	84	42
High	4.86	35.07	95	36.9

*Surface density total (E-selectin/IgG + antibody) **Experimental values obtained by fitting the steady state responses to a 1:1 binding model ***Calculated value obtained with equation 1 **** Ratio Exp. R_{max} /Calc. R_{max}

A decrease of activity following an increase of the surface density of the target has been observed by D. Ricklin [60] with GSLA-2. A similar effect has also been reported by Huber and coworkers [61] with cyclophilin D. In both cases, the target was directly covalently linked to the surface. In our assay a similar observation was witnessed between medium and high surface densities and the corresponding surface activity. However, as shown in Figure 15, the explanation for the observed effect is different due to the capture format applied. Indeed, the surface activity is related to the level of immobilized E-selectin/IgG and not to the total surface density. An increase in the level of immobilized E-selectin/IgG led to an increase of surface activity (Figure 15A-B). As already mentioned, a further increase of the antibody on the surface resulted in a higher total surface density but was not beneficial for the capture of the E-selectin/IgG (Figure 15B-C-D). The most plausible explanations for this effect are steric hindrance and reduce accessibility of the binding sites. This was discussed by Huber *et al.* [61] and can be applied to the antibody-E-selectin/IgG interaction discussed herein.

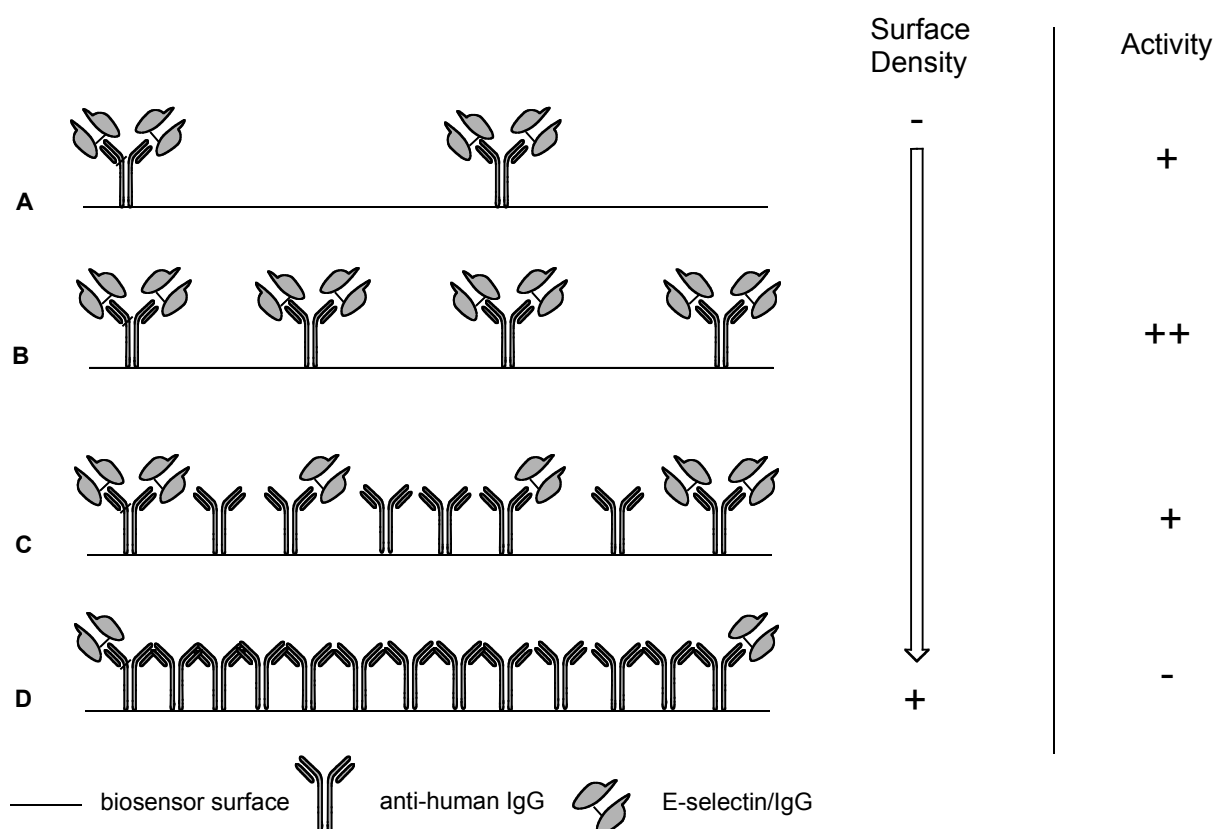


Figure 15. Schematic structure of; **A:** low; **B:** medium; **C:** high and **D:** very high density surfaces of the E-selectin/IgG capture assay.

3.3.2.2 Non-specific contribution from the intermediate used for the capture to the observed binding

It is desirable to have a negligible interaction between the intermediate protein used for the capture and the ligand, although the impact of a non-specific contribution can be determined with the reference flow cell. In order to evaluate the importance of this parameter in our assay, the binding affinity of **GMI-1077** was evaluated with a dextran surface reference cell and an anti-human IgG reference cell (Table 10, Figure 16). The ligand was injected in parallel over the active flow cell and the two types of reference flow cells (Table 10, Figure 16).

Table 10. Binding affinity of **GMI-1077** calculated with two types of reference cells: dextran matrix and anti-human IgG as the intermediate protein used for the capture.

Reference	Exp. K_D [μM]*	R_{max} [RU]
dextran	1.34	21.13
anti-human IgG	1.16	20.07

*Experimental values obtained by fitting the steady state responses to a 1:1 binding model

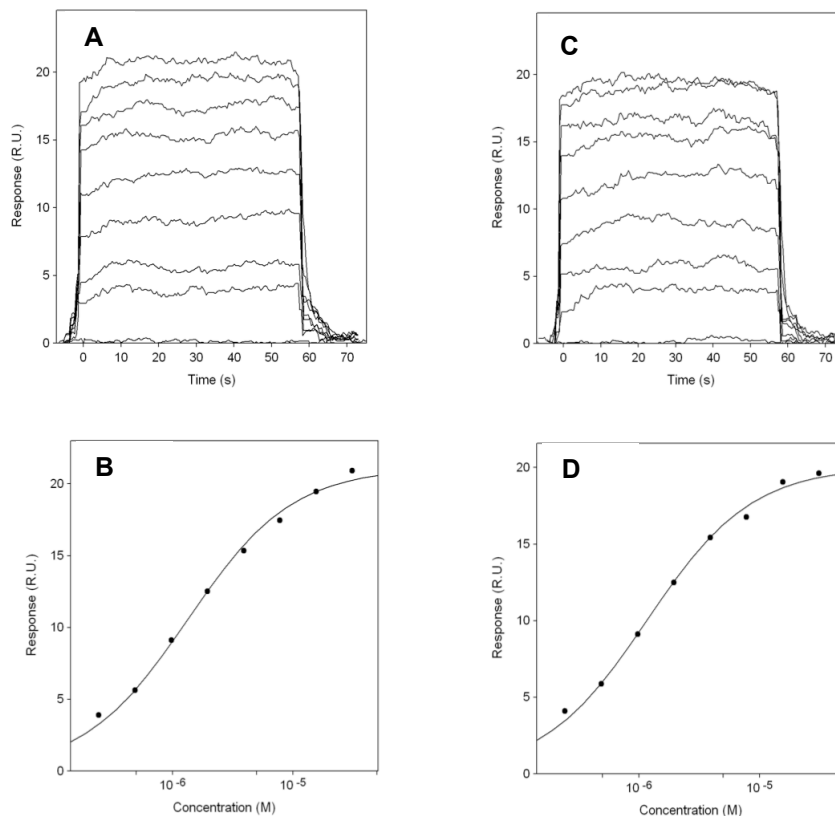


Figure 15. Sensorgrams and affinity isotherm plots of **GMI-1077** with two types of reference cells; **A,B:** dextran matrix; **C,D** anti-human IgG as the intermediate used for the capture.

The interaction between the intermediate protein used for the capture and the ligand appeared to be negligible in the range of the injected concentrations (Table 10 and Figure 16). However, at highest injected concentrations (0.2-1 mM), an increase of the non-specific binding was detected and strongly influenced the signal of the compound (data not shown).

3.3.2.3 Impact of the quality of the protein

In order to study the influence of the quality of the E-selectin on the surface activity and the binding affinity, an increasing proportion of denaturated E-selectin/IgG was captured on a CM5 sensor chip. For this purpose, a solution of E-selectin/IgG was denaturated by heating at 99 °C for 5 minutes and mixed with native protein from the same batch. Three ratios native/denaturated protein were prepared and injected over anti-human IgG surfaces (Table 11) with a similar final concentration of 48 µg/ml of E-selectin/IgG (native and denaturated).

Table 11. Design of a CM5 with increasing proportion of denaturated E-selectin/IgG immobilized.

Percentage native E-selectin/IgG	Surface density of antibody anti human IgG [RU]	E-selectin/IgG [µg/ml] (native + heated)	Surface density of E-selectin/IgG [RU]
100	7'050	48	6'300
50	8'133	48	7'250
25	7'550	48	7'139

As expected, an increasing amount of denaturated protein resulted in a decrease of the experimental R_{max} , indicating a loss of activity on the surface (Table 12 and Figure 17). This drastic decrease cannot be correlated to a difference in surface density and therefore cannot be attributed to it (Table 11). Indeed, the calculated R_{max} was higher with 50 % of active protein but the surface activity decreased by a factor of 1.6 compare to the surface without denaturated protein. A similar surface density (leading to a similar calculated R_{max}) would have led only to minor changes in surface activity if the heated protein was still active.

Table 12. Evaluation of the binding affinity and surface activity of **DS-0565** (0.625-80 μ M, duplicate) at three different ratios of native/denaturated protein captured on the surface.

Percentage native E-selectin/IgG	Exp. K_D [μ M]*	Exp. R_{max} [RU]*	Calc. R_{max} [RU]**	Activity [%]***
100	4.02	21.7	52	41.7
50	2.38	15.6	59.9	26
25	1.70	5.6	57.2	9.8

*Experimental values obtained by fitting the steady state responses to a 1:1 binding model **Calculated value obtained with equation 1 *** Ratio Exp. R_{max} /Calc. R_{max}

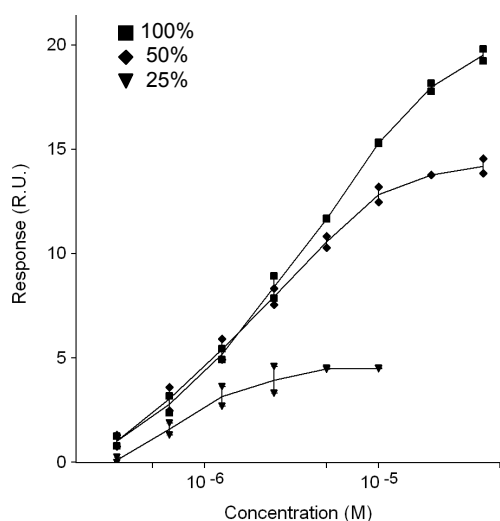


Figure 17. Binding curves are shown of **DS-0565** (0.625-80 μ M, duplicate) at three different ratios of native/denaturated protein captured on the surface.

As a consequence of the decrease in experimental R_{max} , observed with increasing amount of denaturated E-selectin/IgG, a lower quality of the sensorgrams was observed as well as a higher deviation between the duplicates. In addition, the capturing of the denaturated protein indicates that the IgG (Fc) part is still functional. Nevertheless, the loss of R_{max} indicates that denaturated protein does not fully contribute to the binding. Obviously, a reduction of R_{max} affects the observed K_D values. Theoretically, similar K_D s were expected for the different cases. A combination of the parameters mentioned above leads to a variation in the fit of the data points by a 1:1 binding model and therefore explain the variation in K_D s.

The consistency of the data obtained for **DS-0565** binding to E-selectin/IgG is seen in section 3.3.5, Figure 27. The K_D obtained in Table 11 with 100% active E-selectin/IgG differs from average of the earlier measurements in section 3.3.4, Table

17 by 26% and is within the fluctuation between different measurements of the same compound evaluated with the Biacore capture assay.

3.3.2.4 Stability of the surface

A series of E-selectin ligands were measured over the same surface during the course of two weeks. To evaluate the stability of the surface during these measurements, **GMI-1077** was regularly injected and its binding affinity evaluated and compared to previous measurements (Figure 18).

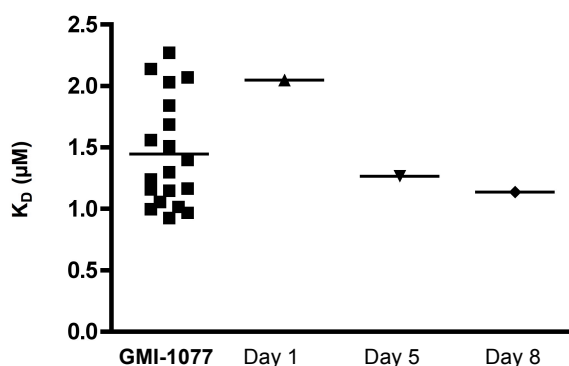


Figure 17. Evaluation of the stability of the surface monitored by three affinity evaluations of **GMI-1077** at day 1, day 5 and day 8 after immobilization. The first column shows the K_D values observed for twenty measurements of **GMI-1077**. The line indicates the mean value (1.45 μM +/- 0.44). A coefficient of variation of 0.3 was calculated.

A variation in the K_D s was observed over the period of eight days, but stayed in the range of fluctuation observed for **GMI-1077** with the capture assay (Figure 18, column 1). A loss of 18% of the density of the surface was observed between first and third measurement and can be correlated to a decrease in R_{max} (Figure 19). This loss has been consistently observed in the capture assay format and reaches a stable value after approximately one week.

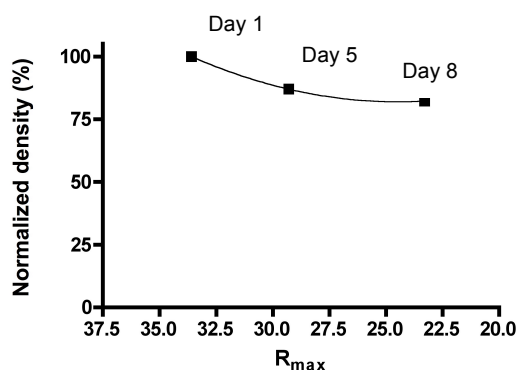


Figure 19. Correlation between the R_{max} obtained with a 1:1 model fit and the stability of the density of the surface.

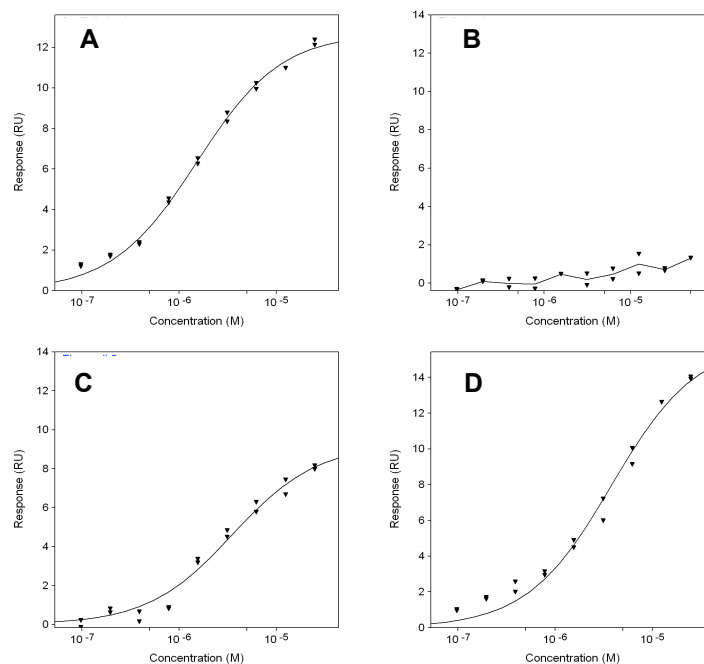
3.3.2.5 Calcium dependence of the binding

It is well-known that E-selectin binds to sialylated carbohydrates in a calcium dependent manner. Therefore, the role of calcium in the Biacore assay was examined in order to confirm that the observed binding results from the desired specific interaction.

DS-0548 was injected over the same surface under different conditions. Results are chronologically shown in Table 13A to D and corresponding binding isotherm plots. As shown with the binding isotherm plot B, no signal was observed in the presence of 3 mM EDTA, which is content in the running buffer, HBS-EP. After equilibration overnight in HBS-P buffer containing 20 mM calcium, a recovery of the signal was observed (Table 13C and binding isotherm plot C). Nevertheless, a lower signal-to-noise of the sensorgrams was observed as well as a shift of the K_D value compare to the binding isotherm plot before treatment with EDTA (Table 13A vs C). A higher R_{max} was observed after equilibration in buffer supplemented with 100 mM calcium chloride (Table 13D). However, this enhancement did not significantly improve the signal-to-noise and could not be correlated with a recovery of the K_D value (Table 13A vs D).

Table 13. Influence of EDTA on the binding affinity of **DS-0548** to E-selectin/IgG and corresponding binding isotherm plots (**A-D**).

Binding isotherm Plot	Buffer	K_D [μ M]	R_{max} [RU]
A	HBS-P + 20 mM CaCl_2	1.52	12.66
B	HBS-EP	-	-
C	HBS-P + 20 mM CaCl_2	3.53	9.24
D	HBS-P + 100 mM CaCl_2	3.80	15.93



These experiments clearly show the correlation between calcium dependency and the specificity of the binding in the Biacore capture assay. It also showed, how the E-selectin/IgG was affected by a depletion of calcium.

3.3.2.6 Removal of sample interactant from the captured surface

In a direct immobilization, the regeneration leads to the removal of the analyte while preserving the activity of the immobilized target (Figure 20A). A clear advantage of the capture assay compare to direct immobilization is the possibility to re-immobilize “fresh” protein by regeneration of the surface (Figure 20B). In both cases, the same terminology of regeneration is used even though it does not lead to the same result. For the capture assay, we will use the term “removal” referring to both captured molecules and analytes (Figure 20B). Obviously, the activity of the

protein used as an intermediate for the capture should not be affected by the removal treatment.

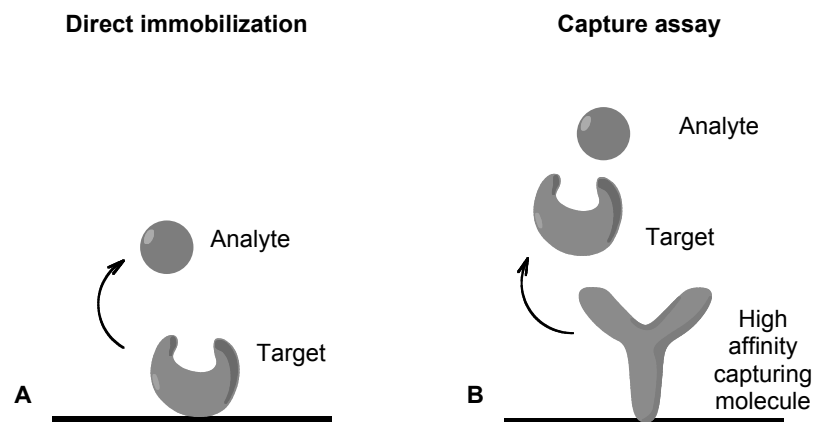


Figure 20. **A:** Regeneration of the surface with direct immobilized target; **B:** removal of the target from a captured surface.

Beauharnois *et al.* described a removal method for P-selectin/IgG and L-selectin/IgG captured by a goat anti-mouse IgG by pulse injection of HCl 20 mM, 50 μ l at 50 μ l/min [58,59].

In our assay, the removal was only partly successful. Fifty percent of the E-selectin/IgG could be removed even after several pulse injections of HCl 20 mM. The achievement of a full regeneration of the surface was never achieved and the quality of the protein remaining on the surface probably suffered from the HCl-treatment. Therefore, another method for removal was explored by injection of glycine 10 mM at low pH. A removal scouting was performed by successive pulse injection of glycine 10 mM with decreasing pH (3, 2, 1.5 and 1). Such a treatment allowed a release of 65 % of E-selectin but also did not allow the complete removal of the target from the surface.

Finally, a third method of regeneration mentioned in an application note and recommended by the manufacturer, GE Healthcare, was tested [62]. This procedure is alternatively proposed for capture assays in which other removal methods failed. The previously tested removal methods were based on injections of acidic solutions. In contrast, in this method, basic conditions are claimed to induce a rapid removal of the target by a single injection of a solution of 0.5 M NaSCN containing 10 mM NaOH for 30 seconds. Several injections were needed to achieve a full regeneration of the

surface. Nevertheless, following regeneration, only 3'400 RU were re-captured (about 40 % of the level obtained with the first capture). A second injection of E-selectin/IgG allowed the capture of an additional 3'300 RU leading to a reasonable level of capture (6'700 RU). However, a significant decay of the signal by 2'000 RU was observed during the equilibration phase of the surface in buffer. In order to evaluate the impact of such a regeneration method, **GMI-1077** was injected. The result was compared to the signal observed directly after the first capture of E-selectin/IgG (Figure 21).

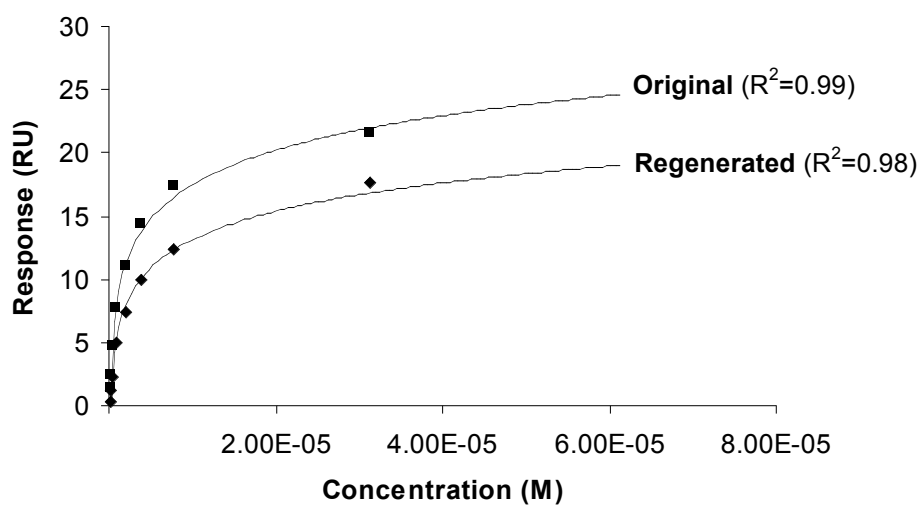


Figure 21. Evaluation of **GMI-1077** on the original and regenerated surface.

The interaction between the Fc fragment of the E-selectin construct and the anti-human IgG is very high (probably in the same order of magnitude as the interaction between IgG and immunoglobulin reported in the nanomolar range [63]). Although this is an advantage for the stability of the surface in the capture assay, it complicates the regeneration of the surface. The strong basic conditions were successful for the removal of E-selectin/IgG from the surface, but also affected the anti-human IgG covalently linked to the surface. Indeed, a sizeable reduction in the R_{max} from the regenerated surface was observed, leading to the conclusion that a regeneration step is not suitable in our assay format.

3.3.3 Evaluation of BW-69669 derivatives

Sialyl Lewis^x (sLe^x) is the minimal carbohydrate epitope of natural E-selectin ligands. This millimolar ligand has served as a starting point for the design of more potent E-selectin antagonists (Figure 22).

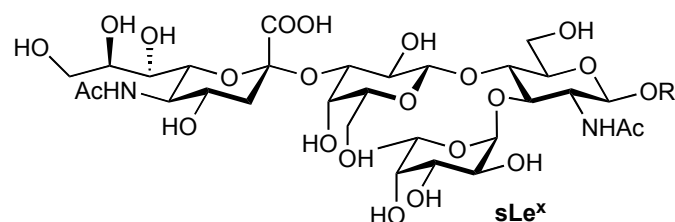


Figure 22. Structure of Sialyl Lewis^x ($K_D = 1\text{mM}$, [64])

In 1994, Graves and coworkers determined by X-ray crystallography the three dimensional structure of the CRD-EGF domain of E-selectin. More recently, in 2000, Somers *et al.* succeeded in resolving the E-selectin/sialyl Lewis^x complex by X-ray crystallography. The crystallography data are in good agreement with NMR studies [10,54,75] concerning the core conformation of the bound sLe^x and revealed important pharmacophores for the binding (Figure 23).

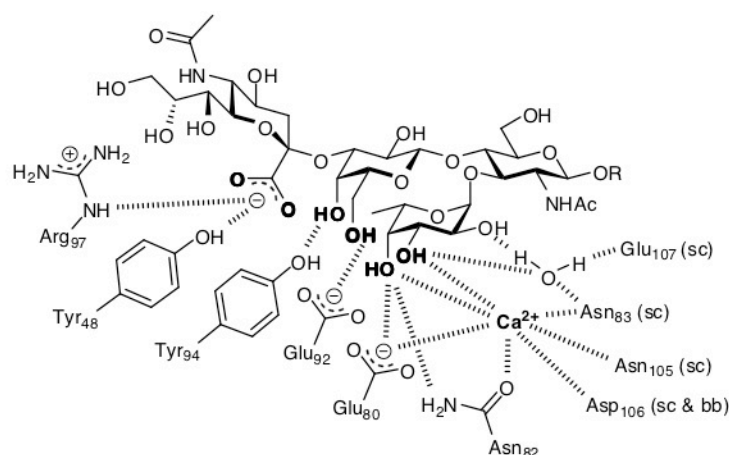


Figure 23. Interactions responsible for sLe^x binding to E-selectin as determined by X-ray crystallography. Part of the amino acid involved in the binding is specified under brackets, side chain (sc) or backbone (bb) (Adapted from [54]).

The tetrasaccharide mimic **BW-69669** (Figure 24A) showed an improved affinity for E-selectin compare to sLe^x. However, for therapeutic use, this

improvement in affinity was not sufficient. In addition, its poor pharmacokinetic profile, mainly due to the presence of polar groups, needed to be improved. Therefore, based on the lead structure **BW-69669**, several antagonists were developed. In order to increase affinity, to improve kinetics and to optimize drug-like properties, derivatives were synthesized by modifying the R groups (Figure 24B). In particular, modifications were sought which led to a stabilization of the bioactive conformation of the ligand in solution. These modifications stabilized the desired conformation through the addition of spatially demanding groups on R² and R³ [65].

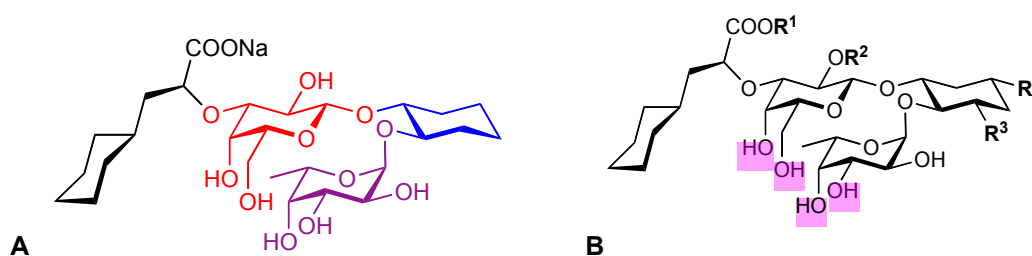


Figure 24. (A) Structure of **BW-69669**. The different carbohydrate derivatives moieties are shown in different colors (galactose in red, fucose in magenta, GlcNAc mimic moiety in blue and cyclohexyl lactic acid in black) (B) Modified sites to improve the potency. Important pharmacophore for the binding were highlighted.

In a first attempt, substitution of the hydroxyl group of **BW-69669** in the 2-position of galactose with a benzoate (**LT-0236**) led to an increase of affinity by a factor of 2.5 (Table 14). A further enhancement was observed by introducing a methyl in the 5-position of GlcNAc mimic moiety (**DS-04115** vs **BW-69669**). By introducing both aforementioned substituents in the R² and R³ positions (**GMI-1077**) a gain in affinity by a factor of 30 was achieved compare to **BW-69669** (Table 14). K_Ds determined by Biacore were in good agreement with the rIC₅₀ determined by static cell-free assay.

Table 14. Initial modifications at R² and R³ and the corresponding K_D values.

Entries	Compound	R ¹	R ²	R ³	R ⁴	rIC ₅₀ (competitive binding assay GMI, sLe ^x =1)	K _D [μM] (Biacore)
1	BW-69669	Na	H	H	H	0.080	45
2	LT-0236	H	Bz	H	H	0.040	18.8
3	DS-04115	Na	H	Me	H	0.016	7.89
4	GMI-1077	Na	Bz	Me	H	0.004	1.45

In parallel, the conformational freedom of **GMI-1077** was evaluated by MC(JBW)/SD-simulations (Dr. Martin Smiesko). This approach originally proposed by Kolb and Ernst [66,67] permits the evaluation of the extent to which the unligated **GMI-1077** sampled the bioactive window.

These results are displayed in a 2D internal coordinate system with the “core-conformation” (x-axis) and the “acid-orientation” (y-axis) as parameters (Figure 25). The z-axis (color code) indicates the frequency of occurrence of the value during the simulation [66,67].

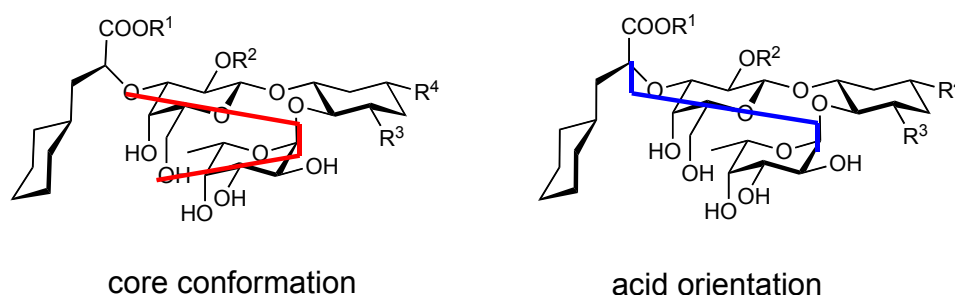


Figure 25. View of the core conformation and the acid orientation [66,67].

This simulation allowed the comparison of the solution and bound conformations of antagonists. The small blue dots indicates bioactive conformation of sLe^x obtained from crystal structure and the larger black square indicates the favorable region determined from trNOE-NMR studies [10,68,69]. Compounds having a high probability for conformations in the bioactive window were shown to

usually have higher affinity to E-selectin, due to their increased pre-organization in the bioactive conformation [66,67].

Figure 26 shows the results obtained with **GMI-1077** in solution (Figure 26B) and bound to E-selectin (Figure 26D) and the corresponding conformational model (respectively, Figure 26A and C). According to the simulation, the reduction of the flexibility of the molecule enhanced in the bound state. The agreement between the acid orientation and core conformation obtained from both states is representative of a good pre-organization of the antagonist. In addition, this pre-organization fits with the bioactive window and the favorable region determined by trNOE-NMR.

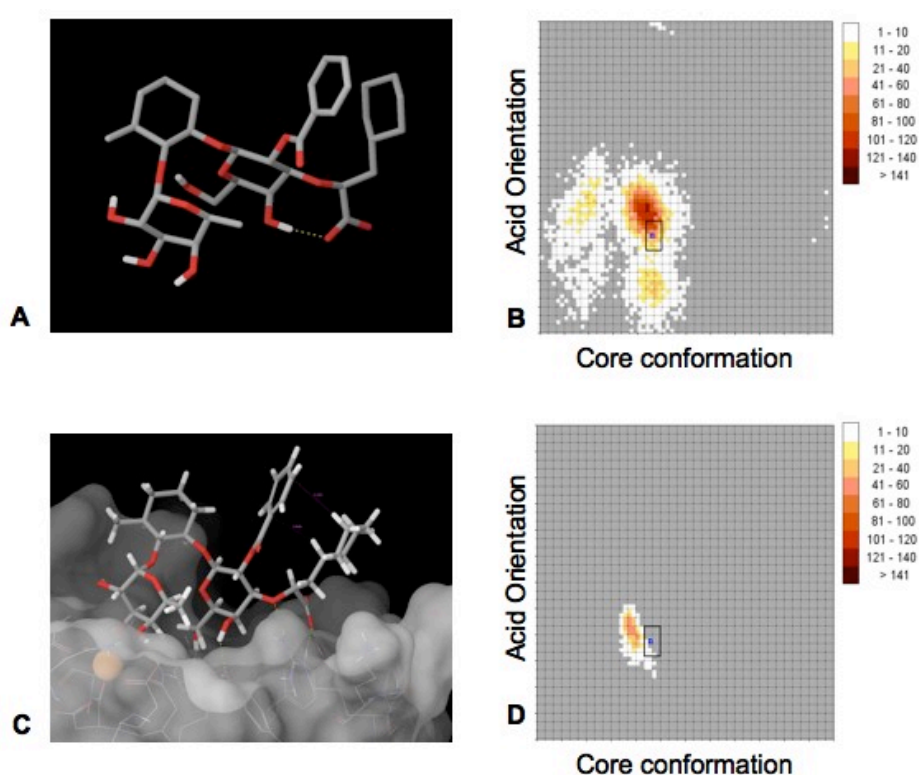


Figure 23. Conformation of **GMI-1077** in solution (A), docking model (C) and MC(JBW)/SD-simulations and obtained for **GMI-1077** in solution (B) and bound to E-selectin (D).

In a next step, R³ was further modified (Table 15). By increasing the steric hindrance in this position, a reduction of the ligand flexibility and therefore, an improvement of the pre-organization of the antagonist in the bioactive conformation is expected. As a consequence, an improved potency of the ligand results.

An affinity similar to **GMI-1077** was observed with R³ being an ethyl group (**DS-0567**) whereas a loss of affinity by a factor of five was observed with a cyclopropyl group (**DS-0565**).

Table 15. Additional modifications at R³ and first modification at R⁴ and the corresponding K_D values.

Entries	Compound	R ¹	R ²	R ³	R ⁴	rIC ₅₀ (competitive binding assay GMI, sLe ^x =1)	K _D [μM] (Biacore)
1	BW-69669	Na	H	H	H	0.080	45
4	GMI-1077	Na	Bz	Me	H	0.004	1.45
5	DS-0567	H	Bz	Et	H	0.007	1.49
6	DS-0565	H	Bz	CyPro	H	0.032	5.36
7	DS-0548	H	Bz	(CH ₂) ₂ COOMe	H	0.008	1.62
8	DS-0560	H	Bz	Me	COOMe	-	1.9

Ester groups introduced in position R³ (**DS-0548**) and R⁴ (**DS-0560**) lead to no significant change in the binding affinity compare to **GMI-1077**. The results obtained with the Biacore assay are in good agreement with the rIC₅₀ of the cell-free competitive binding assay.

In a subsequent series of modifications, the 2-position of galactose was acylated in order to investigate the influence of steric hindrance, polarity, orientation of a substituent in this position (Table 16, entries 7 to 10).

Table 16. Additional modifications at R² and the corresponding K_D values.

Entries	Compound	R ¹	R ²	R ³	R ⁴	rIC ₅₀ (competitive binding assay GMI, sLe ^x =1)	K _D [μM] (Biacore)
4	GMI-1077	Na	Bz	Me	H	0.004	1.45
9	BW-510	Na	<i>para</i> fluoroBz	Me	H	0.005	1.26
10	BW-529	Na	<i>para</i> methoxyBz	Me	H	0.006	0.37
11	BW-534	Na	cyclopropylcarboxylate	Me	H	0.006	2.05
12	BW-570	Na	acetamide	Me	H	-	1.23

In conclusion, an enhancement of the binding by a factor of 120 was observed between the lead compound **BW-69669** (K_D= 45 μM) and the best compound **BW-**

529 ($K_D = 0.37 \mu\text{M}$). An improvement of the affinity by a factor of 30 was observed between **BW-69669** and **GMI-1077**. Nevertheless, none of the modifications in position R^2 and R^3 – despite of **BW-529**, showed a significant improvement of the affinity.

3.3.4 Kinetic evaluation of BW-69669 derivatives

Carbohydrates-lectin interactions usually exhibit low affinity and fast association and dissociation rates. Slectins are not an exception as shown for their interaction with physiological ligands [70-72]. One factor, which rationalizes these fast rates, is certainly the shallowness of selectin binding pocket.

All **BW-69669** derivatives exhibited similar fast kinetic profiles as shown in Table 17. In addition, the steady state was reached within a few seconds and stayed stable during the injection time.

Table 17. Kinetic and affinity evaluation of **BW-69669** derivatives.

Analyte	$k_{on} [10^5 \text{ M}^{-1} \text{ s}^{-1}]$	$k_{off} [\text{ s}^{-1}]$	$K_{D \text{ kin}} [\mu\text{M}]^*$	$K_{D \text{ eq}} [\mu\text{M}]^{**}$	$t_{1/2} [\text{ s}]^{***}$
BW-529	8.9	0.3	0.3	0.3	2.6
BW-570	2.7	0.3	1.3	1.2	2.0
BW-510	2.2	0.3	1.4	1.3	2.3
GMI-1077	8.5	0.9	1.0	1.5	0.8
DS-0567	2.0	0.3	1.6	1.5	2.2
DS-0548	2.0	0.3	1.8	1.8	2.0
DS-0560	77.0	1.9	1.6	1.6	0.4
BW-534	n.d.	0.6	n.d.	2.5	1.1
DS-0565	1.0	0.4	3.8	4.0	1.9
DS-04115	2.0	1.3	6.6	6.5	0.5
LT-0236	n.d.	0.4	n.d.	18.8	1.8
BW-69669	0.2	1.0	51.8	50.4	0.7

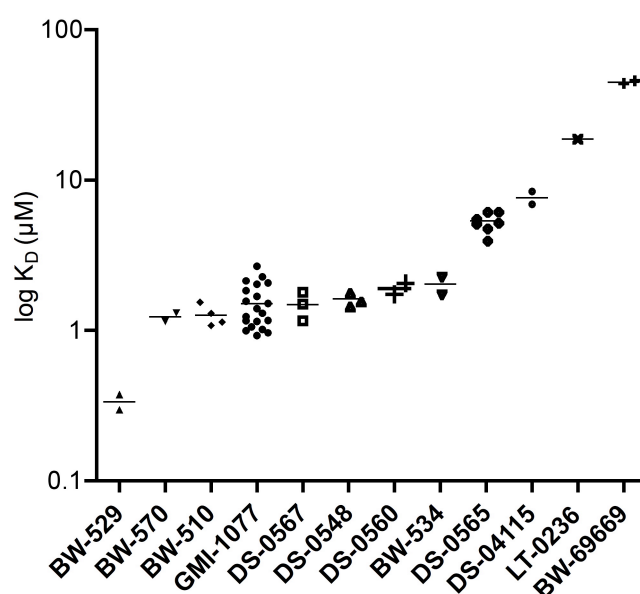
*calculated K_D using $K_D = k_{off}/k_{on}$ ** experimental K_D derived from steady state response fit to a single binding site model *** calculated $t_{1/2}$ using $t_{1/2} = \ln 2/k_{off}$.

While the observed association rates are in a correct range for drug-like molecules, the fast dissociation rates are not suitable. A fast off rate can be compensated by increasing concentrations of the compound and/or by optimizing the ligand. The first approach is prohibitive for a drug molecule. Therefore, the second

approach was used in the selectin project (see Chapter 5). In addition, for a drug-like profile, a further improvement in affinity to the low nanomolar regime would be desired.

3.3.5 Reproducibility in Biacore experiments

Most of the compounds were measured repeatedly on the same surface as well as on different CM5 chips. In order to evaluate the reproducibility of the E-selectin/IgG capture assay, all the K_D s were analyzed by fitting the steady-state to a 1:1 binding model. The results are presented in Figure 27. The number of measurements varies between one (for **LT-0236**) and twenty (for **GMI-1077**).



	BW-529	BW-570	BW-510	GMI-1077	DS-0567	DS-0548	DS-0560	BW-534	DS-0565	DS-04115	LT-0236	BW-69669
Number of values	2	2	4	20	3	3	2	2	7	3	1	2
Mean K_D [μ M]	0.34	1.23	1.27	1.5	1.49	1.62	1.9	2.3	5.36	7.64	18.80	44.90
Std. Deviation	0.06	0.11	0.21	0.51	0.32	0.17	0.23	0.05	0.79	1.07	/	1.27
CV	0.16	0.09	0.16	0.34	0.22	0.11	0.12	0.20	0.15	0.14	/	0.03

Figure 27. K_D reproducibility in Biacore measurements measured at 25°C. For repeated measurements, dashes are drawn indicating average values. **GMI-1077** with the highest number of measurements is highlighted. The coefficient of variation (CV) is defined as the ratio of the standard deviation to the mean. It indicates the variance of the distribution and a $CV < 1$ is considered as low-variance.

As shown in Figure 27, the coefficient of variation (CV) is significantly lower than 1, indicating the stability and the reproducibility of the assay (low-variance). The analysis of these data demonstrates the high degree of reproducibility of the Biacore results and clearly shows the improvement of the affinity achieved by modifying the lead compound **BW-69669**. A linear correlation ($R^2 = 0.83$) between the K_D s (Biacore steady-state signals) and the rIC_{50} (static cell-free assay) was obtained with a double-logarithmic scale (Figure 28). The self-consistency of the measured affinities supported the accuracy of the Biacore data.

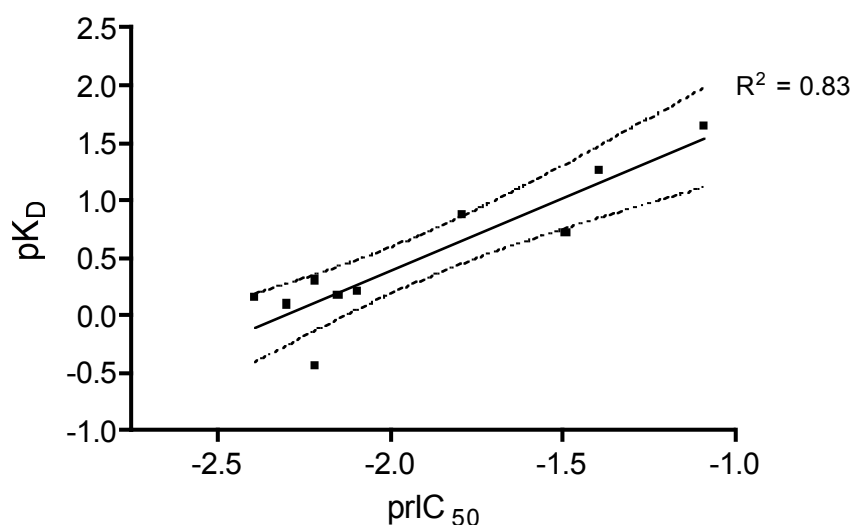


Figure 28. Linear correlation between K_D and rIC_{50} values on a double logarithmic scale. 95% confidence interval is shown in dash lines. **DS-0565** and **DS-04115** are situated at the limit of the interval of confidence and **BW-534** is out of this interval.

3.3.6 Thermodynamic analysis

For a better understanding of the interaction of antagonists with E-selectin, it was of interest to determine the entropic and enthalpic contributions to the binding. A detailed enthalpy/entropy characterization of carbohydrate-plant lectins with a Biacore 2000 was successfully performed and provided interesting information [73]. Biacore 3000 also has the capacity for such thermodynamic studies [74].

DS-04115, **GMI-1077**, **DS-0567** and **DS-0565** were selected for this analysis (Table 15). With **DS-04115** and **GMI-1077**, the influence of a benzoate group in the 2-position of galactose on the enthalpy/entropy contribution could be studied. **DS-0567** and **DS-0565** were chosen for studying the influence of different R^3 substituents.

The analytes were measured at different temperatures between 10 °C and 30 °C with an increment of 2.5 °C and evaluated by applying a van't Hoff plot. Enthalpy (ΔH) and entropy (ΔS) parameters were calculated using Eq. (5) *via* the slope ($\Delta H/R$) and the y-intercept ($-\Delta S/R$). The free enthalpy (ΔG) was calculated using the Eq. (6).

$$\ln(K_D) = (\Delta H/R) \cdot 1/T - (\Delta S/R) \quad (5)$$

$$\Delta G = \Delta H - T\Delta S \quad (6)$$

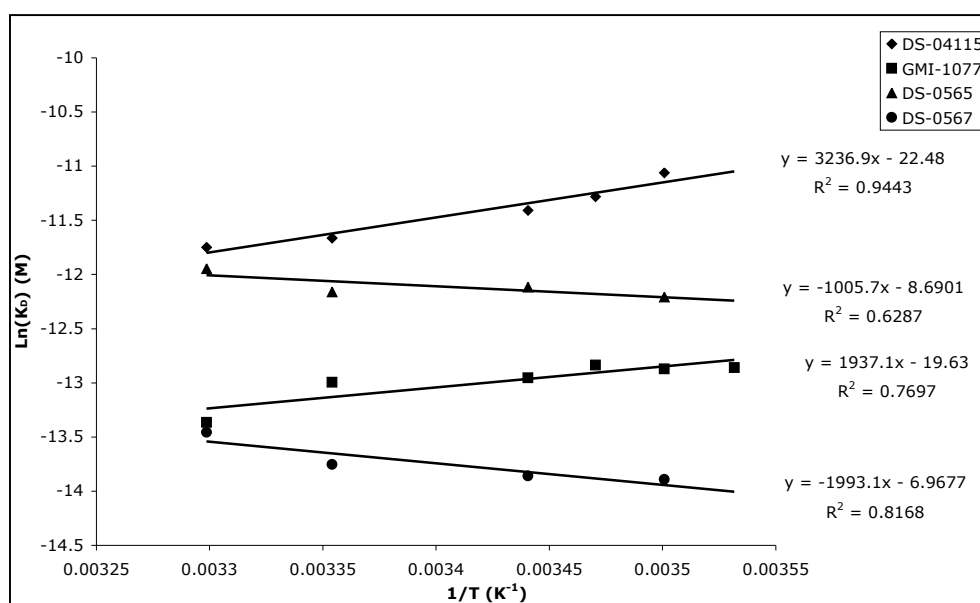
The introduction of a benzoate group in the 2-position of galactose led to an enhancement of enthalpy and a loss of entropy (Table 18, **DS-04115** vs **GMI-1077**). An additional enhancement of enthalpy was observed by replacing the methyl by a cyclopropyl group in the 5-position of GlcNAc mimic moiety (Table 18, **DS-0565**). A further decrease in enthalpy was observed in presence of an ethyl in the 5-position of GlcNAc mimic moiety (Table 18, **DS-0567**).

A drop in the entropy was observed by replacement of the methyl group in R³ position by an ethyl or a cyclopropyl (Table 18, **GMI-1077** vs **DS-0567** and **DS-0565**). The entropy contribution was almost not affected between **DS-0565** and **DS-0567** indicating that both substituents in R³ position contribute in a similar way.

The evolution of the enthalpy contribution was correlated with a variation of the affinity. The unexpected positive enthalpy observed for **DS-04115** and **GMI-1077** remains unclear and cannot be explain by a non-linear heat capacity in the range of temperature analyzed. Indeed, analyses of the data with linear and non-linear heat capacity were performed and the increment between temperature measurements was decreased. However, all conditions led to the same thermodynamic profile.

Table 18. Thermodynamic characterization **DS-04115**, **GMI-1077**, **DS-0567** and **DS-0565** of the binding of to E-selectin/IgG obtained by SPR at 25 °C and associated linear regression of the Van't Hoff plot.

Analyte	K_D [μ M]	N	$\Delta G_{\Delta H-T\Delta S}$ [kJ/mol]	ΔH [kJ/mol]	$T\Delta S$ [kJ/mol]
DS-04115	7.64	1.00	-28.9	+26.89	55.75
GMI-1077	1.5	1.0	-32.54	+16.09	48.6
DS-0565	5.36	1.0	-29.88	-8.35	21.46
			-29.94	-10.2	19.68
			-29.67	-10.89	18.8
DS-0567	1.49	1.0	-33.82	-16.56	17.26



5.3.7 Reverse assay

JE-14 was specifically designed and synthesized in-house by Jonas Egger in order to be covalently linked onto a CM5 sensor chip surface (Figure 29).

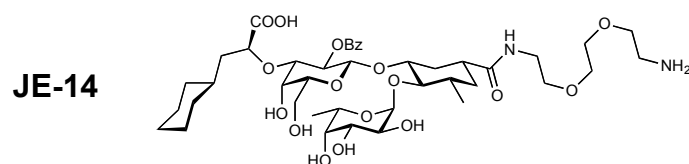


Figure 29. Chemical structure of **JE-14**

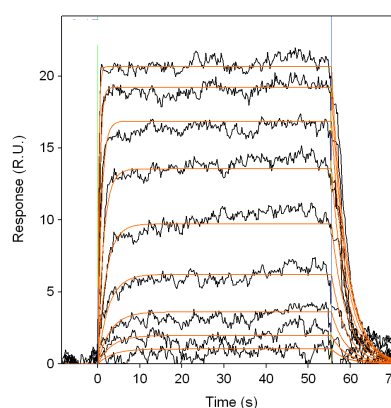
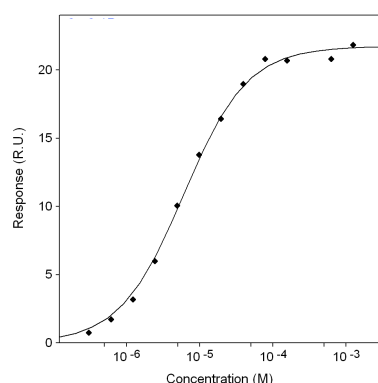
Evaluation of JE-14 with the E-selectin/IgG capture assay

In a first step, **JE-14** was evaluated using the optimized E-selectin/IgG capture assay. Fast binding kinetic were observed and an experimental K_D value of 6.01 μM was measured from the steady state fit of the sensorgrams to a 1:1 binding model (Table 19). The K_D calculated from the kinetic parameters is also reported.

Table 19. Kinetic and affinity evaluation of **JE-14**. Equilibrium binding isotherm plot and kinetic fit of the sensorgrams are shown in the bottom.

Analyte	$k_{\text{on}} [10^4 \text{ M}^{-1} \text{ s}^{-1}]$	$k_{\text{off}} [\text{s}^{-1}]$	$K_{\text{D kin}} [\mu\text{M}]^*$	$K_{\text{D eq}} [\mu\text{M}]^{**}$	$t_{1/2} [\text{s}]^{***}$
JE-14	4.43	0.28	6.32	6.01	2.47

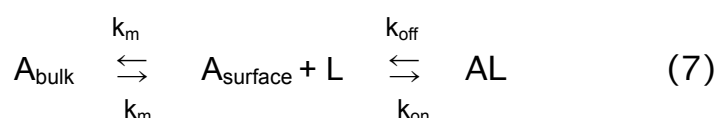
*calculated K_D using $K_D = k_{\text{off}}/k_{\text{on}}$ ** experimental K_D derived from the steady state response fit to a single binding site model *** calculated $t_{1/2}$ using $t_{1/2} = \ln 2/k_{\text{off}}$.



Reverse assay with LecEGF_CR2 construct

In order to validate the quality of the K_D s from the capture assay, **JE-14** was coupled to the surface *via* the standard amine coupling procedure. Four ratios of **JE-14**/ethanolamine (1:1, 1:10, 1:50 and 1:100) were injected on activated surfaces at a final concentration of 1 mM of **JE-14**. Ethanolamine (EA) was co-injected with **JE-14** in order to neutralize activated carboxyl groups of the dextran matrix and therefore modulate the density of **JE-14** immobilized onto the surface. This procedure led to decreased densities of **JE-14** immobilized onto the different surfaces. The affinity of LecEGF_CR2 construct (Ph.D. thesis of Roland Preston) for the linked compound was evaluated by injection of a serial dilution of the LecEGF_CR2 construct starting at 40 μM (Table 20).

Optimal density of **JE-14** needs to be determined for minimizing the mass transfer effect and the phenomenon of rebinding of the LecEGF_CR2 construct to the surface. Diffusion and convection directly influence the mass transfer of the analyte from the bulk solution to the surface. Complications due to mass transfer disturb the binding event by introducing a second equilibrium [Eq.(7)].

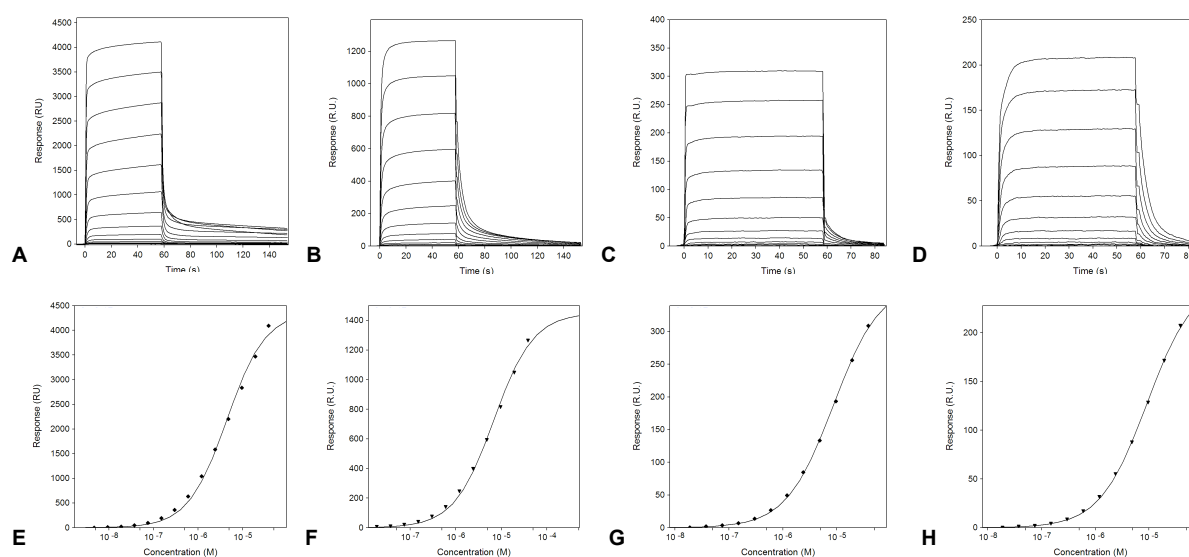


Mass transfer depends on the flow cell dimension (limited impact due to miniaturized flow cells in Biacore system), the diffusion coefficient of the analyte and the flow rate of the bulk solution. Therefore, high molecular weight of analytes such as 70 kDa for the LecEGF_CR2 construct, risk to show mass transfer effects. Increasing the flow rate can reduce the influence of mass transfer. However, since a relatively high flow rate of the bulk solution, 20 $\mu\text{l}/\text{min}$, was already used, it was maintained in order to stay as close as possible to the conditions used in the capture assay.

A second parameter for limiting the mass transfer effect was the density of the immobilized ligand. With a ratio 1:100 of **JE-14**/EA, a 1:1 binding model, which included mass transfer effects showed a coefficient for mass transfer of $10^8 \text{ M}^{-1}\text{s}^{-1}$. The estimate mass transfer coefficient was much higher than the k_{on} of approximately $10^4 \text{ M}^{-1}\text{s}^{-1}$. Therefore, the conditions for immobilization of **JE-14** which led to a high signal-to-noise ratio did not exhibit rebinding of the analyte on the surface (flat steady state and rapid return to the baseline at the end of the injection) and showed a negligible mass transfer effect (Table 20).

Table 20. Evaluation of the affinity and binding kinetics of **JE-14** for the LecEGF_CR2 construct under different conditions of coupling of the ligand on the surface. The corresponding sensorgrams and equilibrium binding isotherm plots are presented below. **A,E:** **JE-14/EA** 1:1; **B,F:** **JE-14/EA** 1:10; **C,G:** **JE-14/EA** 1:50; **D,H:** **JE-14/EA** 1:100.

Ratio JE-14/EA	k_{on} [$10^4 M^{-1}s^{-1}$]	k_{off} [s^{-1}]	$K_{D\ kin}$ [μM]*	$K_{D\ eq}$ [μM **]	$t_{1/2}$ [s]***	R_{max} [RU]
1:1	n.d.	n.d.	n.d.	4.42	n.d.	4'380
1:10	n.d.	n.d.	n.d.	6.81	n.d.	1'450
1:50	n.d.	0.12	n.d.	8.6	5.9	375
1:100	3.23	0.28	8.72	8.88	2.46	254



The k_{on} and k_{off} were similar in the reverse assay and in the captured assay. Except for the 1:1 ratio, higher K_D s were observed in the reverse assay. This fluctuation of about 30% was in the range of those observed with the capture assay. This result confirms the accuracy of the capture assay used for evaluation of E-selectin ligands.

Reverse assay with E-selectin/IgG

The affinity of E-selectin/IgG for the linked compound was also evaluated by injection of a serial dilution of the E-selectin/IgG starting at 58 μM over the surface containing the lowest density of immobilized **JE-14**. The assay was run in presence of 5% DMSO in order to have measurement conditions as close as possible to the capture assay. As shown in Figure 30A, a fit with the simple 1:1 binding site model

failed. Nevertheless, the binding signals obtained showed a nearly perfect fit by using a 1:2 binding model (Figure 30B).

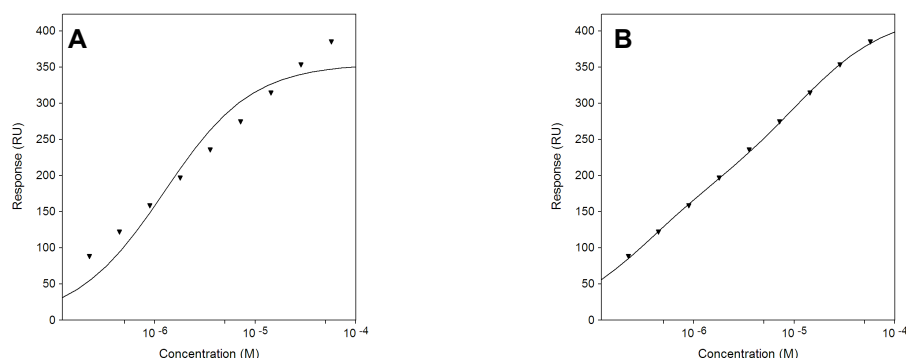


Figure 29. Binding isotherm plot of **JE-14** for E-selectin/IgG using a 1:1 binding model (**A**) and a 1:2 binding model (**B**).

The two binding events were analyzed independently as shown in Figure 31 A first binding event occurred in the micromolar range ($K_D = 12.1 \mu\text{M}$) and a second in the nanomolar range ($K_D = 320 \text{ nM}$).

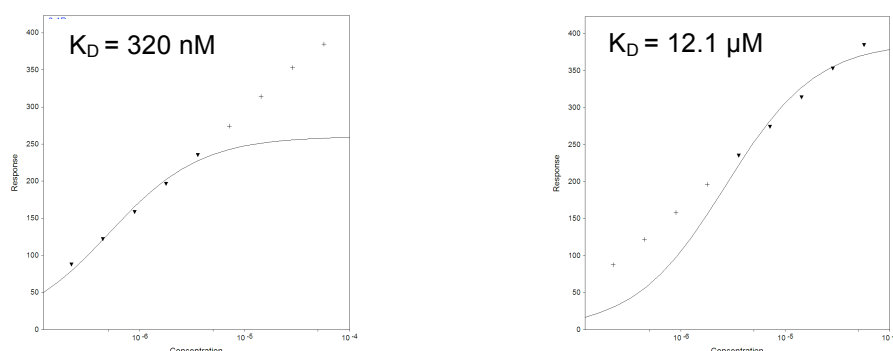


Figure 31. Isolation of the 2 binding events observed in the biacore reverse assay for characterizing the binding of **JE-14** to E-selectin/IgG.

The dimeric form of E-selectin (IgG construct) can explain the two observed binding events. Indeed, the protein is expressed as a dimer due to the presence of the Fc part in the construct. A lower density of **JE-14** on the surface would probably lead to the observation of only one binding event in the micromolar range, similar to the value observed in the capture assay.

It is known from NMR studies (see chapter 4) and from competitive polymer binding assay that both, LecEGF_CR2 construct and E-selectin/IgG have similar affinities for mimics of sLe^x. Therefore, to avoid complications due to the dimer form of the E-selectin with an IgG(Fc) construct, LecEGF_CR2 construct will be used in future reverse assay experiments.

3.4 Conclusion

The selectins have been one of the most actively studied families of carbohydrate-binding proteins since their discovery in the 1980's. Because of their key-role in leukocytes recruitment, selectins are involved in many acute or chronic inflammatory diseases (e.g. arthritis, asthma, allergies, stroke) as well as in cancer. In inflammatory diseases, non-steroidal or steroid-based drugs are available, but show well-documented side effects. An antibody therapy against chronic inflammatory diseases recently emerged, but its utility is limited by high costs. Consequently, the modulation of leukocyte recruitment *via* interference with cell tethering is of high therapeutical interest. For cancer treatment, a combined approach with chemotherapy and administration of a selectin antagonist is likely to be more efficient. Therefore, the identification of a potent selectin antagonist would present new therapeutic opportunities.

One of the research themes at the Institute of Molecular Pharmacy (IMP) is aimed on identifying carbohydrate mimics based on the natural ligand of selectin. By determining the pharmacophores relevant for the binding event and optimizing the pre-organization of the core of the ligands, **BW-69669** was developed as a lead compound. Based on this tetrasaccharide mimic, several ligands were synthesized in order to further improve the potency. In order to evaluate the impact of chemical modification of the ligands on the binding event, a fast and reliable assay was needed. Biacore technology was available in-house with the advantage of lacking the need of any labeling, allowing real-time detection and high degree of automation, the necessity of low consumption of protein and ligands and giving access to kinetic and affinity parameters. Nevertheless, analyzing small molecules like carbohydrates can be very challenging, since the intensity of the signal is directly related to the size of the analyte. After failing in the direct amine coupling of the E-selectin to the surface, a stable capture assay *via* anti-human IgG was successfully established and allowed the evaluation of numerous E-selectin ligands. Together with NMR studies (see Chapter 4), cell-free static assays, ITC measurements and MC(JBW)/SD-simulations, the Biacore results provide useful information for the design of more potent antagonists. As shown in this chapter, an improvement of the affinity by a factor of 120 was observed between **BW-69669** and the highest affinity compound, **BW-529**. Nevertheless, **BW-529** is an exception and for most of the derivatives synthesized, the

affinity reached only low micromolar affinity (e.g. **GMI-1077**, **DS-0567**). Thermodynamic studies showed an evolution of enthalpy and entropy contributions by introducing chemical modification in key positions for the stabilization of the bioactive conformation. However, the parameter influencing the thermodynamic behavior of the tested selectin antagonist could not be clearly attributed.

3.5 References

- [1] J.P. Carver, *Pure Appl. Chem.* **1993**, 65, 763.
- [2] P.Y.S. Lam, P.K. Jadhav, C.J. Eyermann, C.N. Hodge, Y. Ru, L.T. Bacheler, O.M.J. Meek, M.M. Rayner, *Science* **1994**, 263, 380.
- [3] R.S. McGavin, R.A. Gagne, M.C. Chervenak, D.R. Bundel, *Org. Biomol. Chem.* **2005**, 3, 2723.
- [4] R.S. McGavin, D.R. Bundel, *Org. Biomol. Chem.* **2005**, 3, 2733.
- [5] Y.S. Tsantrizos, *Accounts Chem. Res.* **2008**, 41, 1252.
- [6] A. Bastida, A. Hidalgo, J.L. Chiara, M. Torrado, F. Corzana, J.M. Perez-Canadillas, P. Groves, E. Garcia-Junceda, J. Jimenez-Barbero, A.L. Asensio, *J. Am. Chem. Soc.* **2006**, 11, 100.
- [7] B. Ernst, Z. Dragic, S. Marti, C. Müller, B. Wagner, W. Jahnke, J.L. Magnani, K.E. Norman, R. Ohrlein, T. Peters, H.C. Kolb, *Chimia* **2001**, 55, 268.
- [8] H.C. Kolb, B. Ernst, *Chem. Eur. J.* **1997**, 3, 1571.
- [9] H.C. Kolb, B. Ernst, *Pure Appl. Chem.* **1997**, 69, 1879.
- [10] K. Scheffler, B. Ernst, A. Katapodis, J.L. Magnani, W.T. Wang, R. Weisemann, T. Peters, *Angew. Chem. Int. Ed.* **1995**, 34, 1841.
- [11] D. Schwitzer, dissertation, University of Basel, **2007**.
- [12] A. Titz, dissertation, University of Basel, **2008**.
- [13] B. Ernst and L. Magnani, *Nature Review in Drug Disc.* **2009**, 8, 661.
- [14] T. Turbadar, *Proc. Phys. Soc.* **1959**, 73, 40.
- [15] A. Otto, *Z. Phys.* **1968**, 216, 398.
- [16] Surface Plasmon Resonance (Technology note 1), Biacore AB, **2001**, 1-4.
- [17] U. Johnson, L. Fagerstam, B. Ivarsson, B. Johnson, R. Karlsson *et al.* *Biotechniques* **1991**, 11, 620.
- [18] E. Stenberg, B. Persson, H. Roos, C. Urbiniczyk, *J. Colloid Interface Sci.* **1991**, 143, 513.
- [19] K.Y. Tomizaki, K. Usui, H. Mihara, *ChemBioChem* **2005**, 6, 783.
- [20] S. Loefas, *Pure Appl. Chem.* **1995**, 67, 829.
- [21] Y. Suwa, T. Yamauchi, M. Kito, Y. Isono, T. Tamura, M. Tobita, Japanese Patent 20090136482, **2009**.

- [22] K.M. Halkes, P.M. St Hilaire, P.R. Crocker, M. Meldal, *J. Comb. Chem.* **2003**, 5, 18.
- [23] R. Karlsson, M. Kullman-Magnusson, M.D. Hamalainen, A. Remaeus, K. Andersson, P. Borg, E. Gyzander and J. Deinum, *Anal. Biochem.* **2000**, 278, 1.
- [24] D.G. Myszka, T.A. Morton, M.L. Doyle, I.M. Chaiken, *Biophysic. Chem.* **1997**, 64, 127.
- [25] E. Duverger, N. Frison, A.-C. Roche, M. Monsigny, *Biochimie* **2003**, 85, 167.
- [26] R.L. Rich, D.G. Myszka, *J. Mol. Recogn.* **2006**, 19, 478.
- [27] D.G. Myszka, *Curr. Opin. Biotechnol.* **1997**, 8, 50.
- [28] L.D. Roden, D.G. Myszka, *Biochem. Biophys. Res. Commun.* **1996**, 225, 1073.
- [29] M.M. Hann, A.R. Leach, G. Harper, *J. Chem. Inf. and Comput. Sci.* **2001**, 41, 856.
- [30] T.I. Oprea, A.M. Davis, *J. Chem. Inf. and Comput. Sci.* **2001**, 41, 1308.
- [31] S.J. Teague, A.M. Davis, P.D. Leeson, T. Oprea, *Angew. Chem., Int. Ed.* **1999**, 38, 3743.
- [32] H. Kubinyi, *Curr. Opin. Drug Discovery Dev.* **1998**, 1.
- [33] D.G. Myszka, X. He, M. Dembo, T.A. Morton, B. Goldstein, *Biophys. J.* **1998**, 75, 583.
- [34] Y.S. Day, C.L. Baird, R.L. Rich, D.G. Myszka, *Protein Sci.* **2002**, 11, 1017.
- [35] D. Strasser, dissertation, University of Basel, **2008**.
- [36] R.L. Rich D.G. Myszka, *Curr. Opin. Biotechnol.* **2000**, 11, 54.
- [37] I. Abraham, J.S. Tyagi and M.M. Gottesman, *Somatic cells and molecular genetics* **1981**, 8, 23.
- [38] K.P. Jayapal, *et al.*, *Chem. Eng. Pro.* **2007**, 103, 40.
- [39] GE Healthcare, Information sheet: HiTrap protein A HP 1 ml and 5 ml Instructions 71-7002-00 AN.
- [40] J. Yu, dissertation, University of Basel, **2009**.
- [41] Sigma-Aldrich, Information sheet: Cyanogen bromide activated matrices for products Nos. C9210, C9142, C9267.
- [42] H. Towbin, Staehelin T. and J. Gordon, *Proc Natl Acad Sci U S A*, **1979**, 76, 4350.
- [43] M.S. Blake *et al.* *Anal Biochem* **1984**, 136, 175.

- [44] R. Preston, S. Rabbani, B. Ernst, *unpublished results*.
- [45] M.M. Bradford, *Anal. Biochem.* **1976**, 72, 248.
- [46] F. Bitsch, R. Aichholz, J. Kallen, S. Geisse, B. Fournier, J.M. Schlaeppi, *Anal. Biochem* **2003**, 323, 139.
- [47] D. Schwitzer, Dissertation, University of Basel, **2007**.
- [48] J. Egger, B. Ernst, *unpublished results*.
- [49] G. Thoma, J. L. Magnani, R. Oehrlein, B. Ernst, F. Schwarzenbach, R. O. Duthaler, *J. Am. Chem. Soc.* **1997**, 119, 7414.
- [50] G. Thoma, J. T. Patton, J. L. Magnani, B. Ernst, R. O. Duthaler, *J. Am. Chem. Soc.* **1999**, 121, 5919.
- [51] A. Frostell-Karlsson, A. Remaeus, H. Roos, K. Andersson, P. Borg, M. Hämäläinen, R. Karlsson, *J. Med. Chem.* **2000**, 43, 1986.
- [52] K.E. Norman, G.P. Anderson, H.C. Kolb, K. Ley, B. Ernst, *Blood*, **1998**, 91, 475
- [53] C.F. Schuman, M.D. Hamalainen, U.H. Danielson, *J. Mol. Recognit.* **2004**, 17, 106.
- [54] W.S. Somers, J. Tang, G.D. Shaw, R.T. Camphausen, *Cell* **2000**, 103, 467.
- [55] R.L. Rich and D.G. Myszka, *J. Mol. Recognit.* **2001**, 14, 223.
- [56] P. Thillaivinayagalingam, J. Gommeaux, M. McLoughlin, D. Collins, A. R. Newcombe, *J. Chromatogra. B.* **2010**, 878, 149.
- [57] D. Sickert, K. Kroeger, C. Zickler, E.Chokote, B. Winkler, J.M. Grenet, F. Legay and A. Zaar, *J. Immunol. Methods* **2008**, 334, 29.
- [58] M.E. Beauharnois, K.C. Lindquist, D. Marathe, P. Vanderslice, J. Xia, K.L. Matta and S. Neelamegham, *Biochem.* **2005**, 44, 9507.
- [59] M.E. Beauharnois, S. Neelamegham, K.L. Matta, *Meth. Mol. Biol.* **2008**, 347, 343.
- [60] D. Ricklin, dissertation, University of Basel, **2005**.
- [61] W. Huber, S. Perspicace, J. Kohler, F. Muller, D. Schlatter, *Anal Biochem.* **2004**, 333, 280.
- [62] Application note 38, GE Healthcare, **2007**.
- [63] S. Sarikhani, M. Mirshahi, M.R. Gharaati, T. Mirshahi, *Appl. Biochem Biotechnol.* **2010**.
- [64] R. Banteli and B. Ernst, *Bioorg. Med. Chem. Lett.* **2001**, 11, 459.

- [65] Preparation of glycomimetic pseudo-oligosaccharides and replacements for hexoses and *N*-acetylhexosamines, PCT Int. Appl. 2008, WO 2008060378, priority date October 12, **2006**.
- [66] H. C. Kolb, B. Ernst, *Chem. Eur. J.* **1997**, 3, 1571.
- [67] H. C. Kolb, B. Ernst, *Pure Appl. Chem.* **1997**, 69, 1879.
- [68] K. Scheffler, J. R. Brisson, R. Weisemann, J. L. Magnani, W. T. Wong, B. Ernst, T. Peters, *J. Biomol. NMR* **1997**, 9, 423.
- [69] M. Rinnbauer, B. Ernst, B. Wagner, J. Magnani, A.J. Benie, T. Peters, *Glycobiology* **2003**, 13, 435.
- [70] P.Mehta, R.D. Cummings, R.P. McEver, *J. Biol. Chem.* **1998**, 273, 30506.
- [71] M.K. Wild, M.C. Huang, U. Schulze-Horsel, P. A. Van der Merwe, D. Vestweber, *J. Biol. Chem.* **2001**, 276, 31602.
- [72] M. W. Nicholson, A.N. Barclay, M.S. Singer, S.D. Rosen, P.A. Van der Merwe, *J. Biol. Chem.* **1998**, 273, 763.
- [73] P. Critchley and G.J. Clarkson, *Org. Biomol. Chem.* **2003**, 1, 4148.
- [74] C.F. Schuman, M.D. Hammalainen, U.H. Danielson, *J. Mol. Recogn.* **2004**, 17, 106.
- [75] B.J. Graves, R.L. Crowther, C. Chandran, J.M. Rumberger, S. Li, K.S. Huang, D.H. Presky, P.C. Familletti, B.A. Wolitzky, D.K. Burns, *Nature* **1994**, 367, 532.

4. Binding epitope studies of the first generation of E-selectin antagonists by STD-NMR

4.6 Introduction

4.6.1 General points

Isidor Rabi first described a “new method for measuring nuclear magnetic moment” in 1938 [1], a method which form the basis of continuous wave NMR. After the Second World War, in 1946, Felix Bloch and Edward Mills Purcell refined the technique for use on solids and liquids [2,3]. For this work, they shared the Nobel Prize in physics in 1952.

Atomic nuclei are composed of nucleons (neutrons and protons) having an intrinsic quantum property of spin. The spin quantum number I corresponds to the overall spin of the nucleus. As shown by Eq. (1), the important property for NMR is the association of the spin with a magnetic moment (μ) colinear to I , where γ is the gyromagnetic ratio, specific for each nucleus:

$$\mu = \gamma (h/2\pi) I \quad (1)$$

The magnetic moment allows the observation of NMR absorption spectra caused by transitions between nuclear spin levels. In principle, NMR involves two steps:

- Alignment of the magnetic nuclear spins in the magnetic field (B_0)
- Perturbation of the alignment of the spins by applying radio frequency pulse

Most nuclei have no nuclear magnetic moment and do not exhibit NMR absorption spectra. However, certain magnetically active nuclei (e.g. ^1H , ^{13}C , ^{15}N , ^{17}O) can adopt nuclear spin states of different energy in a magnetic field. When a radio-frequency radiation at the resonance frequency of the nucleus (Larmor frequency) is applied, these nuclei can be observed in NMR.

Ideally, each nucleus in a molecule experiences a different chemical environment and thus can be recognized by a characteristic chemical shift. Magnetization can be transferred between nuclei both through chemical bonds (spin-spin coupling) and through space over short distances (dipole-dipole coupling) [4].

NMR spectroscopy was originally dedicated mainly to the characterization of smaller molecular structures. Even in its early stage of development, it was recognized as an important technique to support pharmaceutical research. In 1965, Jardetzky *et al.* detected and characterized the binding of penicillin to serum albumin [5]. This first report of NMR as a “binding-assay”, opened the door to numerous investigations which followed [6-10]. In 1996, the publication of SAR-by-NMR by Abbott Laboratories [11] further demonstrated the potential of NMR in drug design and discovery and catalyzed its impact in pharmaceutical research. Since 15 years, many new methods, adapted to detect and quantify ligand-target interactions with high sensitivity, emerged (e.g. chemical-shift mapping, nuclear-spin relaxation, transferred nuclear overhauser effect). The possibility to obtain structural information of both the target and the ligand are two desired goals that place NMR as a major tool contributing in all phases of drug discovery [12] from primary screening to lead optimization.

4.6.2 Detection of ligand-binding by NMR methods

As already mentioned, NMR methods for detecting ligand binding can be divided in two categories: ligand-based and target-based. The following text will focus on the ligand-based methods, which were used in this thesis. In addition, since detailed theoretical framework to explain and predict how ligand-binding modifies NMR parameters was reported by Peng *et al.* [13], these issues will not be discussed further. Ligand-observation techniques are based on the detection and observation of the resonances of the free ligand. If a ligand was transiently in a bound state during the measurement, its rotational and translational motions were modified. The ligand-observation methods exploit the consequences of the transient bound state on the NMR properties: the ligand behaves as a large molecule (Figure 1) [14]. Thus, bound ligands have large transverse relaxation rates, negative and large NOEs, highly efficient spin-diffusion and small molecular diffusion coefficients.

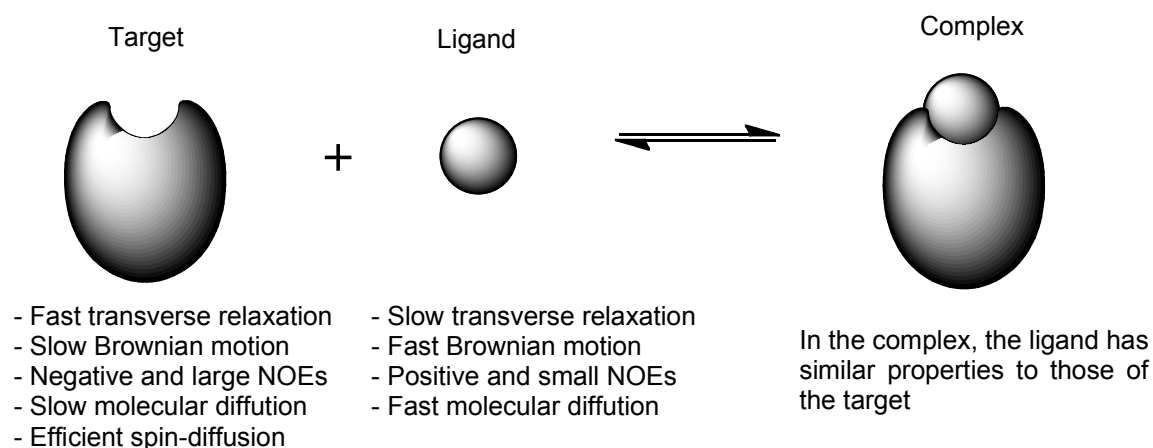


Figure 1. NMR properties of small molecules in a unbound and in an bound form.

One can cited four main advantages of ligand-based methods [15]:

- Small quantities of target are required (typically 1-10 μM).
- No labeling of the target is required.
- Rapid evaluation of new targets is possible.
- Majority of ligand-based screening NMR uses ^1H NMR.

The main disadvantages are the required solubility of the ligands and the inability to localize the binders on the receptor, as well as a risk of non-specific binding increased by the use of high concentration of ligands. Ligand concentrations of a few hundred micromolar are usually required to obtain meaningful data. These limitations tend to be minimized due to improvements in the instrumentation, which require less and less material, while still keeping a similar or even better sensitivity (e.g. cryoprobes, advent of the first 1 GHz NMR spectrometer in 2009 in Lyon, France [16]). Recent development in the methods also greatly ameliorated the previously cited limitations [17,18]. Finally, a major drawback of the ligand-based methods is the need for significant dissociation during the experiments. For this reason, only weak ligands can be observed directly when the concentration of the ligand is considerably larger than that of the receptor (affinity range between few micromolar up to millimolar) [13]. Tightly binding ligands with slow off rates appear as non-binders and therefore the risk of false negative is non-negligible. Several methods exist to overcome this problem, for example competition assays have been

developed e.g. NMR reporter screening [19-21]. If the receptor is available in large quantities, a stoichiometric ratio of the ligand to receptor can directly reveal tight binding.

Two categories of ligand-based experiments are distinguished:

- those exploiting the alteration of the relaxation parameters and diffusion coefficients (selective T_1 and T_2 enhancement) [22],
- those exploiting ^1H magnetization transfer from the target to the bound ligand (STD and waterLOGSY).

These methods are largely used at the Institute of Molecular Pharmacy to provide crucial information in the current drug discovery and development projects from ligand screening to binding epitope and conformational analysis [23]. Their application to the development of E-selectin antagonists is presented in the following two chapters of this PhD work.

4.6.2.1 **Methods based on relaxation enhancement**

In the presence of the protein, an increase of the relaxation rate observed via a faster attenuation of the ligand signal at long relaxation periods is a strong evidence for the binding [7,8, 24, 25]. The effect can be enhanced by the attachment of spin labels to the protein [26].

Transverse relaxation rates

This method was and is the most commonly used, mainly due to its dependence on the overall molecular rotational correlation time, τ_C . Indeed, when the ligand binds to the target, its τ_C becomes transiently as large as for the target. Since the rate of transverse relaxation, R_2 , increases monotonically with τ_C , the $R_{2,\text{bound ligand}} \gg R_{2,\text{free ligand}}$.

To detect the binding, it is possible to compare the height and broadening of resonance lines in the ^1H NMR spectrum of a ligand on the addition of the target.

This is due to the fact that the homogeneous linewidth has a fullwidth at half maximum height (FWHM) for a given resonance of R_2/π . The peak height is also affected and proportional to $1/R_2$.

Comparison of peak heights in the presence and in absence of the target allows the measurement of the free and the bound R_2 rates by using a spin-lock (e.g. a CPMG pulse train or continuous-wave irradiation) as in $R_{1\rho}$ experiments. In such experiment, relaxation times are chosen such that the resonances of the target molecule are filtered away but not the resonances of binding ligands.

In the case of weakly binding molecules and/or low ligand concentrations, the sensitivity of the detection is improved by subtracting the spectrum of the target alone from all spectra prior to analysis [25].

Selective longitudinal relaxation rates

The selective longitudinal relaxation time (sR_1) of a ligand is also a parameter altered by a binding to a macromolecular target. The measurement of a selective R_1 is based on the inversion recovery measurement of a restricted frequency range. Selective R_1 experiments can also be applied in a screening process with the conditions to have isolated and well assigned resonances and to define a separate inversion-recovery pulse for each ligand [27].

4.6.2.2 Methods based on NOEs measurements

A sensitive detection experiment is the saturation transfer difference (STD), which measures the transfer of NOE magnetization from the target to the ligand upon protein saturation [7,9,14,24,28]. In this experiment, a difference spectrum is generated, as indicated in its name. In a first on-resonance experiment, a train of frequency-selective radio-frequency pulses is applied to the receptor in a region of the spectrum that does not contain resonances of the ligand. *Via* an efficient process of spin-diffusion (due to the large molecular weight of the target), the saturation propagates through the target macromolecule. At the ligand-target interface, the saturation is transferred to the bound ligand *via* intermolecular ^1H - ^1H cross relaxation. In a second experiment, so-called reference experiment, the radio-frequency train

pulses are applied off-resonance. The difference between the on- and off-resonance experiments yields the resonances from the ligand that have experienced saturation. Applying an R_2 relaxation filter prior to detection eliminates the resonances of the target in the on-resonance spectrum. The main advantages of STD-NMR are: (i) the efficiency of the method with large target macromolecules, (ii) the requirement of low quantities of target, and (iii) that only ligands which bind are detected. In 2001, Mayer and Meyer introduced the concept of an “amplification factor” in STD experiment [29]. It was suggested to accurately estimate the affinity constant (K_D) of ligands by including this factor that provides an average of the saturated ligand turn-over per target. One limitation of the methods is for high-affinity ligands with a long residence time. Thus, if the turn-over of saturated ligand is too slow, the population of unbound saturated ligands decreases and no STD signal can be recorded. The range of K_D suitable for STD methods was estimated between 10^{-3} and 10^{-8} M [28]. Nevertheless, competition STD NMR methods were developed for the detection of high-affinity ligands [30]. Many parameters also influence the sensitivity of the method such as: efficient magnetization transfer through the target, thus challenging its applicability to low proton density receptors, such as oligonucleotide targets. In addition, the degree of saturation of the receptor is dependent on a competition between the influx of magnetization and various R_1 relaxation and leakage mechanism (by exchange with solvent protons). Finally, STD is compromised for low molecular weight targets (risk of inefficient spin diffusion) [13].

In the context of this thesis, STD was applied to determine the epitope mapping of sLe^x bound to E-selectin [31]. Dr. Brian Cutting enhanced the sensitivity of the methods through optimization of the excitation scheme [32]. In the present chapter, STD experiments were performed on a first-generation of E-selectin antagonists in order to get further information on the binding epitopes of those compounds.

A second method called **Water-Ligand Observed via Gradient Spectroscopy** (waterLOGSY), is based on the magnetization transfer from the bulk solvent (water) to the bound ligand [33]. This experiment is closely related to STD but in that case the energy is transferred first to the water, then to the receptor and finally to the ligand. Binding compounds are distinguished from non-binding by their differential

cross-relaxation properties with water. For the binding ligands, the magnetization is transferred rapidly *via* dipole-dipole interactions to the ligand with a long rotational correlation time due to the concomitant contact with the target. This is not the case for non-binding ligands. As a consequence, cross-relaxation rates are opposite and of different magnitudes and thus, waterLOGSY signals of binding and non-binding ligands are also opposite in sign. In 2008, Günthner and coworkers described a new NMR method called SALMON (Solvent Accessibility, Ligand binding, and Mapping of ligand Orientation by NMR spectroscopy) based on waterLOGSY for the determination of the orientation of a ligand bound to its target by mapping its solvent accessibility [34]. In this approach, all protons on non-exchangeable position were replaced by deuterium. Therefore, the protonation due to the dissolution in water, required for waterLOGSY, was only possible in exchangeable positions of the backbone and side chains. The minimal protonation of the target limited NOEs that were not from H₂O and supported the fact that the magnetization transfer from water to the ligand in the presence of the protein was attributed to water molecules bound to the surface of the target.

4.7 Material and methods

4.7.1 Instrumentation

All spectra were recorded in-house with a Bruker DRX-500 (Bruker BioSpin AG, Fällanden, Switzerland) equipped with Z-gradient SEI probe. Relaxation, STD, COSY and TOCSY experiments were measured at 298.15 K, without spinning, and with a gas flow of 250 l/h. trNOESY experiments were measured at 310 K with a spin rate of 20 Hz, the gas flow increased to 400 l/h. Competitive selective T1 experiment were measured at 278.15 K with a spin rate of 20 Hz, the gas flow increased to 400 l/h.

In order to limit the protein consumption, Shigemi tubes (Sigma Aldrich GmbH, Buchs, Switzerland) were used for samples containing E-selectin. A volume between 230 and 250 μ l was prepared. For samples containing only the ligand, a 500 μ l volume was prepared and ordinary 5 mm NMR tubes were used (Sigma Aldrich GmbH, Buchs, Switzerland). All tubes were cleaned with bidistilled water and washed twice with D₂O. Most of the experiments were manually run. In a few cases the automatic sampler charger (B-ACS 60, Bruker BioSpin AG, Fällanden, Switzerland) was used.

Before each experiment, the spectrometer was optimized for the sample introduced in order to achieve an optimum resolution and sensitivity. The first procedure is the so-called “tuning and matching” of the probe head. It consists of an adjustment of the electrical properties of the coiled circuit for an optimal transmission of the radiofrequency pulses and an optimal reception of the signals. The procedure was done manually or by using the automated command of XWINNMR 3.6 or TOPSPIN 2.1. In a second step, the field frequency was locked according to D₂O in order to keep the magnetic field homogeneity constant. Finally, an optimization of the field homogeneity was done by “shimming”. The procedure was done manually or by using the automated command of XWINNMR or TOPSPIN. To verify the optimization of the spectrometer to the sample, a single-pulse experiment, preceded by a low-amplitude presaturation pulse, was recorded for each sample.

4.7.2 Reagent

After expression and purification, the E-selectin/IgG and the LecEGF_CR2 proteins were concentrated using centrifugal filter devices (Amicon® Ultra-4, 10k molecular weight cut-off from Millipore Corporation, Billerica, MA, USA) at 6,000 rpm at 4 °C. Following the concentration, a buffer exchange was performed with a deuterated buffer (*pH* 7.4, 20 mM *d*11-Tris, 150 mM NaCl, 1 mM CaCl₂ in D₂O, Armar Chemicals) using the same centrifugal filter device. Protein samples between 15 and 60 μM binding site concentrations were used in NMR experiment.

Fifty mM stock solutions of all the ligand used was prepared in *d*6-DMSO. The final concentration of *d*6-DMSO did not exceed 10 % in samples containing protein. Ligand samples without protein were diluted either in D₂O or in deuterated buffer.

4.7.3 Software

Bruker software XWINNMR version 3.6 and TOPSPIN version 2.1, operating on a PC running under Linux OS, were used as the interface with the spectrometer and to analyze the NMR data. MestReNova version 5.2.3-3833 was used for off-line analysis of the spectra. Prism 4 (GraphPad Software Inc., San Diego, USA) was used to fit the relaxation data.

4.7.4 Experiments

4.7.4.1 Relaxation experiments

Spin-spin relaxation experiments

The E-selectin/IgG was present at 20-30 μM in binding site concentration as determined by Bradford assay. A 50 mM stock solution of compound in *d*6-DMSO was prepared and diluted with deuterated buffer (*pH* 7.4, 20 mM *d*11-Tris, 150 mM NaCl, 1 mM CaCl₂ in D₂O, Armar Chemicals) to a final concentration between 1-5 mM in the samples. Prior to the relaxation experiment, a calibration pulse width was performed. For that purpose, a series of experiment with progressively incremented excitation pulse duration were recorded. The 360° null was used for the calibration. The pulse sequence used for T1ρ determination was adapted from Hajduk [35]. To

determine the $T_{1\rho}$ relaxation rate, six experiments were performed with different durations of the continuous-wave spin-locked of 2 kHz (10, 50, 100, 150, 200, 250 ms). The suppression of the signal of water was an important issue due to the presence of residual protons from solvent. Traces of non-deuterated D_2O resulted in enhanced water signals in samples containing the protein. Therefore, a DPFGE water suppression sequence was added at the end of the pulse sequence [36]. For each experiment, 8 scans were measured preceded by two dummy scans. The recovery delay between successive scans was set to 10 s and the receiver gain was adjusted to 256.

Selective spin-lattice relaxation experiment

The E-selectin/IgG was present at a binding site concentration of 10 μM , as determined by Bradford assay. The pulse sequence for a selective inversion recovery was used. A selective 25 ms I-Burp-1⁶ 180° pulse was applied to either the *ortho*-hydrogen of the benzoate group of **GMI-1077** or to the fucose H-6 of **BW-69669**. The resonances of the protons chosen were different from the water resonances to avoid artifacts due to radiation dumping [37]. In order to dephase any residual transverse magnetization, a 1 ms gradient pulse was applied after the selective pulse. For the determination of the selective inversion recovery time, a series of 10 experiments with increasing delays, to allow an increasing recovery of the longitudinal magnetization, were measured (0.075, 0.125, 0.175, 0.225, 0.3, 0.4, 0.5, 1, 2 and 3 sec).

For competitive experiments, a new series of measurements were performed at 278.15 K and the selective pulse was applied to the galactose H-1 of **BW-69669**. This proton was chosen, because, at this temperature, it did not overlap with any of the resonances of **GMI-1077**. In a first step, a sample of E-selectin/IgG (10 μM binding site concentration as determined by the Bradford assay) was titrated by **BW-69669** and the corresponding selT1 values were determined. Then, the selT1 of **BW-69669** at the concentration of 610 μM was measured in presence of E-selectin/IgG from the same batch as the one used for the determination of the titration curve. Finally, 50 μM of **GMI-1077** was added to the sample and the selT1 observed was

correlated to an apparent concentration *via* the titration curve. A relative affinity was calculated by applying the Eq. (2).

$$[\text{BW} - 69669]_{\text{apparent}} = [\text{BW} - 69669]_{\text{real}} + \frac{K_{\text{DBW} - 69669}}{K_{\text{DGMI} - 1077}} * [\text{GMI} - 1077] \quad (2)$$

4.7.4.2 STD-NMR experiments

In order to collect more information about on E-selectin/antagonists interaction, STD-NMR experiments with **GMI-1077**, **DS-0567** and **BW-580** were performed in the presence of E-selectin/IgG or the LecEGF_CR2 construct.

Pulse program parameters

Before recording STD experiment, a calibration pulse was performed on the residual H₂O resonance (4.73 ppm).

The sensitivity of the STD experiment was enhanced through the use of an optimized excitation scheme [36]. The protein was saturated by applying an E-Burp-1 90° cosine modulated selective pulse train split to two sidebands. The protein was saturated with 40 pulses of 50 ms each. The power level (sp11) was at an optimum at 51 dB and the number of scans set to 12K. For each STD, a reference (off-resonance and without inverting the receiver phase) spectrum was measured. In addition, to ensure that there were no subtraction artifacts, a control experiment was measured in the absence of the protein at a similar concentration of ligand. For the control and the reference experiment, the number of scan was reduced to 1K.

Sample

Different batches of protein were used for the STD experiment and the conditions are summarized in Table 1.

Table 1. Description of the samples used to record STD-NMR spectra.

Protein	Protein binding site concentration [μM]	Ligand	Ligand concentration [mM]
E-selectin/IgG	30	DS-0567	5
E-selectin/IgG	30	GMI-1077	1
LecEGF_CR2 construct	15	GMI-1077	1
E-selectin/IgG	60	BW-580	1
E-selectin/IgG	30	BW-69669	1
E-selectin/IgG	30	DS-0560	2

4.7.4.3 Competitive STD-NMR experiment

A competitive STD-NMR experiment was performed with **BW-69669** and **DS-0560** [38]. The same pulse program as described in section 4.2.4.2 was used. The concentration of E-selectin/IgG binding site was 15 μM and 1 mM of **BW-69669** was added to the solution. Then, increasing concentrations of **DS-0560** were added to the mixture (200 μM and 300 μM).

4.7.4.4 Group epitope mapping

Based on the STD experiment, the method of group epitope mapping (GEM) developed by Mayer *et al.* in 2001 was applied to E-selectin antagonists [39]. For each assigned resonance, a fractional STD effect was calculated by applying Eq. (3). I_0 refers to the intensity of the STD signal of the reference spectrum and I_{sat} the intensity of the same resonance in the STD spectrum.

$$\frac{(I_0 - I_{\text{sat}})}{I_0} \quad (3)$$

Each fractional STD effect obtained with Eq. (3) was normalized to the fractional STD effect obtained for the fucose H-6. This normalization allowed the

comparison between the group epitope mapping obtained for different compounds measured.

4.7.4.5 selective TOCSY and COSY experiments

Changes in the chemical shift of **DS-0567** were observed due to both binding to the E-selectin/IgG and use of a different buffer. The majority of the resonances were re-assigned using selective 1D and non-selective 2D TOCSY experiments and a COSY experiment. A sample of E-selectin/IgG, at a binding site concentration of 30 μM , was mixed with 5 mM of **DS-0567** and used to record selective TOCSY spectra. A COSY experiment was measured with a sample containing 5 mM of **GMI-1077** and with a sample containing E-selectin/IgG at a binding site concentration of 60 μM and 1.88 mM of **GMI-1077**.

4.7.4.6 trNOESY experiment

The temperature was increased to 310 K and trNOESY experiments were recorded with a sample containing 5 mM of **GMI-1077** and with a sample containing 1.88 mM of **GMI-1077** and E-selectin/IgG (60 μM binding site).

4.8 Results and discussion

4.8.1 Relaxation experiments of **BW-69669** and **GMI-1077** in the presence of E-selectin/IgG

Measurement of ligand relaxation properties was, and is, largely used to identify and characterize protein-ligand interactions. In this kind of experiment, the resonances of the ligand are observed. If the ligand is transiently bound to the E-selectin/IgG during the observation, the signal will be affected. Indeed, in the bound state, the ligand does not behave like a small molecule, but like the protein. Therefore, a faster relaxation will be observed. This can be explained by the dependence of the relaxation rates on the molecular tumbling rate (inverse of the correlation time, τ_c) [40]. A series of relaxation experiments was performed in order to check the applicability of NMR to our E-selectin/ligand studies and correlate the results with the other techniques used in the project (Biacore and ITC).

Selective spin-lattice relaxation rates (selT1) and spin-spin relaxation rates ($T1\rho$) were measured in the absence and in the presence of the E-selectin/IgG for the lead compound, **BW-69669**, and the optimized ligand, **GMI-1077**. Subsequently, a competitive selT1 experiment between the two compounds was performed.

4.8.1.1 Spin-spin ($T1\rho$) relaxation experiments

*T1 ρ relaxation of **BW-69669***

Signals were recorded after increasing spin locked times (10, 50, 100, 150, 200, 250 ms). For one selected peak, E-selectin/IgG exhibited a relaxation rate six times higher than **BW-69669**, because of the high molecular weight (296 kDa). An increase of the **BW-69669** relaxation rate was observed in presence of the protein, indicated a binding event (Figure 2).

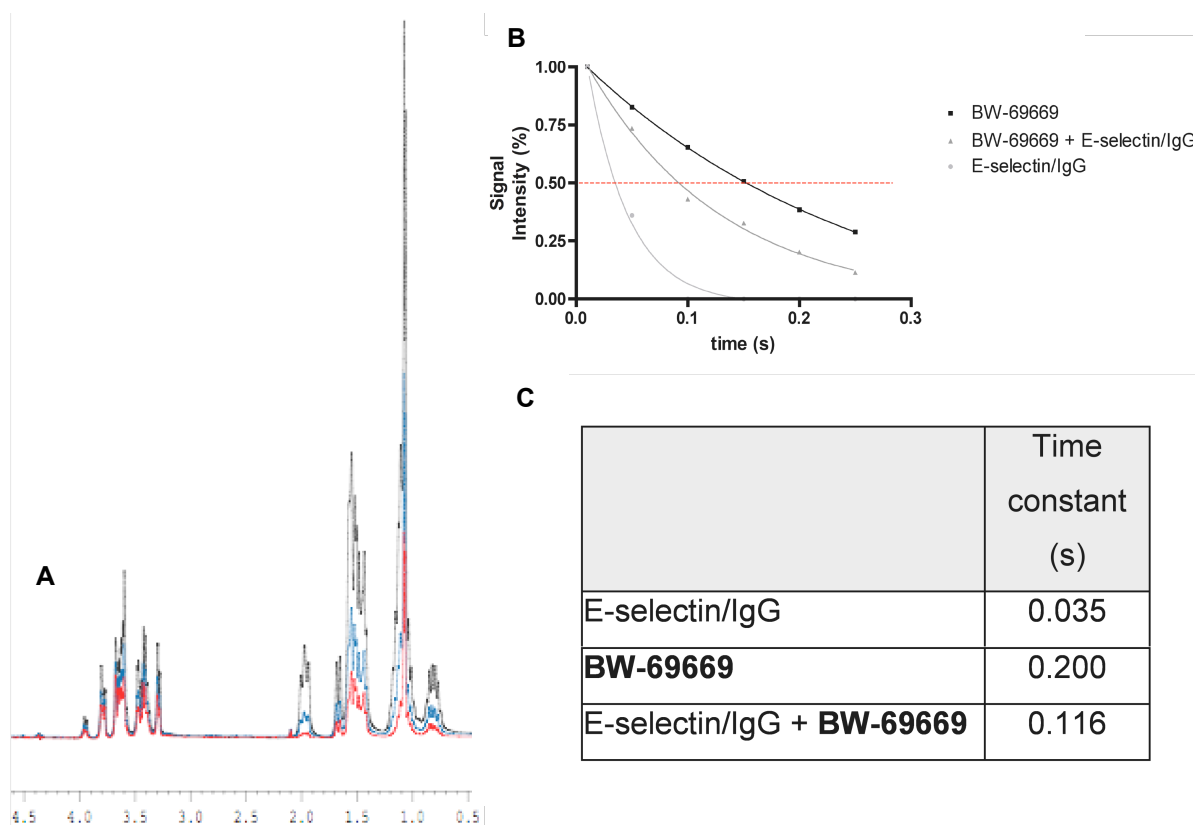


Figure 2. **BW-69669** (1.5 mM) spectra in the presence of E-selectin/IgG at different spin lock times (250 ms red, 150 ms blue, 10 ms black) (**A**). Decay of the signal intensity of **BW-69669**, E-selectin/IgG and mixture of **BW-69669** (1.5 mM) with E-selectin/IgG (10 μ M binding site) (**B**). Calculated time constants (**C**).

In order to verify that no equilibration time was required, a series of measurements was performed immediately after mixing **BW-69669** with the protein and after 4h at room temperature. No significant difference in the relaxation rate could be observed (Figure 3). This indicates, for non-competitive binding, that no equilibration time is required prior measurement.

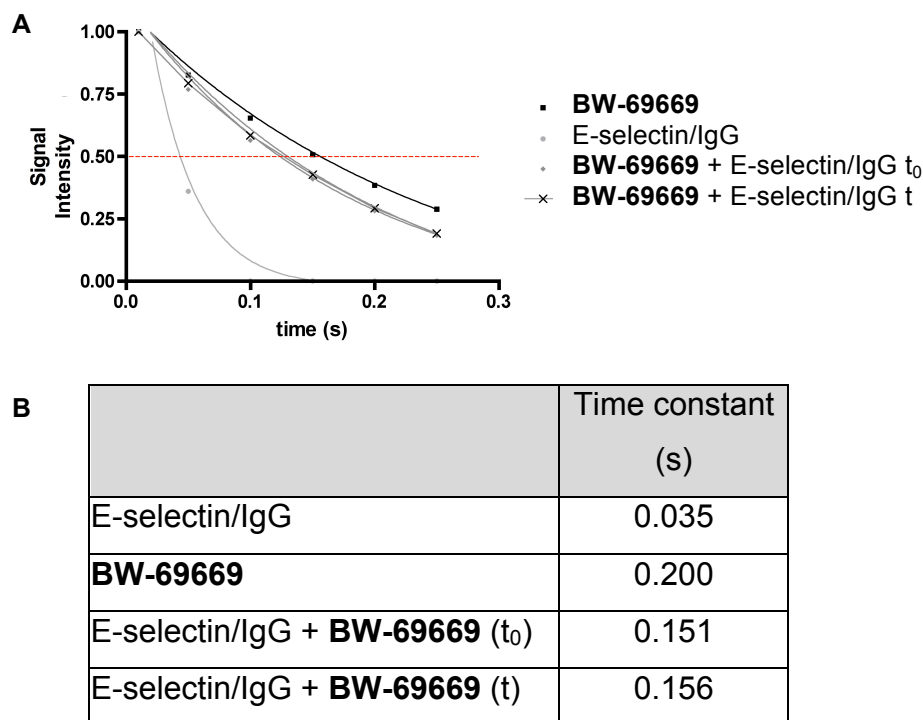


Figure 3. Decay of the signal intensity of **BW-69669** (1.5 mM), E-selectin/IgG and **BW-69669** (1.5 mM) with E-selectin/IgG immediately after preparing the sample (t_0) and after 4h of equilibration at room temperature (t) (A). Calculated time constants (B).

T1 ρ relaxation of **GMI-1077**

A similar experiment was conducted with **GMI-1077**. An enhancement of the binding by a factor of 30 was observed between **BW-69669** and **GMI-1077** with the Biacore captured assay. The relaxation rate was calculated at 2 resonances, 8.01 ppm, corresponding to the resonance of the aromatic ortho-hydrogen of the benzoate in the 2-position of galactose, and 3.86 ppm, corresponding to the resonance of the non-aromatic hydrogen in the 4-position of galactose. In both cases, an enhancement of the relaxation rate by a factor of two was observed in presence of the E-selectin/IgG (Figure 4). This clearly demonstrated the binding between E-selectin/IgG and **GMI-1077**.

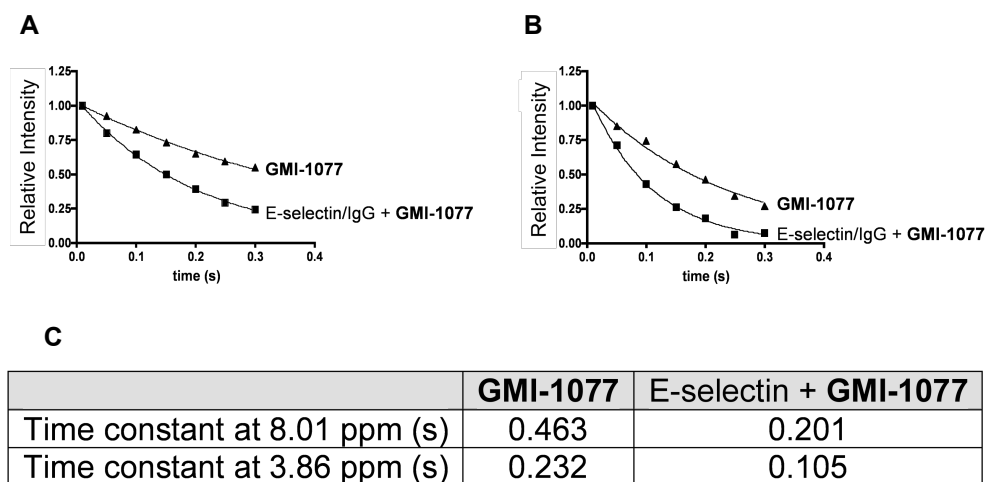


Figure 4. Decays of the signal intensity of the benzoate H-ortho at 8.01 ppm (**A**) of **GMI-1077** and of the non-aromatic hydrogen galactose H-4 of **GMI-1077** at 3.86 ppm (**B**). For both resonances, the measurement was performed with **GMI-1077** (1 mM) in the absence and in the presence of E-selectin/IgG (30 μ M binding site). Calculated time constants for the samples previously described (**C**).

4.8.1.2 Selective T1 relaxation

Selective T1 relaxation of BW-69669

A selective inversion-recovery sequence was used for the measurement. Initially, a selective π pulse was applied at 1.1 ppm corresponding to the fucose H-6. This was followed by a delay of either 0.075, 0.125, 0.175, 0.225, 0.3, 0.4, 0.5, 1, 2 or 3 sec. Finally, a $\pi/2$ pulse to make the magnetization observable, and a water suppression scheme were applied and the signals recorded (Figure 5).

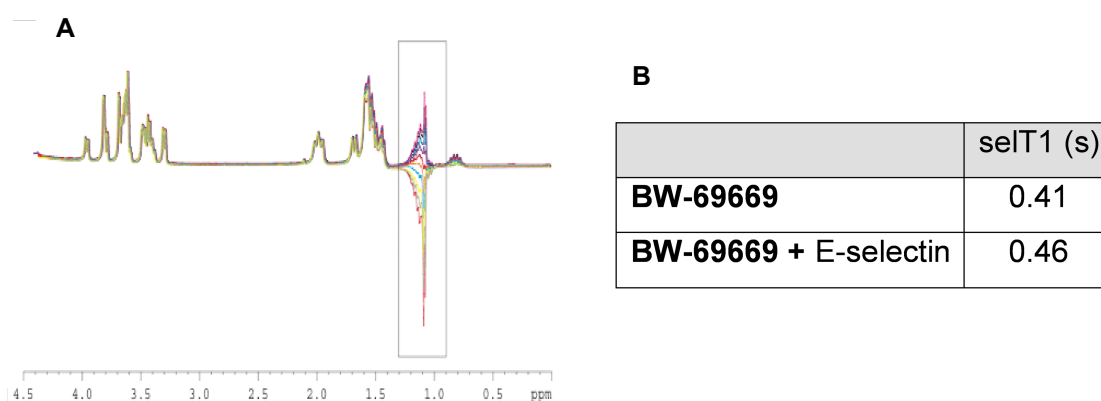


Figure 5. Overlay of spectra of **BW-69669** (1.5 mM) in presence of E-selectin/IgG (**A**). selT1 relaxation of **BW-69669** (3 mM) in the absence and in the presence of E-selectin/IgG (**B**).

An increase in the relaxation rate is observed in the presence of the protein. However, the effect is less pronounced than the increase observed with the $T_{1\rho}$ relaxation experiment.

Selective T_1 relaxation of **GMI-1077**

A selT1 relaxation experiment was performed by applying a selective π pulse on the resonances of the benzoate H-ortho in the 2-position of galactose (Figure 6). As previously observed for **BW-69669**, the relaxation rate of **GMI-1077** was enhanced, indicating the binding. However, the effect was slightly less pronounced than the one observed with $T_{1\rho}$ experiment (see section 4.3.1.1).

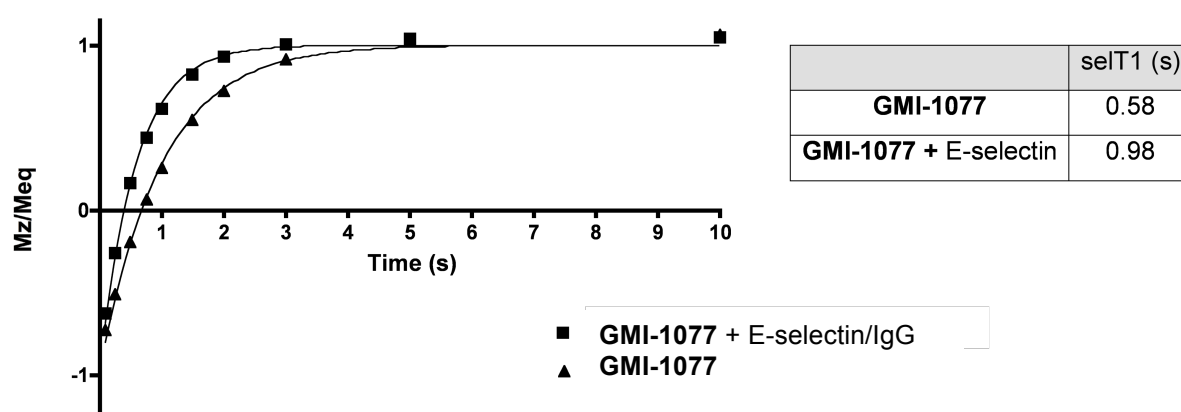


Figure 6. Recovery of the signal intensity of **GMI-1077** at 8.01 ppm following increasing delays and calculated relaxation in the absence (1.88 mM) and in the presence (5 mM) of E-selectin/IgG.

4.8.1.3 Competitive binding measurements using selective T_1 relaxation

*Titration of **BW-69669** with E-selectin/IgG*

The selT1 pulse sequence was selectively applied to galactose H-1 which did not overlap with any of the resonances from **GMI-1077**. The selT1 relaxation time was determined at increasing concentrations of **BW-69669** (0.5 – 3 mM). The large dependence of the selT1 time constant on the concentration of **BW-69669** allowed competitive binding experiments to be performed. For the competitive binding measured by selT1, an optimum concentration of 0.5 mM for **BW-69669** was

determined after titration (Figure 7). At that concentration, a change in the fraction of the free form of **BW-69669** due to the replacement by a competitor will induce a significant change in the selT1 time constant.

	selT1 (s)
BW-69669 (1 mM)	0.54
BW-69669 (0.5 mM) + E-selectin	0.34
BW-69669 (1 mM) + E-selectin	0.41
BW-69669 (1.5 mM) + E-selectin	0.44
BW-69669 (2 mM) + E-selectin	0.46
BW-69669 (2.5 mM) + E-selectin	0.47
BW-69669 (3 mM) + E-selectin	0.48

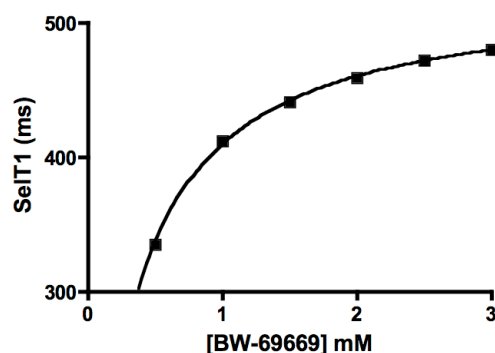


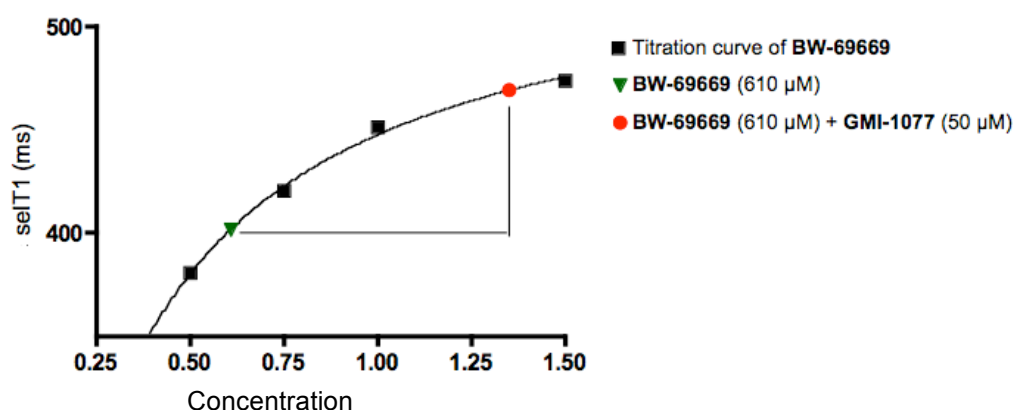
Figure 7. Titration of E-selectin/IgG (10 μ M binding site) with **BW-69669** and the corresponding selT1 observed.

*Competitive binding experiment with **GMI-1077** and relative affinity determination*

The titration of E-selectin/IgG with **BW-69669** was repeated with a new sample of E-selectin/IgG (10 μ M binding site). A slight increase in the selT1 was found at 0.5 mM of **BW-69669** (0.34 s in the first measurement versus 0.38 s in the second sample) and at 1 mM (0.41 s in the first measurement versus 0.45 s in the second sample). Nevertheless, the shift in selT1 was the same between 0.5 mM and 1 mM in both sample ($\Delta = 0.04$ s), indicating that the variation between the measurements was related to the use of different batches of protein samples. This will minimally affect the determination of the relative affinity of **GMI-1077**, because the same batch of protein was used to determine the titration curve and for the competitive measurement. In the presence of 50 μ M of **GMI-1077**, the observed selective relaxation rate was increased to 0.47 s leading to an apparent concentration of **BW-69669** of 1.37 mM. The relative affinity was determined by applying Eq. (4).

$$[\text{BW} - 69669]_{\text{apparent}} = [\text{BW} - 69669]_{\text{real}} + \frac{K_{D\text{BW} - 69669}}{K_{D\text{GMI} - 1077}} * [\text{GMI} - 1077] \quad (4)$$

A relative affinity of **GMI-1077** to **BW-69669** of 0.066 was determined. This result unambiguously showed the considerable enhancement in affinity of **GMI-1077** compare to the lead compound **BW-69669**. The rC_{50} obtained in the static cell free assay and the K_D obtained in Biacore were normalized to the affinity value of **BW-69669** (Figure 8). High consistency of the data from the different assays format was observed confirming the enhancement of the affinity between the lead and the optimized compound.



	rK_D (NMR)	rC_{50} (static cell free assay)	rK_D (μM) (Biacore)
GMI-1077	0.066	0.050	0.033
BW-69669	1	1	1

Figure 8. Titration of E-selectin/IgG (10 μM binding site) with **BW-69669** and the corresponding selT1 observed (black squares). The observed selT1 in the presence of 610 μM of **BW-69669** (green triangle) and the observed selT1 when 50 μM of **GMI-1077** was mixed to 610 μM of **BW-69669** (red circle) are highlighted. Vertical and horizontal lines show the extent to which the relaxation of **BW-69669** in presence of 50 μM of the competitor **GMI-1077** is attenuated and the corresponding apparent concentration of **BW-69669**.

Since the binding of carbohydrate mimics to E-selectin/IgG was successfully observed by ligand-based NMR techniques, further studies by STD-NMR were conducted in order to collect complementary information about the physical basis for the observed affinity.

4.8.2 Transferred NOESY

In the complex of **GMI-1077** with E-selectin/IgG, the proximity between the benzyl substituent in the 2-position of galactose and the cyclohexane groups of **GMI-1077** complexed to E-selectin/IgG was investigated by trNOE NMR experiments. The measurements were conducted at 310 K to displace the residual water resonance. NOEs were observed between galactose H-2 and galactose H-1, galactose H-3, galactose H-4, fucose H-6 (Figure 9). With a 2D-COSY experiment, the assignments were confirmed. Cross-peaks indicating coupling between two protons in correlation spectroscopy are sizable provided they are within two to three bonds. This experiment is frequently used for carbohydrate assignment due to the possibility to determine each proton by “walking” around the ring through the coupling.

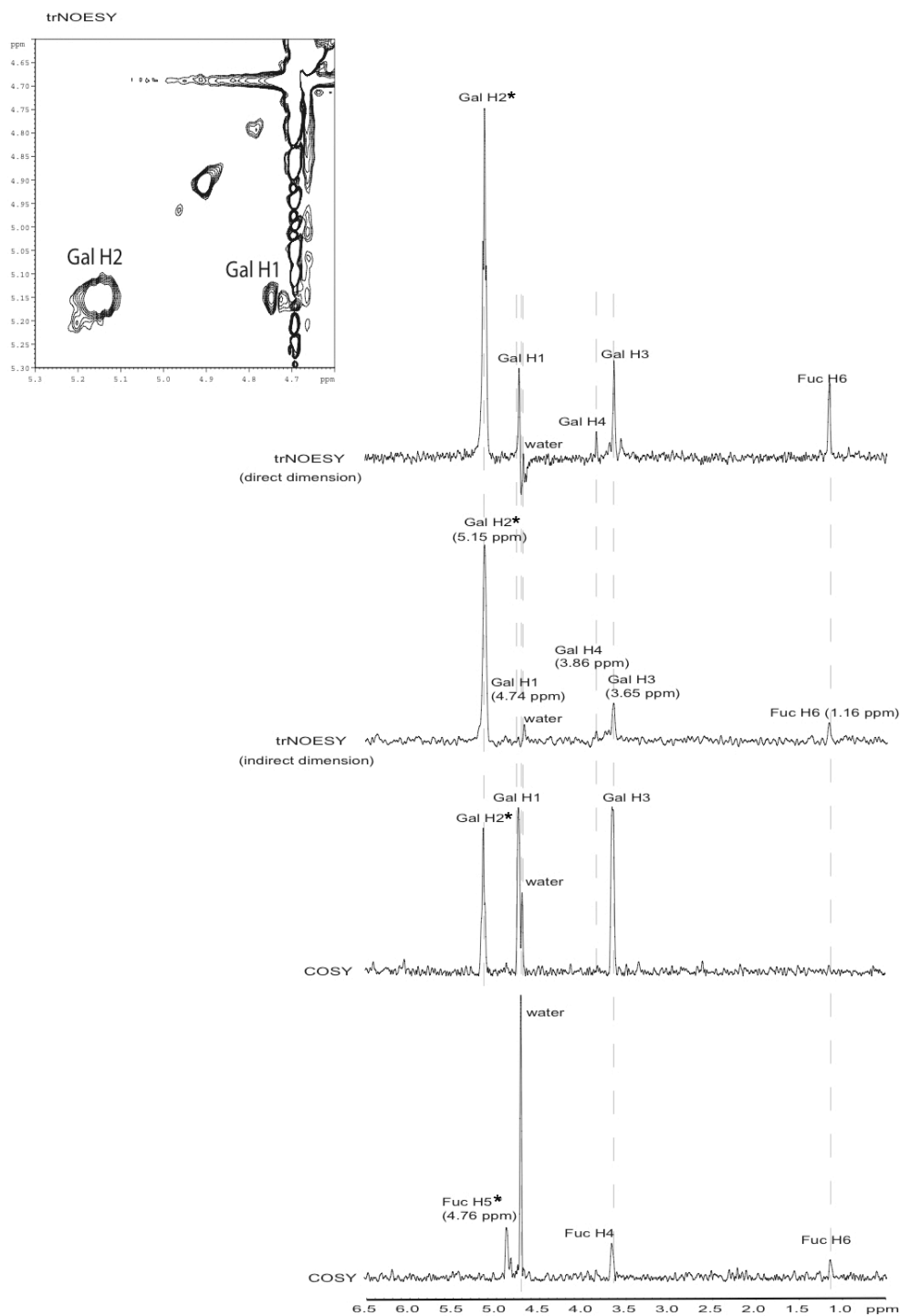


Figure 9. trNOESY of **GMI-1077** (1.88 mM) in presence of E-selectin/IgG (60 μ M binding site) and COSY recorded with the same sample used for the assignment of the resonances. Cross-peaks are indicated with an asterisk.

In the presence of protein, NOEs were also detected between benzoate H-ortho, benzoate H-para and benzoate H-meta in the 2-position of galactose. However, no NOEs with these hydrogens to other resonances were detected (Figure 10).

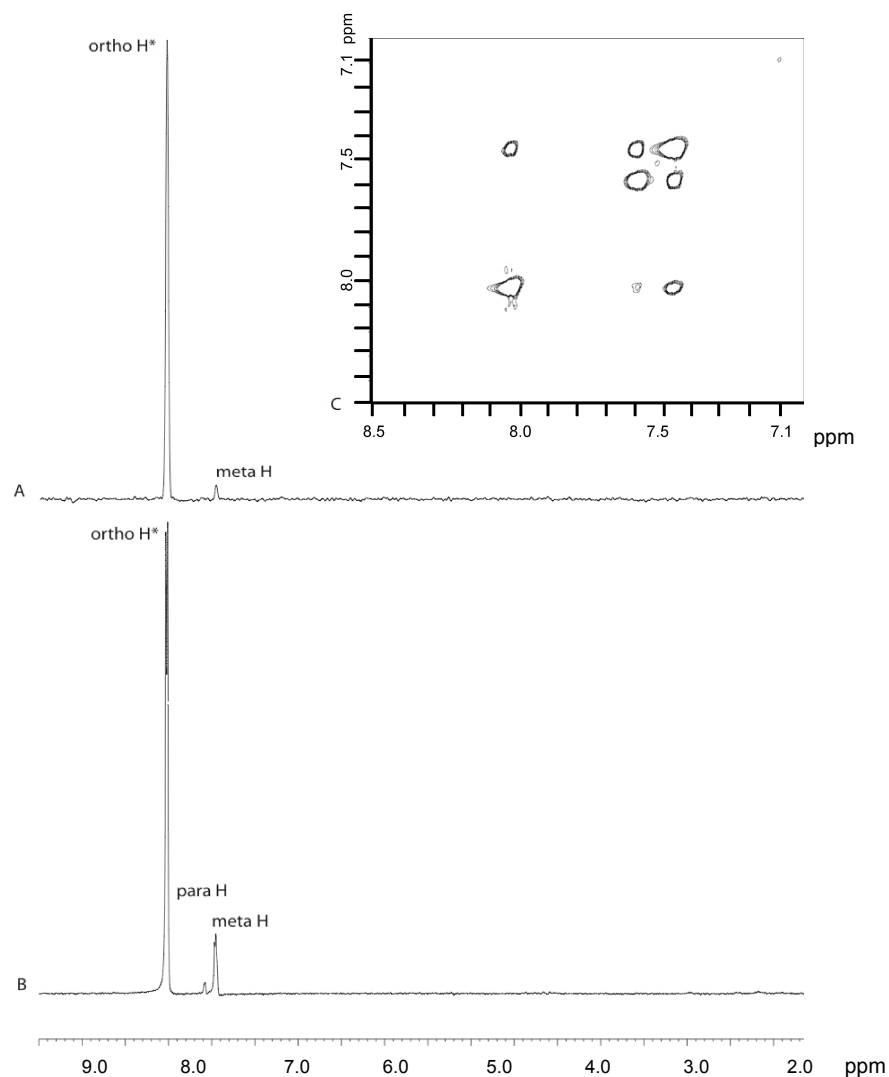


Figure 10. NOESY of **GMI-1077** (5 mM) in the direct dimension (A). trNOESY of **GMI-1077** (1.88 mM) in presence of E-selectin/IgG (B). trNOESY 2D of the benzoate in the 2-position of galactose (C).

The global minimal distance estimated between galactose H-2 and galactose H-3 is 3.06 Å. Therefore, the absence of NOEs between the benzoate in the 2-position of galactose and the cyclohexane groups indicate that these groups are separated by more than 3.06Å.

4.8.3 **2D-TOCSY experiments for assignment of the resonances of DS-0567 in the presence of E-selectin/IgG**

To ensure the purity and the quality of newly synthesized compounds, NMR measurements were performed and resonances were assigned. These NMR experiments were conducted in deuterated organic solvents (usually deuterated methanol) at high concentration of ligand (15-30 mM). In the STD experiments, the measurement was performed in the presence of the protein, at lower concentration of ligand (1-5 mM) in deuterated Tris buffer. These conditions might influence the chemical shift of the resonances. Therefore, 2D-TOCSY (Totally Correlated Spectroscopy) experiments were performed in the buffer used for the STD experiments and led to the assignment of most of the resonances of **DS-0567** (Figure 11). In these experiments, cross-peaks between coupled protons were observed for all protons within a spin-system. In the case of E-selectin ligands, each carbohydrate residue is an isolated spin system. Therefore, it is possible to assign each proton of the natural monosaccharide units. Considerable spectral overlap existed for the non-natural units, such as the cyclohexane spacer, precluding the complete assignment.

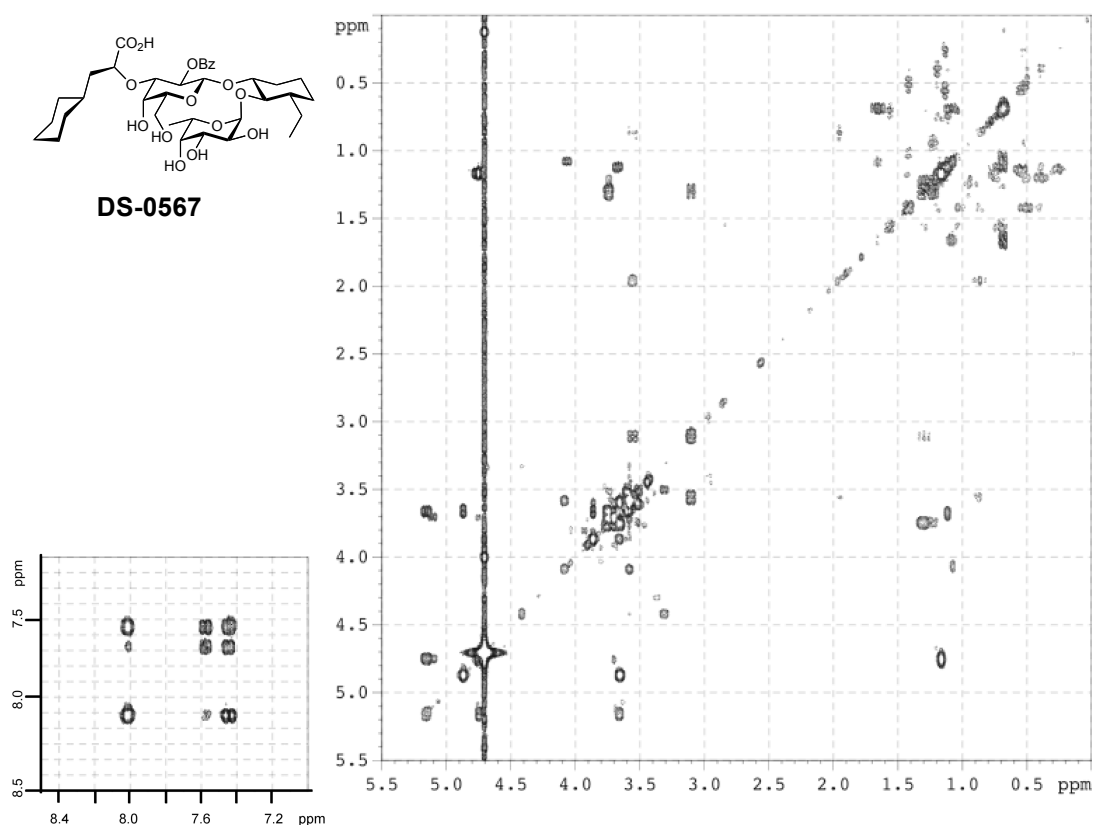


Figure 11. TOCSY experiment of **DS-0567** 5 mM (0.9 mg in 250 μ l) in presence of E-selectin/IgG 30 μ M (1.1 mg in 250 μ l). Signals of the benzoate in the 2-position of galactose are expanded on the bottom left.

4.8.4 STD-NMR experiments of DS-0567 in the presence of E-selectin/IgG

To determine the binding epitope of **DS-0567** interacting with E-selectin/IgG, STD-NMR experiments were performed. The experiment showed large STD values for the benzoate in the 2-position of the galactose moiety (Table 2 and Figure 12), which were unexpected, based on the docking experiments with the crystal structure [41].

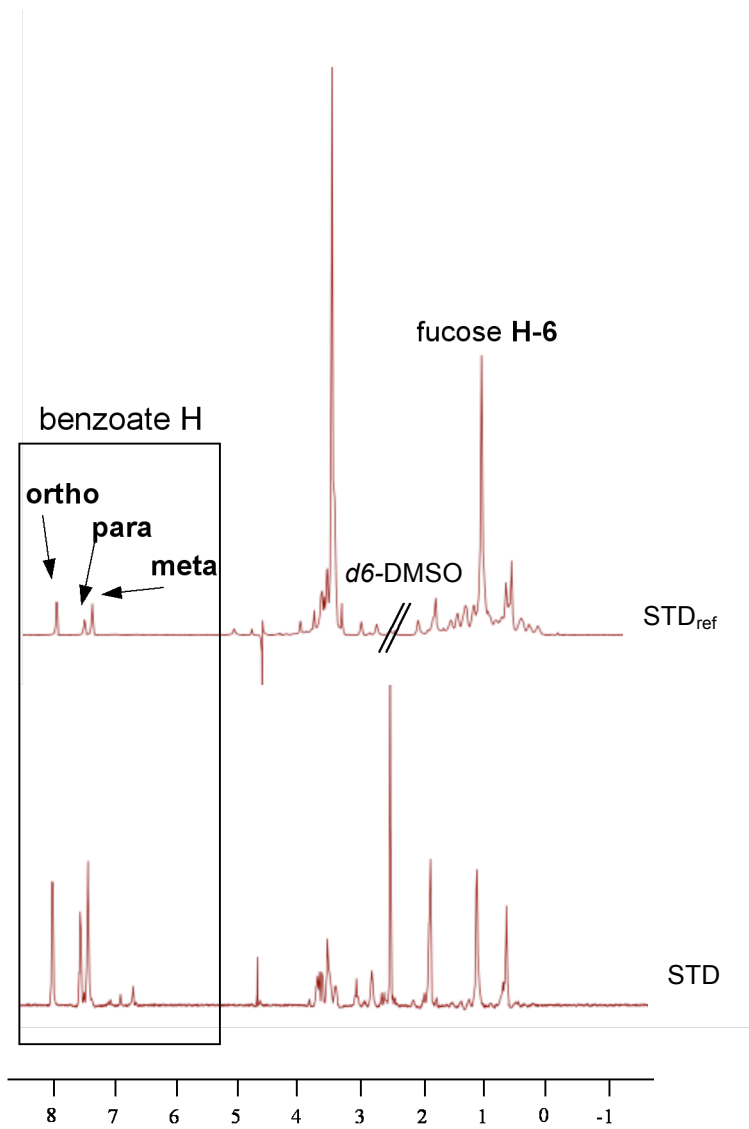
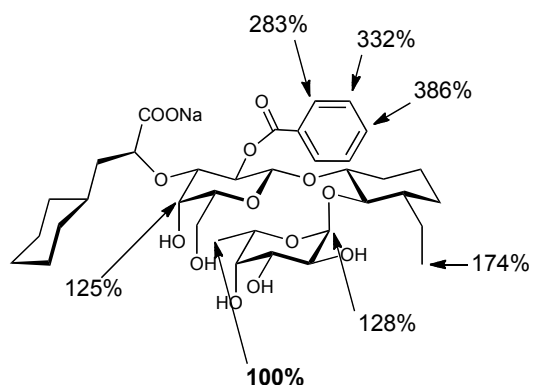


Figure 12: STD and reference spectra of **DS-0567** with E-selectin/IgG. Resonances observed for the benzoate in the 2-position of galactose are indicated as well as the fucose H-6, taken as a reference for the STD-NMR epitope mapping.

Table 2. STD-NMR epitope map of **DS-0567** with E-selectin/IgG.

Resonance	DS-0567 E-selectin/IgG
benzoate H-ortho	283%
benzoate H-para	386%
benzoate H-meta	332%
galactose H-4	125%
cyclohexane 3- ethyl	174%
fucose H-1	128%
fucose H-6	100%



According to docking studies by molecular modeling, the benzoate in the 2-position of galactose is oriented toward the bulk solvent, which is not compatible with large STD values observed. Four hypotheses were suggested to reconcile the differences between the STD-NMR and docking results:

- (i) Non-specific binding,
- (ii) Artifacts,
- (iii) Related to the dimeric form of the protein,
- (iv) Another binding mode.

4.8.5 **Non-specific binding: an issue tested by STD-NMR of DS-0567 with E-selectin/IgG.**

To substantiate or negate hypothesis (i), 2 mM EDTA was added to the sample and the STD-NMR experiments repeated. As seen in Figure 13, the STD-NMR signals are greatly attenuated upon addition of EDTA indicating the calcium dependent interaction observed for other E-selectin antagonists.

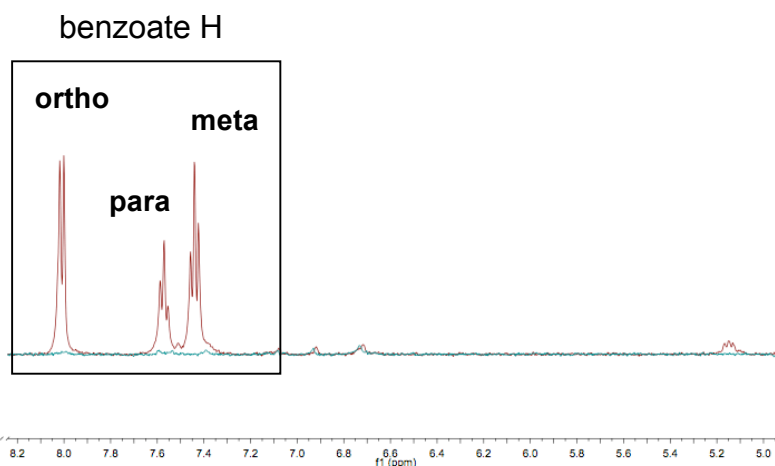


Figure 13: STD-NMR of **DS-0567** with E-selectin/IgG (red spectrum) and STD-NMR of **DS-0567** with E-selectin/IgG and 2 mM EDTA (green spectra).

4.8.6 Artifacts: an issue tested by STD-NMR of **DS-0567** with E-selectin/IgG

Different STD-NMR saturation times were recorded in order to verify that the signals of the aromatic hydrogens are not artifacts of either spin-diffusion or slow relaxation times [42]. As shown in Table 3, the STD-NMR epitope of **DS-0567** with E-selectin/IgG remained essentially constant for all saturation times.

Table 3. Epitope map of **DS-0567** binding to E-selectin/IgG with different saturation times. The epitope for each saturation time is normalized to the value of the benzoate H-para in the 2-position of galactose.

Saturation time (ms)	Bz H-para	Bz H-ortho	Bz H-meta	Non aromatic (5.14 ppm)	Non aromatic (3.85 ppm)
200	1.00	0.67	0.82	0.32	0.33
300	1.00	0.66	0.83	0.34	0.36
400	1.00	0.60	0.82	0.32	0.37
500	1.00	0.62	0.90	0.42	0.32
1000	1.00	0.60	0.89	0.33	0.38

In addition, artifacts from subtraction errors were investigated. Subtraction errors were estimated by repeating the STD-NMR experiments with a 5 mM sample of **DS-0567**, but without the E-selectin/IgG. However, no significant subtraction errors were observed.

4.8.7 **Large STD values of the benzoate in the 2-position of galactose due to the dimeric form of the protein: an issue tested by STD-NMR experiments of GMI-1077 and a monomeric E-selectin construct.**

The binding epitope of **GMI-1077** interacting with E-selectin/IgG was determined by STD-NMR experiments. Again, the experiment showed unexpectedly large STD values for the benzoate in the 2-position of the galactose (Table 4 and Figure 14).

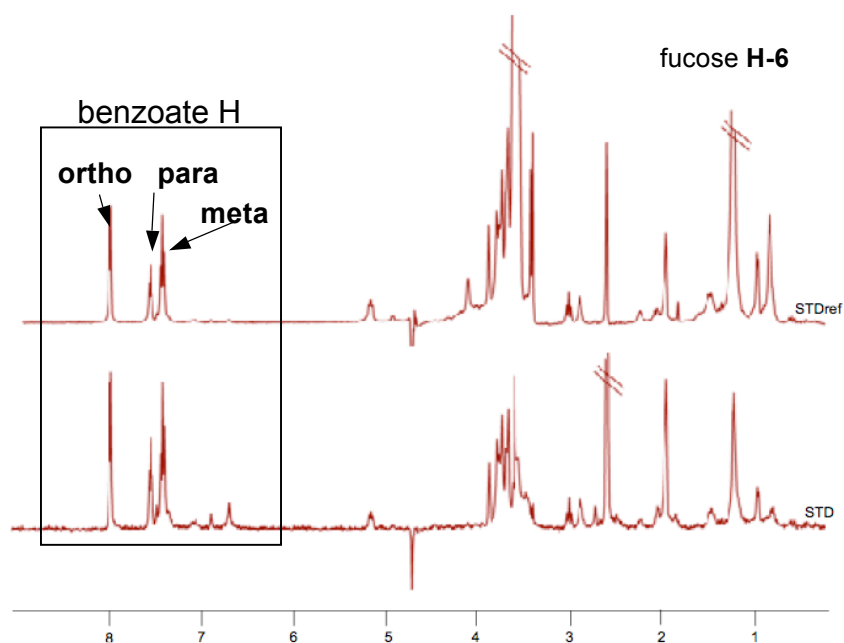
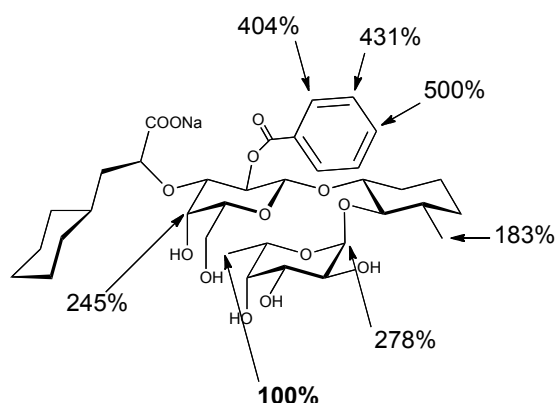


Figure 14: STD and reference spectra of **GMI-1077** (1mM) with E-selectin/IgG. Resonances observed for benzoate in the 2-position of galactose as well as fucose H-6, taken as a reference for the STD-NMR epitope mapping, are indicated.

Table 4. STD-NMR epitope map of **GMI-1077** with E-selectin/IgG.

Resonance	GMI-1077 E-selectin/IgG
benzoate H-ortho	404%
benzoate H-para	500%
benzoate H-meta	431%
galactose H-4	245%
3-methyl cyclohexane	183%
fucose H-1	278%
fucose H-6	100%



To ensure that the STD signals observed were not related to the dimeric form of the E-selectin/IgG construct, an STD-NMR experiment in the presence of a monomeric E-selectin construct, the LecEGF_CR2 construct, was performed (Table 5, Figure 15).

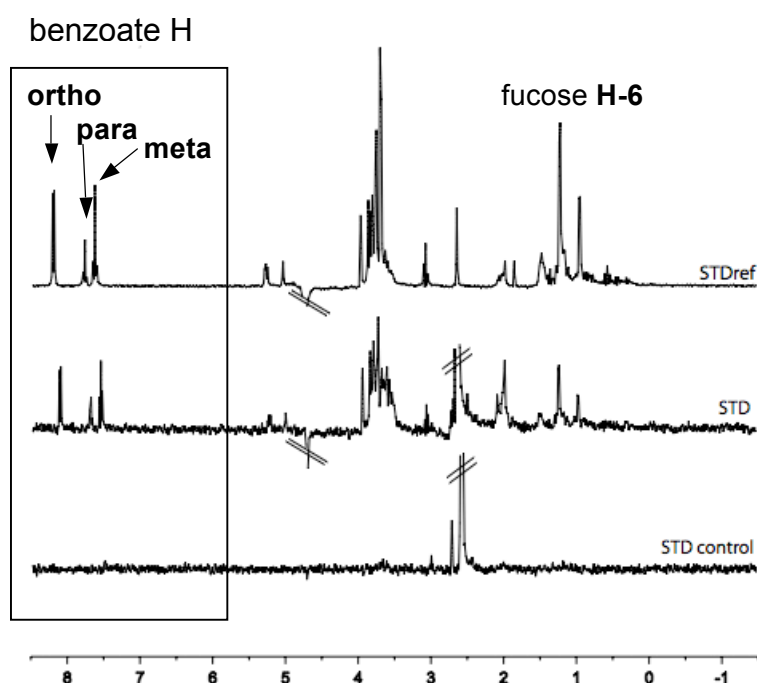
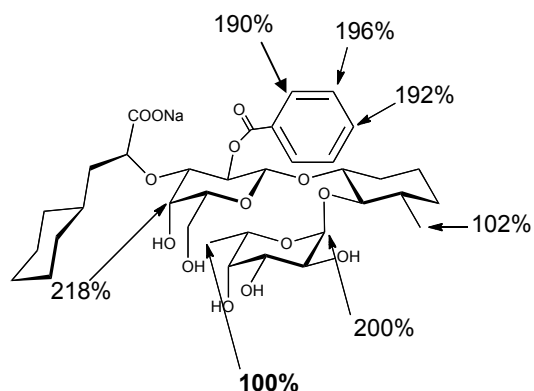


Figure 15: STD-NMR of **GMI-1077** with LecEGF_CR2 construct. Resonances observed for the benzoate in the 2-position of galactose and fucose H-6 are indicated. The latter was taken as a reference for the STD-NMR epitope mapping.

Table 5. STD-NMR epitope map of **GMI-1077** with LecEGF_CR2 construct.

Resonance	GMI-1077 LecEGF_CR2 construct
benzoate H-ortho	190%
benzoate H-para	196%
benzoate H-meta	192%
galactose H-4	218%
3-methyl cyclohexane	102%
fucose H-1	200%
fucose H-6	100%



In the presence of the monomeric form, as well as in the presence of the dimeric form, the STD signals of the benzoate in 2-position of galactose showed large STD values (Figures 14, 15 and 16, Tables 4 and 5). The normalized intensities of the STD epitope in the presence of the LecEGF_CR2 construct (monomeric form) were lower than those obtained with E-selectin/IgG (dimeric form) (Figure 16). The resonances observed for the benzoate in the 2-position of galactose in the presence of the dimeric form showed a normalized intensity twice as big as those observed with the monomer form. The difference may be due to the difference of molecular weight of the two forms (70 kDa vs 396 kDa). In general, the larger the molecular weight, the slower the molecular tumbling, leading to a more efficient Overhauser transfer between nuclei. It is conceivable, although contradicts an earlier publication on the method [43], that different nuclei in E-selectin are saturated to different extents depending on the presence of the monomeric or dimeric form. Furthermore, the number of consensus repeat in the structure of the chimera protein has been shown to influence the binding [44]. Therefore, the presence of less consensus repeat in the monomeric chimera of E-selectin leads to a loss of affinity for antagonists. This might also have a consequence on the STD signals observed, since the different affinities in the two E-selectin forms could be due to a negative impact of the chimera construct on binding site.

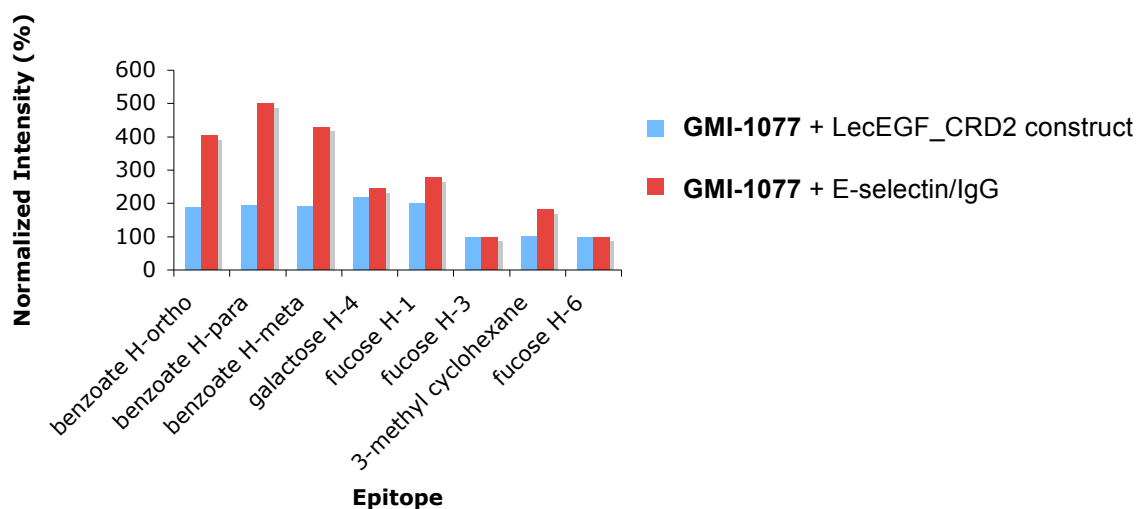


Figure 16: STD-NMR epitope map of **GMI-1077** with the monomeric and the dimeric forms of E-selectin.

4.8.8 STD-NMR experiments of **BW-580**

To provide further insight into the large STD signals observed for the benzoate in the 2-position of galactose, **BW-580** was investigated. **BW-580** has a cyclopropyl carboxylate in the 2-position of galactose. The STD-NMR with E-selectin/IgG showed clear STD signals of the cyclopropyl carboxylate (Figure 17 and Table 6).

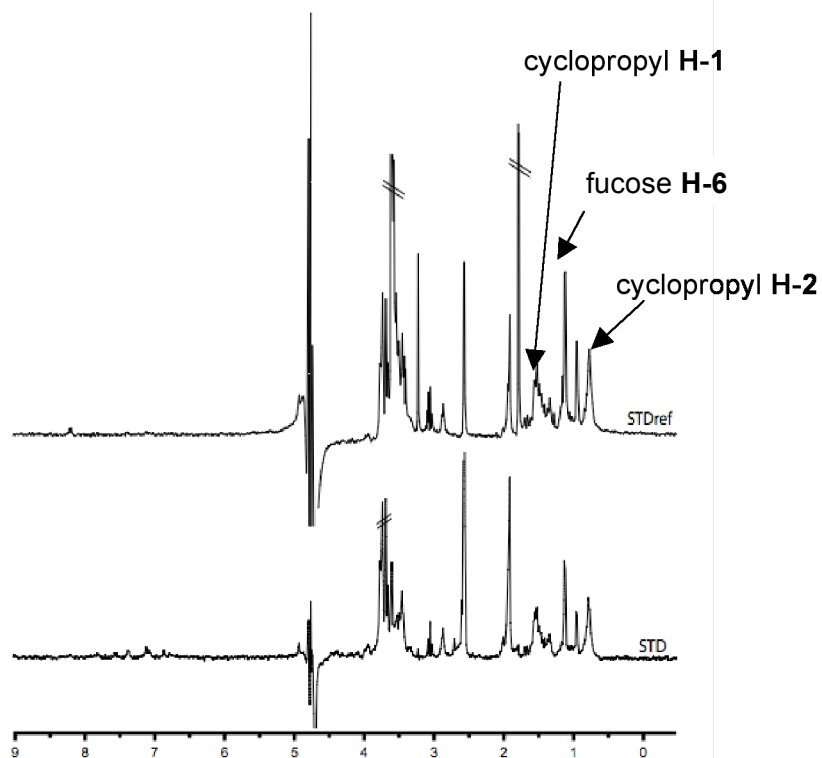
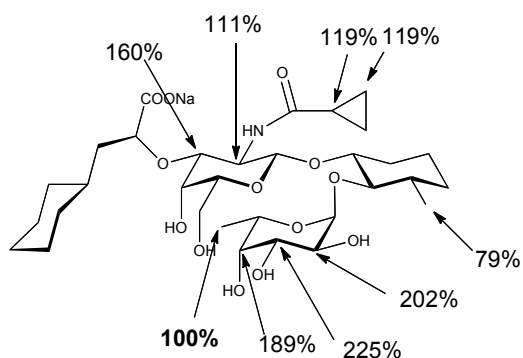


Figure 17: STD-NMR of **BW-580** with E-selectin/IgG. Resonances observed for cyclopropyl in the 2-position of galactose and fucose H-6 were indicated. The latter was taken as the reference for the STD-NMR epitope mapping.

Table 6. STD-NMR epitope map of **BW-580** with E-selectin/IgG.

Resonance	BW-580 E-selectin/IgG
cyclopropyl H-1	119%
cyclopropyl H-2	119%
galactose H-2	111%
galactose H-3	160%
3-methyl cyclohexane	79%
fucose H-2	202%
fucose H-3	225%
fucose H-4	189%
fucose H-6	100%



4.8.9 STD-NMR experiments of BW-69669 and DS-04115

To obtain further insights into the interaction of antagonists with E-selectin, the results of previous STD-NMR experiments of **BW-69669** and **DS-04115** (Figure 18) are included.

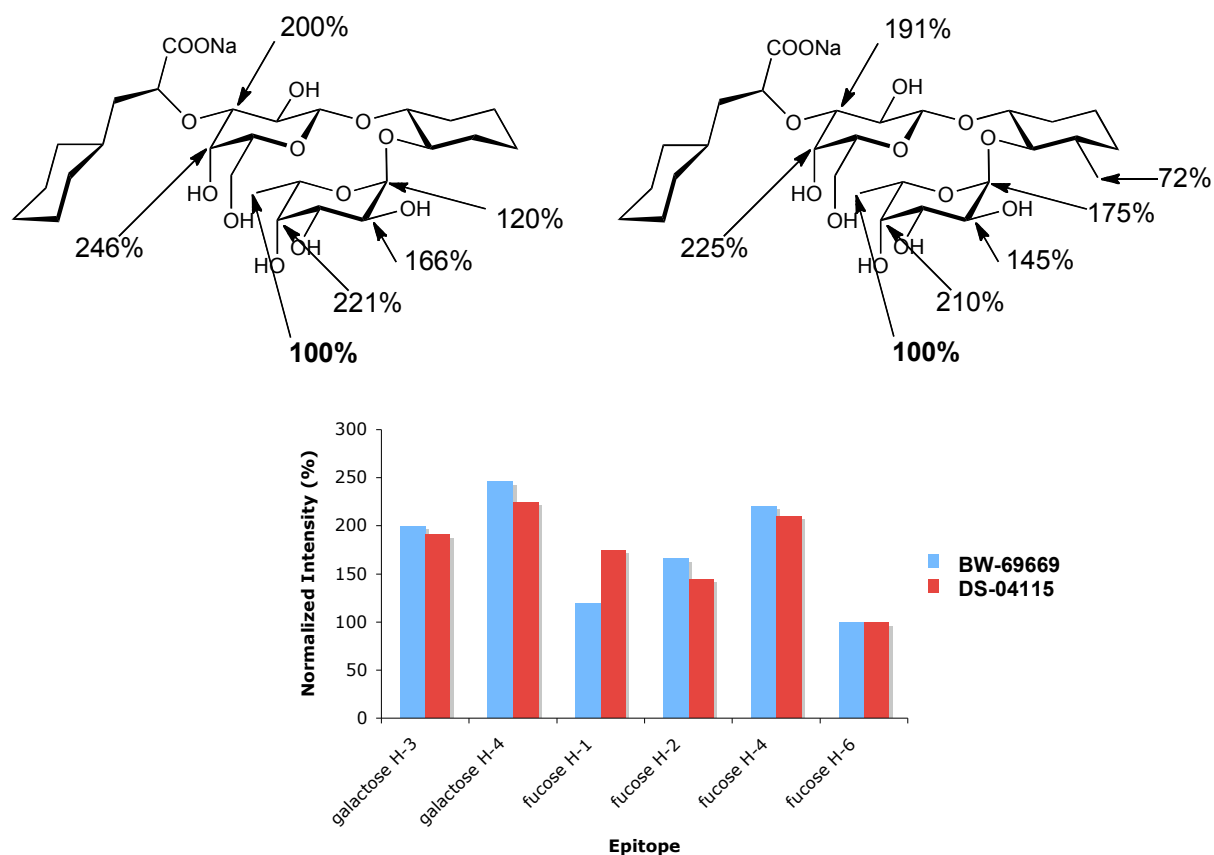


Figure 18: STD-NMR epitope map of **BW-69669** (left) and **DS-04115** (right) with E-selectin/IgG (Dr. Brian Cutting).

The epitope map of **BW-69669** and **DS-04115** showed a high degree of similarity indicating a similar binding mode except for the fucose H-1 (Figure 18). The difference between the fucose H-1 STD values might be explained by the nearby 3-methyl cyclohexane in **DS-04115**, which is absent in **BW-69669**. The steric hindrance of this group might influence the proximity to the protein surface.

4.8.10 Additional studies and comparisons of different epitope maps of compound studied

GMI-1077 and **DS-0567** have similar K_D values (1.46 and 1.49 μM , respectively) determined by Biacore. The epitope map of **GMI-1077** and **DS-0567** showed a similar pattern (Table 2 and 5). The main differences in the epitopes are in the normalized intensities, which are for some resonances 1.2 to 2 times larger than for **GMI-1077** (Figure 19).

Similar STD intensities were observed for the 3-methyl cyclohexane in **GMI-1077** and the 3-ethyl cyclohexane in **DS-0567**. STD intensity of the fucose H-1 was two times larger in **GMI-1077**.

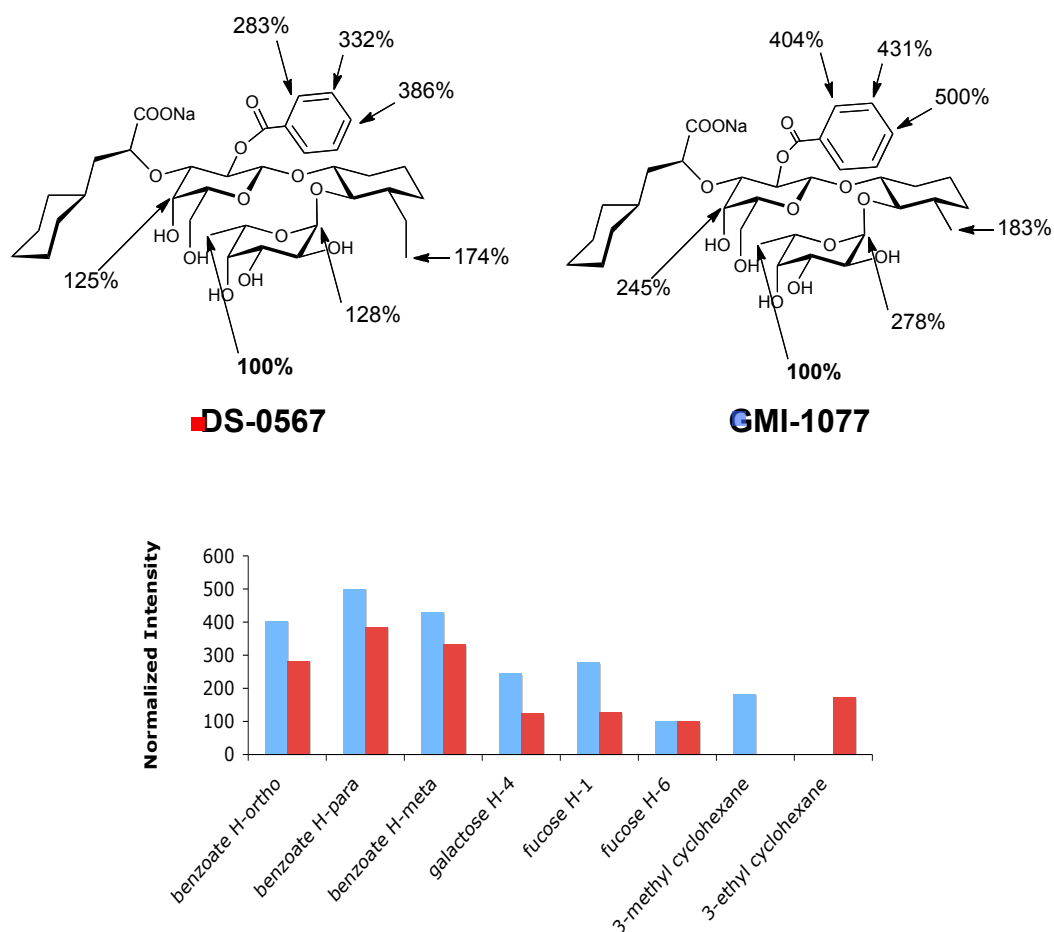


Figure 19. STD-NMR epitope map of **GMI-1077** ($K_D = 1.46 \mu\text{M}$) and **DS-0567** ($K_D = 1.49 \mu\text{M}$) with E-selectin/IgG.

In Figure 20, normalized STD intensities to the fucose H-6 of common assigned resonances of four compounds (**GMI-1077**, **BW-580**, **BW-69669** and **DS-04115**) are compared. For the benzoate in the 2-position of galactose the normalized STDs were more intense than those for the cyclopropyl carboxylate group in the same position in compound **BW-580** (Figure 20). For other resonances from the galactose and the fucose moiety, a similar pattern was observed. We also noticed that the signal of the 3-methyl cyclohexane was significantly stronger for **GMI-1077** (the only compound of the series containing a benzoate group in the 2-position of galactose). A similarity in the intensity of the signal of the 3-methyl cyclohexane from **GMI-1077** and the 3-ethyl cyclohexane of the **DS-0567** (see section 4.3.4, Table 2) was previously observed. Both compounds contain a benzoate in the 2-position of galactose.

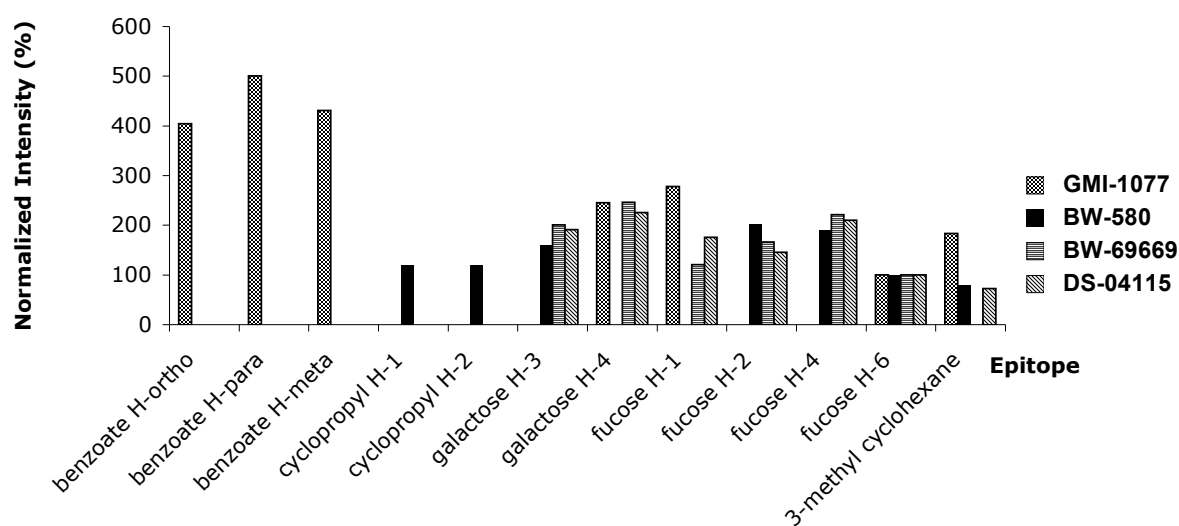


Figure 20. STD-NMR epitope map of common assigned resonances of **GMI-1077**, **DS-04115**, **BW-69669** and **BW-580** with E-selectin/IgG.

4.8.11 STD-NMR experiments of DS-0560

DS-0560 was synthesized as an intermediate planned for further modification. For this reason, an ester group was introduced in the 3-position of cyclohexane. In order to verify that the binding mode was not affected by this modification, STD experiments were performed. The experiment showed again large STD values for the benzoate in the 2-position of galactose (Figure 21).

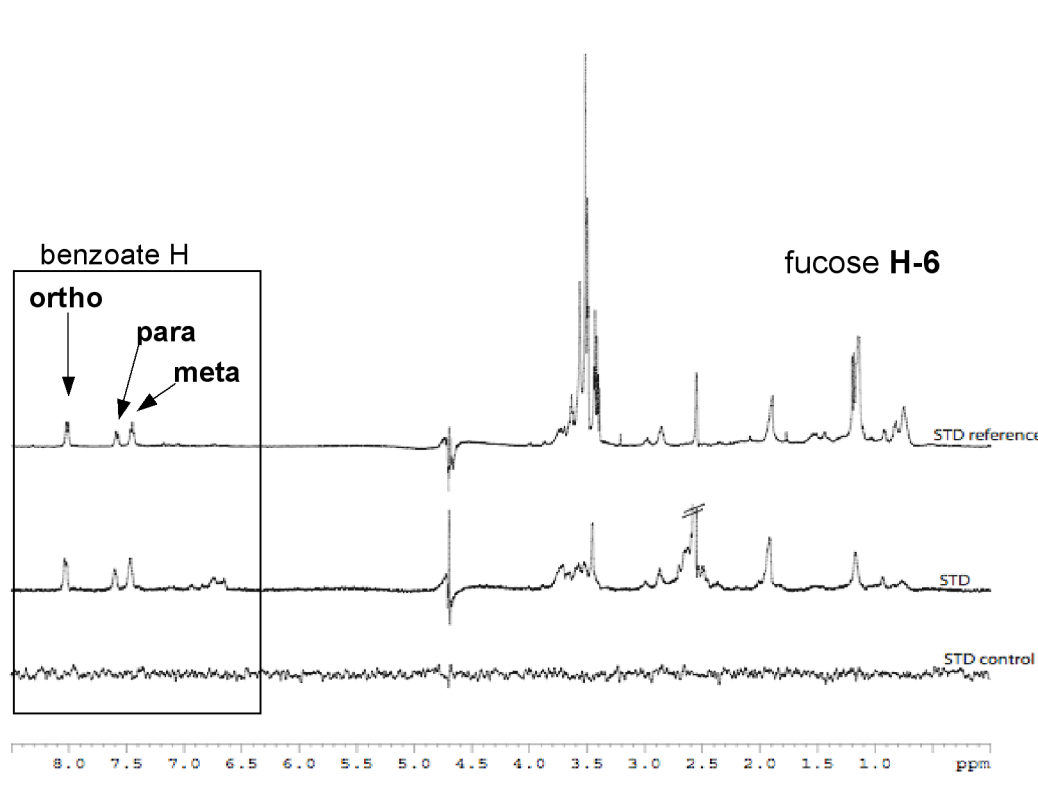
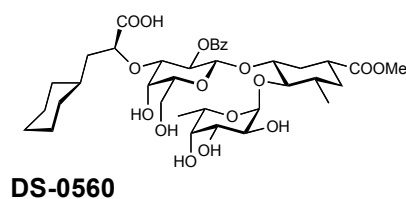


Figure 21: STD-NMR of **DS-0560** with E-selectin/IgG. Resonances observed for benzoate in the 2-position of galactose were highlighted as well as fucose H-6 taken as reference for the STD-NMR epitope mapping.

In competitive STD-NMR experiments, the displacement of **BW-69669** by the **DS-0560** in the presence of E-selectin/IgG (15 μ M binding site) could clearly be shown. The presence of STD signals for the benzoate in the 2-position of galactose, present only in **DS-0560**, demonstrated the displacement of **BW-69669** (Figure 22 A-C). A decay of the intensity of the signal of **BW-69669** of about 50% was observed in the presence of 200 μ M of **DS-0560** (Figure 22 D). The loss of signal in Figure 22 D is attributed to **BW-69669** since no signals from the benzoate of **DS-0560** were visible (Figure 22 B).

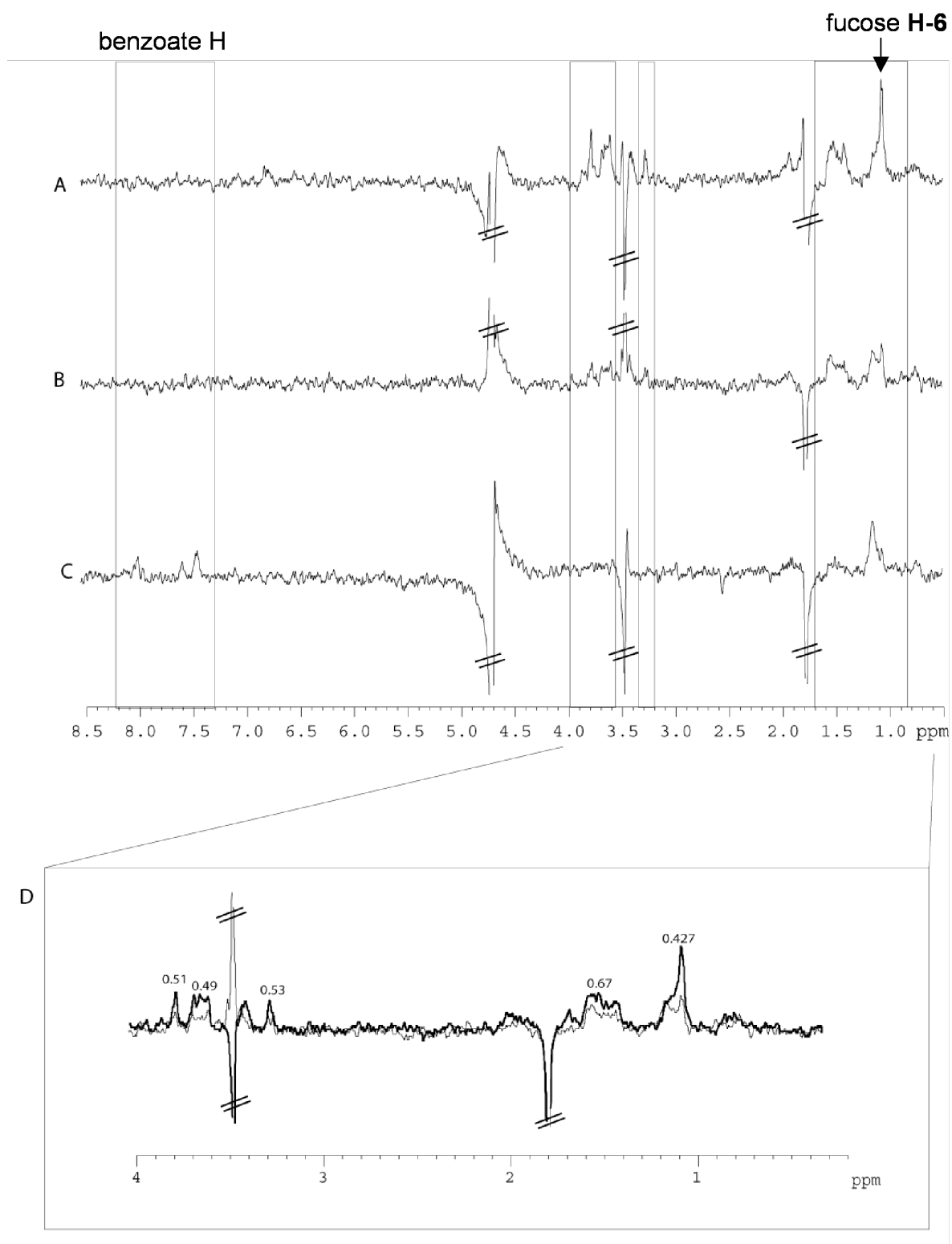


Figure 22. **A:** STD experiment of **BW-69669** (1 mM) in the presence of E-selectin/IgG (15 μ M binding site). **B:** STD experiment of **BW-69669** (1 mM) in presence of E-selectin/IgG (15 μ M binding site) and **DS-0560** (200 μ M). **C:** STD experiment of **BW-69669** (1 mM) in presence of E-selectin/IgG (15 μ M binding site) and **DS-0560** (300 μ M). **D:** Overlay of **A** and **B**. Loss of intensity of the signal is indicated.

4.9 Conclusion

The expression of isotopically enriched E-selectin in mammalian cells such as Chinese Ovarian Cells (CHO) is only possible at high costs [45]. Therefore, we choose NMR techniques based on ligand-observation for the detection and the characterization of interactions between E-selectin and antagonists. Only small amounts of unlabelled protein were required to perform relaxation (10 μ M binding site) and STD experiments (30-40 μ M binding site). Spin-spin and spin-lattice experiments were performed with the lead compound, **BW-69669**, and the optimized first-site ligand, **GMI-1077**. The changes in relaxation induced by the presence of the protein showed the interaction between E-selectin/IgG and these compounds. A competitive spin-spin relaxation experiment was performed and the relative affinity of **GMI-1077** was comparable to those determined by Biacore and ITC.

In order to obtain further information on the binding mode, STD-NMR experiments were performed and the binding epitope of several ligands elucidated. A comparison between STD-NMR epitopes of **GMI-1077** and **DS-0567** with E-selectin/IgG showed large STD values for the benzoate in the 2-position of galactose in both cases. The same experiment was conducted with **GMI-1077** and a monomeric construct of E-selectin (LecEGF_CR2 construct), where large STD values for benzoate in the 2-position of galactose were also observed. The issue of an artifact due to the dimeric form of E-selectin can therefore be excluded. Nevertheless, in the presence of the monomeric and the dimeric forms of E-selectin differences in signal intensities were observed for the same compound (**GMI-1077**). This is probably due to the difference of molecular weight of the protein and to a variation in the number of consensus repeats (CRs).

In the presence of EDTA, STD signals of **DS-0567** in the presence of E-selectin/IgG were significantly attenuated, negating the hypothesis of non-specific binding. Furthermore, it was demonstrated that the observed signals were not due to other artifacts such as spin diffusion, intensity of the power used to saturate the protein, subtraction errors or slow relaxation times. To improve the sensitivity of the measurement, the saturation power was distributed at two frequencies [40]. Performing this experimental setup in the absence of E-selectin/IgG, where no effects

could be observed, indicated that the method used to saturate the protein did not lead to artifacts.

In order to study the structure dependency in the STD signal of groups in the 2-position of the galactose, an STD-NMR experiment with **BW-580** (cyclopropyl in the 2-position of galactose) was performed and compared to **GMI-1077** and **DS-0567**. For all three compounds, a signal was observed for the substituent in the 2-position of galactose. The relative intensity of the STD signals observed for the cyclopropyl in the 2-position of galactose in **BW-580** were lower than those observed for the benzoate in the 2-position of the galactose moiety of **GMI-1077** and **DS-0567**. For these two compounds an explanation for the strong signal might be a closer proximity to the protein surface in the stabilized conformation. Indeed, it is known that a 3-methyl and 3-ethyl cyclohexane (**GMI-1077** and **DS-0567**) stabilized the bioactive conformation [46]. The lower relative intensity of the STD signal of the cyclopropyl in **BW-580** might be attributed to an unfavorable effect of the amide bond which orients the cyclopropyl group differently compare to the ester bond present in **GMI-1077** and **DS-0567**. The differences in steric hindrance and in electron density of the cyclopropyl group compare to the benzyl group probably also influence the observed STD signal. Further investigations are required to see if it is possible to correlate the STD differences with the proximity of the ligand to the surface of the protein and with the structure of the group in the 2-position of galactose.

Finally, two compounds (**DS-0567** and **GMI-1077**) showed a similar affinity in the Biacore assay (1.49 and 1.45 μM , respectively) and similar STD patterns, revealing a similar mode of binding.

After these measurements, the hypothesis of another mode of binding persists. The idea of a reverse binding mode (already postulated by Prof. Beat Ernst ten years ago) was discarded with the elucidation of the crystal structure in presence of the natural ligand **sLe^x**. To provide further insight, an X-ray structure elucidation of the protein co-crystallized with one of the compounds previously cited will be performed (Roland Preston).

4.10 References

- [1] I.I. Rabi, J.R. Zacharias, S. Millman, P. Kusch, *Phys. Rev.* **1938**, 53, 318.
- [2] F. Bloch, *Phys. Rev.* **1946**, 70, 460.
- [3] E.M. Purcell, E.C. Torrey, R.V. Pound, *Phys. Rev.* **1946**, 69, 37.
- [4] D. Canet, J.C. Boubel, E.C. Soulas, *La RMN, Concepts Methodes et Applications, Dunod 2e Ed.* **2002**.
- [5] J.J. Fischer and O. Jardetsky *J. Am. Chem. Soc.* **1965**, 87, 3237.
- [6] D.H. Meadows, G.C. Roberts, O. Jardetsky *J. Mol. Biol.* **1969**, 45, 491.
- [7] P. Balaram, A.A. Bothner-By, E. Breslow, *Biochem.* **1973**, 12, 4695.
- [8] A. De Marco, R.A. Laursen, M. Llinas, *Biochem. Biophys. Acta.* **1985**, 827, 369.
- [9] A.M. Petros, V. Ramesh, M.Llinas *Biochem.* **1989**, 28, 1368.
- [10] M.R. Rejante, I.J. Byeon, M. Llinas *Biochem.* **1991**, 30, 1181.
- [11] S.B. Shuker, P.J. Hajduk, R.P. Meadows, S.W. Fesik, *Science* **1996**, 274, 1531.
- [12] W. Jahnke, H. Widmer, *Cell. Mol. Life Sci.* **2004**, 61, 580.
- [13] J.W. Peng, J. Moore, N. Abdul-Manan, *Prog. NMR Reson. Spect.* **2004**, 44, 225.
- [14] D.J. Craik and K.A. Higgins, *Annual Reports on NMR Spectroscopy* **1990**, 22, 61.
- [15] M. Pellechia, D.S. Sem, K. Wüthrich, *Nat. Rev. Drug Disc.* **2002**, 1, 211.
- [16] www.bruker-biospin.com
- [17] W. Jahnke, P. Floersheim, C. Ostermeier, X. Zhang, R. Hemming, K. Hurth, D.P. Uzunov, *Angew. Chem. Int. Ed.* **2002**, 41, 3420.
- [18] C. Dalvit, M. Fiocco, S. Knapp, M. Mostardini, R. Perego, B. Stockman, M. Veronesi, M. Varasi *J. Am. Chem. Soc.* **2002**, 124, 7702.
- [19] C. Dalvit, M. Flocco, S. Knapp, M. Mostardini, R. Perego, B.J. Stockman *et al.* *J. Am. Chem. Soc.* **2002**, 124, 7702.
- [20] W. Jahnke, P. Floersheim, C. Ostermeier, X. Zhang, R. Hemming, K. hurth *et al.* *Angew. Chem. Int. Ed. Engl.* **2002**, 41, 3420.
- [21] A.H. Siriwardena, F. Tian, S. Noble, and J.H. Prestegard *Angew. Chem. Int. Ed. Engl.* **2002**, 41, 3454.
- [22] H.Y. Carr, E.M. Purcell, *Phys. Review* **1954**, 94, 630.
- [23] B. Cutting, *Chimia* **2006**, 60, 28.

- [24] T. Thewes, K. Constantine, I.J. Byeon, M. Llinas, *J. Biol. Chem.* **1990**, 265, 3906.
- [25] P.J. Hajduk, E.T. Olejniczak, S.W. Fesik, *J. Am. Chem. Soc.* **1997**, 119, 12257.
- [26] W. Jahnke, S. Ruedisser and M. Zurini, *J. Am. Chem. Soc.* **2001**, 123, 3149.
- [27] A. Chen, M.J. Shapiro, *J. Am. Chem. Soc.* **2000**, 122, 414.
- [28] M. Mayer and B. Meyer, *Angew. Chem. Int. Ed. Engl.* **1999**, 38, 1784.
- [29] M. Mayer and B. Meyer, *J. Am. Chem. Soc.* **2001**, 123, 6108.
- [30] Y.S. Wang, D. Liu, D.F. Wyss, *Magn. Reson. Chem.* **2004**, 42, 485.
- [31] M. Rinnbauer, B. Ernst, B. Wagner, J. Magnani, A.J. Benie, T. Peters, *Glycobiology* **2003**, 13, 435.
- [32] B. Cutting, S.V. Schelke, Z. Dragic, B. Wagner, H. Gathje, S. Kelm, B. Ernst, *Magn. Reson. Chem.* **2007**, 45, 720.
- [33] C. Dalvit P. Pavarello, M. Tato, M. Veronesi, A. Vulpetti and M. Sundstrom, *J. Biomol. NMR* **2000**, 18, 65.
- [34] C. Ludwig, P.J. Mihiels, X. Wu, K.L. Kavanagh, E. Pilka, A. Jansson, U. Oppermann, U.L. Günthner, *J. Med. Chem.* **2008**, 51, 1.
- [35] P.J. Hajduk, E.T. Olejniczak, S.W. Fesik, *J. Am. Chem. Soc.* **1997**, 119, 12257.
- [36] B. Cutting, S.V. Schelke, Z. Dragic, B. Wagner, H. Gathje, S. Kelm, B. Ernst, *Magn. Reson. Chem.* **2007**, 45, 720.
- [37] B. Cutting, J.-H. Chen, D. Moskau and G. Bodenhausen, *J. Biomol. NMR* **2000**, 17, 323.
- [38] Y-S. Wang, D. Liu, D.F. Wyss, *Magn. Reson. Chem.* **2004**, 42, 485.
- [39] M. Mayer and B. Meyer, *J. Am. Chem. Soc.* **2001**, 123, 6108.
- [40] C.A. Lepre, J.M. Moore, J.W. Peng, *Chem. Rev.* **2004**, 104, 3641.
- [41] W.S. Somers, J. Tang, G.D. Shaw and R.T. Camphausen, *Cell* **2001**, 105, 971.
- [42] J. Yan, A.D. Kline, H. Mo, M.J. Shapiro, E.R. Zartler *J. Mag. Reson.* **2003**, 163.
- [43] M. Mayer, B. Meyer, *Angew. Chem. Int. Ed.* **1999**, 38, 1784.
- [44] S.H. Li, D.K. Burns, J.M. Rumberger, D.H. Presky, V.L. Wilkinson, M. Jr. Anostario, B.A. Wolitzky, C.R. Norton, P.C. Familletti, K.J. Kim *et al. J. Biol. Chem.* **1994**, 269, 4431.
- [45] H. Takahashi, I. Shimada, *J. Biomol NMR.* **2010**, 46, 3.
- [46] D. Schwitzer, dissertation, University of Basel **2007**.

5. Fragment-based screening approach for the design of a second generation of E-selectin antagonists

5.1 Introduction

5.1.1 Need for fragment-based approaches in drug design

In the early stage of drug discovery, a holistic approach was applied. This approach was based on an early evaluation of molecules using *in vivo* models without the necessity of a preliminary identification of a target. In such an approach, the number of compounds tested was restricted either due to a limited chemical diversity or insufficient pharmacokinetic properties of the compounds (e.g. bioavailability) [1].

The early stage of modern drug discovery is aimed at the identification of molecular targets that are disease relevant and at the identification small organic molecules that can functionally interfere with the characterized target. Progress in genomics, molecular biology and biotechnology allows the rapid identification of targets as well as their expression. In this target-centric approach the *in vivo* evaluation is shifted to a later stage of the drug discovery process.

In parallel, the large libraries of compounds designed *via* combinatorial chemistry necessitate high-throughput screening platforms [2]. Surprisingly, as noted by Betz in 2005, this approach did not fulfill the expectations in terms of return on investment [3,4]. This can be at least partially explained by:

- the hit selection which was frequently not based on physicochemical properties critical for clinical success (e.g. high molecular weight, high lipophilicity, low solubility, poor stability) [5,6]
- the high throughput screening of large libraries of compounds with insufficient diversity.

The above limitations led to the concept of fragment-based approaches as a more efficient alternative for lead generation. Fragment-based approaches include fragment screening, leading to hit identification, and the merging of these hits to

obtain new lead compounds. In this approaches, early selection of compounds showing promising drug-like properties and incorporation of early ADME evaluations are particularly attractive for improving the success rate [7-9]. As consequences, fragment-based drug discovery led to a number of clinical and preclinical candidates within the last decade [10,11].

5.1.2 Fragment-based screening and linked-fragment approaches

The fragment-based screening approach is based on the idea that the binding pocket of a target can be seeing as a collection of subsites. Thus, each subsite is an individual target for low molecular weight compounds (50-250 Da). The identification of these “building blocks” is the aim of fragment-based screening [1]. The main advantage of this approach is the huge diversity of ligands accessible even with a library of limited size. Indeed, the number of ligands virtually assessed in a fragment-based screening is a power function of the number of subsites and of the different possibilities to link them (e.g. 10^9 possible combinations with a library of 10^4 compounds, a target containing two subsites and ten possible linker) [12-13].

The success in the screening is only the first step of fragment-based drug design. The small molecule hits usually exhibit only a weak binding affinity ($> 100 \mu\text{M}$). The required high affinity ligands are only obtained after combination of the selected hits. The linkage of the hits is one possibility to improve the affinity in fragment-based methods. The benefit of the linkage can be explained by the gain in free energy of the linked compound (corresponding to the sum of the free energies of the fragments) and the potential additional gain of entropy (Figure 1) [14]. With this approach, promising new leads can be designed and specificity for a target can be rapidly assessed. In 2004, O'Brien *et al.* showed an overview of fragment-based approaches in drug discovery and success of the fragment-linked method (e.g. improvement of the affinity of a ligand for DNA gyrase by a factor of 660) [8].

Besides the linking of fragments, alternative strategies emerged and can also be used for the generation of high affinity ligands, e.g. merged-fragment, elaboration or design of combinatorial libraries [15,16].

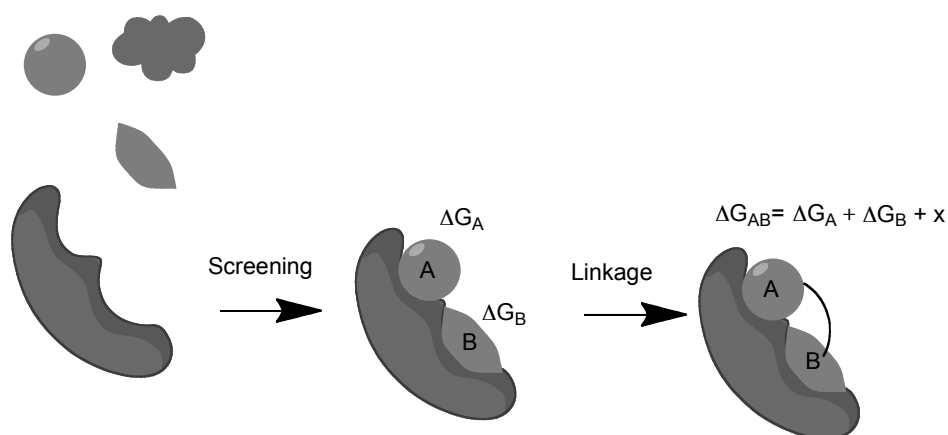


Figure 1. Linked-fragment approach.

In the early stage of fragment-based drug discovery, a large variety of biophysical techniques were used for fragment screening, such as nuclear magnetic resonance (NMR), surface plasmon resonance (SPR), fluorescence anisotropy (FA) and fluorescence life-time (FL) [17]. The weak affinity of the small molecules, their binding to large targets and the necessity of an efficient screening method placed NMR as an ideal technology. In 1996, Fesik *et al.* described for the first time a structure-activity relationship by NMR (SAR by NMR) and the success of its use in a fragment-based approach [18].

5.1.3 SAR by NMR

SAR by NMR is an extension of chemical shift mapping. In this method, protein chemical shift changes are used to identify small molecules binding with a weak affinity to subsites of the binding pocket of a target (Figure 2). Thus, preliminary requirements for SAR by NMR are the assignment of ^{15}N and ^1H backbone resonances and the 3D structure of the target. Limitations are the inherent necessity of the 3D structure and, the isotopic enrichment of the target protein.

In SAR by NMR, HSQC experiments are frequently used to provide informations on both binding constant and binding mode. The structural informations obtained on the ligand-binding mode are used for guiding the linking of the fragments. Indeed, knowledges on the structure of the target and on the relative position of the small ligands are precious for the design of an ideal linker. The

challenge of this crucial step of the process is the maintenance of the spatial orientation of the hits with respect to each other and to the target.

Progress in instrumentation considerably contributed to the efficiency of the process. In 1999, Hajduk *et al.* reported the possibility of screening 1000 small molecules in several hours [19].

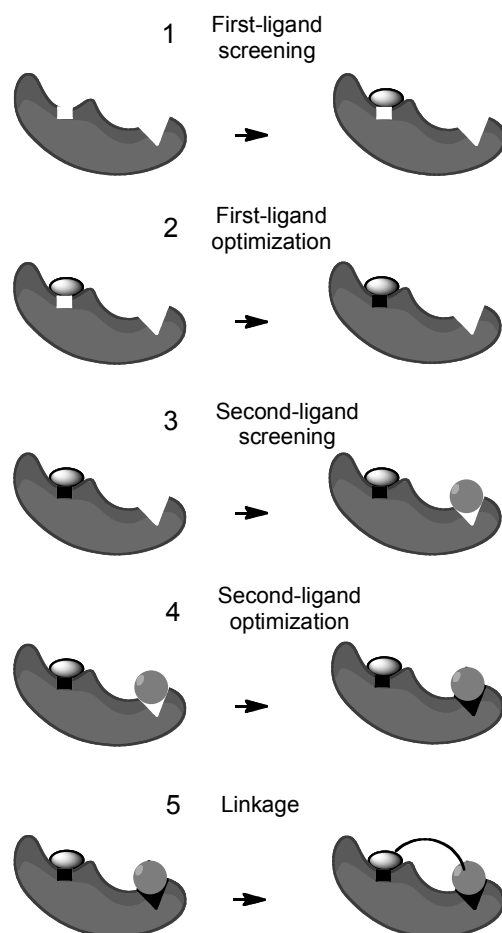


Figure 2. SAR by NMR in five steps for a target containing two subsites; step1: identification of a first-site ligand; step 2: optimization of the first-site ligand identified; step 3: screening for a second site ligand; step 4: optimization of the second-site ligand identified; step 5: linkage of the fragments.

After SAR by NMR, other methods emerged for lead generation by NMR, such as SHAPES screening described by Fejzo *et al.* in 1999. This method differs from SAR by NMR by the screened libraries, which are restricted to low molecular weight compounds corresponding to fragments of existing drugs [20].

In 2002, another method called “structurally oriented library valency engineering” (NMR-SOLVE) was proposed. In this case, the genetic identity existing in large families of targets for the design of focused libraries of small molecules is

used [21]. In that case, only a restricted labeling of the binding site is needed for the identification of the key protons.

The main advantage of SHAPES compare to SAR by NMR is the increase of the hit rate leading to a reduction of the quantity of protein required. The concept of SOLVE is advantageous, because fully labeled protein is not required. Nevertheless, the restricted labeling scheme for an assignment of the key protons in the binding site can also be a complication of the method.

For other approaches, such as inter-ligand transferred NOEs [22,23] isotopically labeling of the target is no longer required. These methods allowed a direct identification of several ligands binding close to each other. In this Ph.D. work, a spin-labeled ligand was used for characterizing protein-mediated ligand-ligand interactions [24]. This led to the identification of small molecules binding in the vicinity of the paramagnetic center.

5.1.4 Spin-label approach

Spin-labels have been used in NMR for many different purposes, such as measuring distances, dynamic studies or protein surface accessibilities [25]. In 2000, Jahnke and coworkers introduced a new application for spin labels with the possibility of detecting the simultaneous binding of different ligands to a target [26]. This method is based on the proportionality between spin-spin relaxation rate (R_2) and the product of the square of the involved spins gyromagnetic ratio γ [Eq. (1)].

$$R_2 \propto \gamma_1^2 \gamma_2^2 \quad (1)$$

The presence of a paramagnetic center (unpaired electron), as it exists in spin-label molecules, dramatically increases R_2 relaxation on protons *via* the larger electron-proton dipole-dipole interaction compared to the effect of a nuclear-nuclear interaction. This enlarged effect is called paramagnetic relaxation enhancement $R_{2\text{para}}$, and is due to the large gyromagnetic ratio of the unpaired electron, which is 658 times that of the proton.

In this thesis, the detection of the paramagnetic relaxation enhancement indicates the simultaneous binding of the two ligands (spin-labeled and second-site ligand), at neighboring binding sites (Figure 3).

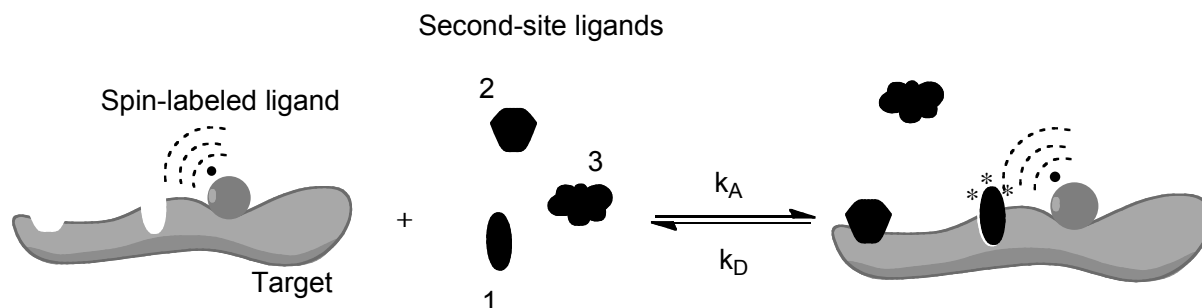


Figure 3. Spin-labels for second-site screening. R_2 of the second-site ligand 1 is enhanced by the paramagnetic interaction with the unpaired electron. The second-site ligand 2 is binding too far away from the spin-labeled ligand and molecule 3 is not binding to the target.

The use of a spin-labeled molecule has a significant practical advantage: the needed amount of target and ligand is considerably reduced (roughly 10 times less target protein than for the majority of other screening methods). Another advantage is the possibility to explore longer distances between the two binding sites ($\approx 20 \text{ \AA}$). Nevertheless, one major limitation is inherently linked to this approach: a possible modification of the binding by the introduction of the spin-labeled cannot be excluded.

Jahnke *et al.* illustrated this approach by linking a TEMPO moiety to a weak ligand of Bcl-xL ($IC_{50} = 140\mu\text{M}$), which failed in the optimization by traditional medicinal chemistry. The affinity of the TEMPO ligand was approximately retained and a second-site screening allowed the identification of hits.

This approach was used in this Ph.D. thesis. A TEMPO spin-label was coupled to a first-site ligand of E-selectin and used for the screening of second-site ligands.

5.2 Materials and methods

For all ligands measured, the chemical structure can be found in Appendix III and IV.

5.2.1 Biacore capture assay

E-selectin/IgG was immobilized following the method described in Chapter 3, section 3.2.5.2 and 3.2.5.3 by capture on an anti-human IgG surface immobilized *via* amine coupling on a CM5 sensor chip. All the compounds analyzed were synthesized in-house by Jonas Egger [27] and dissolved to prepare a 50 mM stock solution in DMSO.

All the binding experiments were performed in HBS-P buffer supplemented with 20 mM calcium chloride and 5% DMSO (v/v) (D8418, Sigma-Aldrich Chemie, Steinheim, Germany). Prior to compound evaluation, the surface was equilibrated in the buffer described above at a flow rate of 5 μ l/min for four hours. For each experiment, ten twofold dilutions of ligand were randomly injected. The stability of the surface after immobilization and its use to determine binding constants was followed by injection of ten twofold dilutions of a reference compound (**GMI-1077**). Prior to each assay, DMSO solutions and blank injection of buffer were performed as described in Chapter 3, section 3.2.5.6.

Data were processed with Scrubber-2.0a (BioLogic Software Pty Ltd., Campbell, Australia). Equilibrium binding constants were determined using a simple steady-state affinity 1:1 binding model. Kinetic data were also fit with Scrubber-2.0a. Double referencing was applied to correct bulk effects and other systematic artifacts (subtraction of reference surface and blank injection) [28].

5.2.1.1 Biacore characterization of TEMPO ligands

Two TEMPO ligands were synthesized by Jonas Egger, respectively with and without a benzoate group in the 2-position of galactose. For the TEMPO ligand with a benzoate in the 2-position of galactose, saturation was reached at a concentration of 15.6 μ M. Nine twofold serial dilutions starting from this concentration were prepared in HBS-P buffer supplemented with 20 mM calcium chloride and injected. A final

concentration of 5% DMSO was kept constant in all the dilutions. An association time and a dissociation time of 60 s were used and the flow rate was set to 20 $\mu\text{l}/\text{min}$. A similar procedure was applied for the characterization of a TEMPO ligand without benzoate in the 2-position of galactose, with dilutions prepared from a concentration at saturation of 312.5 μM .

5.2.1.2 Optimization of the Biacore method used for first-second-site antagonists analysis

All the first-second-site antagonists were synthesized in-house by Jonas Egger and dissolved to prepare a 50 mM stock solution in DMSO. For the first synthesized compound resulting from the second-site screening approach, the association time and the dissociation time were increased to 120 s and the flow rate set to 30 $\mu\text{l}/\text{min}$. Saturation was reached at a concentration of 8 μM and a total of ten twofold dilutions were injected.

The above conditions did not appear optimal for the other first-second-site antagonists. Therefore, a further optimization of the method was performed. The association and dissociation rates were increased up to 600 s and a flow rate of 20 $\mu\text{l}/\text{min}$ was used. Saturation was reached at a concentration of 1 μM and a total of eleven twofold dilutions were injected. In addition, to prevent the presence of residual traces of compound, a blank injection was performed between each injection of ligand dilution. As an additional precaution, the solutions of ligands were injected in an increasing order of concentration. The same method was applied for the analysis of a set of most potent compounds selected according to the data obtained with the ranking procedure.

5.2.1.3 Affinity ranking experiments

The ranking of the antagonists was performed in order to obtain qualitative information about the binding strength of twenty first-second-site antagonists synthesized by Jonas Egger. Similar parameters as described in the previous section were used for the ranking. Prior to each assay, DMSO solutions and blank injection of buffer were performed as described in Chapter 3, section 3.2.5.6. In addition,

blank injections were performed between each injection of ligand. In this type of binding experiment, SPR signals were recorded at a single concentration (0.05 μ M) and divided by the molecular weight of the compounds. The result obtained was normalized to the response obtained with an internal standard (**JE-81**) in order to avoid problems related to the measurement on different chips with different surfaces.

5.2.2 NMR

All spectra were recorded in-house with a Bruker DRX-500 (Bruker BioSpin AG, Fällanden, Switzerland) equipped with Z-gradient SEI probe. E-selectin/IgG was used in all the experiments in this chapter. The preparation of the protein was performed as described in Chapter 4 and concentrations of 15 μ M binding site were prepared (estimated by Bradford assay). As described in the materials and methods section of the Chapter 4, Shigemi tubes (Sigma Aldrich GmbH, Buchs, Switzerland) were used for samples containing E-selectin/IgG and ordinary 5 mm NMR tubes were used for samples containing only ligands (Sigma Aldrich GmbH, Buchs, Switzerland). All tubes were cleaned with bidistilled water and washed twice with D₂O. Before each experiment, the spectrometer was optimized for the sample introduced in order to achieve an optimal resolution and sensitivity (see Chapter 4, section 4.2.1). Identical software packages as described in Chapter 4, section 4.2.3 were used for recording and analyzing the data. The second-site screening approach is based on spin-spin relaxation measurements, which were recorded with the parameters described in Chapter 4, section 4.2.4.1.

5.2.2.1 Pre-selection of promising compounds by screening of small sublibraries of second site compounds

A library of sixty compounds was designed in-house by Dr. Sachin Shelke and Dr. Brian Cutting. To facilitate the screening procedure, the library was divided in sublibraries containing 6-8 compounds each.

T_{1 ρ} measurements at 10 ms and 200 ms spin-lock durations were recorded. Sets of four samples were measured for each sublibrary as described in Table 1. A concentrated stock solution of 100 mM in *d*₆-DMSO of each compound was prepared. The sublibraries were prepared by mixing the compounds at a final

concentration of 15 mM each in *d*6-DMSO. This solution was used to prepare four types of samples as describe in Table 1. This general procedure was applied for all sublibraries. The dilutions were performed in *d*11-Tris buffer (50 mM *d*11-Tris, 150 mM NaCl, 1 mM CaCl₂).

Table 1. Composition of the samples prepared for T1ρ measurements.

Sample	E-selectin/IgG [μM]	Sublibrary [μM of each compound]	JE-16 [μM]	Ascorbic acid [mM]
1	-	300	-	-
2	15	300	-	-
3	15	300	150	-
4	15	300	150	3

For compounds with uncertain assignment, isolated resonances were determined by recording H1-NMR after adding successively each compound in the sublibrary. Then, a series of T1ρ measurements with increasing spin-lock duration (10, 50, 100, 150, 200 and 250 ms) were recorded on samples 2, 3 and 4 for each sublibrary (Table 1). A series of seven promising hits was selected after the screening of all the sublibraries (see section 5.3.5, Figure 12).

5.2.2.2 Analysis of promising hits

The selected hits were individually analyzed. T1ρ measurements with increasing spin-lock duration (10, 50, 100, 150, 200 and 250 ms) were recorded on samples 1, 2, 3 and 4 where the sublibrary was replaced by the selected hit alone (Table 1).

5.2.2.3 STD and waterLOGSY experiments

STD-NMR experiment

The STD experiment confirmed the binding of the best selected second-site compound with the measurement of a sample containing 15 μM of binding site of E-

selectin/IgG mixed with 250 μM of the selected second-site compound. The same procedure as described in Chapter 4, section 4.2.4.2 was applied.

waterLOGSY experiment

A sample containing E-selectin/IgG (15 μM binding site) mixed with the TEMPO ligand (100 μM), the second-site ligand (400 μM) and ascorbic acid (400 μM) was prepared. The sample contained 65% H_2O . Fifty mM stock solutions of TEMPO ligand and of second-site compound in *d*6-DMSO were used for the preparation of the sample.

The pulse program used was described by Dalvit et al. [29,30] and optimized for our sample by Dr. Brian Cutting.

5.3 Results and discussion

The tetrasaccharide mimic **BW-69669** was previously recognized as a lead compound for E-selectin antagonists, and its structure used as a starting point for the development of more potent antagonists. During his PhD, Dr. Daniel Schwitzer worked on two different optimization strategies. One was to target a hydrophobic area on the lectins surface by attaching hydrophobic fragments in the 6-position of the galactose moiety. Unfortunately, the synthesized ligands did not show affinity in the static cell free assay ($rIC_{50} > 10$ mM, relative to sLe^x). The second strategy was dedicated to the optimization of the ligand pre-organization by stabilization of the bioactive conformation. Following this approach, a first generation of a first-site ligand was synthesized and led to a considerable improvement of the affinity by a factor of approximately 100. With this strategy, the low micromolar affinity was reached (**BW-529**, $K_D = 0.37$ μ M, see section 3.3.3, chapter 3). Despite this improvement of the affinity, all new derivatives still exhibited fast kinetic profiles as determined by Biacore. In order to improve the affinity and kinetic profile of E-selectin ligands, a fragment-based approach was initiated. This approach called “fragment-based ligand discovery” was first described by Jencks in 1981. With this approach, two weak binders that bind close to each other on the protein are identified and linked together to produce a high affinity ligand due to additive binding energies and favorable entropic effects. Having already an optimized first-site ligand in the micromolar affinity range, NMR screening was initiated for the identification of a second-site small molecule binding simultaneously and in the vicinity of the first-site ligand. For that purpose, a technique using a spin-labeled analogue of the first-site ligand [31] was applied to E-selectin. **JE-16**, a spin labeled analogue of **GMI-1077** was synthesized in-house by Jonas Egger.

For all ligands measured, the chemical structure can be found in Appendix III and IV.

5.3.1 Evaluation of JE-16 with the Biacore capture assay

As shown in chapter 3, the introduction of a carboxymethyl group in the 5-position of the GlcNAc mimic moiety (**DS-0560**, $K_D = 1.90$ μ M) did not show a drastic impact on the affinity compared to **GMI-1077** ($K_D = 1.45$ μ M). In addition, also further

modification of **DS-0560** for the introduction of a TEMPO moiety (**JE-16**) did not affect the affinity of the ligand for E-selectin/IgG (Table 2).

Table 2. Structures of **GMI-1077**, **DS-0560**, **JE-16** and **JE-61**. The affinities determined by the Biacore capture assay are also reported.

Compound	Structure	K_D^* [μ M] (Biacore)
GMI-1077		1.45
DS-0560		1.90
JE-16		1.25
JE-61		12.46

* experimental K_D derived from steady state response fit to a single binding site model

To study the influence of the benzoate group the spin labeled first-site compounds **JE-16** and **JE-61** were studied. In Biacore experiments, **JE-61** showed a ten-fold reduced affinity compared to **JE-16**. As shown in chapter 3, a similar decrease of the affinity was observed between **DS-04115** (absence of the benzoate in the 2-position of galactose) and **GMI-1077**. This observation suggests that the presence of the TEMPO moiety did not affect the binding mode of the first-site ligand. For both compounds, **JE-16** and **JE-61**, fast kinetics were observed (Table 3).

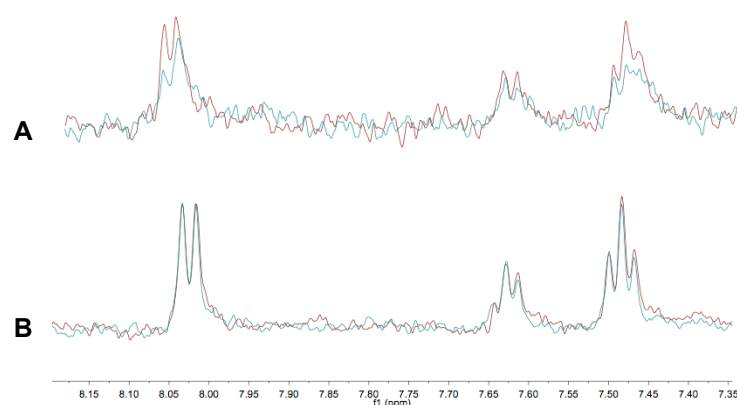
Table 3. Kinetic and affinity evaluation of **GMI-1077**, **DS-0560**, **JE-16** and **JE-61**.

Analyte	k_{on} [$10^5 M^{-1} s^{-1}$]	k_{off} [s^{-1}]	$K_{D\ kin}$ [μM]*	$K_{D\ eq}$ [μM **]	$t_{1/2}$ [s]***
GMI-1077	8.5	0.9	1.0	1.45	0.8
DS-0560	77.0	1.9	1.6	1.60	0.4
JE-16	3	0.36	1.2	1.25	1.9
JE-61	-	0.2	-	12.46	3.5

*calculated K_D using $K_D = k_{off}/k_{on}$ ** experimental K_D derived from steady state response fit to a single binding site model *** calculated $t_{1/2}$ using $t_{1/2} = \ln 2/k_{off}$.

5.3.2 NMR evaluation of the paramagnetic activity of **JE-16** and reducing conditions

To find the conditions for the reduction and to validate the paramagnetic activity of **JE-16**, $T_{1\rho}$ relaxation was measured. Two spectra of **JE-16** were recorded at 50 ms and 150 ms durations of spin lock at a concentration of 1 mM. Broad signals as well as strong decay in intensity due to paramagnetic relaxation were observed (Figure 4A). The same experiments were repeated after addition of an excess of 10 mM ascorbic acid to the sample. The ten-fold excess ensured the complete reduction of the radical (Figure 4B). The line narrowing and a negligible decay (less than 2 %) of the intensity were observed compared to the paramagnetically active form of **JE-16**, demonstrating the diamagnetic form of the molecule in presence of ascorbic acid.

**Figure 4.** (A) Paramagnetic activity of **JE-16** (B) Reduction of **JE-16** in the presence of 10-fold excess of ascorbic acid.

5.3.3 Second site screening by NMR

A library of sixty compounds was composed in-house by Drs. Sachin Schelke and Brian Cutting in 2004 for MAG project (Myeline-associated glycoprotein). The compounds were selected based on diversity, drug-like character, solubility, dispersion of their NMR signals and synthetic accessibility.

The library was divided into eight sublibraries containing 6-8 compounds each. The compounds were associated according to their chemical compatibility (chemical reaction of the compounds in a sublibrary was not suitable) and in a way to have at least one isolated resonances each in a H1-NMR spectrum.

5.3.4 Assignment of isolated resonances for each compound of each sublibrary

The process below describes the procedure for one of the sublibraries (Figure 5). A similar procedure was applied to the other sublibraries as well.

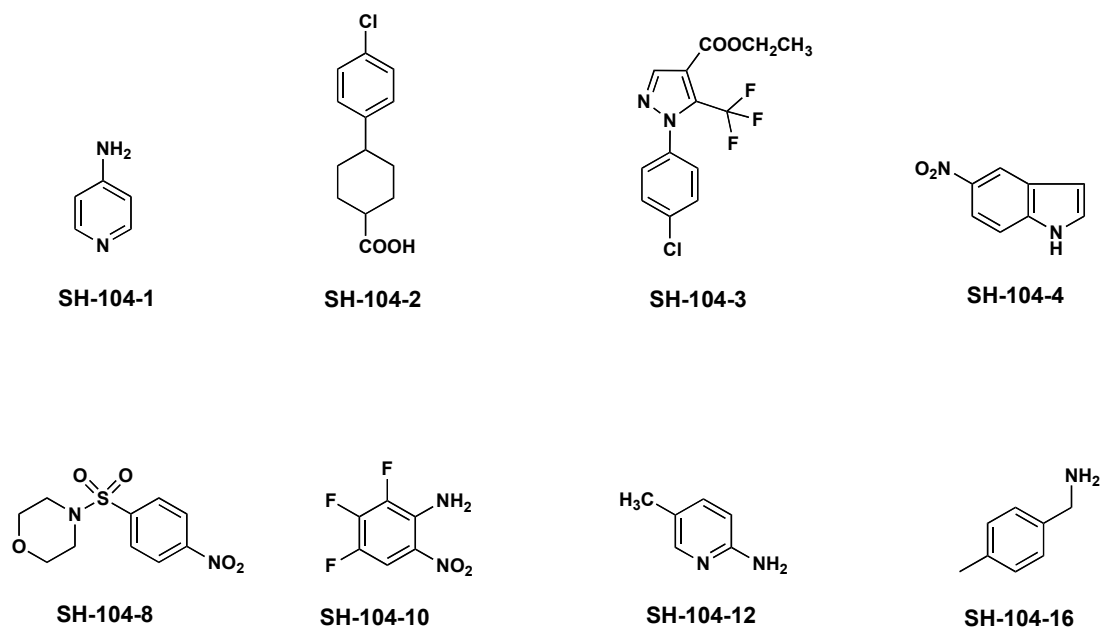


Figure 5. Composition of sublibrary 1.

A hypothetical spectrum of the sublibrary was created by overlaying H1-NMR spectra of each compound individually recorded (Figure 6A). By comparison with the

H1-NMR spectrum of the sublibrary (Figure 6B), unambiguous and isolated resonances were assigned for each compound (Figure 6C).

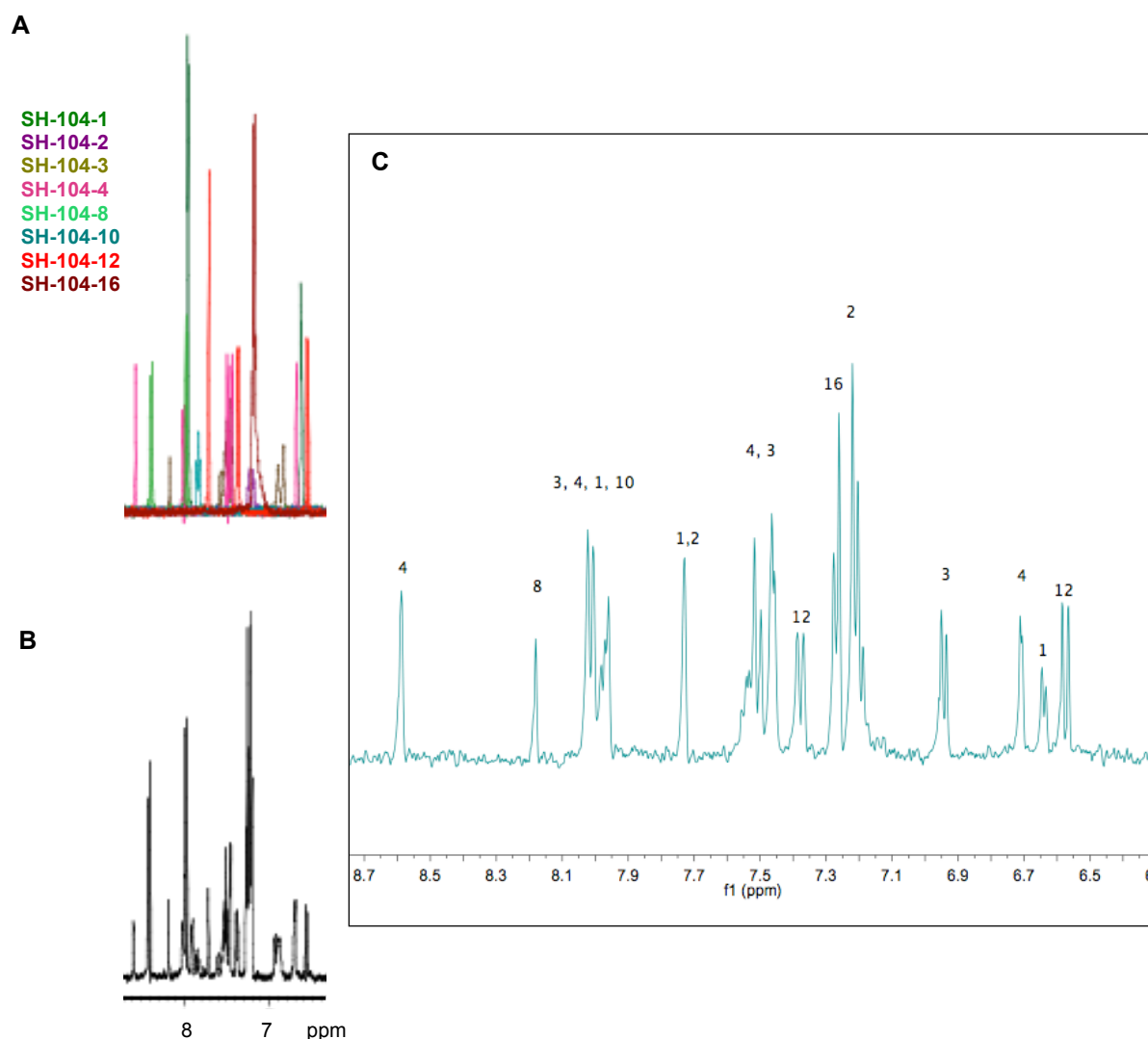


Figure 6. Hypothetical H1 spectrum of sublibrary 1 (A). H1 spectrum of sublibrary 1 (B). Resonance assignment of the sublibrary (C).

5.3.5 Screening of the sublibraries

In order to qualitatively estimate the binding potential of each compound to E-selectin, a first relaxation measurement was performed with a sample containing E-selectin/IgG (15 μ M binding site) and sublibrary 1 (300 μ M) at two spin-lock durations (10 and 200 ms). All compounds of sublibrary 1 except **SH-104-12** showed an enhancement of their relaxation rate in presence of E-selectin/IgG indicating a binding to E-selectin/IgG (Figure 7 and 8). As shown in Figure 8, a further decay of

the relative intensity roughly estimated between 15% and 55 % was observed for **SH-104-1**, **SH-104-2**, **SH-104-3**, **SH-104-4**, **SH-104-8**, **SH-105-10** and **SH-104-16**. The relaxation of **SH-104-12** was not strongly modified (less than 5% decay of the relative intensity, Figure 8) in the presence of E-selectin/IgG indicating minimal binding.

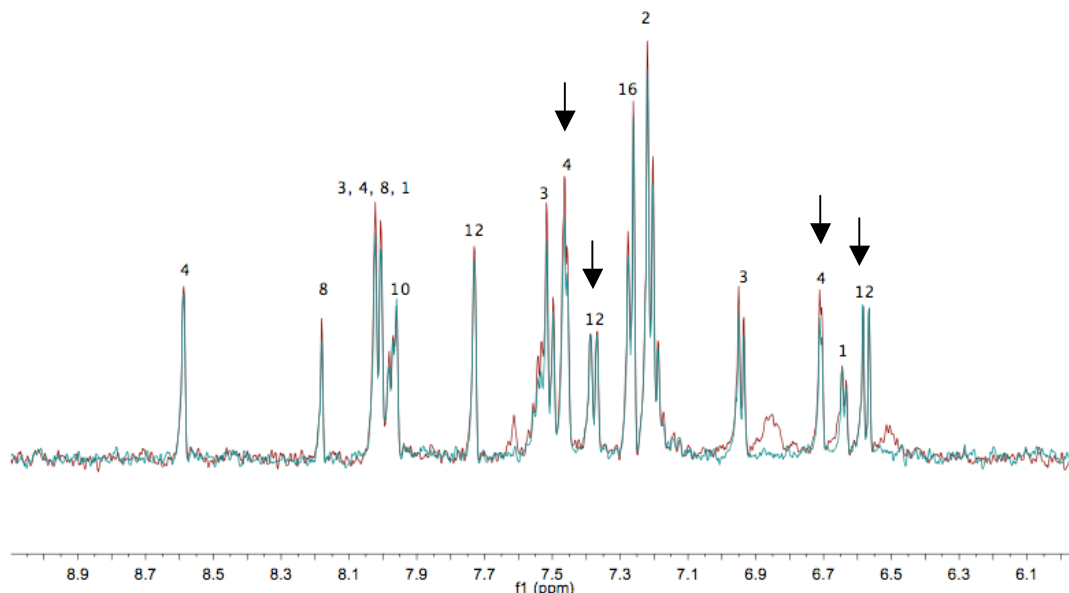


Figure 7. T1 ρ relaxation measurement of sublibrary 1 at 10 ms (red) and 200 ms (green) spin-lock in the presence of E-selectin/IgG. Isolated resonances of compound **SH-104-4** and **SH-104-12** are indicated by arrows.

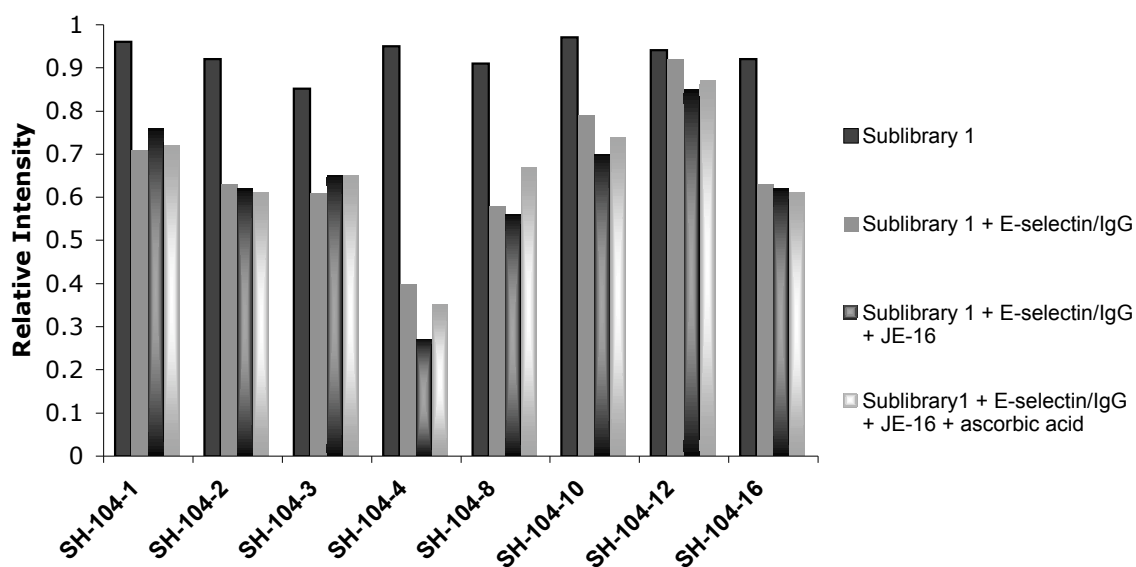


Figure 8. Variation of the intensity of the signal of each compound of sublibrary 1 in T1 ρ relaxation experiments recorded at two spin-lock durations (10 ms and 200 ms). The experiments were recorded on the sublibrary 1 alone, in the presence of E-selectin/IgG, after adding **JE-16** and after reduction of **JE-16** by ascorbic acid.

This cycle of two measurements was repeated with a sample containing E-selectin/IgG (15 μM binding site), sublibrary 1 of second-site ligand (300 μM each) and **JE-16** (150 μM). The cycle was recorded again after reduction of the TEMPO-ligand by adding ascorbic acid (3 mM) (Figure 9). An enhancement of the relaxation rate was expected in presence of **JE-16** if the compound bound in the vicinity of **JE-16**. This effect should be cancelled after reduction of the TEMPO moiety with ascorbic acid.

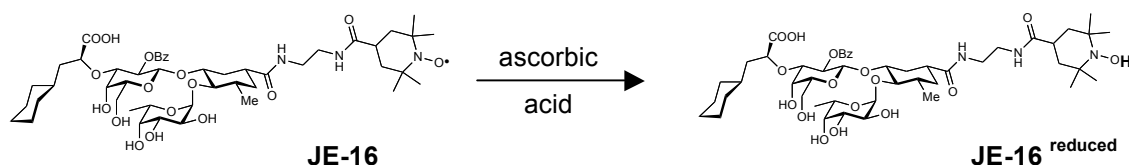


Figure 9. Reduction of **JE-16** with ascorbic acid.

The effect of **JE-16** on the relaxation rate was not the same for all the compounds of sublibrary 1 indicating differences in the proximity between the ligands (Figure 8):

- Compounds **SH-104-2**, **SH-104-3** and **SH-104-16** were not significantly affected by the presence of **JE-16** in either state: radical and reduced. These compounds bound to the protein but not in the vicinity of **JE-16**.
- Compound **SH-104-8** showed an unexpected behavior with a recovery of 110% of the relaxation rate in presence of the reduced form of **JE-16**.
- Compound **SH-104-1** indicated its binding to E-selectin/IgG but probably does not experience a paramagnetic effect.
- Compound **SH-104-12** showed a low affinity for the E-selectin/IgG as previously mentioned. Nevertheless, the relaxation rate seemed to be disturbed in the presence of **JE-16** indicating that **SH-104-12** might bind in its proximity.
- The additional relaxation due to **JE-16** appeared only significant for compounds **SH-104-4** and **SH-104-10**. However, the proximity of the assigned resonance of **SH-104-10** used for the analysis to the resonance of other compounds underscored the need for caution in our conclusions.

According to these results, after screening sublibrary 1, **SH-104-4** was the only compound clearly recognized as a hit. Indeed, in the presence of the E-selectin/IgG, the decay in intensity of the signals of **SH-104-4** was twice as large as that without E-selectin/IgG. This quicker relaxation rate is due to the longer rotational correlation time of the ligand in a bound form, indicating an interaction with the protein. In the presence of **JE-16**, a further enhancement of the decay in intensity by a factor of 1.5 was observed due to the presence of the radical in the vicinity of **SH-104-4** (within a radius of about 20 Å) [32,33]. This effect was cancelled by reduction of **JE-16** with ascorbic acid leading to a recovery of 90 % of the relaxation (Figure 7 and 8).

Due to uncertainty in the results obtained for compounds **SH-104-1**, **SH-104-8**, **SH-104-10** and **SH-104-12**, a new analysis of their relaxation rates was performed. In that purpose, series of six T1ρ experiments with increasing spin-lock duration (10, 50, 100, 150, 200 and 250 ms) were measured.

Prior to the relaxation measurements, each of these four compounds was added independently to a E-selectin/IgG sample and a H-1 spectrum was recorded in order to ensure a precise assignment and to verify that an isolated resonance was observed for **SH-104-10** (Figure 10).

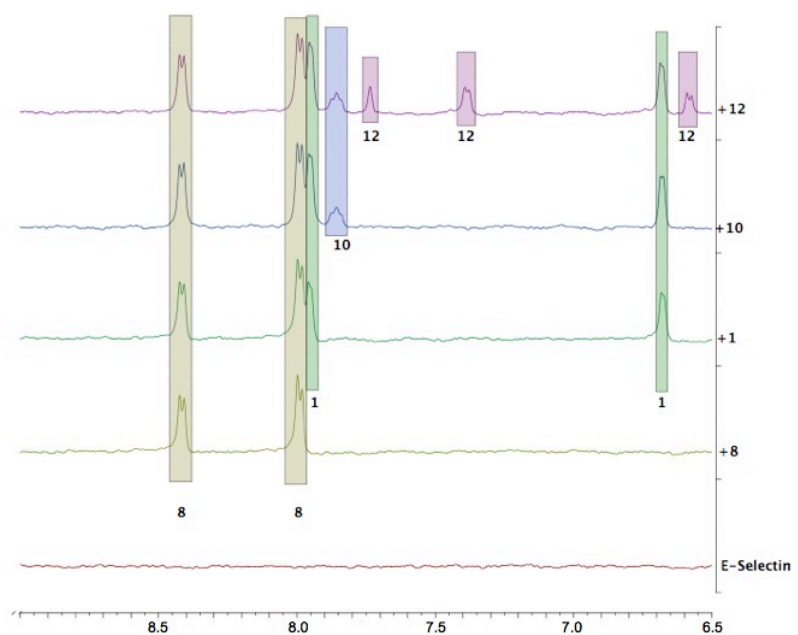


Figure 10. Assignment of the resonances by adding successively the compounds **SH-104-1**, **SH-104-8**, **SH-104-10** and **SH-104-12** to E-selectin/IgG and recording H-1 spectrum.

Then, new cycles of relaxation measurement were performed. As shown on Figure 11, none of the compounds, whose binding was questionable when analyzed in the sublibrary, were confirmed as a hit. A similar relaxation rate was observed in the presence of **JE-16** under both states: radical active or reduced. The variation observed for **SH-104-10** in Figure 8 was probably due to the overlap of the signal with other resonances of other compounds.

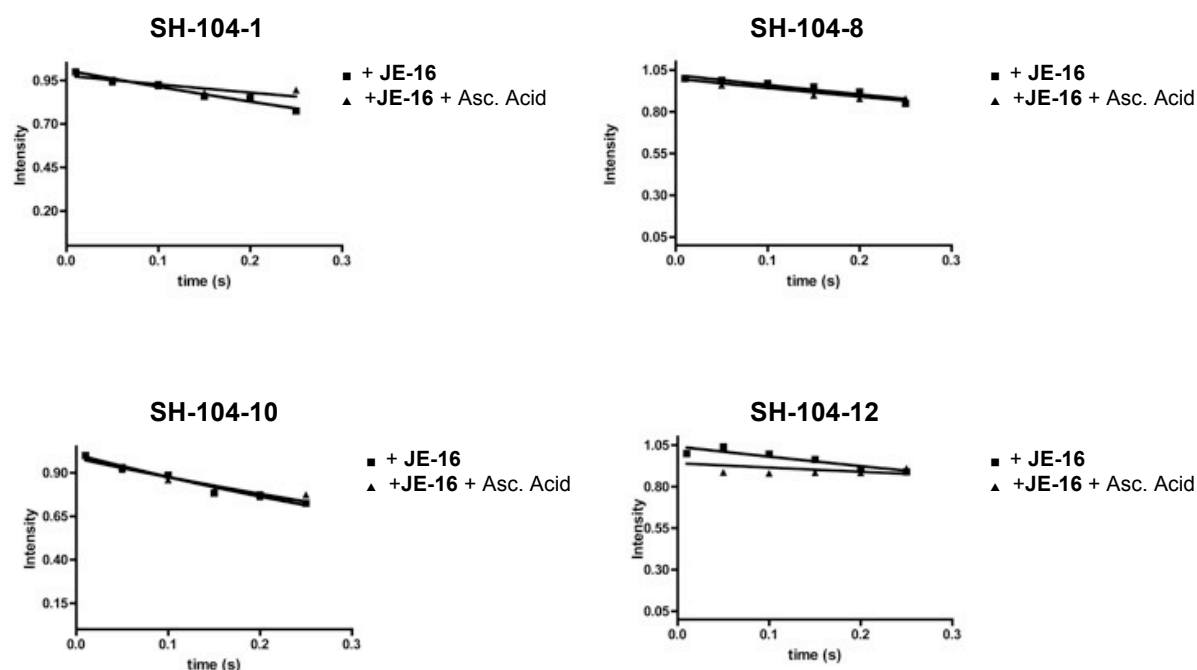


Figure 11. $T_{1\rho}$ relaxation measurement of compounds **SH-104-8**, **SH-104-1**, **SH-104-10** and **SH-104-12** in the presence of E-selectin/IgG, **JE-16** (■) and with **JE-16** reduced by ascorbic acid (▲).

A similar procedure of $T_{1\rho}$ relaxation measurement on isolated resonances from compounds within the different sublibraries of the library was performed. This global screening leads to the identification of six promising hits in addition to the **SH-104-4** (Figure 12). As shown in Figure 13, for all of the hits, a binding to E-selectin/IgG in the vicinity of **JE-16** was observed.

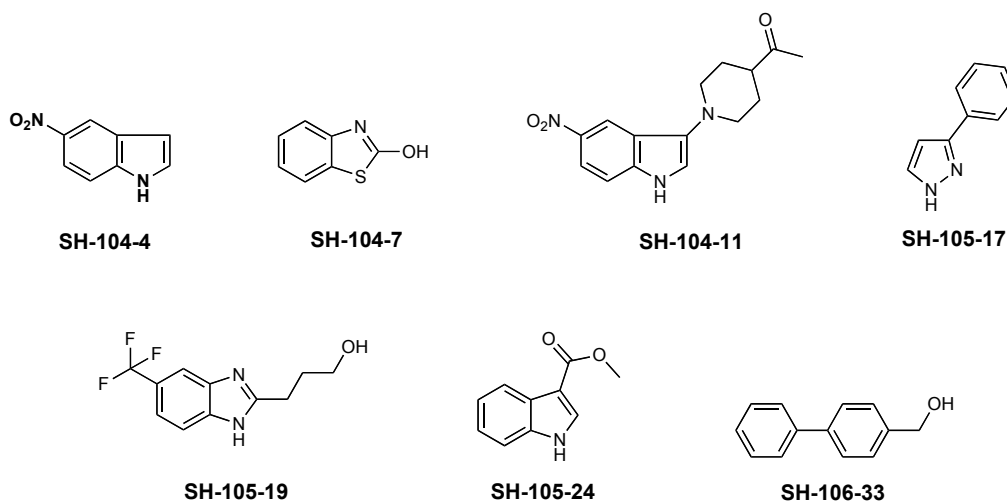


Figure 12. Structure of promising hits selected by NMR screening.

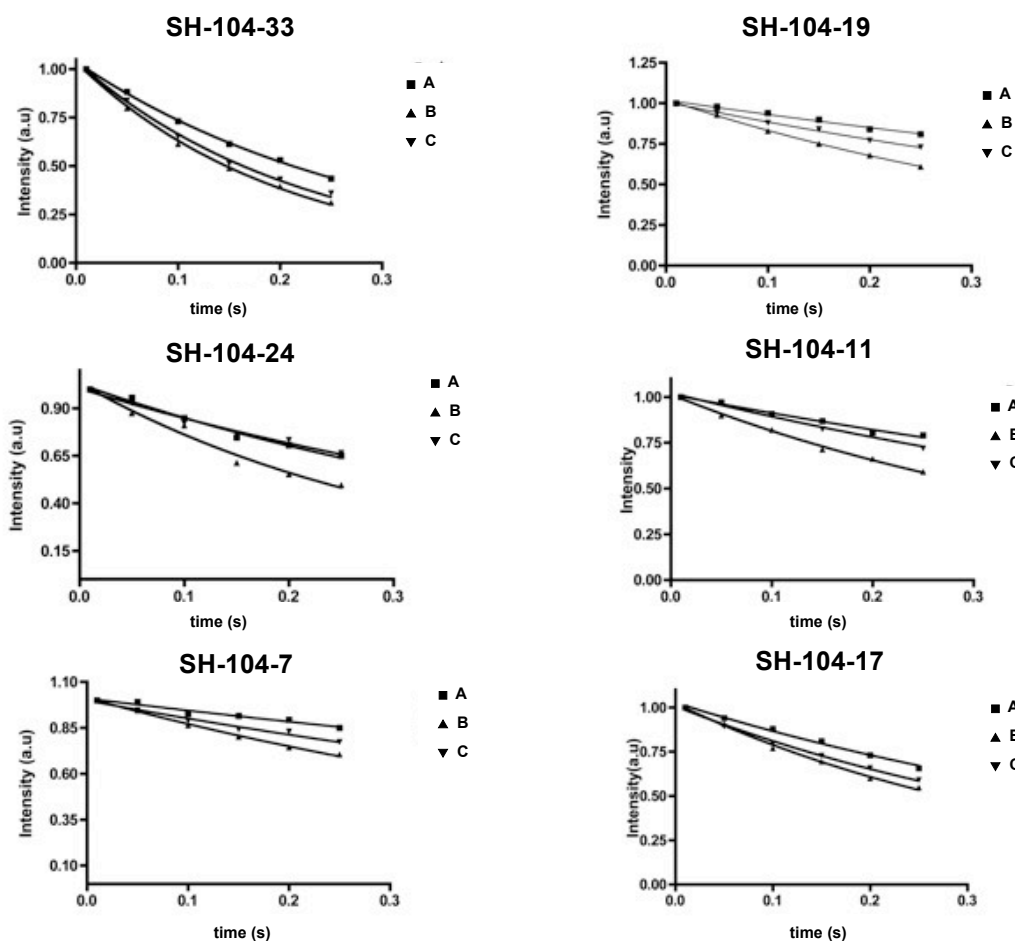


Figure 13. T₁ρ relaxation measurement on isolated resonances of compounds SH-104-33, SH-104-19, SH-104-24, SH-104-11, SH-104-7 and SH-104-17 in the presence of E-selectin/IgG (■A), with JE-16 (▲B) and with JE-16 reduced by ascorbic acid (▼C).

The indole moiety appeared to be an important epitope for binding to the second-site (see ligands **SH-104-4**, **SH-104-7**, **SH-104-11**, **SH-104-19** and **SH-104-24**, Figure 12). Three of the hits found were chosen for further studies: **SH-104-4**, **SH-104-19** and **SH-104-17**. Each of these compound was analyzed individually in the presence of E-selectin/IgG, **JE-16** and **JE-16** reduced with ascorbic acid.

5.3.6 **SH-104-17**

The relaxation rate of **SH-104-17** was measured in the presence of E-selectin/IgG, **JE-16** was then added to the sample and a last cycle of relaxation measurements were performed after reducing **JE-16** with ascorbic acid. A set of four resonances of **SH-104-17**, which did not overlap with the resonances of **JE-16**, was chosen for the study (Figure 14). As shown in Figure 14B, an enhancement of the relaxation rate was observed in the presence of E-selectin/IgG, demonstrating the binding of **SH-104-17** to E-selectin/IgG. Nevertheless, no additional effect was observed in presence of **JE-16**, as well as after reduction of the radical by ascorbic acid (Figures 15, 14C and 14D). Therefore, **SH-104-17** was found to be a hit in the global screening (binding to E-selectin/IgG in the proximity of **JE-16**) but could not be confirmed as a hit when isolated (binding to E-selectin/IgG but not in the vicinity of **JE-16**).

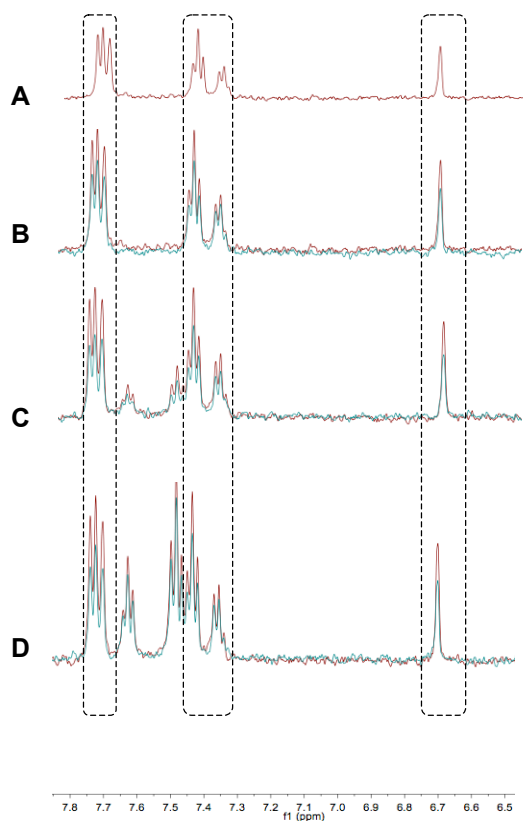


Figure 14. $T_{1\rho}$ relaxation measurement at 10 ms (red) and 250 ms (green) spin-lock durations. **(A)** SH-104-17, **(B)** SH-104-17 and E-selectin/IgG, **(C)** SH-104-17, E-selectin/IgG and JE-16, **(D)** SH-104-17, E-selectin/IgG, JE-16 and ascorbic acid. Resonances of SH-104-17 are indicated (dashed square).

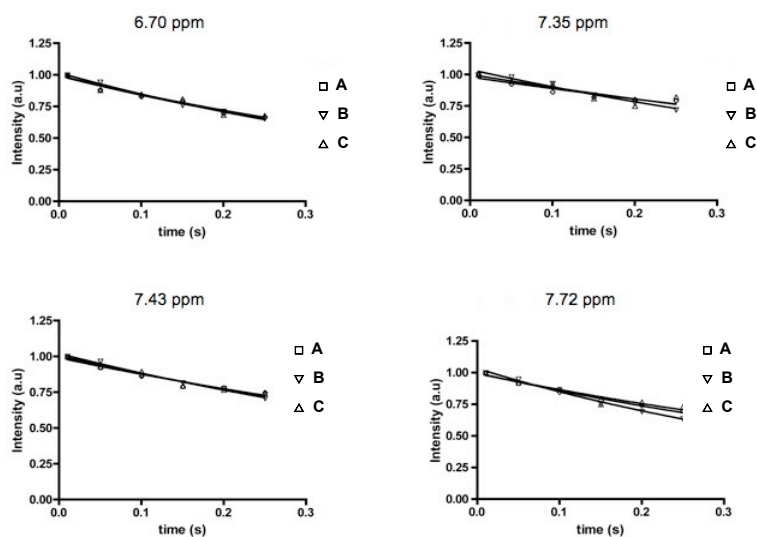


Figure 15. $T_{1\rho}$ relaxation measurement on isolated resonances of compounds SH-104-17 in the presence of E-selectin/IgG (\square A), with JE-16 (\triangle B) and with JE-16 reduced by ascorbic acid (∇ C).

5.3.7 SH-104-19

A set of five isolated resonances of **SH-104-19** was chosen for $T_{1\rho}$ relaxation studies in order to substantiate or negate the result of the global screening (Figure 16).

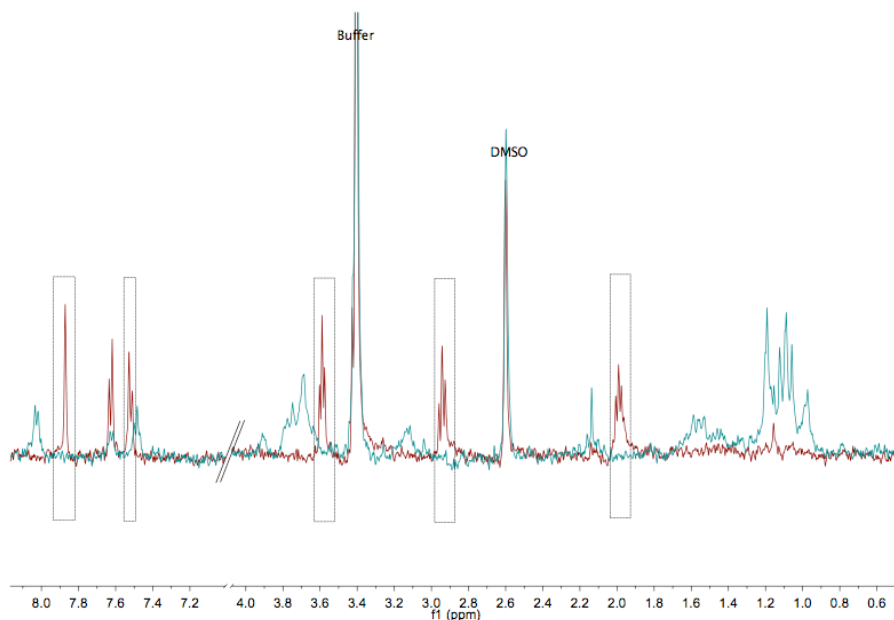


Figure 16. Overlay of H-1 spectrum of **SH-104-19** (200 μ M, red) and **JE-16** (200 μ M, green). Resonances of **SH-104-19** chosen for the $T_{1\rho}$ relaxation experiments are inscribed in rectangles.

As shown in Figure 17, an enhancement of the relaxation was observed in the presence of E-selectin/IgG confirming the binding of **SH-104-19** to the protein. The relaxation rate was significantly affected in presence of **JE-16** and restored after reduction of the TEMPO-ligand by ascorbic acid. Therefore, **SH-104-19** was confirmed as a hit binding in the vicinity of the first-site ligand.

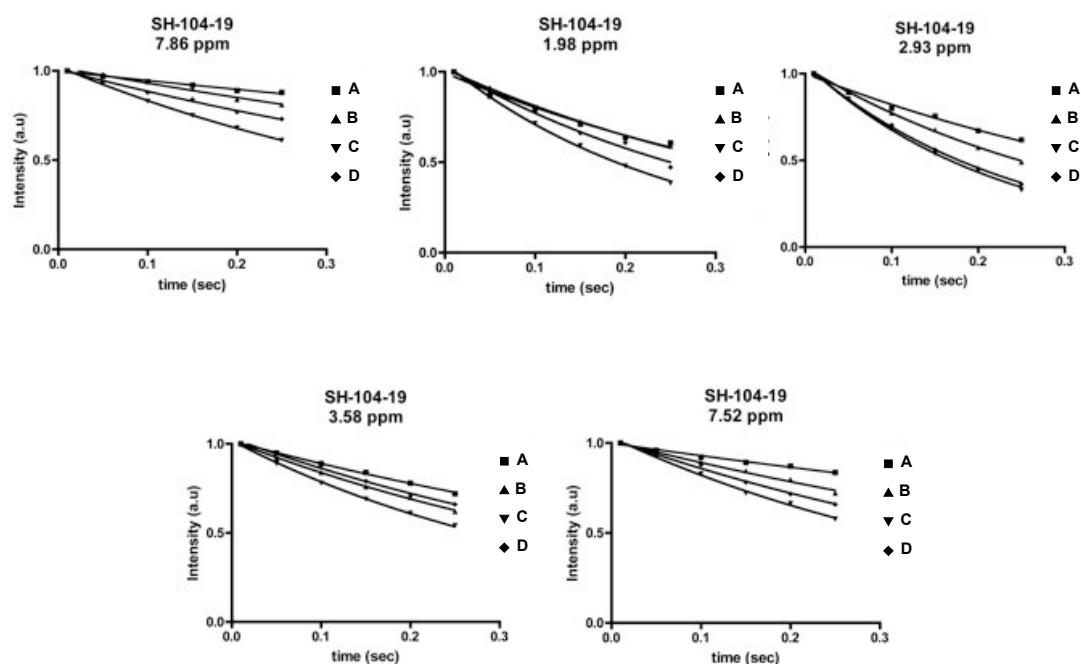


Figure 17. $T_{1\rho}$ relaxation measurement on isolated resonances of compounds **SH-104-19** alone (■A), in the presence of E-selectin/IgG (▲B), with **JE-16** (▼C) and with **JE-16** reduced by ascorbic acid (◆D).

As previously shown, the relaxation rate of the screening hit was affected by the paramagnetic influence of **JE-16**. The size of this influence is directly related to the distance between the observed hydrogen and the radical. Therefore, it was possible to estimate the orientation of the second-site ligand. Indeed, an optimal placement of the linker is crucial for the potency of the linked compounds.

The four best-isolated resonances of **SH-104-19** were chosen for a detailed analysis of the orientation (7.86 ppm, 3.58 ppm, 2.93 ppm and 1.98 ppm). Relaxation data were fit using Eq. (2) and relaxation rates estimated from the fit where C is a constant, Y is the relative intensity obtained for each spin-lock duration, X is the spin-lock duration and K corresponds to relaxation rate, $R_{1\rho}$.

$$Y = C * \exp (-R_{1\rho} * X) \quad (2)$$

Because of an incomplete recovery of the signal after reduction of **JE-16** by ascorbic acid, the relaxation of **SH-104-19** in the presence of E-selectin differed from its relaxation in the presence of E-selectin and the reduced form of **JE-16**. For this reason, the differences in the relaxation rate obtained for **SH-104-19** mixed to E-selectin/IgG in the presence and absence of **JE-16** were chosen for the analyses (indicated as Δ in Figure 18). An example is shown in Figure 18 on the left for the resonance at 7.86 ppm and the results obtained for the different resonances are summarized in the table.

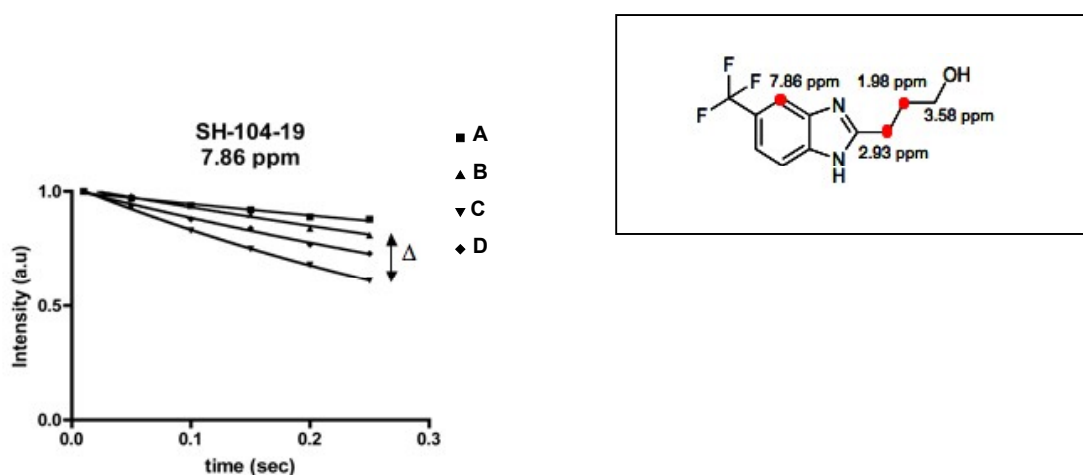


Figure 18. Enhancement of the relaxation rate observed for **SH-104-19** mixed with E-selectin/IgG in presence and absence of **JE-16** (Δ). Plot A: **SH-104-19** alone, plot B: **SH-104-19** and E-selectin/IgG, plot C: **SH-104-19**, E-selectin/IgG and **JE-16**, plot D: **SH-104-19**, E-selectin/IgG, **JE-16** and ascorbic acid. The hydrogen found to be closer to the radical are highlighted in red on the structure of **SH-104-19** (top right).

As a result, hydrogen in position 4 of the indole moiety and hydrogens in position 1' and 2' of the propanol chain were more affected by the presence of the TEMPO, indicating their proximity to **JE-16**. A schematic view of the orientation of **JE-16** and **SH-104-19** is presented in Figure 19. In the linked compound, the linker should be preferentially attached on the site of **SH-104-19** closest to **JE-16** in order to obtain the ideal orientation of the molecules.

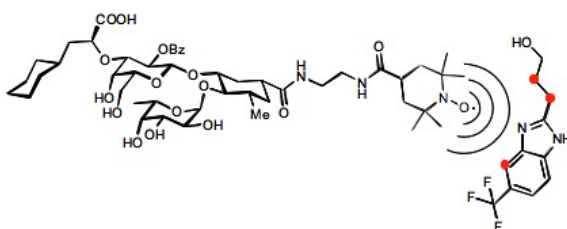


Figure 19. Schematic view of **JE-16** and **SH-104-19**.

5.3.8 SH-104-4

SH-104-4 was immediately recognized as a hit after the screening of sublibrary 1. Indeed, the relaxation rate of **SH-104-4** was enhanced in the presence of E-selectin/IgG (proving the binding) and was further enhanced by the presence of **JE-16** (proving the proximity between the two molecules). The same procedure as previously described for **SH-104-19** was applied to **SH-104-4**. Thus, the first step was the validation of **SH-104-4** as a hit by repeating the $T_{1\rho}$ relaxation measurement with the isolated compound.

Assignment of **SH-104-4**

transferNOE experiment were recorded with **SH-104-4** and E-selectin/IgG and assigned by Dr. Cutting and Jonas Egger. As shown in Figure 20, only resonances of hydrogens in position 3 and 4 of **SH-104-4** were completely isolated from those of **JE-16**. Signals of hydrogens in position 2 and 7 of **SH-104-4** were partially overlapping with resonances of **JE-16**.

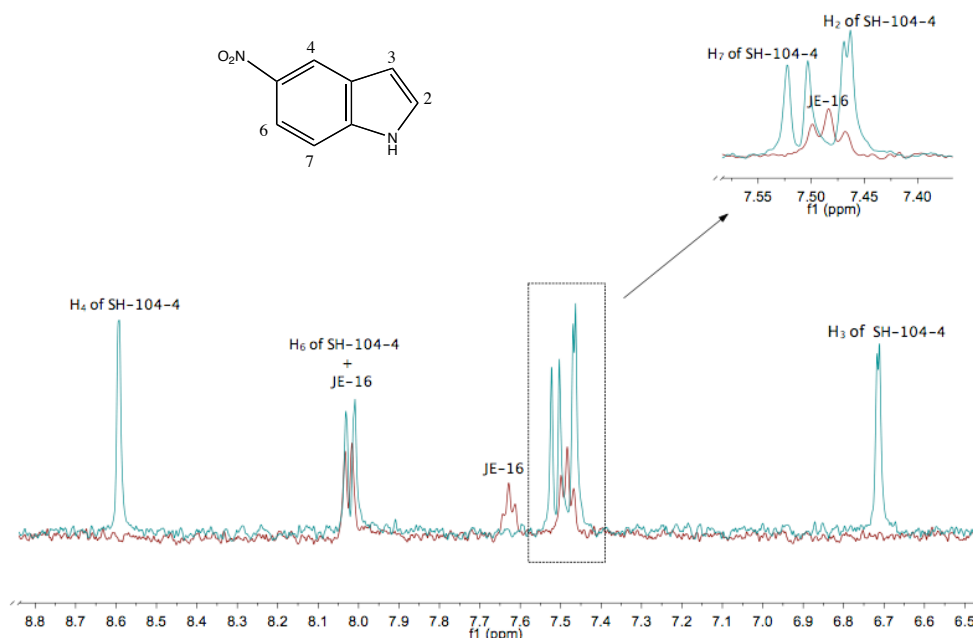


Figure 20. Overlay of H-1 spectrum of **JE-16** reduced by ascorbic acid (red) and H-1 spectrum **SH-104-4** in the presence of E-selectin/IgG (green).

Validation of **SH-104-4** as a hit

The relaxation curves are displayed for the H-1 resonances in position 3, 4 and 7 of **SH-104-4** (Figure 21). The interaction with E-selectin/IgG was clearly confirmed as well as the proximity to the radical.

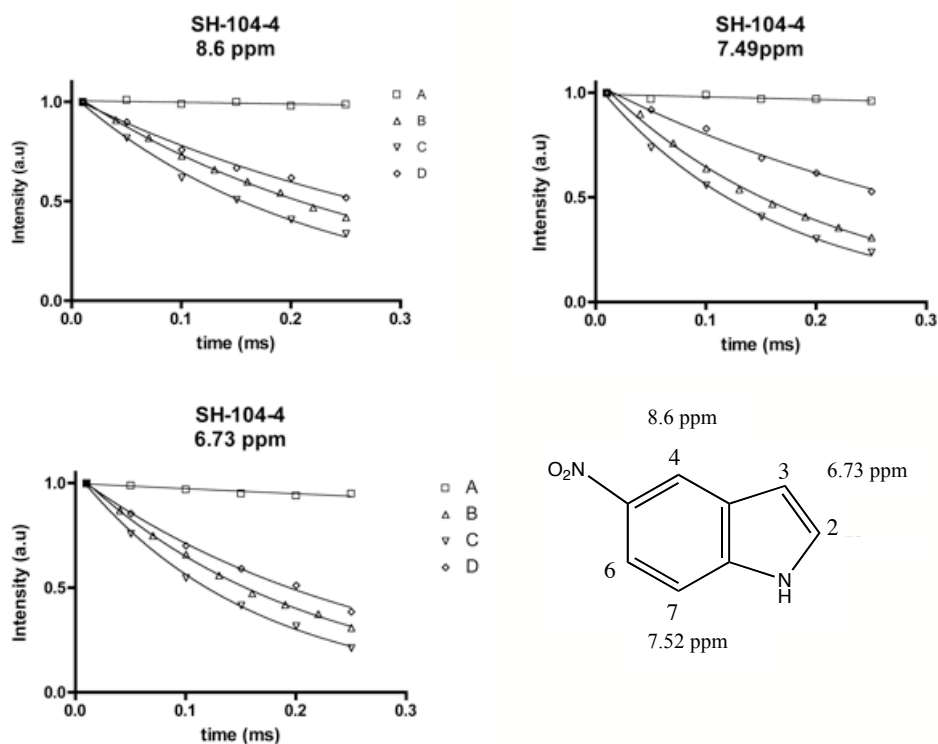


Figure 21. Variation of the relaxation rate observed for **SH-104-4**. Plot A: **SH-104-4** alone, plot B: **SH-104-4** and E-selectin/IgG, plot C: **SH-104-4**, E-selectin/IgG and **JE-16**, plot D: **SH-104-4**, E-selectin/IgG, **JE-16** and ascorbic acid. The hydrogen studied are indicated on the structure of **SH-104-4** (bottom right).

STD-NMR measurements were used as a complementary approach to confirm the binding of **SH-104-4** to E-selectin/IgG. As shown in Figure 22B, the binding was confirmed through the observation of the nitroindole STD signals.

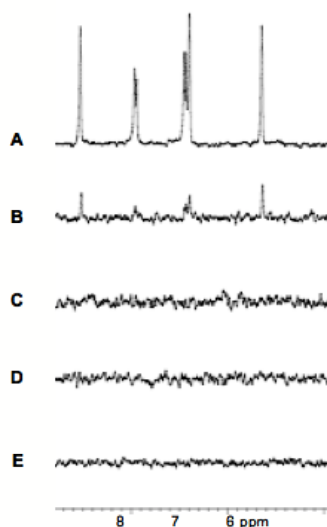


Figure 22. Confirmation of the binding of **SH-104-4** to E-selectin/IgG with STD-NMR experiments. (A); H-1 spectrum of **SH-104-4** (250 μ M) in the presence of E-selectin/IgG (B), (C); STD-NMR and reference spectra of **SH-104-4** (250 μ M) in the presence of E-selectin/IgG (D), (E); STD-NMR and reference spectra of **SH-104-4** (250 μ M) without E-selectin/IgG.

An example of the high reproducibility of the relaxation rate measurement of **SH-104-4** in the presence of E-selectin/IgG is shown in Figure 23. The level of reproducibility suggests that the method could be applied to check the quality of an E-selectin sample after purification.

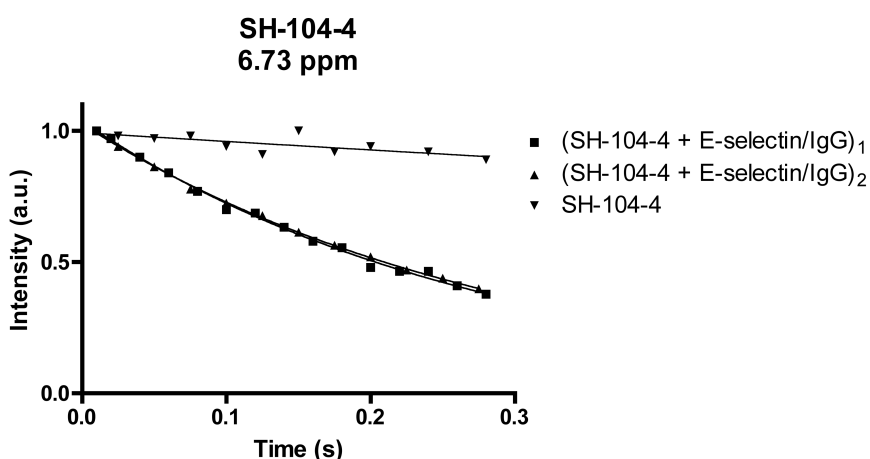


Figure 23. Relaxation rate of **SH-104-4** in the absence and in the presence of two different batches of E-selectin/IgG.

WaterLOGSY was used as a complementary approach in order to verify the independent binding of **SH-104-4** and **JE-16** to E-selectin/IgG. This method is used

to identify compounds that bind to a target using water-mediated NOEs [31,34,35]. In this experiment, it is possible to distinguish binding and non-binding ligands, since, provided the fraction of unbound ligand is not too large, their resonances appear with opposite sign.

Ascorbic acid and DMSO did not bind to E-selectin/IgG and showed resonances with an opposite sign as those of **SH-104-4** and **JE-16** (Figure 24). Therefore, the independent binding of **JE-16** and **SH-104-4** to E-selectin/IgG was confirmed.

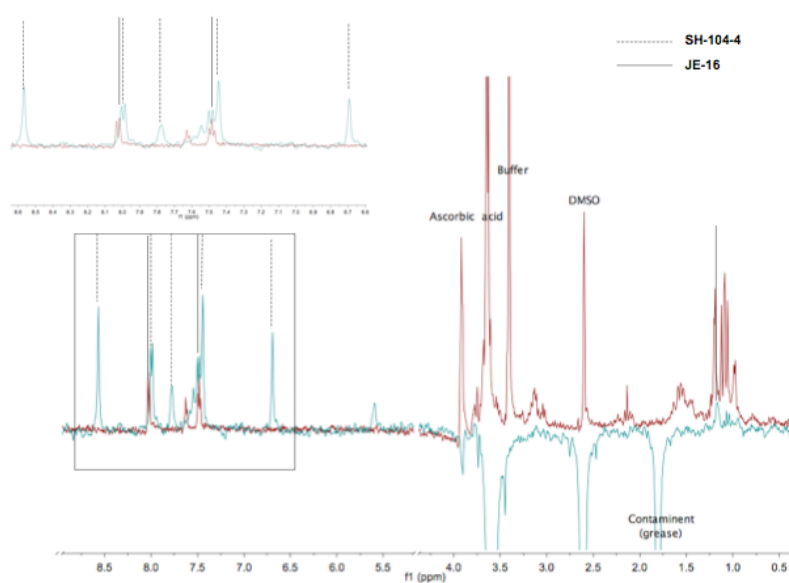


Figure 24. Overlay of H-1 spectrum of **JE-16** reduced by ascorbic acid (red) and WaterLOGSY spectrum of **SH-104-4** in the presence of E-selectin/IgG and **JE-16** reduced by ascorbic acid (green). Resonances of **SH-104-4** and **JE-16** (respectively dashed and solid lines) were highlighted.

*Orientation of **SH-104-4***

The determination of the orientation of **SH-104-4** to the radical was performed for the resonances of hydrogens in positions 3, 4 and 7. For hydrogens in positions 3 and 4, the analysis was straightforward since no overlap with the resonances of **JE-16** was present. The data obtained for the hydrogen in position 7 were also processed. A minimal overlap was observed for the component of the multiplet at 7.52 ppm, justifying the use of hydrogen 7 in this analysis. Two measurements on two different samples were performed. A nearly complete removal of the effect of the radical on the relaxation was obtained by reduction of **JE-16** with

ascorbic acid. Therefore, the differences in relaxation rates obtained for **SH-104-4** mixed with E-selectin/IgG in the presence of **JE-16** and in the presence of reduced **JE-16** were calculated and compared (indicated as Δ in Figure 25). As shown in Figure 25, the hydrogen in position 7 of **SH-104-4** (7.52 ppm) appeared to be closer to the radical, followed by the hydrogen in position 3 of **SH-104-4** (6.73 ppm) and finally, the hydrogen in position 4 of **SH-104-4** (8.6 ppm), which appeared to be the most remote.

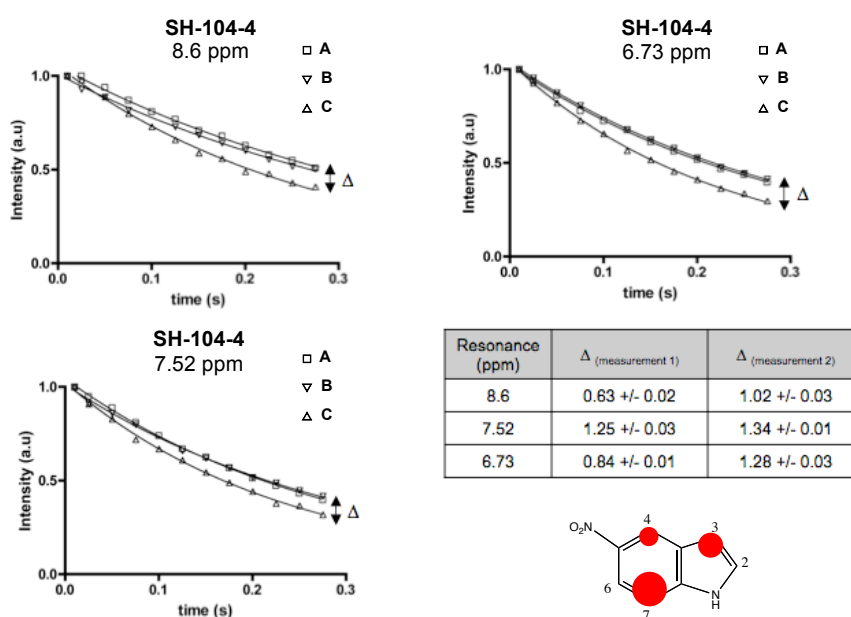


Figure 25. Enhancement of the relaxation rate observed for **SH-104-4** mixed with E-selectin/IgG in the presence and in the absence of **JE-16** (Δ). Plot A: **SH-104-4** and E-selectin/IgG, plot B: **SH-104-4**, E-selectin/IgG and **JE-16**, plot C: **SH-104-4**, E-selectin/IgG, **JE-16** and ascorbic acid. Red circles indicate the proximity of the hydrogen of **SH-104-4** to **JE-16** according to their size (the bigger the closer).

Complementary studies

The influence of the high concentration of ascorbic acid (5 mM) on the relaxation of **SH-104-4** (150 μ M) was checked in the absence of E-selectin/IgG immediately after mixing the compounds, after 48h of incubation and after 72h of incubation. No significant perturbation of the relaxation was observed ($0.017 <$ coefficient of variation < 0.042 , Figure 26A). In addition, no perturbation of the

relaxation was observed in presence of a first-site ligand (**BW-69669**), in the absence and in the presence of E-selectin/IgG was observed (Figure 26B).

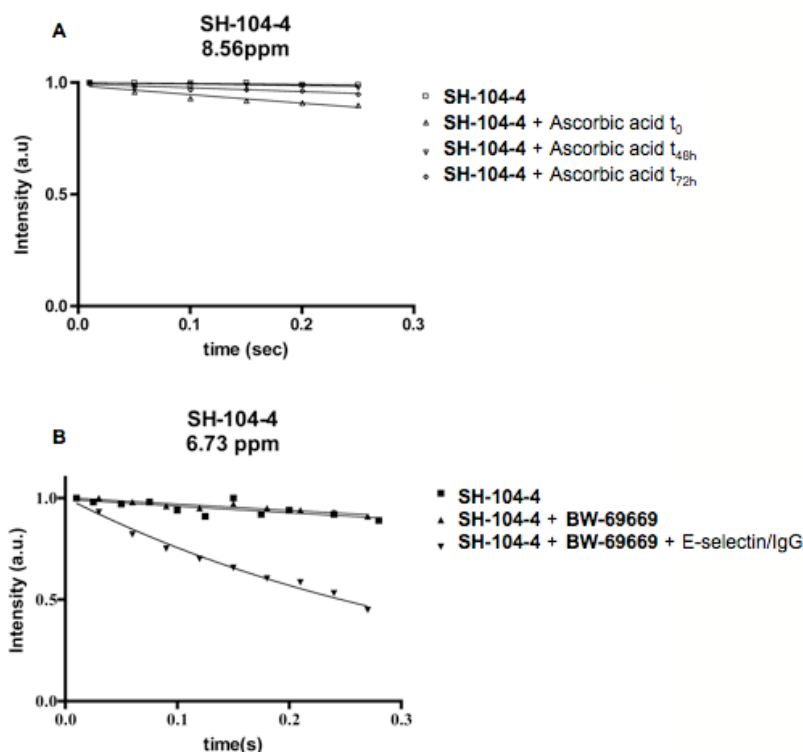


Figure 26. (A) Relaxation rate of **SH-104-4** (150 μ M) in presence of ascorbic acid (5 mM). (B) Relaxation rate of **SH-104-4** in presence of **BW-69669** with and without E-selectin/IgG.

Conclusion

After being successfully used with the MAG for the development of more potent ligands [32,36-38], **SH-104-4** was chosen for further development of E-selectin antagonists. According to the results previously shown for E-selectin, the hydrogen in position 7 of **SH-104-4** (7.52 ppm) appeared to be closest to the radical. Nevertheless, the partial overlap of the hydrogen in position 7 indicated that caution is required when choosing the position of **SH-104-4** for the linkage of first and second site ligands. Therefore, 2 series of new generations of E-selectin antagonists were synthesized in-house by Jonas Egger. In the first series, the linker in the second-site ligand is connected to the nitrogen of the indole system. In the second series, the linker is connected to the carbon in position 3 of the indole system (Figure 27). Compounds belonging to the same series differ from each other by the length of the spacer on either side of the triazole.

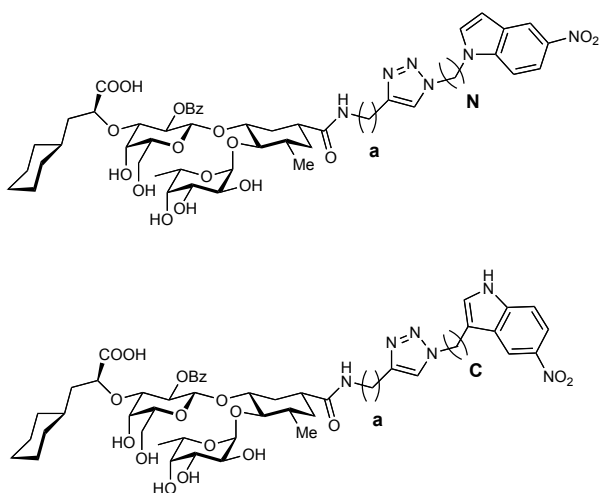


Figure 27. Schematic view of the two series of first-second-site antagonists. For the linker, the nomenclature refers to the number of carbons on the first-site side or on the second-site side of the triazole. **a** indicates that anti-triazoles are investigated, **N** indicates that the linker is connected to the nitrogen of the indole system, **C** indicates that the linker is connected to the carbon in the 3 position of the indole system.

5.3.9 Analysis of the first compound synthesized and optimization of the Biacore method

JE-63 was the first synthesized compound resulting from the second-site screening approach. A first evaluation of **JE-63** was performed under the conditions used in the Biacore assay for the first-site ligand (Flow rate = 20 $\mu\text{l}/\text{min}$, association time = dissociation time = 60 s, see chapter 5). As shown in Figure 28A, the association time was too short to reach the steady state. Therefore, three conditions were tested:

- (i) Flow rate = 20 $\mu\text{l}/\text{min}$, association time = dissociation time = 120 s
- (ii) Flow rate = 30 $\mu\text{l}/\text{min}$, association time = dissociation time = 120 s
- (iii) Flow rate = 30 $\mu\text{l}/\text{min}$, association time = dissociation time = 150 s

For the optimization of the conditions, only four concentrations were injected, starting at 2.5 μM with a dilution factor of 2. Conditions (ii) were optimal and were therefore used for the complete analysis of **JE-63** (Figure 28B).

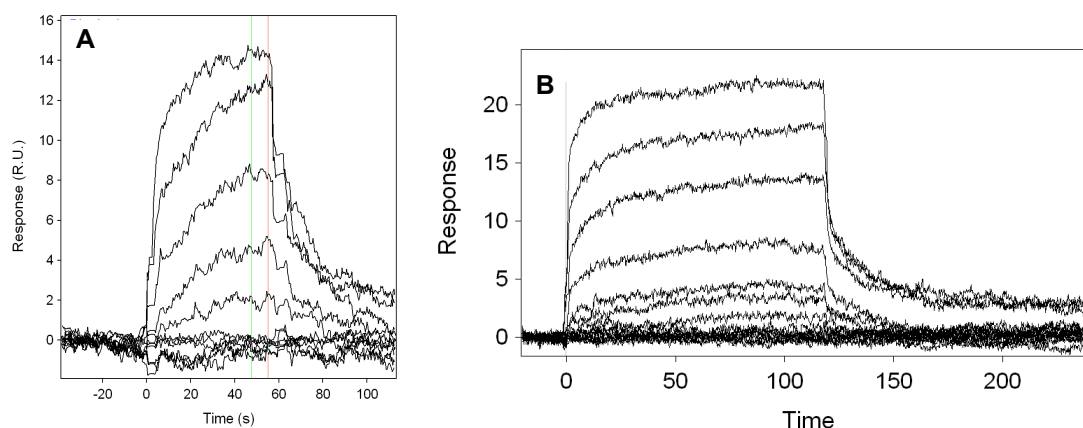


Figure 28. Sensorgrams of **JE-63** binding to E-selectin/IgG immobilized on the CM5 surface by capture assay *via* anti-human IgG. **(A)** Flow rate 20 $\mu\text{l}/\text{min}$, association time 60 s, dissociation time 60 s **(B)** Flow rate 30 $\mu\text{l}/\text{min}$, association time 120 s, dissociation time 120 s.

The linked compound showed an improvement in the affinity by a factor of 3 compared to the unlinked compound **DS-04115** (Figure 29). When the three most concentrated samples were injected, an incomplete return to the baseline was observed. This was probably due to a small “rebinding effect” of the compound on the surface [38] and these concentrations were not taken into account for the kinetic evaluation.

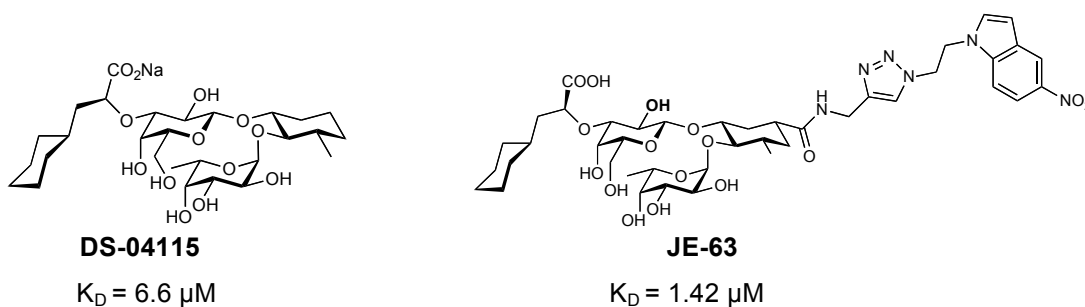


Figure 29. Structure of **DS-04115** and **JE-63** and related K_D s calculated from the kinetic parameters measured by Biacore.

The kinetic parameters of the binding were different for **JE-63** compared to all other E-selectin ligand until then investigated. Although both k_{on} ($5.15 \times 10^4 \text{ M}^{-1}\text{s}^{-1}$) and k_{off} (0.073 s^{-1}) rates were slower, the k_{off} rate showed a stronger reduction and resulted in a $t_{1/2}$ of 9.49 s (Figure 30).

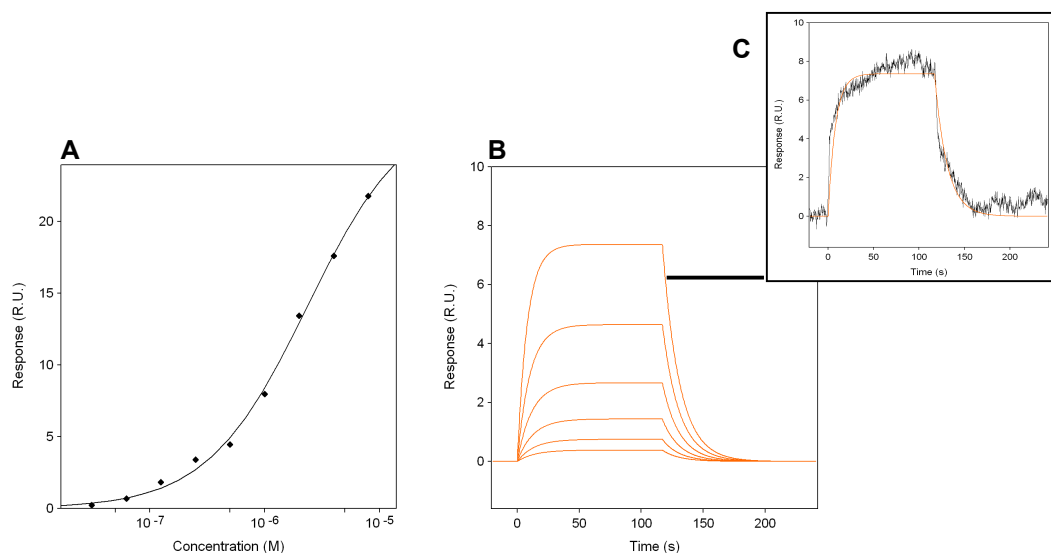


Figure 30. (A) Plot of the binding isotherm for **JE-63** binding to E-selectin/IgG fit with a 1:1 binding model. (B) Kinetic fit of the sensorgrams for injections of **JE-63** between 1 μM and 31.25 nM. (C) Example of a kinetic fit using the 1 μM concentration.

5.3.10 Optimization of assay conditions for **JE-57**

The parameters of the method optimized for **JE-63** were not optimal for **JE-57** (Figure 31). In particular, an association time of 120 s was not sufficient to reach the steady state. Therefore, the association time was increased to 600 s. The dissociation time was also increased to 600 s to reach a stable baseline in-between each sample injection and a flow rate of 20 μl/min was used. In addition, one blank injection was performed between each injection of **JE-57**. This blank injection ensured that the system did not contain any residual of **JE-57** prior to each new injection of the compound. These buffer injections washed the surface without risk of damaging the E-selectin/IgG immobilized (data not shown).

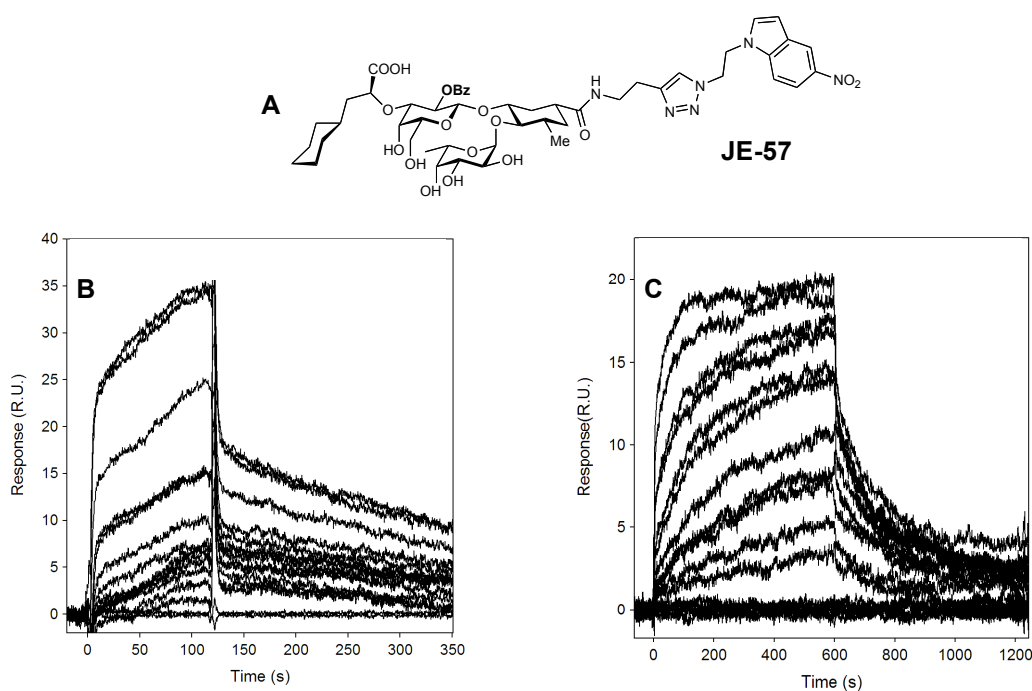


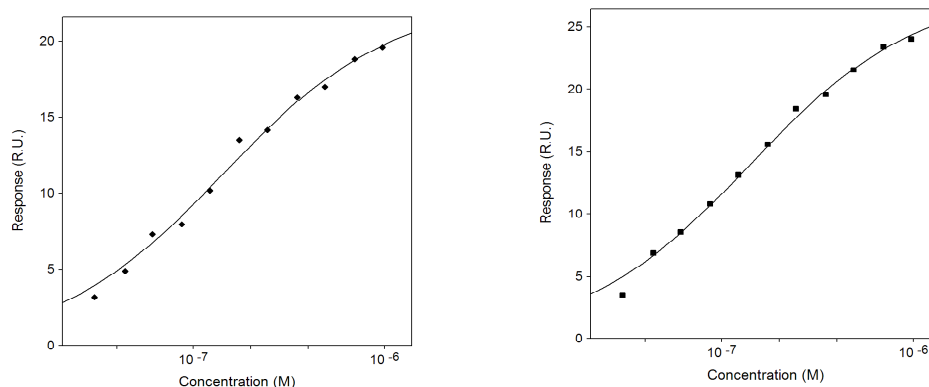
Figure 31. (A) Structure of **JE-57**. Sensorgrams of **JE-57** binding to E-selectin/IgG immobilized on the CM5 surface by the capture assay via anti-human IgG. (B) Flow rate 20 $\mu\text{l}/\text{min}$, association time 120 s, dissociation time 600 s (C) Flow rate 20 $\mu\text{l}/\text{min}$, association time 600 s, dissociation time 600 s.

JE-57 was measured over two surfaces in order to study the reproducibility. The affinity was improved by a factor of 10 compared to the first generation of compounds, as e.g. **GMI-1077**, tested on the same surface ($K_D = 1.24\mu\text{M}$). In addition, the k_{on} was 10 times slower and k_{off} 180 times slower (Table 4).

Table 4. Kinetic and affinity evaluation of **JE-57**. Plots of the equilibrium binding isotherm plots are shown in the bottom (A) **JE-57** measurement 1 (B) **JE-57** measurement 2.

Analyte	$K_{D \text{ eq}} [\mu\text{M}]^{**}$	$K_{D \text{ kin}} [\mu\text{M}]^*$	$k_{\text{on}} [10^4 \text{ M}^{-1} \text{ s}^{-1}]$	$k_{\text{off}} [\text{s}^{-1}]$	$t_{1/2} [\text{s}]^{***}$
JE-57 _{meas. 1}	0.14	0.15	2.6	0.004	173
JE-57 _{meas. 2}	0.13	0.13	3.9	0.005	138
GMI-1077	1.24	1.2	46.5	0.560	1.24

*calculated K_D using $K_D = k_{\text{off}}/k_{\text{on}}$ ** experimental K_D derived from the steady state response fit to a single binding site model *** calculated $t_{1/2}$ using $t_{1/2} = \ln 2/k_{\text{off}}$.



The same parameters were applied to determine the affinity and kinetic parameters of other first-second-site antagonists as well as for the ranking study.

5.3.11 Ranking

A ranking of the antagonists was performed in order to obtain qualitative information about the binding strength of 20 first-second-site antagonists synthesized by Jonas Egger.

Preliminary studies for optimization of the ranking procedure.

The binding constant of **JE-57** was previously determined ($K_D = 0.14 \mu\text{M}$). Saturation was reached with a $1 \mu\text{M}$ injection. Therefore, in a first attempt, **JE-56**, **JE-57** and **JE-58** were injected at a concentration of $1 \mu\text{M}$ and $0.1 \mu\text{M}$ over the same surface. To ensure that all analyte is removed from the chip surface, before the injection of a new compound, two injections of buffer were performed after each injection of analyte. The response observed in Biacore is directly related to the molecular weight of the analyte. Therefore, in order to rank the ligands, the response obtained for each injection was divided by the molecular weight of the corresponding compound. All the compounds showed a similar normalized response (Figure 32). Indeed, the ranking observed for the two concentrations injected appeared nearly identical.

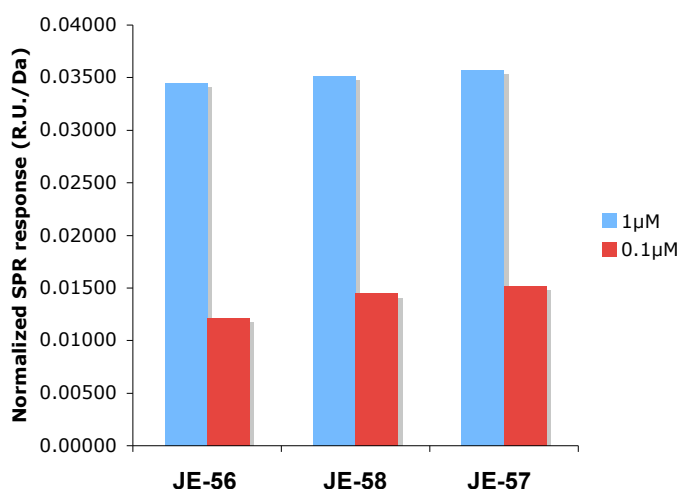


Figure 32. Response of **JE-56**, **JE-57** and **JE58** at $0.1 \mu\text{M}$ and $1 \mu\text{M}$ normalized to the respective molecular weight of the compounds.

Following these preliminary studies for the ranking procedure, **GMI-1077** was used as a test compound in order to check the quality of the surface. As shown in Figure 33, the lack of activity did not allow further studies and a new surface had to be prepared.

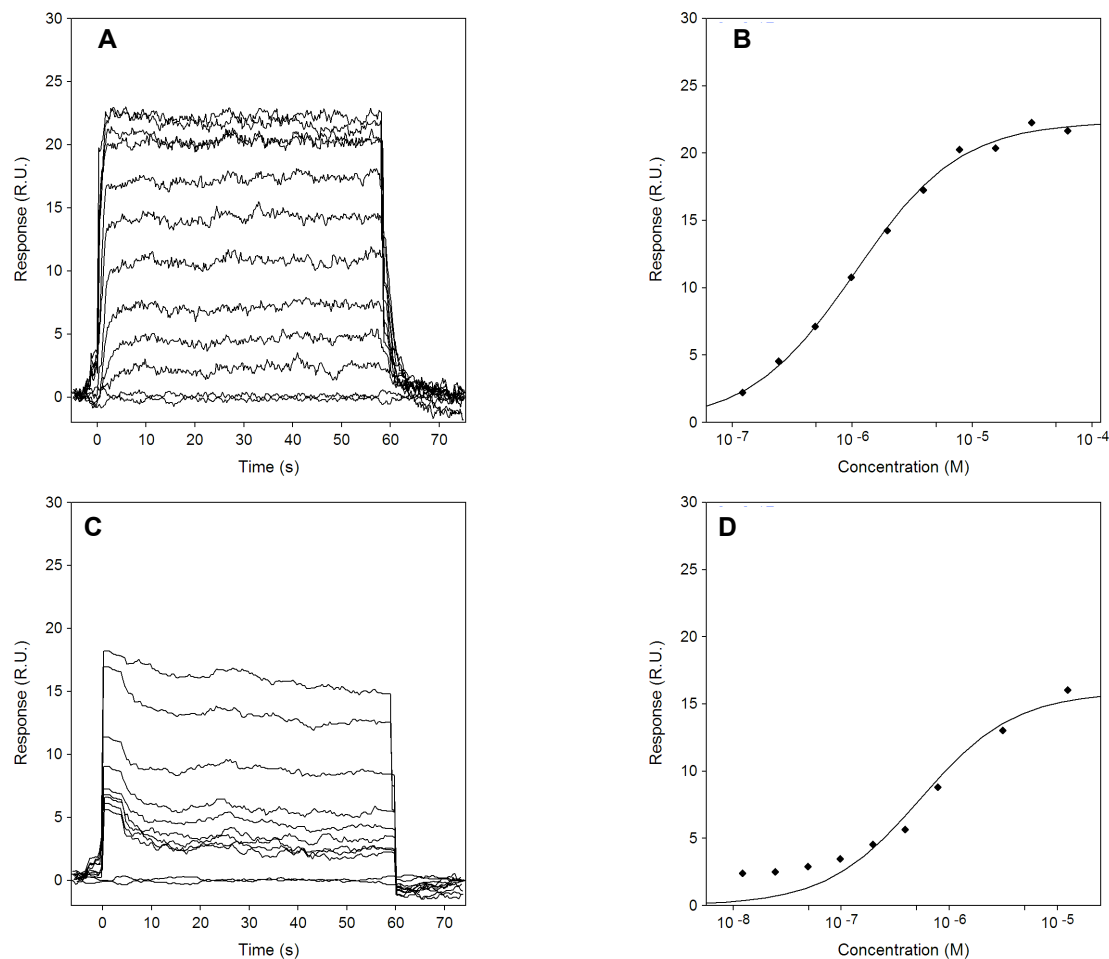


Figure 33. Sensorgrams and binding isotherm plots of **GMI-1077** for E-selectin/IgG before (**A** and **B**) and after (**C** and **D**) injections of **JE-56**, **JE-57** and **JE-58** for ranking studies.

Use of different surfaces for the ranking

A new E-selectin/IgG surface was prepared and 0.5 μ M of **JE-56**, **JE-57** and **JE-58** were injected. As shown in Figure 34A, it appeared not possible to directly compare the results obtained with measurements over different surfaces. Specifically, the intensity of the response obtained is related to the level of immobilization of protein (E-selectin/IgG and anti-human IgG used for the capture). The proportionality of the concentration injected and the response recorded is not identical between different surfaces due to a variation in the level of protein

immobilized (e.g. 0.5 μM exhibits a higher normalized response than 1 μM measured on a different surface, Figure 34A). The level of immobilization can differ considerably from one to another immobilization, even when a similar standard operating procedure is followed (Table 5). In addition, because all ligands analyzed exhibited a low response, the density of the immobilized protein was increased, resulting in a significant change in the response recorded. This variation had a strong impact on the result of the ranking in which compounds are evaluated according to the response obtained for a single injection. As shown in Figure 34B, the relative ranking order was the same with a set of compound tested over the different surfaces but the normalized response of a compound tested over surface 2 can not be included in the ranking obtained over surface 1.

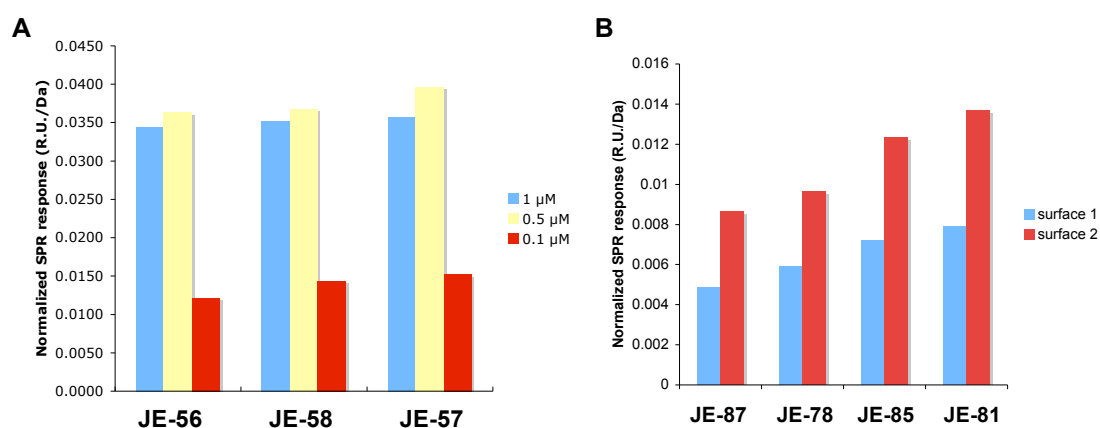


Figure 34. (A) Normalized response obtained for **JE-56**, **JE-57** and **JE-58** at 1 μM , 0.5 μM and 0.1 μM . 1 μM and 0.1 μM were recorded on the same surface. (B) Normalized response obtained for **JE-87**, **JE-78**, **JE-85** and **JE-81** at 0.05 μM on two different surfaces described in Table 1.

Table 5. Comparison of the response obtained for a 1.9 μM injection of **GMI-1077**, as well as a full series to obtain the K_D over 2 surfaces with different levels of immobilization of protein (anti-human/IgG and E-selectin/IgG).

Surface	Analyte	Surface Capacity Antibody anti-hIgG(Fc) [RU]	Surface Capacity E-selectin/IgG [RU]	Response at 1.9 μM [RU]	R_{max} [RU]	Exp. K_D^* [μM]
1	GMI-1077	10971	4290	14.2	23.4	1.3
2	GMI-1077	16350	9446	17.6	30.2	1.4

*Experimental values obtained by fitting the steady state responses to a 1:1 binding model

In order to compare compounds analyzed over different surfaces, two possibilities were considered: (i) a normalization to the R_{max} observed for each compound (ii) a normalization to an internal standard. The first option was unacceptable, because it implied a complete analysis of each compound, thus

negating any advantage in time and cost from a ranking. Therefore, **JE-81** was chosen as an internal standard for the next series of measurements. With this internal standard, measurements made over different surfaces showed similar normalized response and could be compared between each other (Figure 35).

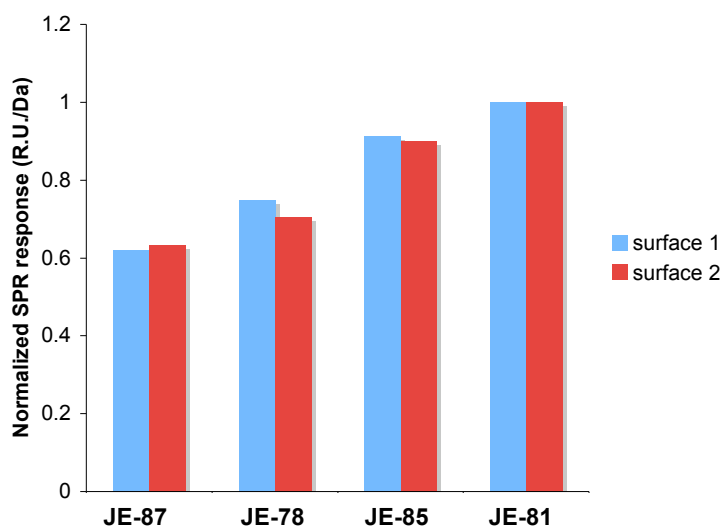


Figure 35. Normalized response obtained for **JE-78**, **JE-81**, **JE-85** and **JE-87** at 0.05 μM on two different surfaces (Table 4) with a second normalization to **JE-81** chosen as an internal standard.

Justification of the choice of the concentration injected for the ranking

As previously mentioned, in the preliminary test performed with **JE-56**, **JE-57** and **JE-58**, three concentrations were tested based on the results obtained for the complete characterization of **JE-57**. Therefore, the concentration at saturation (1 μM) was injected as well as a concentration close to the K_D value [K_D (**JE-57**) = 0.14 μM , concentration injected 0.1 μM]. With both concentrations, a similar ranking was observed. An intermediate concentration of 0.5 μM was also successfully tested and was applied for the ranking of a second series of compounds: **JE-78**, **JE-81**, **JE-85** and **JE-87**. However, as shown in Figure 36, this concentration appeared to be too high for these compounds. An increasing slope in steady state and no return to the baseline during the dissociation phase were observed showing a persistence of the compound on the surface.

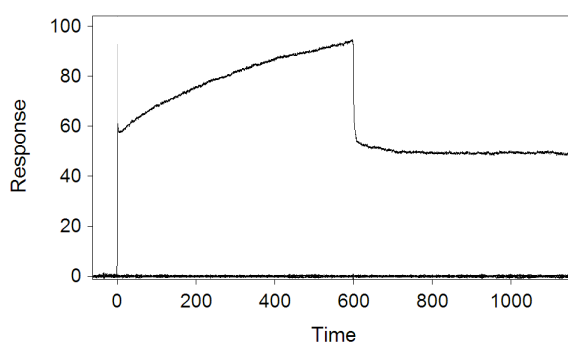


Figure 36. Sensorgram obtained after injection of 0.5 μM of **JE-78** and a blank injection.

Therefore, a new cycle of injections was performed at a concentration of 0.05 μM . This concentration was finally suitable for the entirety set of compound and was used for the global ranking of 20 first-second-site antagonists synthesized by Jonas Egger.

Final result of the ranking

The results obtained were normalized to both, the response of **JE-81**, and their molecular weight (Figure 37). A mean value is reported for the compounds measured more than once (labeled with *).



Figure 37. Ranking of 20 first-second-site antagonists according to their normalized response at a concentration of 0.05 μM (SPR signal divided by the molecular weight and normalized to **JE-81**).

The ranking clearly showed a higher binding strength for the compounds linked to the nitrogen of 5-nitroindole. Indeed, four out of the five compounds showing the highest affinity were linked to the nitrogen of the 5-nitroindole (**JE-81**, **JE-85**, **JE-**

86, JE-97). In addition, a linker length of six carbons (Figure 34, $a+N = 6$) led to improved binding affinities (**JE-86** and **JE-81**) in the N-linked case. A significant decrease in affinity was observed between the **JE-86** and **JE-89** showing that a linker length of six carbons was not optimal for compounds linked to the carbon-3 of the 5-nitroindole. Only one compound (**JE-83**) linked to the carbon-3 on the 5-nitroindole belongs to the five compounds with the best affinities. Its homologue (**JE-78**) with a similar length of the linker ($2a+3N = 5$) but linked to the nitrogen of the 5-nitroindole showed a clear decrease in affinity. In addition, all the N-linked compounds with a total length of five carbons for the linker exhibited a lower affinity (**JE-58, JE-78, JE-87** and **JE-113**) than the one with the extended linker.

Based on the previous observations, it is apparent that the total length of the linker influenced the binding strength. Additionally, the site of linkage on the 5-nitroindole also influenced the binding strength. These effects are compensatory, for example, **JE-81** and **JE-83** exhibited different linker length and at the same time are not linked to the same position of the 5-nitroindole, but showed similar binding strengths. Finally, among the compounds investigated, **JE-86** possessed the best affinity.

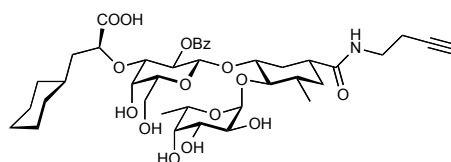
5.3.12 Binding assay for JE-55, JE-81, JE-83, JE-85, JE-86 and JE97

A detailed study of the five compounds with the highest affinities was performed with the Biacore. In addition, **JE-55**, a first-site ligand with an *n*-butinyl linker, was investigated as well. Affinity and kinetic characterization of this compound was of interest as a precursor for *in-situ* click chemistry experiment. In Table 6, affinity and kinetic parameters are summarized.

Table 6. Kinetic evaluation of **JE-55**, **JE-83**, **JE-81**, **JE-86**, **JE-85** and **JE-97**. The reported K_D s are derived from the steady-state fit to a single binding site model. Structure of **JE-55** is shown in the bottom.

Analyte	$K_{D\text{ eq}}$ [μM]**	$K_{D\text{ kin}}$ [μM]*	k_{on} ($\text{M}^{-1}\cdot\text{s}^{-1}$)	k_{off} (s^{-1})	$t_{1/2}$ (s)***
JE-55	1.12	1.12	3.54×10^6	3.98	0.174
JE-81 (2a4N)	0.049	0.035	7.97×10^4	0.0028	240
JE-86 (3a3N)	0.030	0.018	1.42×10^5	0.0026	250
JE-85 (1a3N)	0.057	0.037	6.79×10^4	0.0025	280
JE-83 (2a3C)	0.050	-	-	-	-
JE-97 (3a1N)	0.089	0.036	6.35×10^4	0.0023	310

*calculated K_D using $K_D = k_{\text{off}}/k_{\text{on}}$ ** experimental K_D derived from the steady state response fit to a single binding site model *** calculated $t_{1/2}$ using $t_{1/2} = \ln 2/k_{\text{off}}$.



JE-55

5.4 Conclusion

A second-site screening approach based on a spin-labeled first-site ligand was previously applied in-house to MAG and led to substantial improved antagonist. A similar approach was applied to E-selectin. For that purpose, Jonas Egger synthesized a first-site ligand with a TEMPO moiety (**JE-16**). The presence of the TEMPO did not significantly affect the affinity of the ligand, as shown with Biacore investigations. From an NMR screening of a small library of second-site compounds, seven promising hits were selected. Three of them contain an indole moiety, and two others are indole derivatives (either an imidazol or a thiazol). Finally, the 5-nitroindole (**SH-104-4**) was chosen for further development.

The best first-second-site antagonists showed a 1300-fold improvement of the K_D compared to the lead **BW-69669**. This improvement can mainly be attributed to the pre-organisation of the core in the bioactive conformation and the successful linking of a second-site fragment. Concerning the kinetic characteristics, all first-site ligands (e.g. **GMI-1077**) showed fast association and dissociation rates, which are typical for carbohydrate-protein interactions (flat, solvent-accessible binding site) [39-42]. A significant change in the kinetic profile of the first-second-site antagonist was observed. For the proper analysis of these new compounds, a Biacore assay was developed to allow a preliminary ranking. Later on, a complete analysis of the five best compounds was performed. Figure 38 shows K_D values, as determined from the ratio of their off and on rates. As already mentioned, fast association and dissociation rates are clearly observed in Figure 38 for all the first-site ligands: all are located on the right side of the chart. However, the successfully first-second-site antagonists displayed dissociation rates that were at least one order of magnitude slower than those of the first-site compounds. Therefore, a displacement to the left side of the chart is observed.

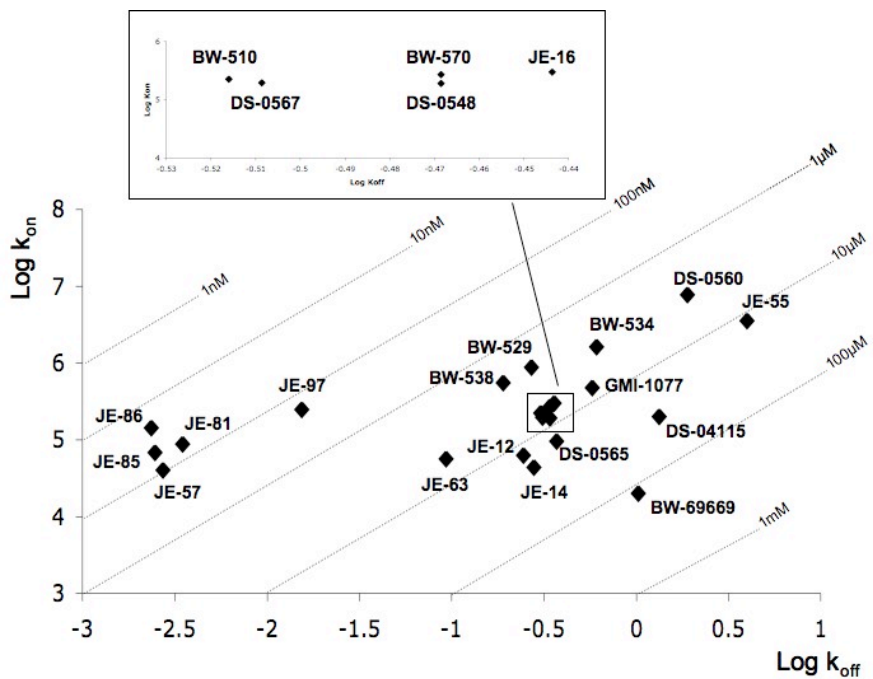


Figure 38. Map of on and off rates of E-selectin antagonists.

The association of a first-site ligand with a second-site fragment was chemically achieved. In a near future, *in-situ* click chemistry will be used for the combination of the two partners [43].

5.5 References

- [1] P.J. Hajduck, *Molecular Interventions* **2006**, 6, 266.
- [2] B.A. Posner, *Curr. Opin. Drug Discov. Devel.* **2005**, 8, 487.
- [3] U.A. Betz, *Drug Discov. Today* **2005**, 10, 1057.
- [4] U.A. Betz, *Curr. Opin. Chem. Biol.* **2005**, 9, 387.
- [5] S.J. Teague, A.M. Davis, P.D. Leeson, T. Oprea, *Angew. Chem. Int. Ed. Engl.* **1999**, 38, 3743.
- [6] C.A. Lipinski, *J. Pharmacol. Toxicol. Methods* **2000**, 44, 235.
- [7] T.I. Oprea, A.M. Davis, S.J. Teague, P.D. Leeson, *J. Chem. Inf. Comput. Sci.* **2001**, 41, 1308.
- [8] D.A. Erlanson, R.S. McDowell, T. O'Brian, *J. Med. Chem.* **2004**, 47, 1.
- [9] R.A. Carr, M. Congreve, C.W. Murray, D.C. Rees, *Drug Discov. Today* **2005**, 10, 987.
- [10] P.J. Hajduk and J. Greer *Nat. Rev. Drug. Discov.* **2007**, 6, 211.
- [11] M. Congreve *et al.* *J. Med. Chem.* **2008**, 51, 3661.
- [12] T. Fink, H. Bruggesser, J.L. Reymond, *Angew. Chem. Int. Ed. Engl.* **2005**, 44, 1504.
- [13] P.J. Hajduk, R.P. Meadows, S.W. Fesik, *Science* **1997**, 278, 497.
- [14] E.T. Olejniczak, P.J. Hajduk, P.A. Marcotte, D.G. Nettlesheim, R.P. Meadows, R. Edalji, T.F. Holzman, S. W. Fesik, *J. Am. Chem. Soc.* **1997**, 119, 5828.
- [15] W. Jahke and H. Widmer, *Cell Mol. Life Sci.* **2004**, 61, 580.
- [16] M. Fischer and R.E. Hubbard, *Molecular Interventions* **2009**, 9, 1.
- [17] C. Dalvit, *Drug Disc. Today*, **2009**.
- [18] S.B. Shuker, P.J. Hajduk, R.P. Meadows, S.W. Fesik, *Science* **1996**, 274, 1531.
- [19] P.J. Hajduk *et al.* *J. Med. Chem.* **1999**, 42, 2315.
- [20] J. Fejzo *et al.* *Chem. Biol.* **1999**, 6, 755.
- [21] M. Pellechia *et al.* *J. Biomol. NMR* **2002**, 22, 165.
- [22] D.W. Li, E.F. DeRose, R.E. London, *J. Biomol. NMR* **1999**, 15, 71.
- [23] R.E. London, *J. Magn. Reson.* **1999**, 141, 301.
- [24] W. Jahnke *et al.* *J. Am. Chem. Soc.* **2000**, 122, 7394.
- [25] P.A. Kosen, *Methods Enzymol.* **1989**, 177, 86.

- [26] W. Jahnke, L.B. Perez, G. Paris, A. Strauss, G. Fendrich, C.M. Nalin, *J. Am. Chem. Soc.* **2000**, 122, 7394.
- [27] J. Egger, B. Ernst, *unpublished results*.
- [28] R.L. Rich D.G. Myszka, *Curr Opin Biotechnol* **2000**, 11, 54.
- [29] C. Dalvit, P. Pevarello, M. Tato, M. Veronesi, A. Vulpetti, M. Sundström. *J. Biomol. NMR* **2000**, 18, 65.
- [30] C. Dalvit, G. Fogliatto, A. Stewart, M. Veronesi, B. Stockman. *J. Biomol. NMR* **2001**, 21, 349.
- [31] B.J. Stockman and C. Dalvit, *Progress in Nuclear Magnetic Resonance Spectroscopy* **2002**, 41, 187.
- [32] Sachin Schelke Dissertation, University of Basel, **2007**.
- [33] I. Bertini, C. Luchinat, P. Giacomo, R. Pierattelli, *ChemBioChem* **2005**, 6, 1536.
- [34] C. Dalvit, D. Caronni, N. Mongelli, M. Veronesi and A. Vulpetti, *Curr. Drug Discov. Technol* **2006**, 3, 115.
- [35] C. Dalvit G. Fogliatto, A. Stewart, M. Veronesi and B. Stockman, *J. Biomol. NMR* **2001**, 21, 349.
- [36] D. Strasser, Dissertation, University of Basel, **2008**.
- [37] S.V. Shelke, B. Cutting, X. Jiang, H. Koliver-Brandl, D.S. Strasser, O. Schwardt, S. Kelm and B. Ernst, *Angew. Chem., Int. Ed.*, in press.
- [38] L. Nieba, A. Krebber and A. Plückthun, *Anal. Biochem.* **1996**, 234, 155.
- [39] P. Mehta, R.D. Cummings, R.P. McEver, *J. Biol. Chem.* **1998**, 273, 32506.
- [40] M.K. Wild, M. C. Huang, U. Schultze-Horsel, P.A. van der Merwe, D. Vestweber, *J. Biol. Chem.* **2001**, 276, 31602.
- [41] L. Herfurth, B. Ernst, R. Ohrlein, B. Wagner, J.L. Magnani, A.J. Benie, T. Peters, *J. Med. Chem.* **2005**, 48, 6879.
- [42] O. Schwardt, H. Gaethje, A. Vedani, S. Mesch, G. Gao, M. Spreafico, J. von Orelle, S. Kelm, B. Ernst, *J. Med. Chem.* **2009**, 52, 989.
- [43] S.K. Mamidyala, M.G. Finn, *Chem. Soc. Rev.* **2010**, 39, 1252.

6. Conclusions and outlook

In acute and chronic inflammatory diseases, an excessive recruitment of leukocytes is problematic. Therefore, the modulation of leukocyte recruitment by interfering with cell tethering is of therapeutical interest. This modulation can be achieved by targeting CAMs like selectins, which play a key role in leukocytes transmigration.

Selectins are calcium dependant carbohydrate-binding proteins involved in the early stage of the homing process. This family of protein, discovered in 1989, was intensively studied and their role in the leukocytes recruitment is well understood. Therefore, selectins are regarded as potential target in drug discovery. Recent advances in the development of selectin antagonists are aiming on carbohydrates-mimetics drugs. Nevertheless, the development of carbohydrate-derived drugs is still challenging due to unfavorable pharmacokinetic profiles inherently linked to carbohydrates (e.g. fast association and dissociation rates, poor solubility, high polarity) and insufficient pharmacodynamics properties (low K_{DS}).

Based on the relevant pharmacophores of the natural ligand of selectins, the tetrasaccharide sLe^x, a first mimic was identified (**BW-69669**). Then, several antagonists were synthesized in order to achieve a stabilization of the bioactive conformation and thereby to improve the potency.

For the evaluation of new antagonists synthesized reliable assay formats became necessary. Biacore was available in-house with all the advantages linked to this technology (e.g. direct evaluation, real-time measurement, labeling not required, access to affinity and kinetic parameters). For a better understanding of the binding mode, Biacore data were combined with STD-NMR and NMR relaxation studies.

6.1 Biacore assay development

The presence of lysines in the vicinity of the binding pocket of E-selectin led to the failure of the direct immobilization of the E-selectin/IgG, *i.e.* binding pocket no longer accessible. Therefore, a capture assay format was established with the advantage of generating oriented surfaces. Two intermediate proteins for the capture, both targeting the Fc part of the E-selectin construct, were tested: protein A and anti-human IgG (Fc specific). In both cases, the capture surfaces allow the

analysis of E-selectin antagonists. Nevertheless, the anti-human IgG was preferred, because it allows a better level of capture of E-selectin was achieved, leading to a better quality of the data. Indeed, reasonable levels of response for antagonists were obtained ($R_{\max} \approx 30$ RU), when considering the difficulties to evaluate low molecular weight compounds with Biacore technology. In addition, a higher stability of the surface was observed. The drawback of the high stability of the surface was the impossibility of complete removal of E-selectin.

The evaluation of the first generation of E-selectin antagonists showed an improvement of the binding by a factor of two when introducing a benzoate in the 2-position of the galactose moiety (**LT-0236**). An improvement of the affinity by a factor of five was observed in the presence of a methyl group in the 5-position of the GlcNAc mimic (**DS-04115**). By combining these modifications, a gain in affinity by a factor of 30 was obtained (**GMI-1077**). The introduction of a *p*-fluorobenzoate in the 2-position of galactose did not improve the affinity (**BW-510**), whereas the *p*-methoxybenzoate (**BW-529**) showed an increase in the affinity by another factor of four compare to **GMI-1077**. Unfortunately, none of the other modifications showed a significant improvement of the affinity.

Concerning the kinetic profile of this generation of E-selectin antagonists, a fast association and a fast dissociation rates were always observed and could not be improved.

6.2 STD-NMR and relaxation experiments

In parallel to Biacore evaluation, spin-spin and spin-lattice NMR experiments were performed. This qualitatively confirmed binding and helped to establish the conditions for competitive spin-spin relaxation experiments. These experiments allowed determining the affinity of E-selectin antagonists relative to **BW-69669**. The data obtained were consistent with the affinity observed in Biacore.

In order to obtain further informations on the binding mode, STD-NMR experiments were performed for some of the antagonists in presence of E-selectin/IgG and in presence of the Lec EGF_CRD2 construct. With both proteins, similar STD patterns were observed with all antagonists, revealing a similar binding mode. The observed contact of the substituent in the 2-position of galactose with the protein observed by STD-NMR led to the hypothesis of another binding mode.

6.3 Second-generation of E-selectin antagonists

In order to improve affinity and kinetic of E-selectin ligands, a fragment-based approach was initiated. An optimized first-site ligand of the first generation of E-selectin antagonists with a micromolar affinity was chosen as a starting point.

A spin-labeled analogue of this ligand (**JE-16**) was synthesized in-house by Jonas Egger and used for the identification of small second-site ligands binding to the E-selectin in the vicinity of **JE-16**. After screening of a library of second site ligands, seven promising hits were found. One representative thereof, 5-nitroindole was further developed.

The design of the linker of first- and second-site ligands was guided by NMR. Thus, relaxation rates of the second-site ligand proton in the presence of the spin-labeled ligand first-site ligand gave information on its relative orientation.

Jonas Egger synthesized a library of twenty “first-second-site” antagonists with linkers of different length. Their binding affinity to E-selectin/IgG was evaluated by a ranking procedure on the Biacore. Subsequently, a complete characterization of the best five antagonists was performed. The two first-second-site antagonists with the highest affinity contained linkers with a total length of six carbons and were linked to the nitrogen in the 1-position of the 5-nitroindole. The best first-second-site antagonist showed a 1300-fold improvement of the K_D compared to the lead **BW-69669** and displayed a 380-fold slower dissociation rate.

6.4 Outlook

The capture Biacore assay is well established and can be routinely used for the evaluation of E-selectin antagonists. Nevertheless, the difficulties to remove E-selectin from the chip surface make the assay less feasible. When the E-selectin antagonist is immobilized on the sensorchip, affinity data comparable to the capture assay format were obtained. The immobilization of high affinity ligands on the surface will:

- decrease the protein consumption,
- reduce the necessity of frequent new immobilization,

- allow the evaluation of new compounds in a competitive format and
- allows the characterization of the affinity of other proteins, such as murine E-selectin.

After STD-NMR experiments of ligands from the first-generation, the possibility of another binding mode persists. An X-ray structure elucidation E-selectin co-crystallized of with a first-generation ligand will provide further insight.

Until now, STD-NMR and group epitope mapping (GEM) of first-second-site antagonists was compromised by their limited solubility at the concentration required for STD-NMR experiments. An improvement of the solubility could be achieved e.g. by replacement of the nitro group of the 5-nitroindole by an amine or an acetamide.

Finally, after the second-site screening, seven hits were selected. So far, only one of them was used for the development of first-second-site antagonists. The six hits left offers promising perspective for the design and synthesis of other libraries of first-second-site antagonists.

CURRICULUM VITAE

Name, Address: Céline WECKERLE
Magdenstrasse 25
4058 BASEL (CH)
Mobile: +41 (0) 789 09 16 25
CEWeckerle@gmail.com

Date of birth: September 16, 1979

Place of birth: Strasbourg (67) - FRANCE

Nationality: French

Marital status: Common-law marriage, one child



LANGUAGES

French	Native language
English	Fluent
German	Conversational

EDUCATION

University of Basel – Institute of Molecular Pharmacy Basel SWITZERLAND

2007-2010 Ph.D. in Pharmaceutical Sciences under the direction of Prof. Dr. B. Ernst.

„E-selectin antagonists: Fragment-Based Drug Discovery and Lead Optimization by NMR and BIAcore“.

Université Louis Pasteur - Strasbourg FRANCE

2005 Master – M2 in Biological and Chemical Analysis
Analysis and Biotechnology option with honours
Training period of end of study in research and development.
Pierre Fabre Dermo Cosmetic
Service of Cutaneous Biochemistry –Toulouse (FR)
Identification and study of serine-proteases of the human skin

2004 Master – M1 biochemistry mention biochemistry molecular and cellular
Molecular biology option with honours

2003 Licence in Biochemistry (Equivalent to a Bachelor's degree) with honours
Training period of third year in fundamental research.

2002 CNRS - Molecular institute of Plants Biology - Strasbourg (FR)
Laboratory of Virology
Studies in vivo and in vitro of the interactions between viral proteins.
First cycle (DEUG) of studies in Biology with honours

Training period for the second year.
Laboratory of medical analysis – Strasbourg (FR)
Blood analysis, Elisa tests, identification of pathogens.

PROFESSIONAL EXPERIENCE

2005-06	CNRS–Laboratory of NMR and biophysics of membranes – Strasbourg (FR) Under the direction of Prof. Dr. Burkhard Bechinger Research assistant. Publication in 2008 (see section Scientific Qualifications) <i>Expression, purification and structural studies of proteins from the Bcl-2 family.</i>
2005	Laboratory of Histo-cyto-pathology – Strasbourg (FR) Cytopathology technician.
2001-04	Point Accueil Etudiant - University Louis Pasteur - Strasbourg (FR) Stewardess.

SCIENTIFIC SKILLS

Biacore	Biacore 3000. Assay development, thermodynamic and kinetic evaluations.
Molecular Biology	Binding assays, micro-plates (UV and fluorescence), HPLC, FPLC, Western blot Farwestern, cloning, PCR, mini-preparation of DNA, transformation of bacterial cells, bacterial and mammalian (CHO) cell culturing, affinity chromatography, gel filtration, ELISA, SDS-PAGE, production and purification of ¹⁵ N and ¹³ C labeled protein for NMR studies.
NMR	Bruker DMX 500 MHz and ADVANCE III spectrometer. STD-NMR, competition STD-NMR, transverse relaxation rate, longitudinal relaxation rate, waterLOGSY, epitope mapping, second-site screening. Brucker DMX 300 MHz spectrometer Solid-state NMR
Far UV-CD Spectroscopy	JASCO Model J-810 CD spectropolarimeter. Studies of conformational changes in secondary structure.
Fluorescence Spectroscopy	Spectra Max M5 (Molecular Devices Inc.) spectrofluorimeter. Studies of accessibility of the binding pocket and competitive binding.

ADDITIONAL SKILLS

IT	Windows, MacOS X, Microsoft Office XP, MestReNova, Minitab, advanced skills in Microsoft Excel, Adobe Illustrator, Prism,
----	---

SCIENTIFIC QUALIFICATIONS

Publications

S. Nedelkina, I. Gokce, H. Ridley, C. Weckerle, T. Magnin, F. Vallette, F. Pattus, J.H.Lakey, B. Bechinger, *High-yield expression and purification of soluble forms of the anti-apoptotic Bcl-xL and Bcl-2 as TolAIII- fusion proteins*, Protein Expression and Purification (2008)

Unpublished data from PhD work due to confidentiality reasons. Patents are pending.

Posters

Celine Weckerle, Jonas Egger, Brian Cutting and Beat Ernst. Fragment based lead optimization for carbohydrate mimics binding to E-selectin. Annual Research Meeting **2010**, Basel, Switzerland.

Jonas Egger, Céline Weckerle, Daniel Schwitzer and Beat Ernst. Synthesis, Development and optimization of E-selectin ligands guided by NMR and Biacore studies. Annual Research Meeting **2009**, Basel, Switzerland.

Educational Experience

Since 2007 Supervisor of several practical courses in Pharmaceutical Biology.
In-house technical support for Biacore users

2006 Supervisor of a master thesis on expression and purification of N¹⁵ labelled Bax for structural studies.

Courses

2009 Key Issues in Drug Discovery.
GE Healthcare Innovation Meeting.

2008 Second NMR School of GERM (Groupement de Resonance Magnetique),
Biacore Interaction Day (Central Europe).

2007 Formation pratique en RMN liquide et solide – University of Lille (FR),
Numerous lectures and seminars (drug discovery, analytics).

REFERENCES

Prof. Dr. B. Ernst Institute of Molecular Pharmacy, University of Basel (CH)
(+41 61 267 15 51) beat.ernst@unibas.ch
Thesis advisor

Dr. B. Cutting Institute of Molecular Pharmacy, University of Basel (CH)

(+41 61 267 15 63) brian.cutting@unibas.ch

Prof. Dr. B. Bechinger

Faculty of Chemistry, University Louis Pasteur (FR)
(+33 36 824 51 50) bechinger@chimie.u-strasbg.fr

INTERESTS AND ACTIVITIES

Travelling (England, Italy, Martinique, Switzerland, Slovenia).

Reading (thriller, suspense, novel, detective story).

Salsa dancing.

Water sports (holder of the BNSSA licence).

Appendix I

E-Selectin-IgG(Fc)-secreted construct (Novartis: frank Kolbinger)

MIASQFLSALTLVLLIKESGAWSYNTSTEAMTYDEASAYCQQRYPYTHLVAIQNKEEIEYLN
SILSYSPSYWIGIRKVNNVWVWVGTQKPLTEEAKNWAPGEPNNRQKDEDCVEIYIKREK
DVGMMWDERCSKKKLALCYTAACTNTSCSGHGECVETINNYTCKCDPGFSGLKCEQIVNC
TALESPEHGSLVCSHPLGNFSYNSSCSISCDRGYLPSSMETMQCMSSGEWSAPIACNVV
ECDAVTNPANGFVECFQNPFSFPWNTTCTFDCEEGFELMGAQSLQCTSSGNWDNEKPTCK
AVTCRAVRQPQNGSVRCSHSPAGEFTFKSSCNFTCEEFGFMLQGPQVECTTQGQWTQQIP
VCEAFQCTALSNPERGYMNCLPSASGSFRYGSSECFSCQGFVFLKGSKRLQCGPTGEWDN
EKPTCEAVRCDVAHQPPKGLVRCASHPIGEFTYKSSCAFSCEEFGFELYGSTQLECTSQGQ
WTEEVPSCQVVKCSSLAVPGKINMSSCSGEPVFGTVCKFACPEGWTLNGSAARTCGATGHW
SGLLPTECEVDKKEPKSCDKTHTCPPCPAPELLGGPSVFLFPPKPKDTLMISRTPEVTCV
VVDVSHEDPEVKFNWYVDGVEVHNAKTKPREEQYNSTYRVVSVLTVLHQDWLNGKEYKCK
VSNKALPAPIEKTISKAKGQPREPQVYTLPPSRDELTKNQVSLTCLVKGFYPSDIAVEWE
SNGQPENNYKTTTPVLDSGDSFFLYSKLTVDKSRWQQGNVVFSCSVMHEALHNHYTQKSLS

LSPGK

E-Selectin-IgG(Fc) [Theoretical pI: 5.41 / Mw (average mass): 86692.61]

The molecular weight is around 148 KDa on a reducing SDS-PAGE.

E-selectin: Amino acids 1-548



IgG (Fc): Amino acids 549-785



CH1: 549-554
Hinge: 555-570

CH2: 571-682

CH3: 682-785

Appendix II

Lec EGF_CD2 domain construct (Roland Preston)

0

WSYNTSTEAMTYDEASAYCQORYTHLVAIQNKEEIEYLNSILSYSPSYWIGIRKVNNVVWVGTQKPLTEEAKN
WAPGEPNNRQKDEDCVEIYIKREKDVGMWNDERCSKKKLALCYTAACTNTSCSGHGECVETINNYTCKCDPGFSG
LKCEQIV

157

158

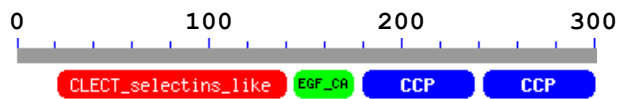
NCTALESPEHGSLVCSHPLGNFSYNSSCSISCDRGYLPSSMETMQCMSSGEWSAPIPACNVVE
CDAVTNPANGFVECFQNPFSFPWNTTCTFDCEEFGFELMGAQSLQCTSSGNWDNEKPTCKA

E-Selectin-IgG (Fc) [Theoretical pI: 4.74/ Mw (average mass):31281.72]

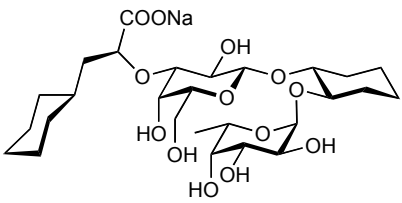
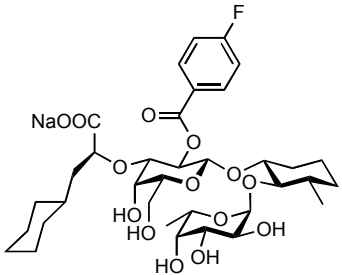
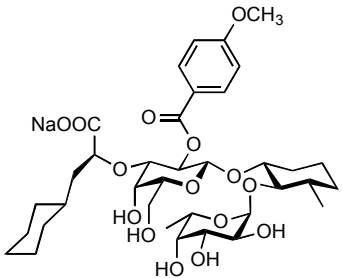
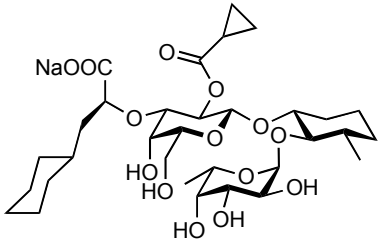
The molecular weight is around 70 KDa on a reducing SDS-PAGE.

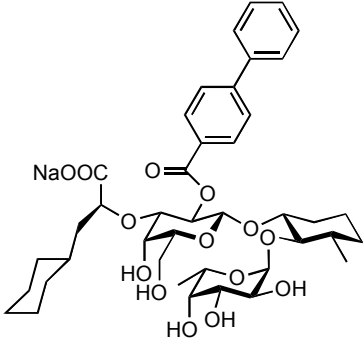
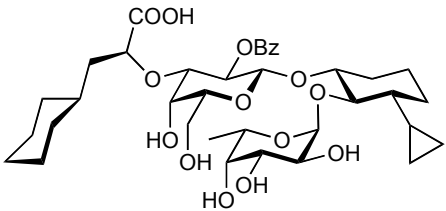
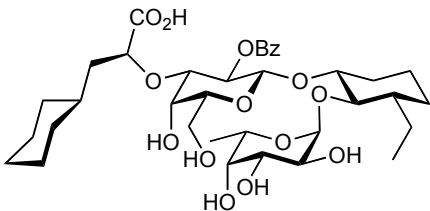
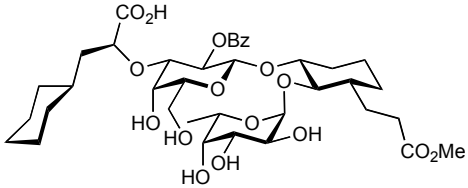
Lec and EGF domains: Amino acids 1-157

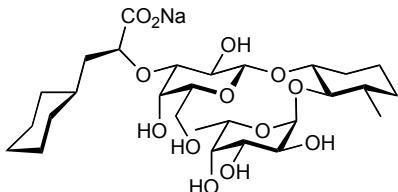
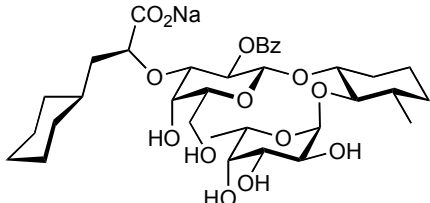
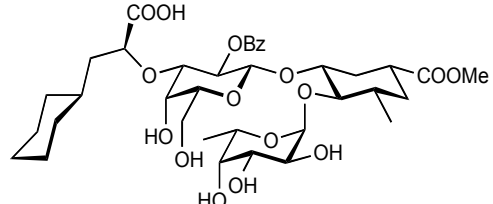
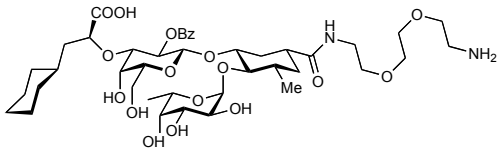
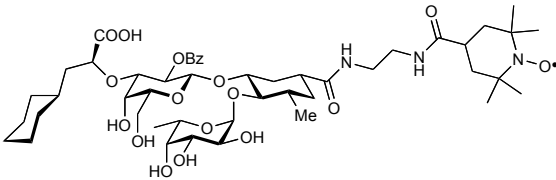
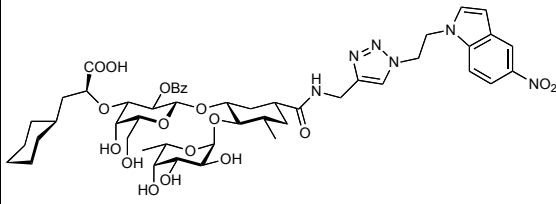
CRD domains: Amino acids 158-281

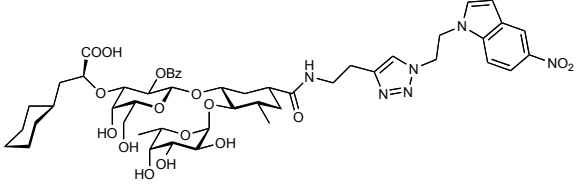
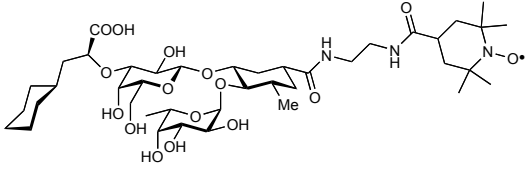
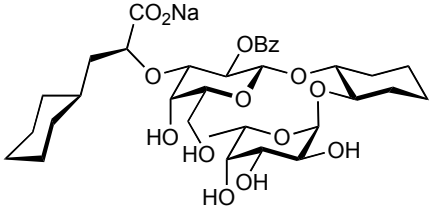


Appendix III

Compound	Structure	Mol. Wt.	rI _C ₅₀ competitive binding assay GMI, ref. sLe ^x	K _D (μM) Biacore, 25°C
BW-69669		600.64	0.08 – 0.12	44.90
BW-510		736.75	0.00515	1.27
BW-529		748.79	0.00626	0.34
BW-534		682.73	0.00618	2.32

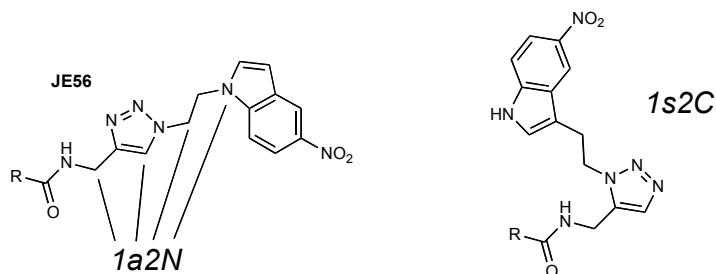
Compound	Structure	Mol. Wt.	rIC ₅₀ competitive binding assay GMI, ref. sLe ^x	K _D (μM) Biacore, 25°C
BW-538		794.85	0.0147	n.d.
DS-0565		722.82	0.032	5.36
DS-0567		710.35	0.007	1.49
DS-0548		768.36	0.008	1.62

Compound	Structure	Mol. Wt.	rI _C ₅₀ competitive binding assay GMI, ref. sLe ^x	K _D (μM) Biacore, 25°C
DS-04115 BW-40800		614.29	0.016	7.64
GMI-1077 BW-40801		718.32	0.004	1.50
JE-12 DS-0560		754.82	-	1.90
JE-14		870.98	-	6.01
JE-16		964.5	-	1.25
JE-56		904.96	-	2.45

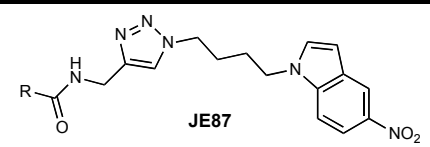
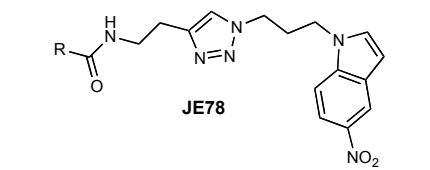
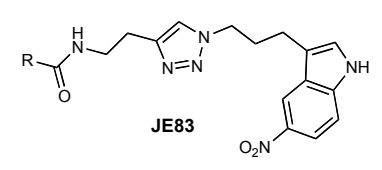
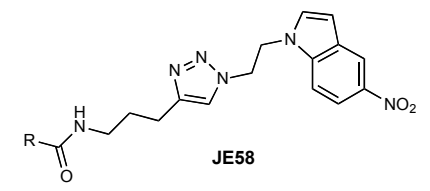
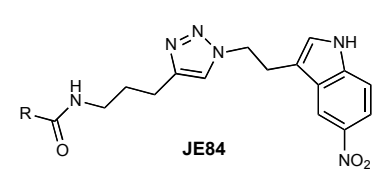
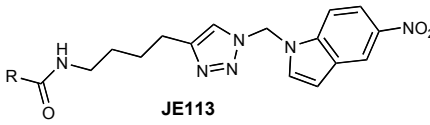
Compound	Structure	Mol. Wt.	rI _C ₅₀ competitive binding assay GMI, ref. sLe ^x	K _D (μM) Biacore, 25°C
JE-57		1023.09	-	0.138
JE-61		860.48	-	12.46
LT-0236		704.30	-	18.8

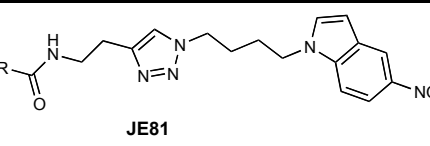
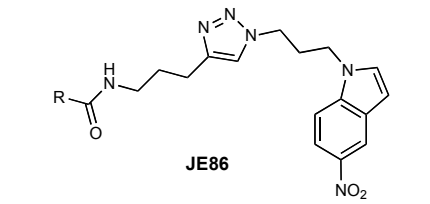
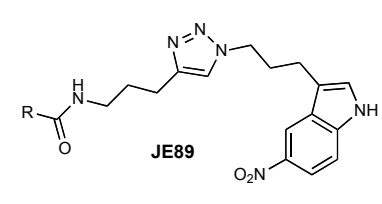
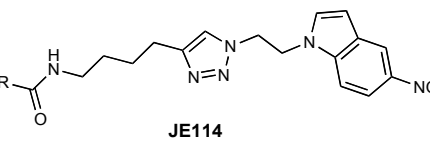
Appendix IV

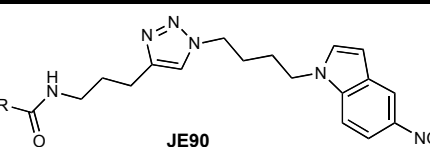
Nomenclature for identification of the linking pattern. 1: number of CH₂ groups in the first-site linker; a: type of conjunction (a = *anti*; s = *syn*); 2: number of CH₂ groups in the second-site linker; N: site of attachment at the second-site linker (N: nitrogen, C: carbon).



2	1a1N			
3	1a2N		1a2C	
	2a1N			
4	1a3N		1a3C	
	2a2N		2a2C	
	3a1N			

5	1a4N	 JE87		
	2a3N	 JE78	2a3C	 JE83
	3a2N	 JE58	3a2C	 JE84
	4a1N	 JE113		

6	2a4N	 JE81		
	3a3N	 JE86	3a3C	 JE89
	4a2N	 JE114		

7	3a4N	 JE90		
---	------	---	--	--